

UNCLASSIFIED

AD NUMBER: AD0875226

LIMITATION CHANGES

TO:

Approved for public release; distribution is unlimited.

FROM:

Distribution authorized to US Government agencies and their contractors; Export Controlled; 1 Jan 1970. Other requests shall be referred to Air Force Flight Dynamics Laboratory, ATTN: FDCC, Wright-Patterson AFB, OH 45433.

AUTHORITY

AFFDL ltr dtd 25 Oct 1972

AFFDL-TR-69-124

PART I

VOLUME I

AD875226

# WING ROLL CONTROL DEVICES FOR TRANSONIC HIGH LIFT CONDITIONS

25

PART I - FIXED WING CONFIGURATION

VOL. I - GENERAL CONFIGURATION, DEVICES,  
TEST RESULTS, CONCLUSIONS

JACK D. McALLISTER  
DAVID B. BENEPE  
PERRY D. WHITTEN  
GARY KAFTAN

DDC  
RECEIVED  
OCT 9 1970  
REGISTERED  
B

GENERAL DYNAMICS, FORT WORTH DIVISION

AD NO. \_\_\_\_\_  
DDC FILE COPY

TECHNICAL REPORT AFFDL-TR-69-124, PART I, VOL. I

JANUARY 1970

This document is subject to special export controls and each transmittal to foreign governments or foreign nationals may be made only with prior approval of AFFDL (FDCC), W-PAFB, Ohio 45433

AIR FORCE FLIGHT DYNAMICS LABORATORY  
AIR FORCE SYSTEMS COMMAND  
WRIGHT-PATTERSON AIR FORCE BASE, OHIO

ERRATA - March 1971

AD-875-226

Attached are corrected pages of AFFDL-TR-69-124, Volume 1, Part I,  
"Wing Roll Control Devices for Transonic High Lift Conditions - Fixed Wing  
Configuration". Unclassified report, January, 1970.

Page 8

Delete Page 8 and replace with this revised page.

Page 96

Delete Page 96 and replace with this revised page.

Air Force Flight Dynamics Laboratory  
Air Force Systems Command  
Wright-Patterson Air Force Base, Ohio

Table I GEOMETRIC CHARACTERISTICS

| ITEM   | SYMBOL                              | FULL SCALE VALUE               | MODEL SCALE VALUE              |
|--|-------------------------------------|--------------------------------|--------------------------------|
| WING AREA                                    | $S_{ref}$                           | 498.31 ft <sup>2</sup>         | .86512 ft <sup>2</sup>         |
| ASPECT RATIO                                 | $AR_{basic}$                        | 4.07                           | 4.07                           |
| ROOT CHORD (AT $\phi$ )                      | $C_r$                               | 231.14 In                      | 9.631 In                       |
| TIP CHORD (OF BASIC TRAPEZOIDAL WING)        | $C_{Ttrap}$<br>(Lateral Pos)        | 69.34 In<br>SS224.24           | 2.889 In<br>S.S.9.343          |
| WING SPAN                                    | $b_{ref}$                           | 540.57 In                      | 22.524 In                      |
| MEAN AERODYNAMIC CHORD                       | MAC                                 | 157.98 In                      | 6.583 In.                      |
| LOCATION OF MAC<br>LONGITUDINAL (L.E.)       | $\bar{X}$                           | F.S. 450.03                    | F.S.18.751                     |
| LATERAL                                      | $\bar{Y}$                           | S.S. 101.22                    | S.S. 4.218                     |
| MOMENT<br>CENTER - 25% MAC                   | $c.g.ref$                           | F.S. 489.52                    | S.S.20.397                     |
| BASIC TRAPEZOIDAL WING<br>LEADING EDGE SWEEP | $\Delta L.E.w$                      | 31.50 Deg                      | 31.50 Deg                      |
| TRAILING EDGE SWEEP                          | $\Delta T.E.w$                      | -6.207 Deg                     | -6.207 Deg                     |
| TAPER RATIO                                  | $\Delta T$                          | .300                           | .300                           |
| GLOVE<br>LEADING EDGE SWEEP                  | $\Delta L.E.G$                      | 70.0 Deg                       | 70.0 Deg                       |
| OVERALL LENGTH                               |                                     | 866.64 In                      | 36.11 In                       |
| F.S. OF NOSE                                 |                                     | F.S. 22.01                     | F.S. 0.917                     |
| COMPOSITE WING-GLOVE<br>PLANFORM             | $S_{composite}$<br>$AR_{composite}$ | 618.72 Ft <sup>2</sup><br>3.28 | 1.0741 Ft <sup>2</sup><br>3.28 |

NOTE: Airfoil section coordinates are given in Figure 5, page 15

This page of AFFDL TR-69-124 Part I, Volume I, revised February 1971

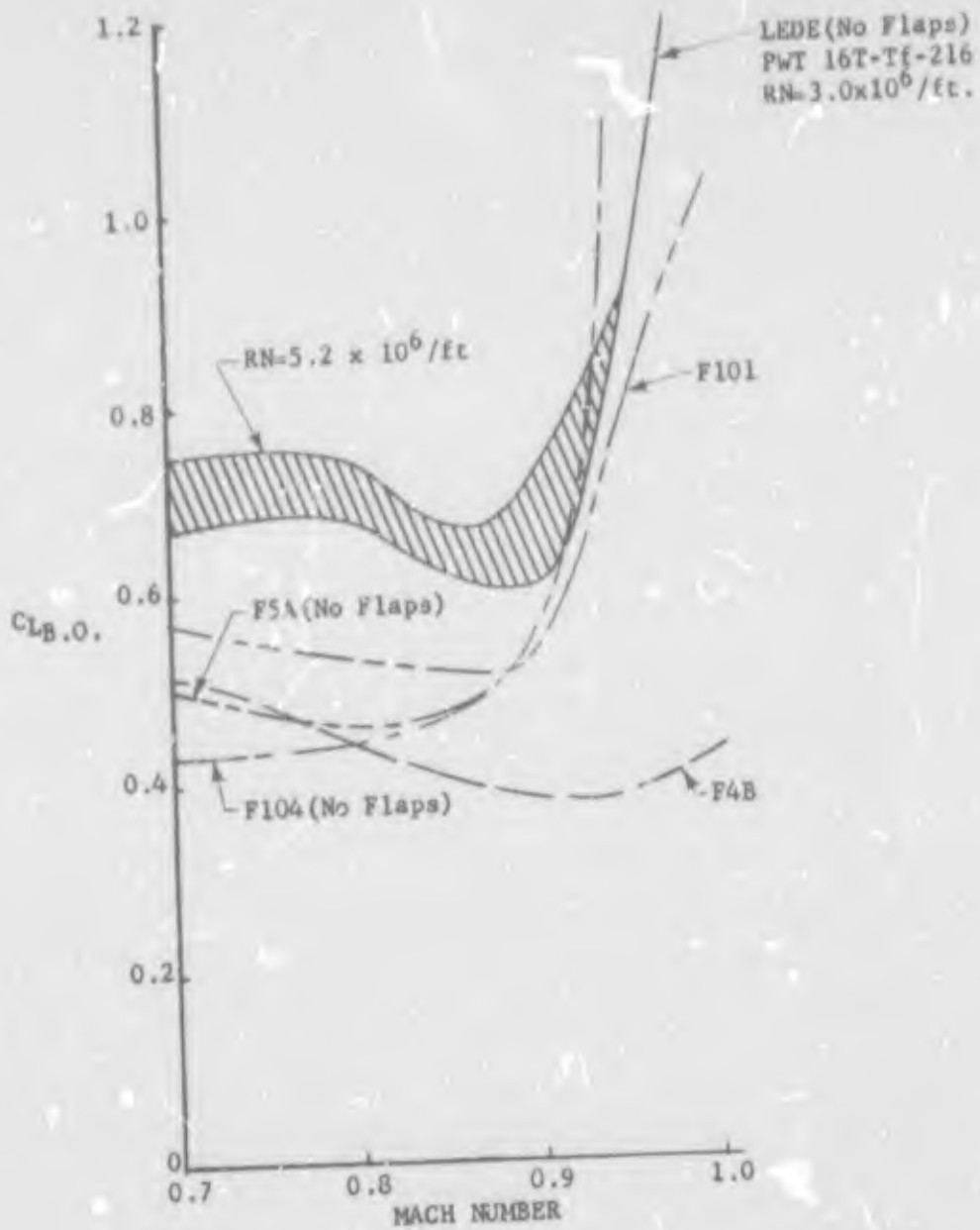


Figure 31 COMPARISON OF BUFFET ONSET

This page of AFFDL TR-69-124 Part I, Volume I, revised February 1971.

NOTICE

When Government drawings, specifications, or other data are used for any purpose other than in connection with a definitely related Government procurement operation, the United States Government thereby incurs no responsibility nor any obligation whatsoever; and the fact that the Government may have formulated, furnished, or in any way supplied the said drawings, specifications, or other data, is not to be regarded by implication or otherwise as in any manner licensing the holder or any other person or corporation, or conveying any rights or permission to manufacture, use, or sell any patented invention that may in any way be related thereto.

|                                 |   |                |
|---------------------------------|---|----------------|
| ACCESSION NO.                   |   |                |
| COPY                            | WRITE SECTION <input type="checkbox"/>          |                |
| NO                              | NOY SECTION <input checked="" type="checkbox"/> |                |
| UNANNOUNCED                     | <input type="checkbox"/>                        |                |
| JUSTIFICATION                   |   |                |
| BY                              |   |                |
| DISTRIBUTION/AVAILABILITY CODE: |   |                |
| REG.                            | AVAIL.  | NO. OF SPECIAL |
| 2                               |   |                |

Copies of this report should not be returned unless return is required by security considerations, contractual obligations, or notice on a specific document.

# WING ROLL CONTROL DEVICES FOR TRANSONIC HIGH LIFT CONDITIONS

PART I — FIXED WING CONFIGURATION

VOL. I — GENERAL CONFIGURATION, DEVICES,  
TEST RESULTS, CONCLUSIONS

*JACK D. McALLISTER*  
*DAVID B. BENEPE*  
*PERRY D. WHITTEN*  
*GARY KAFTAN*

This document is subject to special export controls and each transmittal to foreign governments or foreign nationals may be made only with prior approval of AFFDL (FDCC), W-PAFB, Ohio 45433

## FOREWORD


This report summarizes the work accomplished by the Fort Worth Division of General Dynamics, Fort Worth, Texas, under USAF Contract F33615-69-C-1225, Project 8219. This is the final report on the Fixed Wing Configuration phase of the study.

The work was accomplished during the period from 1 January to 26 November 1969 under the direction of the Air Force Project Engineer, Mr. Welbourne G. Williams, Control Criteria Branch, Flight Dynamics Laboratory (FDCC). Mr. John H. Watson served as the General Dynamics Program Manager for this study. The success of this work is due to the contributions made by the following persons in the areas designated:

|                      |   |
|----------------------|---|
| Malley R. Bass       | Configuration lines development and design of model components                              |
| David B. Benepe      | Selection of the basic wing body configuration and analysis of longitudinal characteristics |
| Gary Kaftan          | Test Conductor for wind tunnel evaluations and model test lead man                          |
| Jack D. McAllister   | Principal Investigator, selection and analysis of roll control devices                      |
| Thomas F. Paniszczyn | Consultant on roll control devices and assistance on the final report                       |
| Perry D. Whitten     | Prediction and analysis of longitudinal characteristics                                     |

The report was released by the authors in March, 1970.

This technical report has been reviewed and is approved.



C. B. Westbrook

Chief, Control Criteria Branch  
Flight Control Division  
Air Force Flight Dynamics Laboratory



## ABSTRACT

The Wing Mounted Roll Control Study (Contract F33615-69-C-1225) was an investigation of various methods for improving control effectiveness at high-lift transonic conditions. Emphasis was placed upon the use of leading edge devices as primary controls and also as auxiliary devices with conventional controls. Selected configurations were tested in AEDC 4T facility and limited validation was obtained in the AEDC 16T facility. Control configurations investigated included leading edge flaps and ailerons both singly and in combination, as well as spoilers, differential horizontal tail and several auxiliary devices. Use of differential leading edge deflection significantly improved aileron effectiveness at high-angle-of-attack transonic conditions. Because of the important effects that the wing-body configuration has upon wing mounted control devices, considerable data and analysis are presented for the longitudinal characteristics. Testing of the same model in two different size facilities provided significant information on wall interference effects at transonic conditions.

## TABLE OF CONTENTS

|                                     |       |
|-------------------------------------|-------|
| FOREWORD                            | ii    |
| ABSTRACT                            | iii   |
| LIST OF FIGURES                     | x     |
| LIST OF TABLES                      | xviii |
| LIST OF SYMBOLS AND ABBREVIATIONS   | xix   |
| SECTION I INTRODUCTION              | 1     |
| 1. OBJECTIVE                        | 1     |
| 2. SCOPE                            | 1     |
| 3. TECHNICAL APPROACH               | 2     |
| 4. REPORT ORGANIZATION              | 3     |
| SECTION II CONFIGURATION SELECTION  | 5     |
| 1. GENERAL ARRANGEMENT              | 5     |
| a. Wing Planform                    | 9     |
| b. Wing Section                     | 14    |
| c. Fuselage Modifications           | 16    |
| 2. LEADING EDGE FLAPS               | 19    |
| 3. AILERONS AND TRAILING EDGE FLAPS | 22    |
| 4. VENTED SPOILER                   | 22    |
| 5. SPLIT FLAPS                      | 26    |
| 6. VORTEX GENERATOR PATTERN         | 28    |
| 7. KRUGER GLOVE FLAP                | 30    |

|             |   |     |
|-------------|---|-----|
| SECTION III | WIND TUNNEL TECHNIQUES AND TEST PROGRAMS        | 33  |
| 1.          | FACILITIES                                      | 33  |
| 2.          | TEST TECHNIQUES                                 | 34  |
|             | a. Full Scale Simulation                        | 35  |
|             | b. Flow Visualization                           | 36  |
|             | c. Basic Test Configuration                     | 38  |
| 3.          | FORCE AND MOMENT MEASUREMENTS                   | 39  |
| 3.          | TEST PROGRAMS                                   | 41  |
| SECTION IV  | COMPARISONS BETWEEN WIND TUNNELS                | 49  |
| 1.          | TIE-IN RUNS                                     | 49  |
| 2.          | LEDE CONFIGURATION LONGITUDINAL DATA            | 57  |
| 3.          | LATERAL-DIRECTIONAL DATA                        | 68  |
| SECTION V   | REYNOLDS NUMBER EFFECTS                         | 74  |
| SECTION VI  | SYMMETRICAL CONFIGURATION EFFECTS               | 93  |
| 1.          | TEST CONFIGURATION VERIFICATION                 | 94  |
| 2.          | LEDE CONFIGURATION LONGITUDINAL CHARACTERISTICS | 94  |
|             | a. Lift Curve Slope                             | 100 |
|             | b. Angle of Zero Lift                           | 104 |
|             | c. Minimum Drag Coefficient                     | 104 |
|             | d. Drag Due to Lift                             | 104 |
|             | e. Aerodynamic Center                           | 107 |
| 3.          | LEADING EDGE FLAP EFFECTS                       | 110 |
|             | a. Test Results for Basic Leading Edge          | 117 |
|             | b. Comparison of Test Results with Predictions  | 129 |

|    |  |     |
|----|--|-----|
| 4. | ALTERNATE LEADING EDGE                     | 135 |
| 5. | AUXILIARY DEVICES                          | 140 |
|    | a. Vortex Generators                       | 141 |
|    | b. Drooped Trailing Edge                   | 141 |
|    | c. Split Trailing Edge Flaps               | 144 |
|    | SECTION VII ROLL CONTROL DEVICES           | 147 |
| 1. | DIFFERENTIAL LEADING EDGE FLAPS            | 147 |
| 2. | AILERONS                                   | 153 |
|    | a. Basic Geometric Effects                 | 153 |
|    | b. Symmetrical Leading Edge Deflection     | 167 |
|    | c. Linearity with Deflection               | 172 |
| 3. | COMBINED LEADING AND TRAILING EDGE DEVICES | 185 |
| 4. | VENTED SPOILER                             | 194 |
| 5. | DIFFERENTIAL HORIZONTAL TAIL               | 194 |
| 6. | AUXILIARY DEVICES                          | 200 |
|    | a. Vortex Generators                       | 200 |
|    | b. Trailing Edge Droop                     | 200 |
|    | c. Split Flap                              | 204 |
|    | d. Kruger Glove Flap                       | 204 |
|    | e. Canopy Fairing Effects                  | 204 |
| 7. | ROLL CONTROL COORDINATION                  | 207 |
|    | SECTION VIII CONCLUDING REMARKS            | 218 |
| 1. | ROLL CONTROL CONFIGURATIONS                | 218 |
| 2. | SYMMETRICAL CONFIGURATIONS                 | 220 |
| 3. | TEST TECHNIQUES                            | 221 |

|  |     |
|--|-----|
| REFERENCES   | 223 |
| VOLUME II  | 226 |
| APPENDIX I ROLL RATE EFFECTS ON AIR-TO-AIR COMBAT                      | 226 |
| 1. SIMULATION  | 226 |
| 2. RESULTS   | 228 |
| APPENDIX II ROLL CONTROL POWER CRITERIA                                | 236 |
| 1. GENERAL RESPONSE ANALYSIS   | 236 |
| 2. HANDLING QUALITIES CONSIDERATIONS                                   | 242 |
| 3. ROLLING MOMENT REQUIREMENT  | 248 |
| APPENDIX III FORCE AND MOMENT COMPARISONS<br>VARIOUS WIND TUNNELS USED | 251 |
| 1. TIE-IN RUNS   | 251 |
| 2. LEDE CONFIGURATION LONGITUDINAL DATA                                | 258 |
| 3. LEDE CONFIGURATION LATERAL-DIRECTIONAL DATA                         | 271 |
| APPENDIX IV FORCE AND MOMENT COMPARISONS<br>SYMMETRICAL CONFIGURATIONS | 277 |
| 1. LEDE CONFIGURATION LONGITUDINAL CHARACTERISTICS                     | 277 |
| 2. LEADING EDGE FLAP EFFECTS   | 281 |
| 3. ALTERNATE LEADING EDGE  | 314 |
| 4. AUXILIARY DEVICES   | 347 |
| a. Vortex Generators   | 347 |
| b. Drooped Trailing Edge   | 364 |
| c. Split Trailing Edge Flaps   | 381 |

|             |  |     |
|-------------|--|-----|
| APPENDIX V  | FORCE AND MOMENT COMPARISONS               |     |
|             | ROLL CONTROL DEVICES                       | 398 |
| 1.          | DIFFERENTIAL LEADING EDGE FLAPS            | 398 |
| 2.          | AILERONS                                   | 411 |
| 3.          | COMBINED LEADING AND TRAILING EDGE DEVICES | 476 |
| 4.          | VENTED SPOILER                             | 521 |
| 5.          | DIFFERENTIAL HORIZONTAL TAIL               | 533 |
| 6.          | AUXILIARY DEVICES                          | 538 |
| APPENDIX VI | TABULATED FORCE AND MOMENT DATA            | 535 |

## LIST OF FIGURES

| <u>Figure</u> |  | <u>Page</u> |
|---------------|--|-------------|
| 1             | RESEARCH MODEL GENERAL ARRANGEMENT<br>(ROLL CONTROL L.E.D.E. FORCE MODEL<br>PROGRAM) | 6           |
| 2             | LEDE MODEL   | 7           |
| 3             | TYPICAL THREE DIMENSIONAL SHOCK PATTERN AND<br>QUALITATIVE SEPARATION BOUNDARIES     | 10          |
| 4             | QUALITATIVE BUFFET BOUNDARIES OF VARIOUS<br>AIRCRAFT                                 | 12          |
| 5             | AIRFOIL SECTION OF BASIC TRAPEZOIDAL WING  | 15          |
| 6             | NORMAL CROSS SECTIONAL AREA WITH TAILS   | 17          |
| 7             | FUSELAGE FAIRINGS  | 18          |
| 8             | LEADING AND TRAILING EDGE FLAP PLANFORMS   | 20          |
| 9             | LEADING-EDGE-FLAP AIRFOIL GEOMETRIES   | 21          |
| 10            | CURVATURE DISTRIBUTIONS  | 23          |
| 11            | UPPER SURFACE SLOPE DISTRIBUTIONS  | 23          |
| 12            | ESTIMATED AILERON ROLLING MOMENT   | 24          |
| 13            | SPOILER GEOMETRY   | 25          |
| 14            | TYPICAL SPLIT FLAP SECTIONS  | 27          |
| 15            | VORTEX GENERATOR ARRAY   | 29          |
| 16            | VIEW OF VORTEX GENERATORS  | 31          |
| 17            | GLOVE-MOUNTED KRUGER FLAP  | 32          |

| <u>Figure</u> |   | <u>Page</u> |
|---------------|---|-------------|
| 18            | TRANSITION STRIP LOCATIONS<br>(LEDE RESEARCH FORCE MODEL)                               | 37          |
| 19            | STABILITY AXES SIGN CONVENTION  | 40          |
| 20            | WING STRAIN GAGE LOCATIONS  | 42          |
| 21            | LEDE MODEL IN PWT 16T   | 44          |
| 22            | TIE-IN COMPARISON BETWEEN CAL AND PWT 4T  | 51          |
| 23            | LEDE, CLEAN WING COMPARISON BETWEEN<br>PWT 4T and 16T                                   | 58          |
| 24            | LEDE, MID AILERONS, COMPARISONS BETWEEN<br>PWT 4T AND 16T,                              | 69          |
| 25            | LEDE, DIFFERENTIAL L.E. FLAP AND MID<br>AILERONS COMPARISON BETWEEN PWT 4T and 16T      | 72          |
| 26            | LEDE, DIFFERENTIAL L.E. FLAP AND EXTENDED<br>AILERONS COMPARISON BETWEEN PWT 4T and 16T | 73          |
| 27            | REYNOLDS NUMBER EFFECT ON LEDE CLEAN WING<br>PWT 4T                                     | 76          |
| 28            | REYNOLDS NUMBER EFFECT ON LEDE CLEAN WING<br>PWT 16T                                    | 82          |
| 29            | REYNOLDS NUMBER EFFECT ON MID AILERONS  | 91          |
| 30            | COMPARISON OF LIFT/DRAG RATIOS  | 95          |
| 31            | COMPARISON OF BUFFET ONSET  | 96          |
| 32            | MACH NUMBER EFFECTS ON LEDE CLEAN WING  | 97          |
| 33            | LEDE CONFIGURATION BUFFET CHARACTERISTICS<br>WING-ROOT-BENDING MOMENT                   | 101         |



| <u>Figure</u> |   | <u>Page</u> |
|---------------|---|-------------|
| 34            | LEDE CONFIGURATION BUFFET CHARACTERISTICS,<br>AXIAL FORCE COEFFICIENT             | 102         |
| 35            | LIFT CURVE PARAMETERS, LEDE CLEAN WING<br>HORIZONTAL TAIL ON                      | 103         |
| 36            | COMPARISON OF $C_{D\text{MIN}}$ VARIATION WITH<br>MACH NUMBER, HORIZONTAL TAIL ON | 105         |
| 37            | SQUARE ROOT PLOT FOR DRAG-DUE-TO-LIFT<br>ANALYSIS OF CAMBERED CONFIGURATIONS      | 106         |
| 38            | DRAG-DUE-TO-LIFT PARAMETERS, LEDE CLEAN<br>WING HORIZONTAL TAIL ON                | 108         |
| 39            | AERODYNAMIC CENTER  | 109         |
| 40            | FLOW VISUALIZATION LEADING EDGE EFFECTS   | 111         |
| 41            | SKETCH OF FLOW PATTERNS FOR DIFFERENTIAL<br>LEADING EDGE DEFLECTION               | 112         |
| 42            | SYMMETRIC LEADING EDGE FLAP EFFECTS, H.T.<br>ON                                   | 118         |
| 43            | SYMMETRIC LEADING EDGE FLAP EFFECTS, H.T.<br>OFF                                  | 119         |
| 44            | EFFECT OF LEADING EDGE FLAP DEFLECTION<br>ON CRITICAL LIFT COEFFICIENT            | 120         |
| 45            | EFFECT OF LEADING EDGE FLAP DEFLECTION ON<br>DRAG-DUE-TO-LIFT FACTOR              | 121         |
| 46            | EFFECT OF LEADING EDGE FLAP DEFLECTION ON<br>LIFT COEFFICIENT FOR MINIMUM DRAG    | 122         |
| 47            | EFFECT OF LEADING EDGE FLAP DEFLECTION<br>ON MINIMUM DRAG COEFFICIENT             | 123         |
| 48            | SYMMETRIC LEADING EDGE FLAP EFFECTS, H.T.<br>ON                                   | 125         |

| <u>Figure</u> |  | <u>Page</u> |
|---------------|--|-------------|
| 49            | SYMMETRIC LEADING EDGE FLAP EFFECTS, H.T. OFF  | 126         |
| 50            | VARIATION OF LEADING EDGE FLAP INCREMENTS WITH MACH NUMBER, HORIZONTAL TAIL ON                   | 127         |
| 51            | VARIATION OF LEADING EDGE FLAP INCREMENTS WITH MACH NUMBER, HORIZONTAL TAIL OFF                  | 128         |
| 52            | COMPARISON OF PREDICTED AND MEASURED LIFT CURVES   | 130         |
| 53            | COMPARISON OF PREDICTED AND MEASURED DRAG POLARS   | 132         |
| 54            | COMPARISON OF PREDICTED AND MEASURED LIFT-CURVE PARAMETERS                                       | 134         |
| 55            | COMPARISON OF PREDICTED AND MEASURED MODEL MINIMUM DRAG LEVELS                                   | 136         |
| 56            | COMPARISON OF PREDICTED AND MEASURED MINIMUM DRAG INCREMENTS DUE TO LEADING EDGE FLAP DEFLECTION | 137         |
| 57            | EFFECT OF ALTERNATE LEADING EDGE, $\delta_{LE}=0^{\circ}$  | 138         |
| 58            | EFFECT OF ALTERNATE LEADING EDGE, $\delta_{LE}=10^{\circ}$                                       | 139         |
| 59            | EFFECT OF VORTEX GENERATORS  | 142         |
| 60            | VARIATIONS OF DROOPED TRAILING EDGE FLAP INCREMENTS WITH MACH NUMBER                             | 143         |
| 61            | EFFECT OF DROOPED TRAILING EDGE ON DRAG-DUE-TO-LIFT PARAMETERS                                   | 145         |
| 62            | VARIATION OF SPLIT FLAP INCREMENTAL EFFECTS  | 146         |
| 63            | DIFFERENTIAL L.E. FLAP EFFECTS   | 148         |
| 64            | COMPARISON OF LEADING EDGE FLAP EFFECTS HORIZONTAL TAIL ON                                       | 152         |

| <u>Figure</u> |   | <u>Page</u> |
|---------------|---|-------------|
| 65            | AILERON SPANWISE POSITION EFFECTS<br>HORIZONTAL TAIL OFF                    | 155         |
| 66            | AILERON SPANWISE POSITION EFFECTS<br>HORIZONTAL TAIL ON                     | 156         |
| 67            | AILERON EFFECTIVENESS LOW ANGLES OF ATTACK                                  | 158         |
| 68            | FLOW VISUALIZATION MID AILERON 20/-20                                       | 161         |
| 69            | SKETCH OF FLOW PATTERNS FOR DEFLECTED MID-<br>AILERONS                      | 162         |
| 70            | HORIZONTAL TAIL INTERFERENCE, SMALL<br>AILERON DEFLECTION                   | 168         |
| 71            | HORIZONTAL TAIL INTERFERENCE, LARGE<br>AILERON DEFLECTION                   | 171         |
| 72            | SYMMETRICAL L.E. EFFECTS ON MID AILERONS                                    | 173         |
| 73            | LINEARITY OF AILERON WITH DEFLECTION  | 174         |
| 74            | LINEARITY WITH DEFLECTION MID SPAN AILERON -<br>HORIZONTAL TAIL ON          | 176         |
| 75            | LINEARITY WITH DEFLECTION MID SPAN AILERON -<br>HORIZONTAL TAIL OFF         | 179         |
| 76            | COMPARISON OF UP DEFLECTED AND DOWN DEFLECTED<br>SURFACES, MID SPAN AILERON | 180         |
| 77            | COMPARISON OF UP DEFLECTED MID-AILERON AND<br>SPOILER, CLEAN LEADING EDGE   | 182         |
| 78            | FLOW VISUALIZATION OF SPOILER   | 184         |
| 79            | DIFFERENTIAL L.E. FLAP WITH MID SPAN AILERONS                               | 186         |
| 80            | COMBINED LEADING AND TRAILING EDGE ROLL<br>CONTROL                          | 188         |
| 81            | DIFFERENTIAL L.E. FLAP WITH EXTENDED SPAN<br>AILERONS                       | 192         |

| <u>Figure</u> |  | <u>Page.</u> |
|---------------|--|--------------|
| 82            | VENTED SPOILER EFFECTS   | 195          |
| 83            | SPOILER ROLLING MOMENT   | 197          |
| 84            | DIFFERENTIAL HORIZONTAL TAIL EFFECTS   | 198          |
| 85            | VORTEX GENERATOR EFFECTS ON EXTENDED SPAN<br>AILERONS                        | 201          |
| 86            | TRAILING EDGE DROOP EFFECTS ON MID AILERONS                                  | 202          |
| 87            | FLOW VISUALIZATION OF SPLIT FLAP EFFECTS                                     | 205          |
| 88            | SPLIT TRAILING EDGE FLAP EFFECTS ON MID<br>AILERONS                          | 206          |
| 89            | COORDINATION CHARACTERISTICS MID-SPAN<br>AND OUTBOARD AILERONS               | 208          |
| 90            | COORDINATION CHARACTERISTICS EXTENDED<br>SPAN AILERONS                       | 210          |
| 91            | COORDINATION CHARACTERISTICS MID AILERON<br>AND DIFFERENTIAL HORIZONTAL TAIL | 213          |
| 92            | EFFECTS OF CONTROL MOMENT RATIO ON COORDINATION                              | 216          |
| 93            | TYPICAL COORDINATION BOUNDARIES MID AILERON                                  | 217          |
| 94            | BATTLE CONDITIONS  | 227          |
| 95            | PLAN VIEWS OF BATTLE TYPES   | 230          |
| 96            | AVERAGE POINTING ANGLE   | 231          |
| 97            | AIM SCORE  | 232          |
| 98            | AVERAGE BATTLE SCORE   | 233          |
| 99            | REACQUISITION TIME ANALYSIS  | 234          |
| 100           | GENERALIZED ROLL PERFORMANCE   | 241          |
| 101           | GENERALIZED PERFORMANCE FOR ROLL AND STOP<br>MANEUVER                        | 243          |

| <u>Figure</u> |   | <u>Page</u> |
|---------------|---|-------------|
| 102           | SUMMARY OF ROLL HANDLING QUALITIES CRITERIA   | 244         |
| 103           | GENERALIZED LATERAL COORDINATION EFFECTS  | 247         |
| 104           | EFFECTS OF CONTROL MOMENT RATIO ON<br>COORDINATION                                      | 249         |
| 105           | TIE-IN COMPARISON BETWEEN CAL AND PWT 4T  | 252         |
| 106           | LEDE, CLEAN WING COMPARISON BETWEEN PWT 4T<br>AND 16T                                   | 259         |
| 107           | LEDE, MID AILERONS, COMPARISONS BETWEEN PWT<br>4T AND 16T                               | 272         |
| 108           | LEDE, DIFFERENTIAL L.E. FLAP AND MID AILERONS<br>COMPARISON BETWEEN PWT 4T AND 16T      | 275         |
| 109           | LEDE, DIFFERENTIAL L.E. FLAP AND EXTENDED<br>AILERONS COMPARISON BETWEEN PWT 4T and 16T | 276         |
| 110           | MACH NUMBER EFFECTS ON LEDE CLEAN WING  | 278         |
| 111           | SYMMETRIC LEADING EDGE FLAP EFFECTS, H.T. OFF   | 282         |
| 112           | SYMMETRIC LEADING EDGE FLAP EFFECTS, H.T. ON  | 298         |
| 113           | EFFECT OF ALTERNATE LEADING EDGE  | 315         |
| 114           | EFFECT OF VORTEX GENERATORS   | 348         |
| 115           | EFFECT OF DROOPED TRAILING EDGE   | 365         |
| 116           | EFFECT OF SPLIT TRAILING EDGE FLAPS   | 382         |
| 117           | DIFFERENTIAL L.E. FLAP EFFECTS  | 399         |
| 118           | AILERON SPANWISE POSITION EFFECTS, HORIZONTAL<br>TAIL OFF                               | 412         |
| 119           | AILERON SPANWISE POSITION EFFECTS, HORIZONTAL<br>TAIL ON                                | 414         |
| 120           | HORIZONTAL TAIL INTEFERENCE, SMALL AILERON<br>DEFLECTION                                | 424         |

| <u>Figure</u> |  | <u>Page</u> |
|---------------|--|-------------|
| 121           | HORIZONTAL TAIL INTERFERENCE, LARGE AILERON DEFLECTION     | 436         |
| 122           | REYNOLDS NUMBER EFFECT ON MID AILERONS                     | 448         |
| 123           | SYMMETRICAL L.E. EFFECTS ON MID AILERONS                   | 450         |
| 124           | EFFECTS OF LEADING EDGE SECTION GEOMETRY WITH MID AILERONS | 452         |
| 125           | LINEARITY OF AILERON WITH DEFLECTION                       | 453         |
| 126           | LINEARITY OF AILERON WITH DEFLECTION (H.T. OFF)            | 461         |
| 127           | DIFFERENTIAL L.E. FLAP WITH MID SPAN AILERONS              | 477         |
| 128           | DIFFERENTIAL L.E. FLAP WITH EXTENDED SPAN AILERONS         | 487         |
| 129           | VENTED SPOILER EFFECTS                                     | 522         |
| 130           | DIFFERENTIAL HORIZONTAL TAIL EFFECTS (CLEAN L.E.)          | 534         |
| 131           | VORTEX GENERATOR EFFECTS ON EXTENDED SPAN AILERONS         | 539         |
| 132           | TRAILING EDGE DROOP EFFECTS ON MID AILERONS                | 540         |
| 133           | SPLIT TRAILING EDGE FLAP EFFECTS ON MID AILERON            | 548         |
| 134           | KRUGER LEADING EDGE GLOVE FLAP EFFECTS                     | 549         |
| 135           | CANOPY FAIRING EFFECTS ON MID AILERONS                     | 550         |
| 136           | EFFECT OF CANOPY FAIRING                                   | 551         |

## LIST OF TABLES

| <u>Table</u> | <u>Page</u> |
|--------------|-------------|
| I            | 8           |
| II           | 45          |
| III          | 48          |
| IV           | 50          |
| V            | 405         |
| VI           | 463         |
| VII          | 464         |
| VIII         | 469         |
| IX           | 472         |
| X            | 474         |
| XI           | 499         |
| XII          | 508         |
| XIII         | 513         |

## LIST OF SYMBOLS AND ABBREVIATIONS

### Symbols

|                 |   |
|-----------------|---|
| b               | wing span   |
| c               | chord   |
| $\bar{c}$       | wing mean geometric chord   |
| $C_D$           | drag coefficient, Drag/q $S_{ref}$  |
| $C_{Dmin}$      | minimum value of drag coefficient at particular Mach number                                   |
| $C_l$           | rolling moment coefficient, rolling moment/q $S_{ref}b$                                       |
| $C_{lP}$        | damping due to roll rate coefficient, $\frac{\partial C_l}{\partial \dot{\phi}} \frac{b}{2V}$ |
| $C_{l\delta_a}$ | aileron effectiveness coefficient, $\frac{\partial C_l}{\partial \delta_a}$                   |
| $C_L$           | lift coefficient, lift/q $S_{ref}$  |
| $C_{L\alpha}$   | lift curve slope, $\frac{\partial C_L}{\partial \alpha}$                                      |
| $C_{LC}$        | lift coefficient at which drag polar becomes non-parabolic, see Figure 39, pg 105             |
| $C_{LC_{Dmin}}$ | lift coefficient for minimum drag coefficient   |
| $C_m$           | pitching moment coefficient, pitching moment/q $S_{ref}\bar{c}$                               |
| $C_n$           | yawing moment coefficient, yawing moment/q $S_{ref}b$   |
| g               | acceleration due to gravity   |
| GW              | gross weight  |
| $I_x$           | moment of inertia about longitudinal stability axis   |



## LIST OF SYMBOLS AND ABBREVIATIONS (CONT'D)

|             |  |
|-------------|--|
| $I_z$       | moment of inertia about z stability axis   |
| $I_{xz}$    | cross product of inertia   |
| K           | drag due to lift factor defined by equation (1) pg 103   |
| L           | fuselage length  |
| $L\delta_a$ | roll acceleration per unit lateral control input   |
| L/D         | lift to drag ratio   |
| M           | Mach number  |
| $P_{ss}$    | steady state roll rate   |
| q           | dynamic pressure   |
| $R_n$       | Reynolds number  |
| $R_I$       | inertia ratio, $I_x/I_z$   |
| $R_\beta$   | stability ratio, directional stability/effective dihedral, $C_{n\beta}/C_{l\beta}$                                 |
| $R_\delta$  | control moment ratio, $\left[ \frac{\Delta C_n}{\Delta C_l} \right]$ roll control or $C_{n\delta_a}/C_{l\delta_a}$ |
| $S_f$       | planform area of flap segment  |
| $S_{ref}$   | reference area, area of wing planform excluding the highly swept inboard glove                                     |
| $S_w$       | reference wing area  |
| s           | Laplace operator   |
| t           | local thickness of wing section  |

LIST OF SYMBOLS AND ABBREVIATIONS (CONT'D)

|               |  |
|---------------|--|
| $t$           | time   |
| $v$           | velocity   |
| $\bar{y}$     | lateral distance to centroid of flap segment planform  |
| $\alpha$      | wing angle of attack   |
| $\alpha_{LO}$ | angle of attack for zero lift  |
| $\beta$       | aircraft point angle, see Figure 94, page 213  |
| $\delta$      | deflection, positive leading edge down (leading edge devices), or trailing edge down (trailing edge devices) |
| $\delta_a$    | average aileron deflection, $1/2 (\delta_{right} - \delta_{left})$   |
| $\zeta_\phi$  | damping ratio of numerator quadratic in $\phi/\delta_a$ transfer function                                    |
| $\zeta_d$     | damping ratio of dutch roll mode   |
| $\phi$        | roll angle   |
| $\Lambda$     | sweep angle  |
| $T_R$         | time constant of the rolling convergence mode  |
| $T_s$         | time constant of the spiral mode   |
| $T_1$         | time to obtain maximum control input, see Appendix I   |
| $\omega_\phi$ | natural frequency of numerator quadratic in $\phi/\delta_a$ transfer function                                |
| $\omega_d$    | natural frequency of the dutch roll mode   |

## LIST OF SYMBOLS AND ABBREVIATIONS (CONT'D)

### Subscripts

|          |  |
|----------|--|
| aero     | aerodynamic contribution   |
| eff      | effective value of coefficient including approximation of control system effects |
| FCS gain | control system feedback gain   |
| o        | initial condition  |
| pa       | principal axis value   |

### Abbreviations

|      |  |
|------|--|
| AEDC | Arnold Engineering Development Center                    |
| CAL  | Cornell Aeronautical Laboratory                          |
| FDCC | Control Criteria Branch of AF Flight Dynamics Laboratory |
| F.S. | Fuselage Station   |
| H.T. | Horizontal Tail  |
| L.E. | Leading Edge   |
| LEDE | Leading Edge Device Effectiveness                        |
| L/R  | Left/Right Surface Deflection in Degrees                 |
| M.S. | Model Scale  |
| NACA | National Advisory Committee for Aeronautics              |
| NASA | National Aeronautics and Space Administration            |
| PWT  | Propulsion Wind Tunnel                                   |
| RMS  | root-mean-square   |
| VG   | Vortex Generators  |

## SECTION I

### INTRODUCTION

Maneuvering of aircraft in the transonic speed regime is an item currently receiving critical attention. The high maneuvering load factors necessary for combat at these speeds require flight at high lift coefficients ( $C_L > 1.0$ ) and corresponding high angles of attack. At these extreme conditions, shock-induced separation of the boundary layer occurs on the wing and results in buffet, severe drag increases, losses in lift and control effectiveness. Present aircraft operating at transonic speeds and high lift coefficients encounter serious stability and control problems, including loss of roll control power. Adverse yaw can also be a severe problem, one example being the use of stabilators for both roll control and longitudinal trim.

The control criteria branch (FDCC) of the AF Flight Dynamics Laboratory recognized the need for research on effective wing-mounted roll control devices. To fill this need, they initiated a program to assess the effectiveness of various types of devices used both singly and in combinations where phasing may be a function of angle of attack or other measurable physical parameter or parameters.

#### 1. OBJECTIVE

The long term objective of this program is research into wing-mounted roll control devices on both fixed wing and variable-sweep configurations for transonic high-lift conditions. The initial study reported herein is limited to devices suitable for fixed-wing configurations. The second phase of the study, devoted to control devices for variable-sweep configurations, will be covered by a separate report at a later date.

#### 2. SCOPE

The basic concern of the investigation is the improvement of control effectiveness at high lift transonic conditions. However, since the control device is an integral part of the complete wing-body configuration, the study included selection of a configuration representative of current thinking for advanced fighter applications. The inadequacy of theoretical analysis in the transonic speed range required that primary emphasis be

placed on experimental results of scaled wind tunnel tests. Since adequate roll control is highly dependent upon good wing design, detailed analysis of longitudinal characteristics is also presented for the selected configuration. Modification and use of existing wind tunnel model components was encouraged to minimize program costs.

### 3. TECHNICAL APPROACH

Available literature, including British publications, on the subject on wings and wing mounted control devices at transonic high lift conditions was reviewed for applicability to the specific program and general insight into particular tasks. Since analytical solutions for the complex configurations at the high lift coefficient transonic conditions, meaningful to this study, are not mathematically tractable at this time, primary emphasis was placed upon semi-empirical methods and available experimental results useful for configuration design and wind tunnel testing.

Two brief studies were accomplished to establish criteria for roll control power and control coordination characteristics. Air-to-air combat encounters were simulated on the General Dynamics Fort Worth Division ATAC digital program to assess the effects of roll performance on the tactical characteristics of advanced fighter configurations. The handling qualities aspects of roll performance were reviewed from the standpoint of pilot control capability and the interrelated effects of inertia, lateral-directional stability, and control coordination throughout the wide angle of attack range of interest.

Design of the wing body configuration was accomplished based on the criteria of eliminating or minimizing the strength of the shock patterns on the wing upper surface over a wide angle of attack range. This criteria minimizes shock induced boundary layer separation on the basic wing planform and hence enhances control effectiveness. Reliance was placed on applicable experimental data, general design guidelines, and semi-empirical techniques.

In selecting suitable wing mounted control devices, the Flight Dynamics Laboratory desired that primary emphasis be

placed on the use of leading edge devices for primary controls and also auxiliary devices to be used with conventional controls. This led to designating the study by the acronym LEDE (Leading Edge Device Effectiveness). However the study was more general than this title in that several other wing mounted controls and differential horizontal tail deflection were also investigated. These other devices consisted of flaperons at three spanwise locations and a vented spoiler for primary control, split trailing edge flaps, vortex generators, and a Kruger leading edge flap on the glove for auxiliary devices.

Two items received special attention in the specification of wind tunnel test techniques. In the past, wind tunnel measurements have experienced problems in the simulation of boundary-layer shock-wave interaction due to Reynolds number mismatch and in the tunnel wall interference effects at transonic speeds. Simulation of the boundary-layer shock-wave interaction was investigated by testing over a wide Reynolds number range. The majority of the wind tunnel testing was accomplished in the AEDC PWT four foot by four foot test section with a 22.5 inch span model. Wind tunnel wall interference effects were evaluated in a brief validation test using the AEDC PWT sixteen foot by sixteen foot transonic facility.

Six component force and moment measurements were obtained to afford the best possible understanding of the degradations in control effectiveness at high angles of attack and the origins of control yawing moments as well as to record the basic longitudinal and control effectiveness characteristics of the LEDE configurations. Numerous flow visualization runs were accomplished using a mixture of oil and titanium oxide pigment prepared by AEDC personnel. In addition, buffet characteristics were obtained for several configurations through wing root bending measurements.

#### 4. REPORT ORGANIZATION

A detailed description of the LEDE configuration is presented in Section II together with the information and criteria employed to establish the selected design. The various techniques

employed in the wind tunnel testing are reviewed in Section III. The detailed wind tunnel programs, denoting the configurations and conditions tested, are also presented in this section.

The discussion of tests results is provided in Sections IV through VII covering comparisons between data from various wind tunnels, simulation of full scale characteristics, symmetrical configuration effects, and data for the various roll controls. In the interest of brevity, only representative data plots as necessary to illustrate the key points are included in these sections. Extensive presentation of these data is given in Appendices III, IV and V. Concluding remarks on symmetrical configuration items, roll-control devices, and specific wind tunnel test techniques are provided in Section VIII.

Several other items only generally related to the main objective of the study are included as appendices. A brief study of roll performance effects on tactical suitability in air-to-air combat is summarized in Appendix I. Background information used to select the control power criteria for sizing the various wing mounted roll controls is documented in Appendix II. And, in the interest of completeness, a tabulation of all force and moment measurements obtained from wind tunnel tests is provided in Appendix VI.

## SECTION II

### CONFIGURATION SELECTION

The configuration selection task was guided by three basic ground rules:

- 1) The configuration should be representative of the current thinking with respect to high performance fighter aircraft design;
- 2) Primary emphasis should be placed on stability and control characteristics rather than performance;
- 3) Existing model components should be used where feasible to reduce fabrication costs.

Within this framework of guidelines the project team had a high degree of freedom in selecting the test configuration. The final configuration chosen represents a compromise among application of advanced wing design concepts, constraint of wing area imposed by model loads and consideration of the overall fighter-aircraft design problem. In particular, consideration was given to roll-control devices compatible with the high-lift system for low-speed conditions. This led to the emphasis upon plain leading- and trailing-edge devices which might be used for a simple high lift system at low speeds as well as roll control over a wide speed range.

#### 1. GENERAL ARRANGEMENT

The general arrangement of the test configuration is shown in Figure 1 . Several details of the model are illustrated in the model photograph of Figure 2 . A complete set of geometric data for the LEDE configuration, including all manufacturing drawings, is given in Reference 1 . For convenience to the reader, key geometric data are presented in Table I in both model scale and full scale dimensions. Unless specifically noted, the full scale values are used for discussions in this report.



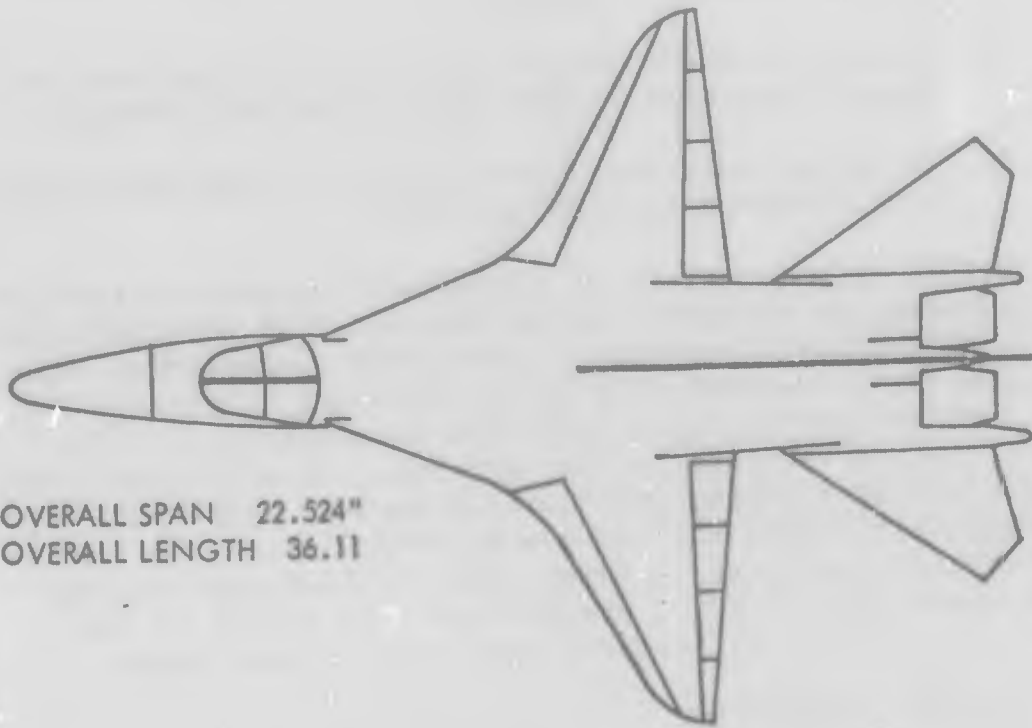


Figure 1 RESEARCH MODEL GENERAL ARRANGEMENT  
(ROLL CONTROL L.E.D.E. FORCE MODEL PROGRAM)



Figure 2 LEDE MODEL Note R.H. Leading Edge Deflected Down  $10^{\circ}$   
and Differential Aileron Setting

TABLE I GEOMETRIC CHARACTERISTICS

| ITEM   | SYMBOL  | FULL SCALE VALUE                | MODEL SCALE VALUE               |
|--|---|---------------------------------|---------------------------------|
| WING AREA  | $S_{ref}$   | 498.31 FT <sup>2</sup>          | .86512 FT <sup>2</sup>          |
| ASPECT RATIO   | $AR_{basic}$                                      | 4.07                            | 4.07                            |
| ROOT CHORD (AT $\xi$ )   | $C_r$   | 231.14 IN                       | 9.631 IN                        |
| TIP CHORD (OF BASIC TRAPEZOIDAL WING)  | $C_{ttrap}$<br>(Lateral Pos)                      | 69.34 IN<br>SS224.24            | 2.889 IN<br>SS9.343             |
| WING SPAN  | $b_{ref}$   | 540.57 IN                       | 22.524 IN                       |
| MEAN AERODYNAMIC CHORD   | MAC   | 157.98 IN                       | 6.583 IN                        |
| LOCATION OF MAC<br>LONGITUDINAL(L.E.)<br>LATERAL                                   | $\bar{X}$<br>$\bar{Y}$                            | F.S. 450.03<br>S.S. 101.22      | F.S. 18.751<br>S.S. 4.218       |
| MOMENT<br>CENTER - 25% MAC   | c.g.ref   | F.S. 522.97                     | F.S. 20.397                     |
| BASIC TRAPEZOIDAL WING<br>LEADING EDGE SWEEP<br>TRAILING EDGE SWEEP<br>TAPER RATIO | $\Lambda_{LEw}$<br>$\Lambda_{TEw}$<br>$\lambda_T$ | 31.50 deg<br>-6.207 deg<br>.300 | 31.50 deg<br>-6.207 deg<br>.300 |
| GLOVE<br>LEADING EDGE SWEEP  | $\Lambda_{LEG}$                                   | 70.0 deg                        | 70.0 deg                        |
| OVERALL LENGTH   |   | 866.64 IN                       | 36.11 IN                        |
| F.S. OF NOSE   |   | F.S. 22.01                      | F.S. 0.917                      |
| COMPOSITE WING-GLOVE<br>PLANFORM   | $S_{composite}$<br>$AR_{composite}$               | 618.72 FT <sup>2</sup><br>3.28  | 1.0741 FT <sup>2</sup><br>3.28  |

NOTE: Airfoil section coordinates are given in Figure 5, page 15.

Study of various possible wing-body arrangements for the LEDE program led to the conclusion that existing 1/24-scale model components could be employed for the fuselage-inlet and empennage. These components were previously fabricated and used in the F-111 program; however, several minor geometric differences exist between these parts and the selected F-111 configuration. The wing planform, which resembles an ogee type, was actually derived from a low-aspect-ratio tapered planform that was mated to the existing "glove" planform. The curved wing tip and curved leading edge in the region of the glove-wing intersection are modifications selected to improve performance and stability and control characteristics at transonic speeds.

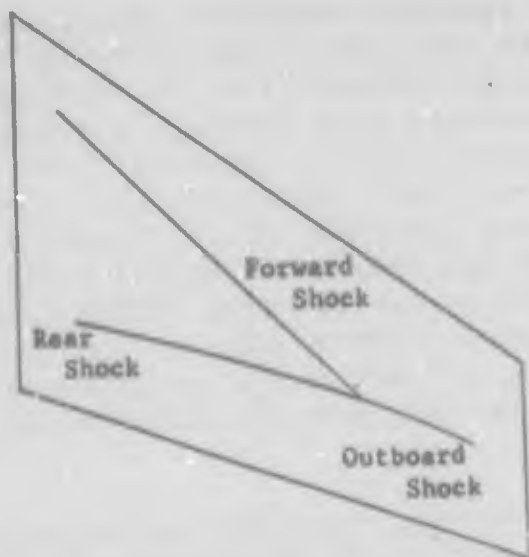
The cross-sectional area distribution resulting from addition of the fixed wing to the basic F-111 fuselage-inlet package exhibits rather severe slopes both ahead of and behind the maximum area. Fairings were added to the canopy, the nacelles and the aft upper fuselage to obtain a "good" Mach one area distribution.

The rationale behind the design approach and the background details are discussed in the following subsections.

#### a. Wing Planform

The basic goal of the wing planform selection was to provide an aerodynamic surface free from adverse effects of shock-induced boundary layer separation insofar as possible. Control problems associated with maneuvering in the high-lift transonic speed regime are caused primarily by such shock-induced separations. The shock wave patterns which produce adverse separation are essentially caused by inadequacies in the basic wing-body geometries of currently operational aircraft.

The complexity of the problem is illustrated in Figure 3, which presents a typical transonic shock pattern on a moderately swept wing and a qualitative sketch of the flow separation boundaries for such a wing as a function of lift coefficient and Mach number. A reader familiar with the problem will recognize these illustrations which were presented in the open



TYPICAL TRANSONIC FLOW CONDITION

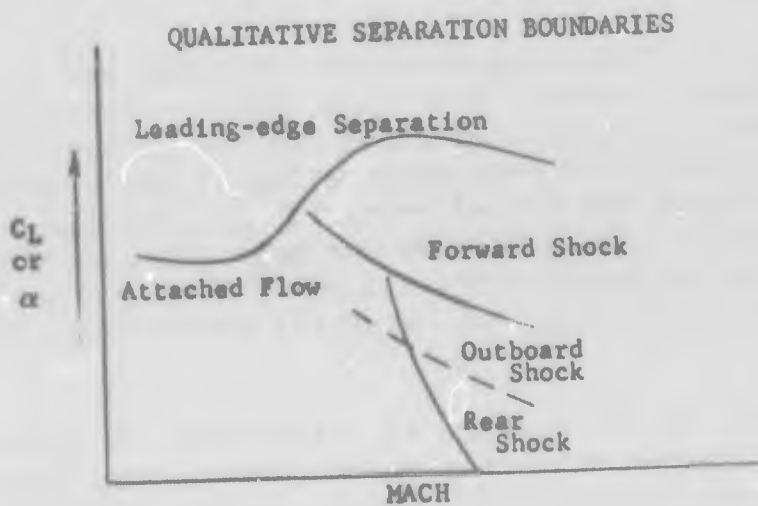
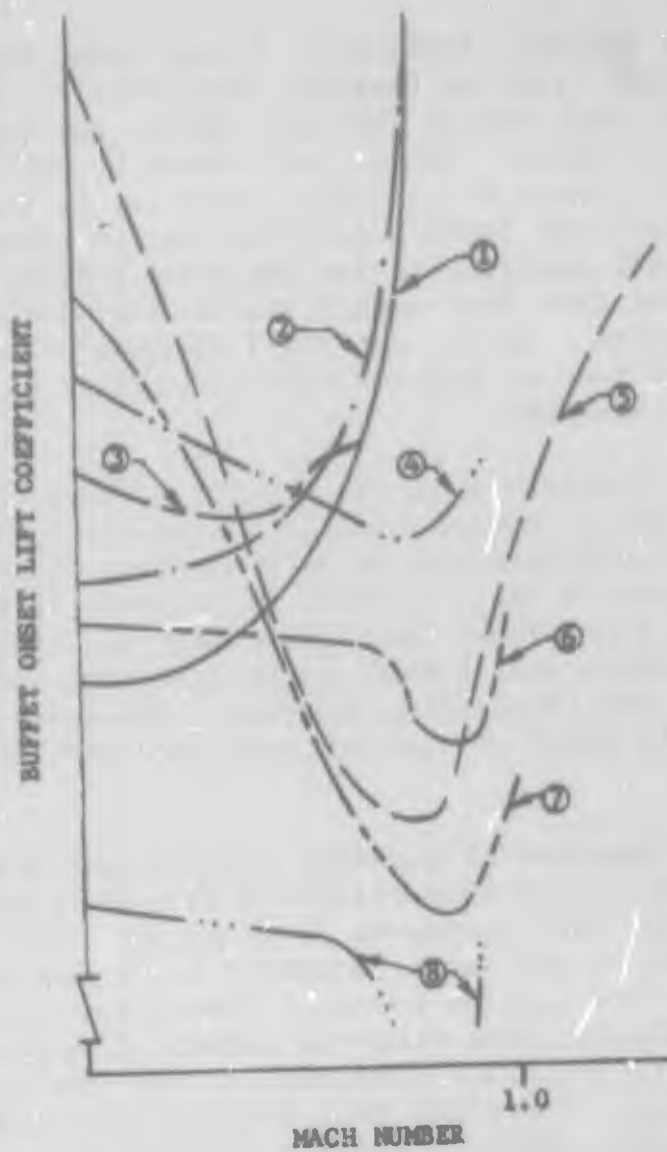


Figure 3 TYPICAL THREE-DIMENSIONAL SHOCK PATTERN AND QUALITATIVE SEPARATION BOUNDARIES

literature by Rogers and Hall (Reference 2) and later appeared in the excellent survey paper by Pearcey, Reference 3. Adverse flow separations can occur aft of the rear shock, the forward shock, or the outboard shock. The pattern shown is only typical and of course is altered by planform geometry, airfoil section, and wing twist and camber distributions in addition to Mach number and lift coefficient (or angle of attack). Pearcey points out the fact that severe separation usually occurs aft of the outboard shock, but the formation of an outboard shock can be delayed to higher angles of attack by judicious choice of planforms.

One of the best indicators of the effects of wing geometry on the formation of shock-induced separations is the variation of buffet onset lift coefficient with Mach number. Figure 4 presents buffet boundaries qualitatively for several different aircraft as obtained from flight data (Reference 4). The planforms associated with each buffet onset curve are indicated in the figure by the identifying numbers. The geometric characteristics of the wings of each aircraft are tabulated on the figure.

The significant features of Figure 4 are (1) that a dip in the buffet boundary occurs when buffet is caused by shock-induced separation, (2) that increased leading edge sweep tends to delay the dip in the buffet boundary to higher Mach numbers, and (3) that the general trend of the buffet boundaries for thin wings (especially those with low values of leading and trailing edge sweep) is different from that of the thicker and more highly swept wings. There are four factors that contribute to this behavior. First, the thin airfoils do not perturb the flow as severely as do thicker airfoils; therefore, the strength of the shock waves which do form is lower. Second, the pressure gradients due to airfoil shape are lower over the aft portion of the airfoil, therefore, less tendency towards trailing edge flow separation exists even if shock waves do form on the wing. Third, low values of leading edge sweep tend to delay the onset of leading edge flow separation for a given streamwise and airfoil thickness ratio. Fourth, the interval of Mach numbers between initial formation of supersonic flow on the wing and supersonic flow reaching the trailing edge is smallest for low values of trailing edge sweep. The four factors combine to give a buffet boundary which is low at subcritical Mach numbers and then rises very rapidly with Mach number. The low buffet boundary at lower Mach numbers can be raised significantly by use of leading edge flaps.



| AIRCRAFT | ASPECT RATIO | LEADING EDGE SWEEP-Degree | TAPER RATIO | AIRFOIL THICKNESS RATIO |
|----------|--------------|---------------------------|-------------|-------------------------|
| 1        | 3.09         | 23.1                      | 0.39        | 0.045                   |
| 2        | 2.45         | 27.0                      | 0.38        | 0.034                   |
| 3        | 3.75         | 32.0                      | 0.20        | 0.048                   |
| 4        | 3.40         | 46.0                      | 0.25        | 0.060(Root),0.050(Tip)  |
| 5        | 3.86         | 49.5                      | 0.26        | 0.070                   |
| 6        | 2.20         | 60.0                      | -           | 0.055                   |
| 7        | 2.90         | 41.1                      | 0.23        | 0.080(Root),0.050(Tip)  |
| 8        | 2.31         | 60.0                      | 0           | 0.065                   |

Figure 4 QUALITATIVE BUFFET BOUNDARIES OF VARIOUS AIRCRAFT

One can infer from the previous discussions that a prime planform candidate for achieving improved transonic aerodynamic characteristics should be a derivative of a thin wing having low to moderate sweep. This avenue of approach was pursued. A thorough review of NACA, NASA, and British reports was undertaken to identify planform and airfoil section effects on shock patterns. In addition, a large amount of General Dynamics transonic wind tunnel test data on variable sweep and fixed wing high performance configurations was analyzed in terms of lift and drag characteristics. On the basis of this review, it was decided to mate a basically low aspect ratio trapezoidal wing of moderate leading edge sweep and taper ratio to the F-111 glove planform. The highly developed wing-body junction design of the F-111 would be preserved and thus reduce the probability of a forward shock originating from the wing-body juncture. However, it was recognized that the kink in leading edge sweep at the intersection of the glove and outer wing panel would be another possible source of a forward shock.

Previous General Dynamics work on the aerodynamic characteristics of non-straight-taper wings (Reference 5) provided the knowledge that the change in leading edge sweep at the intersection of the glove and outboard wing panel would cause high interference velocities and that the high velocities could be significantly reduced by using a curved leading edge to give a smooth transition of leading edge sweep. Investigation of British papers on transonic wing design (References 6, 7, and 8) indicated that further improvements might be obtained by using a parabolic leading edge shape at the tip. The curved tip tends to produce a nearly constant spanwise distribution of minimum pressure coefficient due to angle of attack in the tip region and thus reduces the possibility of formation of a tip shock.

The lift and drag analyses mentioned earlier indicated that a slightly higher aspect ratio than that provided by the basic trapezoidal planform would be desirable so the curved tip was added to the trapezoidal planform to increase the overall wing span.



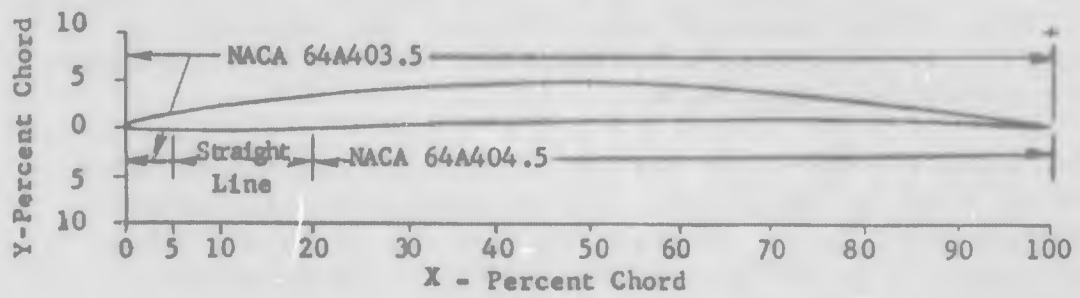
Originally the planform was designed to have a full scale wing area of approximately 600 square feet (not including the glove). Predictions of model loads at the desired test Reynolds numbers indicated that angle of attack would be too severely limited with such a large wing area. The final wing area used on the model represents a compromise made to obtain angles of attack considered useful for the investigation.

b. Wing Section

The primary airfoil section chosen for the LEDE configuration wing employs considerably more camber than those that have previously been used for fighter aircraft which have supersonic capability. The airfoil section is conventional in the sense that the surface ordinates are derived from NACA 64A series sections. It is unconventional in the sense that the surface ordinates are taken from two different values of thickness ratio. The basic airfoil geometry is shown in Figure 5. The surface ordinates from five percent chord on the lower surface forward, around the leading edge and on the upper surface back to the trailing edge are those for the NACA 64A403.5 section. From twenty percent chord on the lower surface aft to the trailing edge, the ordinates are those of the NACA 64A404.5 section. A straight line fairing between five percent chord and twenty percent chord joins the two ordinate distributions.

The airfoil selection was purely empirical and was made for the following reasons:

- 1) Detailed review of the literature indicated that the leading edge and upper surface geometry are the primary airfoil factors that set the upper surface flow field.
- 2) The analysis of available wind tunnel data previously mentioned indicated that a 64A403.5 section provided good aerodynamic characteristics at transonic high lift conditions.
- 3) The additional span due to the added curved wing tips predicated an increase in thickness ratio to four percent to improve structural characteristics.



COORDINATES - Percent Chord

| X/C   | (Y/C) <sub>U</sub> | (Y/C) <sub>L</sub> | X/C | (Y/C) <sub>U</sub> | (Y/C) <sub>L</sub> | X/C  | (Y/C) <sub>U</sub> | (Y/C) <sub>L</sub> |
|-------|--------------------|--------------------|-----|--------------------|--------------------|------|--------------------|--------------------|
| 0     | 0                  | 0                  | 25  | 3.7138             | +.0367             | 75   | 3.0977             | .9605              |
| .50   | .4133              | -.1551             | 30  | 3.9875             | .1253              | 80   | 2.6225             | .9075              |
| .75   | .5174              | -.1776             | 35  | 4.1852             | .2149              | 85   | 2.0113             | .7196              |
| 1.25  | .6895              | -.1848             | 40  | 4.3074             | .3077              | 90   | 1.3623             | .4953              |
| 2.50  | 1.0300             | -.1665             | 45  | 4.3461             | .4185              | 95   | .6853              | .2426              |
| 5.00  | 1.5485             | -.0900             | 50  | 4.3080             | .5394              | 100  | 0                  | 0                  |
| 7.50  | 1.9645             | -.0838             | 55  | 4.2014             | .6614              | LER  | .072               |                    |
| 10.00 | 2.3196             | -.0782             | 60  | 4.0263             | .7739              |      |                    |                    |
| 15.00 | 2.8994             | -.0665             | 65  | 3.7878             | .8687              | θLER | 12°40'             |                    |
| 20.00 | 3.3566             | -.0547             | 70  | 3.4798             | .9362              |      |                    |                    |

Figure 5 AIRFOIL SECTION OF BASIC TRAPEZOIDAL WING

The airfoil section in the tip region was developed by taking the first forty percent of the section at span station 224.24 (full scale) and placing it perpendicular to the leading edge at span stations 246.98 and 259.10. The remainder of the geometry was determined by smoothly fairing in both spanwise and chordwise directions.

The wing incidence is set at a negative one degree with respect to a waterline plane. The origin of the incidence is the line joining the intersection of the glove and wing leading edges at fuselage station 443.01. No geometric twist is used in the basic wing chord plane.

The glove upper surface lines from fuselage station 400.00 aft are refaired to provide a smooth transition to the trapezoidal outer wing panel. In the region of the glove-wing intersection additional leading edge droop is used to further reduce interference velocities over the curved leading edge.

#### c. Fuselage Modifications

The model fuselage is modified at the aft end to accommodate the sting mount. For the LEDE configuration the sting mount is larger in the vertical direction than those previously used; therefore, the lower fuselage lines are modified more between the ducts. A cover plate encloses the sting cavity.

The cross-sectional area distributions for the LEDE configuration are shown in Figure 6. The addition of the fixed wing caused a rather sharp peak in the area distribution and high values of slope both ahead of and aft of the peak. Fairings have been added in three regions to fill the slopes and improve the area distribution in the region of the wing-fuselage intersection. The fairings are indicated by the cross-hatched areas in Figure 7. An upper surface fairing which extends the canopy fairing from fuselage station 280 to fuselage station 496 has been added to the upper surface to fill the forward facing slopes. Fairings have been added to the nacelle sides and to the aft upper

- STING MODIFICATION INCLUDED
- INLET AREA = 2110 IN<sup>2</sup>

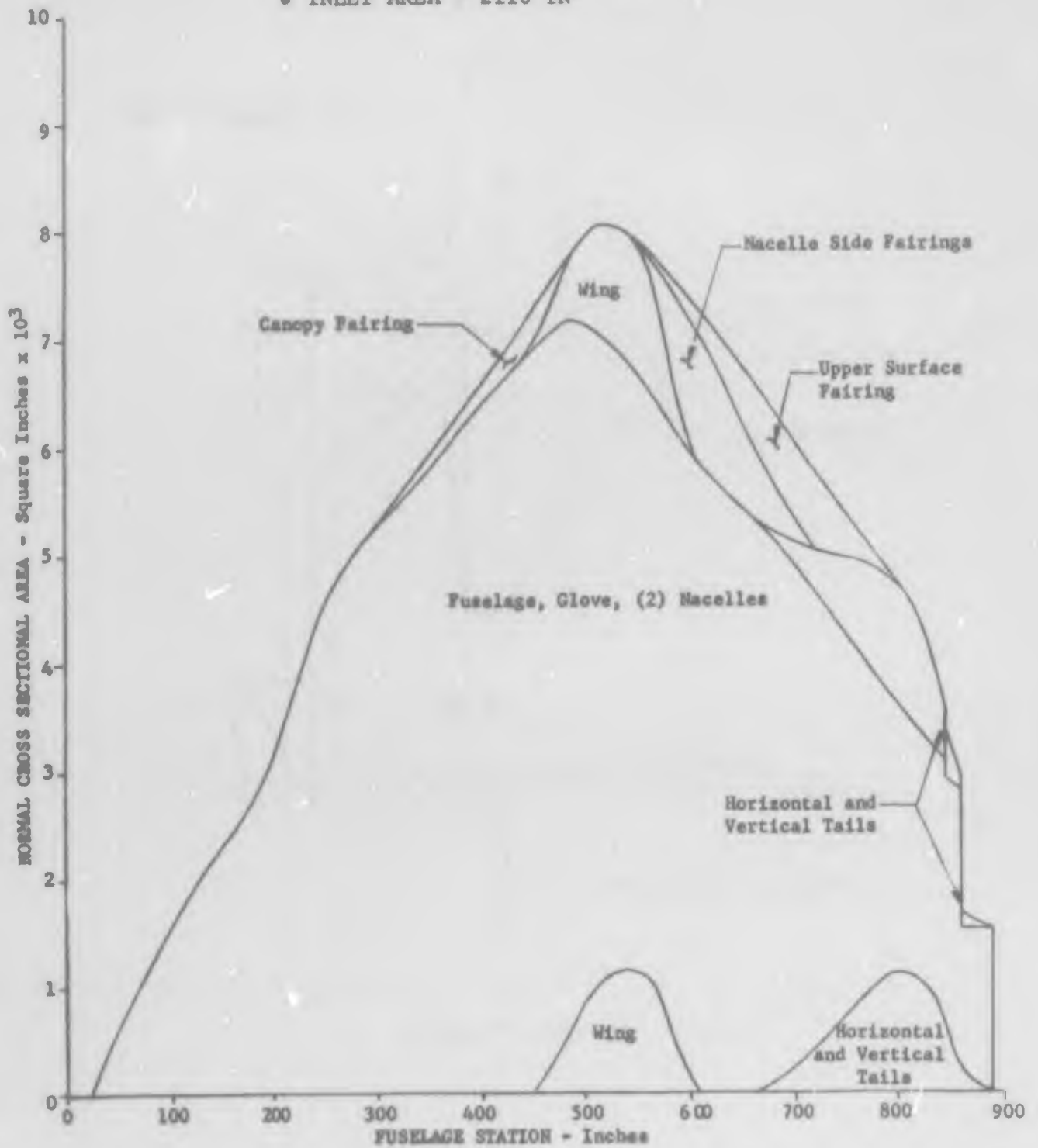


Figure 6 NORMAL CROSS SECTIONAL AREA WITH TAILS

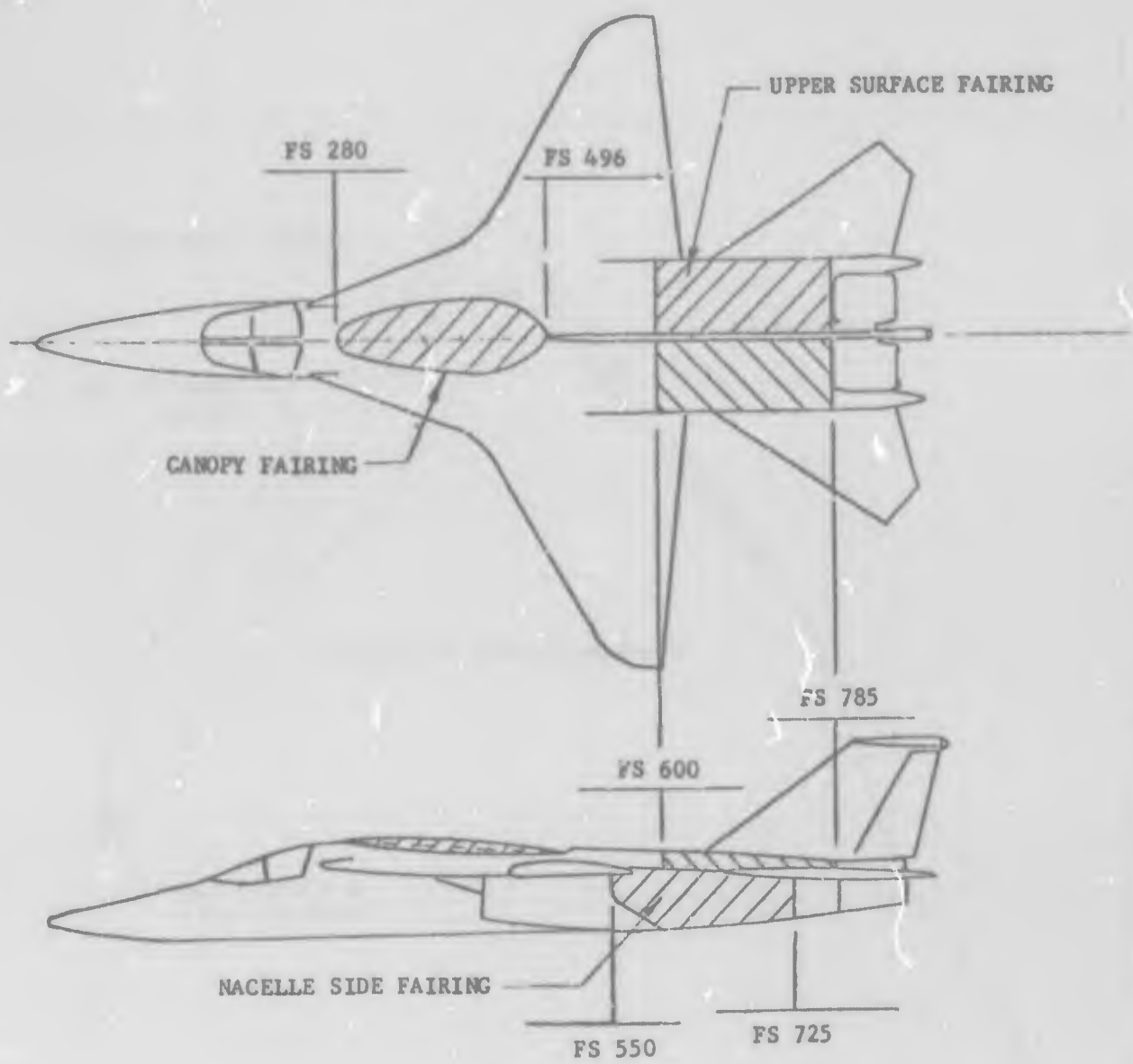


Figure 7 FUSELAGE FAIRINGS

fuselage to fill the aft facing slopes. The amount of area added by these fairings has been determined such that a smooth overall area distribution is obtained with or without the horizontal and vertical tail areas included in the test configuration area distribution.

## 2. LEADING EDGE FLAPS

Available wind tunnel data on the effects of leading edge droop or leading edge flaps were surveyed to assess flap planform effects. Most NACA and NASA data are for relatively small chord flaps having a chord length which is either a constant or a constant percent of wing chord. Recent General Dynamics wind tunnel tests have obtained data on leading edge flap planforms having chord lengths which vary with span but are not a constant percent wing chord.

Based on the results of the data survey, the leading edge flap planform shown in Figure 8 was selected for the LEDE configuration. The hinge line is defined at eighteen percent chord at the root and thirty percent chord at the tip of the basic trapezoidal planform. The inboard edge of the flap upper surface is defined by a line which passes through the intersection of the theoretical glove and trapezoidal wing leading edges and is oriented at 7.5 degrees to the aircraft centerline. The hinge line extends to intersect the curved tip. The mating surfaces of the flap and wing at the inboard edge are cut on a forty - five degree plane to the wing manufacturing chord plane.

Leading edge deflections of zero, five, ten and fifteen degrees are provided for both left and right leading edge flaps. The deflections are obtained by using brackets fabricated for each angle, thus the leading edge airfoil geometry which is critical in setting the upper surface flow field is identical for each deflection.

A set of alternate leading edge flaps was designed to investigate the effects of a "peaky" airfoil. The airfoil geometry is modified as shown in Figure 9. Guidelines for design of the modifications were obtained from References 9, 10 and 11. The

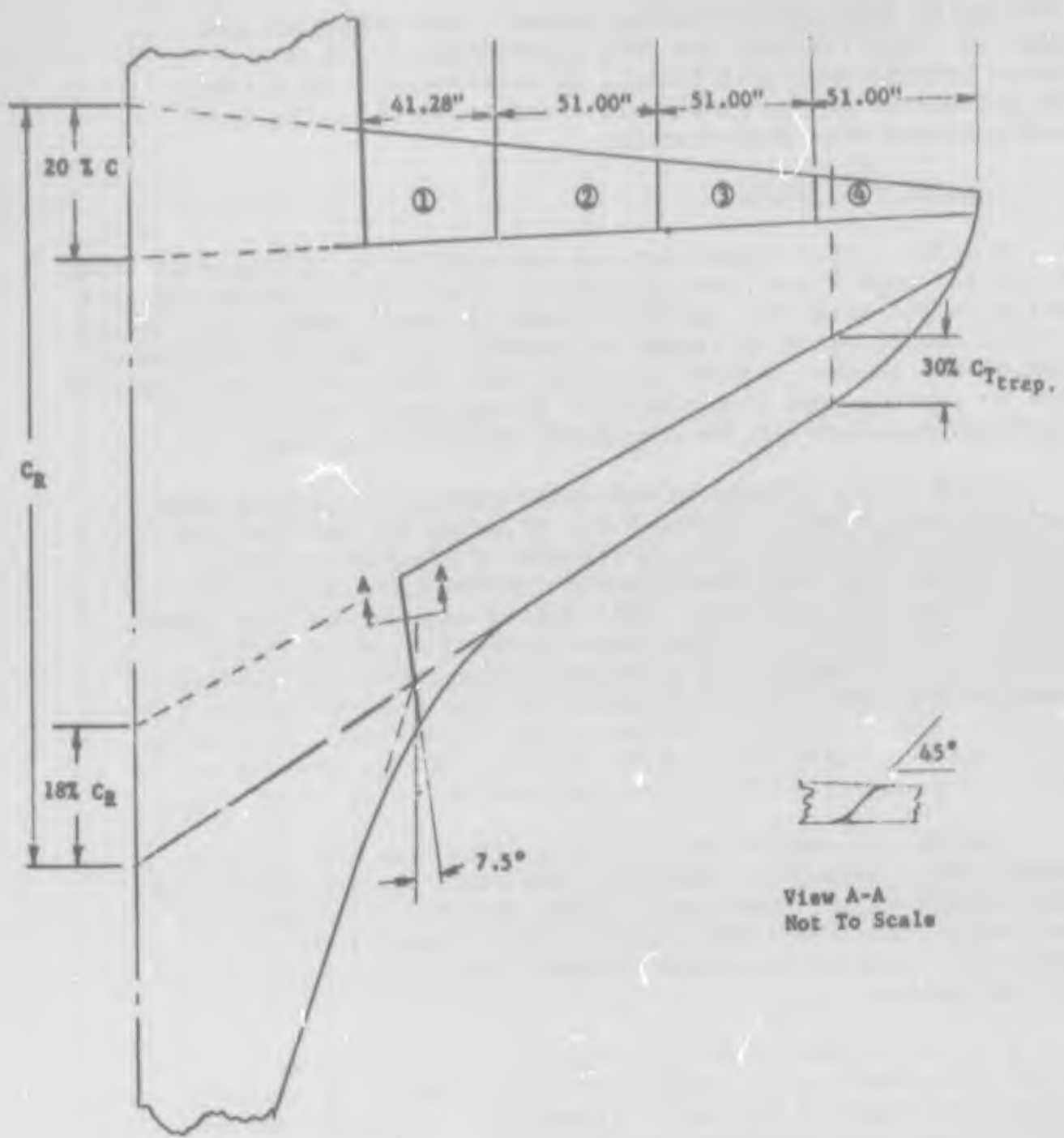


Figure 8 LEADING AND TRAILING EDGE FLAP PLANFORMS

| X/C% | (y/C)U-% | (y/C)I.-% |
|------|----------|-----------|
| 0    | .260     | .260      |
| .5   | .700     | -.165     |
| .75  | .765     | -.180     |
| 1.00 | .825     | -.183     |
| 1.25 | .880     | SAME      |
| 2.00 | 1.025    | AS        |
| 3.00 | 1.210    | BASIC     |
| 4.00 | 1.378    |           |
| 5.00 | 1.545    |           |
| 6.00 | 1.720    |           |

——— MODIFIED (K2 Leading Edge)  
 - - - BASIC (K1 Leading Edge)

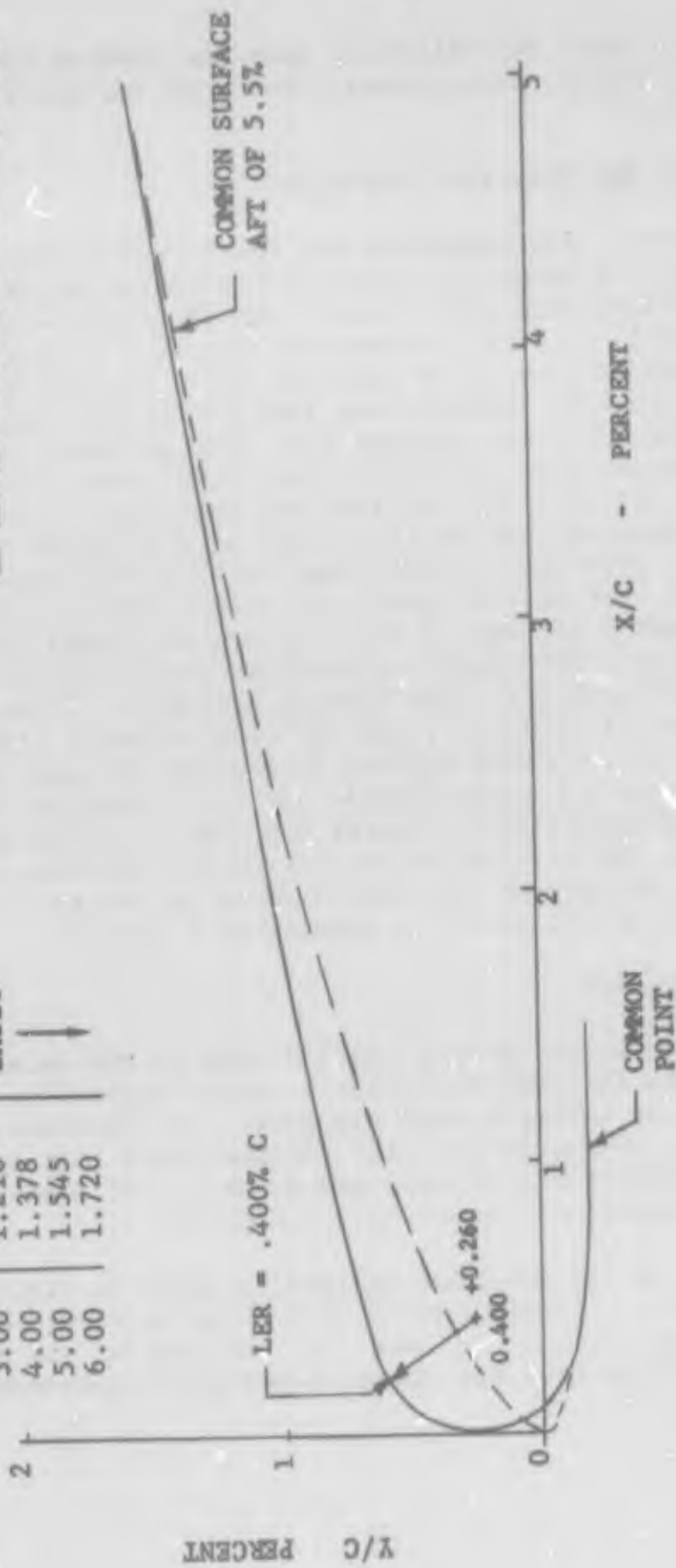


Figure 9 LEADING-EDGE-FLAP AIRFOIL GEOMETRIES



curvature and slope distributions near the leading edge are shown in Figures 10 and 11, respectively, for both the basic and alternate airfoils.

### 3. AILERONS AND TRAILING EDGE FLAPS

Selection of the planforms for the trailing edge devices was accomplished in a manner to allow investigation of several spanwise aileron locations and simple transonic maneuvering flaps. A relatively small chordwise extent was selected so that the main portion of the wing could be employed for a structural box even though a rather wide leading-edge flap is incorporated. The aft twenty percent chord was divided into four spanwise segments. It was planned to have each fifty-one inches wide, (full scale) however, the nacelle side fairings necessitated a reduction in the inboard segment span to 41.28 inches, see Figure 8. Control effectiveness estimates, based upon the USAF DATCOM, Reference 12, confirmed that the desired level of control power could be attained by using any two of the four trailing edge segments. These estimates, based upon fifteen degrees aileron deflection, are given in Figure 12 for the inboard (segments 1 and 2), mid-span (segments 2 and 3), and outboard ailerons (segments 3 and 4). A conservative surface deflection was used for surface sizing since control effectiveness has been found to decrease drastically at deflections greater than ten to fifteen degrees depending upon the particular configuration, see for example Reference 13. Details of the work leading to the roll control power criteria may be found in Appendices I and II.

### 4. VENTED SPOILER

A representative spoiler was included in the selected roll control devices in order to obtain a direct comparison of various roll controls on a single wing planform. An additional consideration is that configurations with advanced high-lift systems, such as slotted and/or Fowler flaps, are normally incompatible with the design requirements of conventional ailerons.

Geometry of the selected spoiler is shown in Figure 13. A nominal ten percent chord hinged at 0.75 was selected with the device spanning segments 2 and 3. Venting of one percent chord at the hinge line was chosen based upon experience

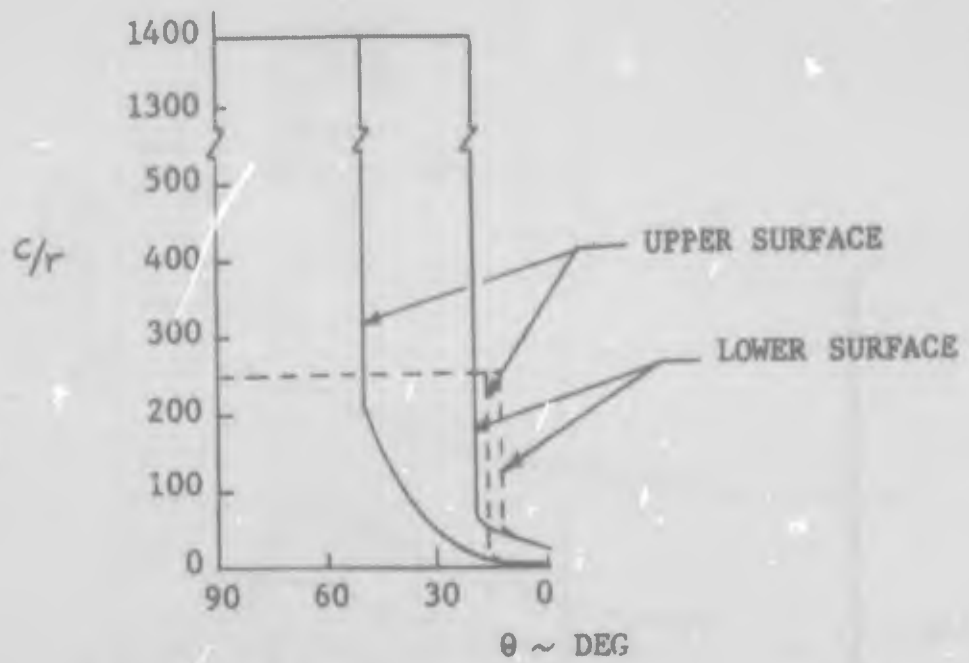


Figure 10 CURVATURE DISTRIBUTIONS

——— BASIC AIRFOIL (K1 Leading Edge)  
 - - - - MODIFIED AIRFOIL (K2 Leading Edge)

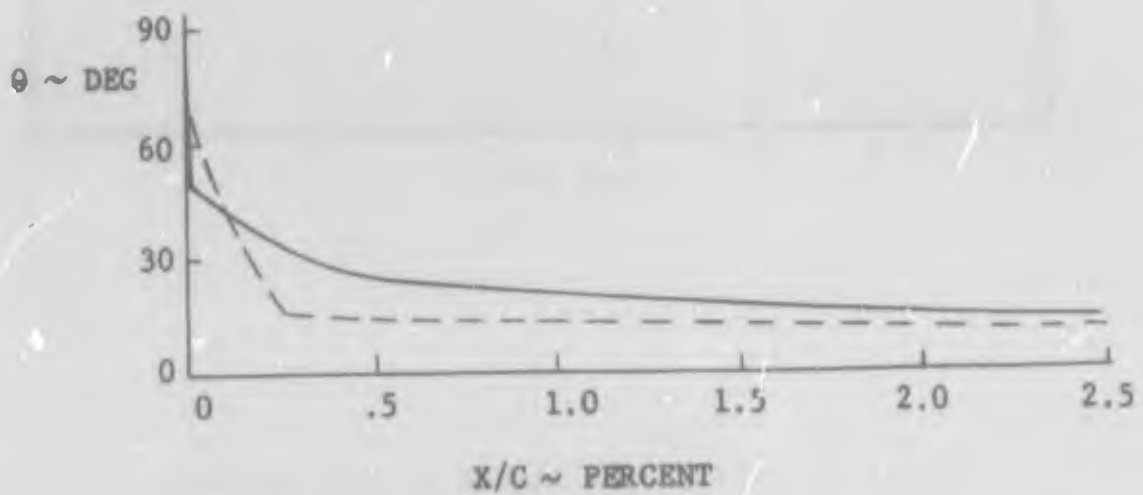


Figure 11 UPPER SURFACE SLOPE DISTRIBUTIONS

$C_L = 0.4$   
 $\delta_a = 15^\circ$   
 20% Chord

| Code | Aileron Location | % bw/2        |
|------|------------------|---------------|
| —    | Inbd.            | 28.1 to 62.6  |
| —    | Mid.             | 43.4 to 81.0  |
| —    | Outbd.           | 62.6 to 100.0 |

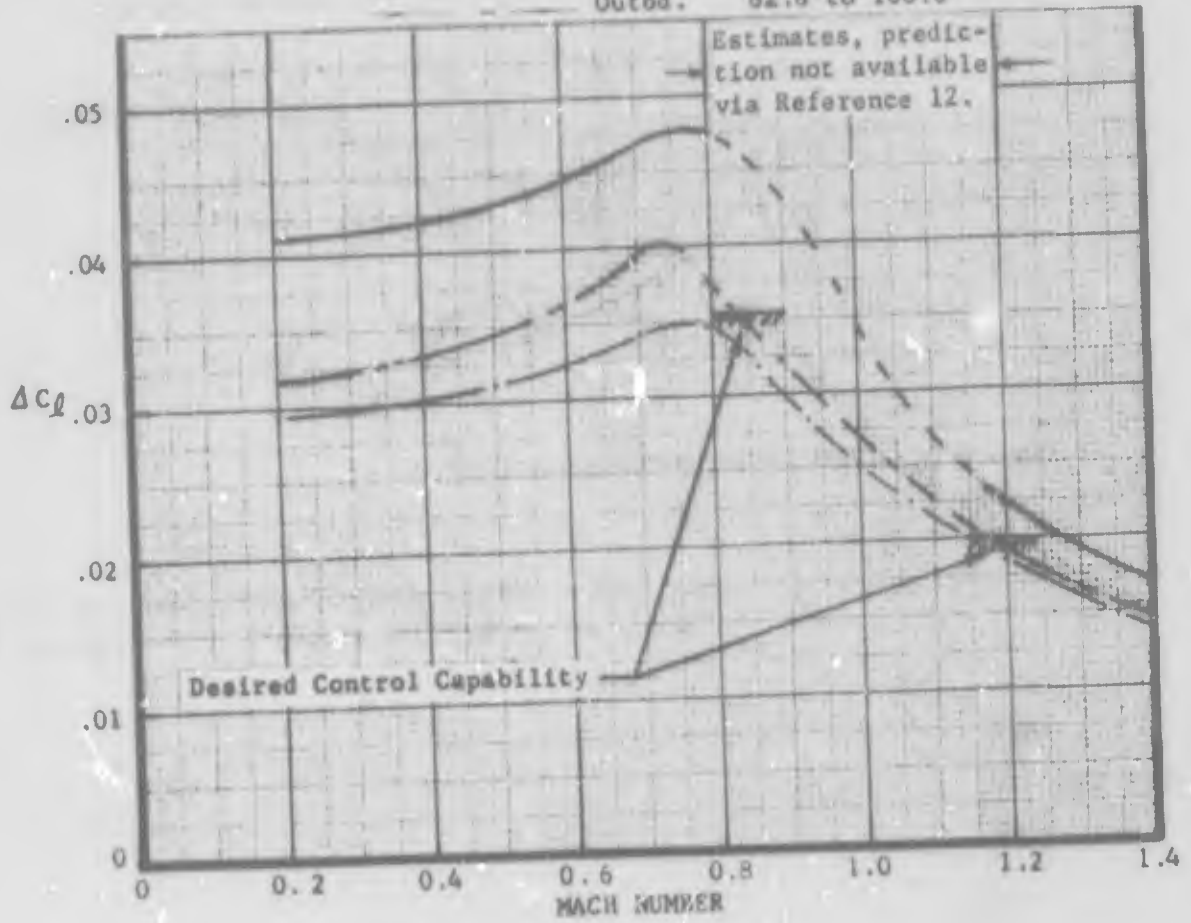


Figure 12 ESTIMATED AILERON ROLLING MOMENT

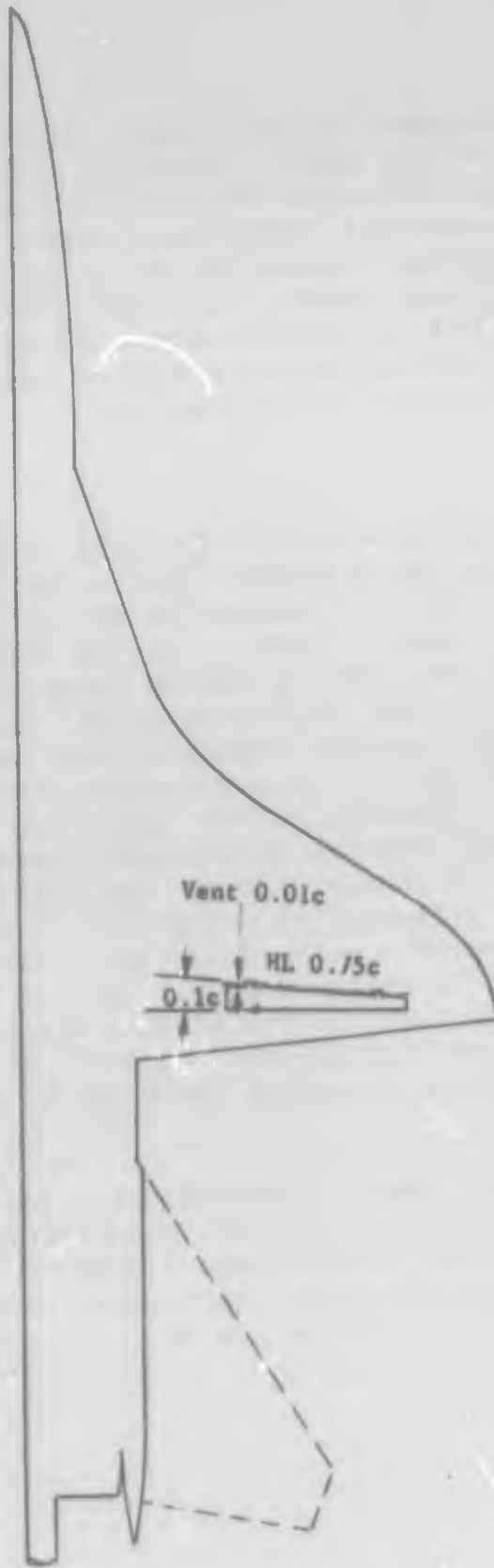


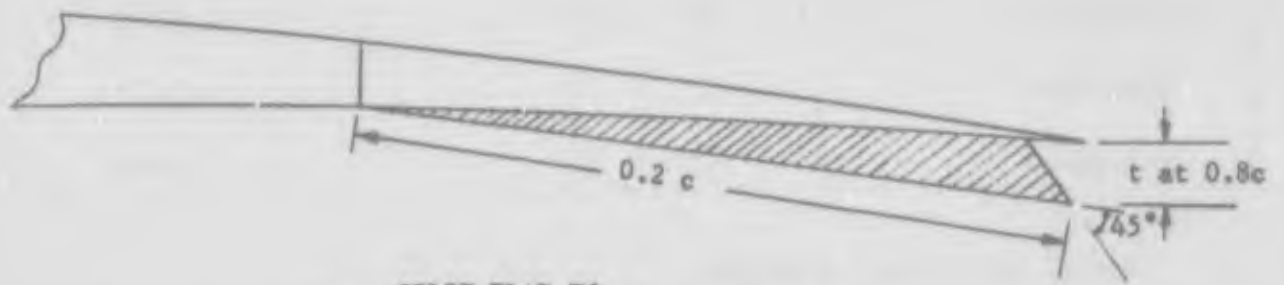
Figure 13 SPOILER GEOMETRY

that such an arrangement significantly reduces hinge moments while improving rolling moment linearity at small deflections. This device is geometrically similar to the mid-span aileron and thus affords a meaningful comparison between the two types of control devices without strict regard to the rolling moment attainable. (Estimate based on the USAF DATCOM indicated that to meet the selected transonic control criteria, the spoiler would have to be fifteen percent chord spanning segments 1, 2 and 3 with a ninety degree deflection).

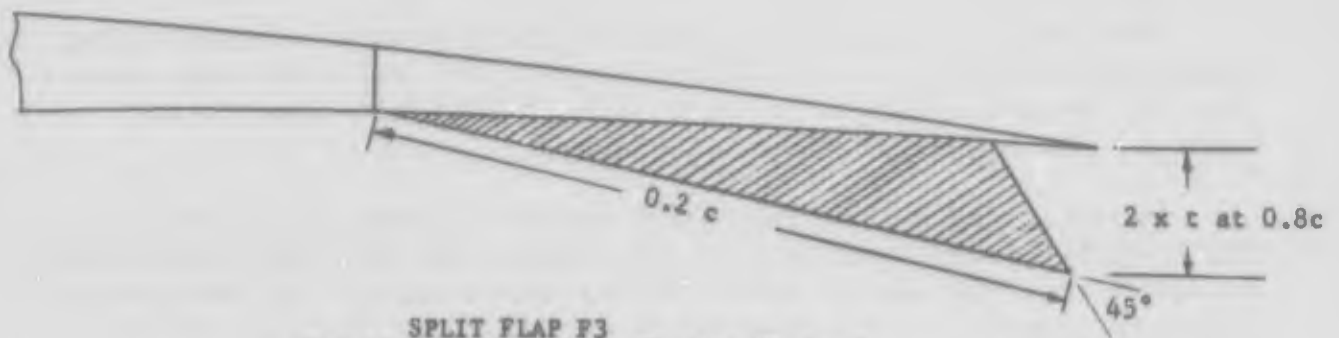
## 5. SPLIT FLAPS

Available experimental data for wing sections and ailerons with blunt trailing edges suggest that a split trailing-edge flap offers two basic advantages when employed to effectively blunt the trailing edge. First, trailing edge bluntness reduces static pressure at the aft stagnation point causing a significant aft movement of the shock/wave on the wing upper surface. This minimizes shock-induced boundary-layer separation at transonic speeds. Similarly, in a few cases blunt trailing edge ailerons have been found to be more effective than conventional sharp trailing edge controls at transonic speeds, see References 14 and 15. To evaluate these effects, the split flaps of Figure 14 were selected. Differential deflection is obtained by deflecting the appropriate aileron and split flap as an integral unit. Flap F2, to be employed on all aileron segments, has a trailing edge depth equal to the airfoil thickness at eighty percent chord. Flap F3 (for aileron segments 2 and 3) has a trailing edge depth of twice the thickness at eighty percent chord.

The experimental data of References 14 and 15 have been used to estimate the increase in control capability with blunt trailing edges as indicated in the Table. However, it was not felt that this data was sufficiently applicable to estimate differences between blunting effects for split-flap configurations F2 and F3.



SPLIT FLAP F2  
FOR AILERON SEGMENTS ①, ②, ③, ④



SPLIT FLAP F3  
FOR AILERON SEGMENTS ② AND ③ ONLY

Figure 14 TYPICAL SPLIT FLAP SECTIONS

| Aileron Location | Sections | Estimated Increase in $\Delta C_l$ Produced by Blunt Trailing Edge |
|------------------|----------|--|
| Inboard          | ① + ②    | 0.0118   |
| Mid-Span         | ② + ③    | 0.0127   |
| Outboard         | ③ + ④    | 0.0109   |

## 6. VORTEX GENERATOR PATTERN

One of the auxiliary devices proposed for investigation was an array of vortex generators. Vortex generators have been used very successfully in the past to reduce the extent of shock-induced separation. Pearcey presents an excellent discussion of vortex generator design principles and uses in Reference 16. The application in the present investigation is to reduce the extent of shock-induced separation in the region of trailing-edge control devices at transonic speeds at moderate to high angles of attack.

The generator planform, size and spacing were selected using guidelines established in References 16 and 17 and from data generated by General Dynamics in tests of a 1/10-Scale flow field model of the F-111A at supersonic speeds.

The selected vortex generator array is shown in Figure 15. The design is unconventional in the sense that the generators are oriented such that their chord planes are parallel to the aircraft plane of symmetry. The generators are constant in size and the leading edges are located at the hinge line of the leading-edge flap. The array extends spanwise from the inboard edge of the leading-edge flap nearly to the wing tip.

This array was selected to produce low drag at low angles of attack and yet produce sufficient vortex strength at high angles of attack to reduce the extent of shock induced flow separation in the trailing-edge region. Surface flow photographs from a

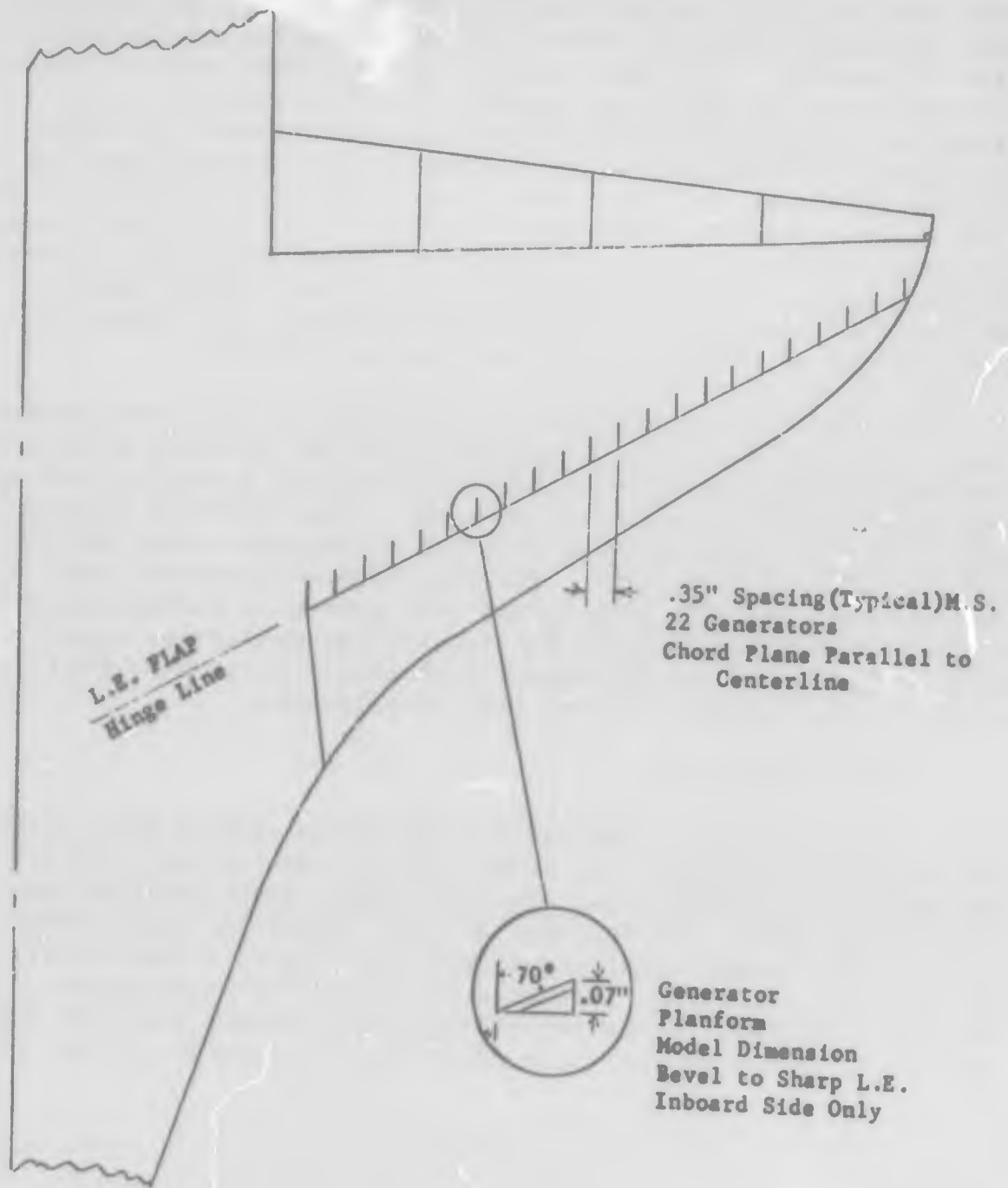


Figure 15 VORTEX GENERATOR ARRAY



NACA test of a 38.5 degree leading-edge-sweep wing of four percent thickness ratio (Reference 18) were used to set the generator orientation. The photographs show that the surface flow is streamwise at low angles of attack. The flow takes on a progressively increasing inboard direction with increasing angle of attack. For the LEDE configuration it was assumed that the surface flow over the outer wing panel would be qualitatively similar to that over the NACA wing. On this basis, the highly swept generator planforms were anticipated to start producing corotating vortices of significant strength at about six degrees angle of attack and that the increase in vortex strength with angle of attack would be sufficient for the intended purpose.

The physical construction and mounting of such small generators presented a difficult problem which was overcome by machining the vortex generators as integral parts of a separate set of leading-edge-flap brackets (Figure 16). The choice of leading-edge-flap deflection for use with the vortex generators had to be made prior to the tests. The five degree deflection was chosen because it was anticipated that generator effectiveness would be sufficient to make the five degree deflection equal to or superior to the ten degree deflection in terms of roll control effectiveness at high lift coefficients.

#### 7. KRUGER GLOVE FLAP

A Kruger flap was devised for the glove leading edge during the testing in PWT 4T. The intent of this device was to alter the vortex flow originating from the highly swept leading edge of the wing glove, particularly at high angles of attack where such a vortex might adversely effect the control effectiveness of roll control devices located outboard on the wing proper. The basic geometric characteristics of this Kruger flap and the location relative to the glove planform are shown in Figure 17.



Figure 16 VIEW OF VORTEX GENERATORS

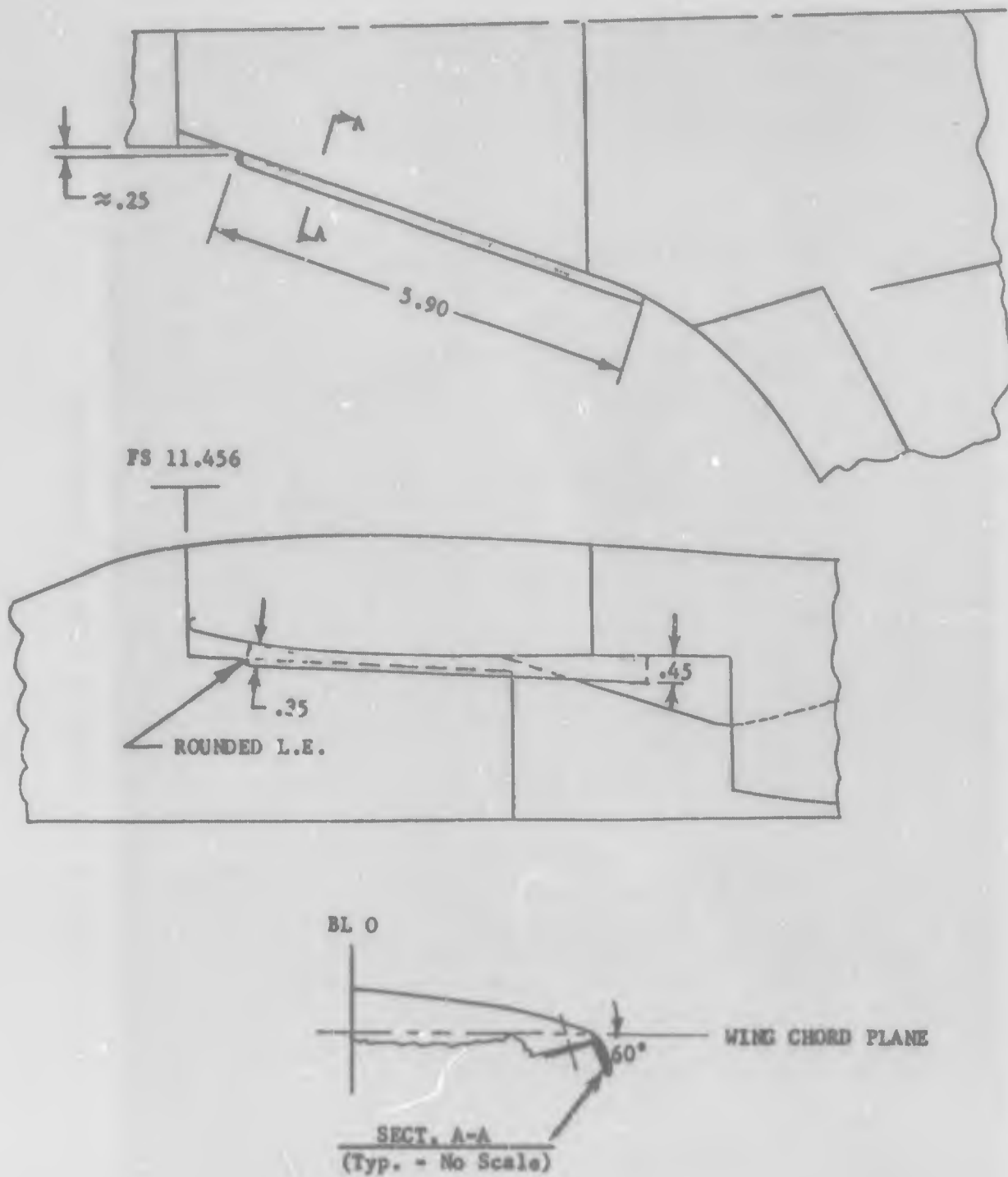


Figure 17 GLOVE-MOUNTED KRUGER FLAP

## SECTION III

### WIND TUNNEL TECHNIQUES AND TEST PROGRAMS

The objective of the test program was to investigate methods of improving roll control effectiveness at transonic high lift conditions. Recently developed concern about methods of testing to adequately simulate flight conditions for shock induced flow separation had an impact on the experimental program. Two different problems had to be resolved. First, how could the effects of transonic wind tunnel wall constraints be minimized or at least evaluated? Second, which of several recently proposed methods of simulating boundary-layer conditions at flight Reynolds numbers should be used? The first problem affected the choice of test facilities and the second problem the mode of conducting the test programs.

#### 1. FACILITIES

The Request for Proposal stated FDCC's desire to have the investigation run in the Arnold Engineering Development Center Propulsion Wind Tunnel (AEDC PWT 4T) transonic facility. Calibration data available at the time of the contractor's proposal did not indicate that significant effects due to tunnel size would be encountered in that facility. Some anomalous results had been obtained in General Dynamics tests in other small transonic facilities and, therefore, it was proposed to use two approaches to validate the 4T test data. First, an F-111A configuration which has been tested in a larger facility would be included in the 4T test program. Comparisons of force and moment results from the two facilities would be evaluated to assess possible tunnel wall effects. Second, a short verification test program was proposed to be run in the PWT 16T facility. The first proposal was accepted as part of the basic contracted effort. The second proposal was originally rejected due to uncertainties in the schedule and demand for 16T occupancy time. Later the proposal was accepted and the 16T test program was funded under an extension to the original contract.

The test conducted in the Propulsion Wind Tunnel 4-Foot Facility (PWT 4T) was designated TC-043, and was accomplished during the time periods from 21 to 31 July and from 2 to 5 September 1969, for a total of 120 hours of installed time. The first entry was terminated when the 1.5 inch Task MK-VI-A balance failed during the testing of Part Number 316, at which time 92 hours of installed time had been utilized. The 1.5 inch Task MK-VI-B balance was obtained for the second entry into PWT 4T, and the remaining 28 hours of test time were utilized. The PWT 16T test, designated TF-216, was run during 10 and 11 September 1969, and required 26 tunnel occupancy hours.

An arrangement was made among FDCC, Directorate of Test at AEDC, ARO, Inc. and General Dynamics to loan the LEDE model to ARO for calibration tests in the PWT 4T. In addition to the two tests discussed in the previous paragraph, calibration data was obtained during test TC-045 performed on 6 September 1969 for the model in both the upright and inverted positions for various tunnel wall porosity settings at several Mach numbers in the range from 0.7 to 1.2. General Dynamics, in turn, was permitted use of the calibration data to assess differences between PWT 4T and PWT 16T results.

## 2. TEST TECHNIQUES

General Dynamics proposed to use A. B. Haines' approach to investigate possible transonic scaling effects during the experimental program. The approach described briefly in Reference 19 is essentially to use a boundary layer trip well forward on the wing, but size the trip to be smaller in height than is normally used. In this way the thinnest possible turbulent boundary layer can be obtained ahead of all significant shock waves. The test unit Reynolds number was to be the highest possible consistent with model loads and tunnel operating modes.

Six-component force and moment data were to be obtained in pitch runs including a nominal angle of attack range from -2 to

28 degrees. The basic test configuration was to be the wing-body configuration less horizontal tail. Data were to be obtained at three subsonic and one supersonic Mach numbers. Numerous surface flow visualization photographs were to be obtained to aid interpretation of the force and moment data.

During the actual conduct of the test program several unexpected operational problems were encountered which required changes to the planned test procedures. The changes included:

- 1) modification of the approach to simulating full scale conditions;
- 2) implementation of surface flow visualization;
- 3) addition of the horizontal tail to the configuration for most of the roll control device tests.

The operational problems and their solutions are discussed in the following subsections. Details apropos to the overall conduct of the tests and data reduction and summaries of the configuration tested complete this section.

#### a. Full Scale Simulation

As mentioned earlier, it was originally intended to use the A. B. Haines approach to investigate transonic scaling effects during the experimental program. Unfortunately, the initial runs with the check configuration indicated that wall interference effects were severe in the PWT 4T. This fact aroused concern about interpretation of data for the roll control study if any significant deviations from normal test practice were used.

Preliminary runs made on the LEDE configuration, without horizontal tail, to develop the surface flow visualization technique indicated that natural transition was occurring on the outer-wing upper surface near the leading-edge flap hinge line at low angle of attack and moving forward as angle of attack

increased. This situation indicated that fixing transition near the leading edge was necessary to prevent this movement. Carborundum grit was applied as shown in Figure 18 using a sparse distribution. The first series of fixed-transition runs were made using #120 grit on the wing. For the rest of the tests #180 grit was used at all Mach numbers and Reynolds numbers. This grit size was also used for all other boundary layer trips except for #150 grit on the nose.

The maximum unit Reynolds number that could be obtained at all test Mach numbers was 5.2 million per foot and the majority of the tests were run at that condition. Some configurations were tested also at 3.0 million per foot at all Mach numbers and at the maximum obtainable values at .8 and .9 Mach number.

During the 16T test the clean-wing and clean-wing with midspan-aileron configurations were tested at unit Reynolds numbers of 5.2 and 3.0 million per foot to provide a check on the 4T results.

#### b. Flow Visualization

Surface flow visualization was accomplished in both the 4T and 16T tests. PWT personnel have not had success in attempts to use the fluorescent oil film technique. Therefore, a mixture of titanium oxide and oil was used as the surface flow indicator. The flow patterns were recorded on 16mm movie film at each of several angles of attack. During the first entry in the PWT 4T facility, color film was used. The films were processed overnight and were viewed by the project team to aid in the interpretation of the force and moment data and also to aid in selecting configurations to be tested later in the experimental program. Unfortunately attempts to produce black and white reproductions of single frames gave some poor results. Therefore, black and white film was used for the second entry in the PWT 4T and during the test in PWT 16T.

Several runs early in the first entry in PWT 4T were devoted to arriving at a suitable mixture of the surface flow indicator. The problem encountered was the high operating temperature in the test facility. Prior to each oil flow run the model was

GRIT SIZES

- #150 - Nose
- #180 - Elsewhere

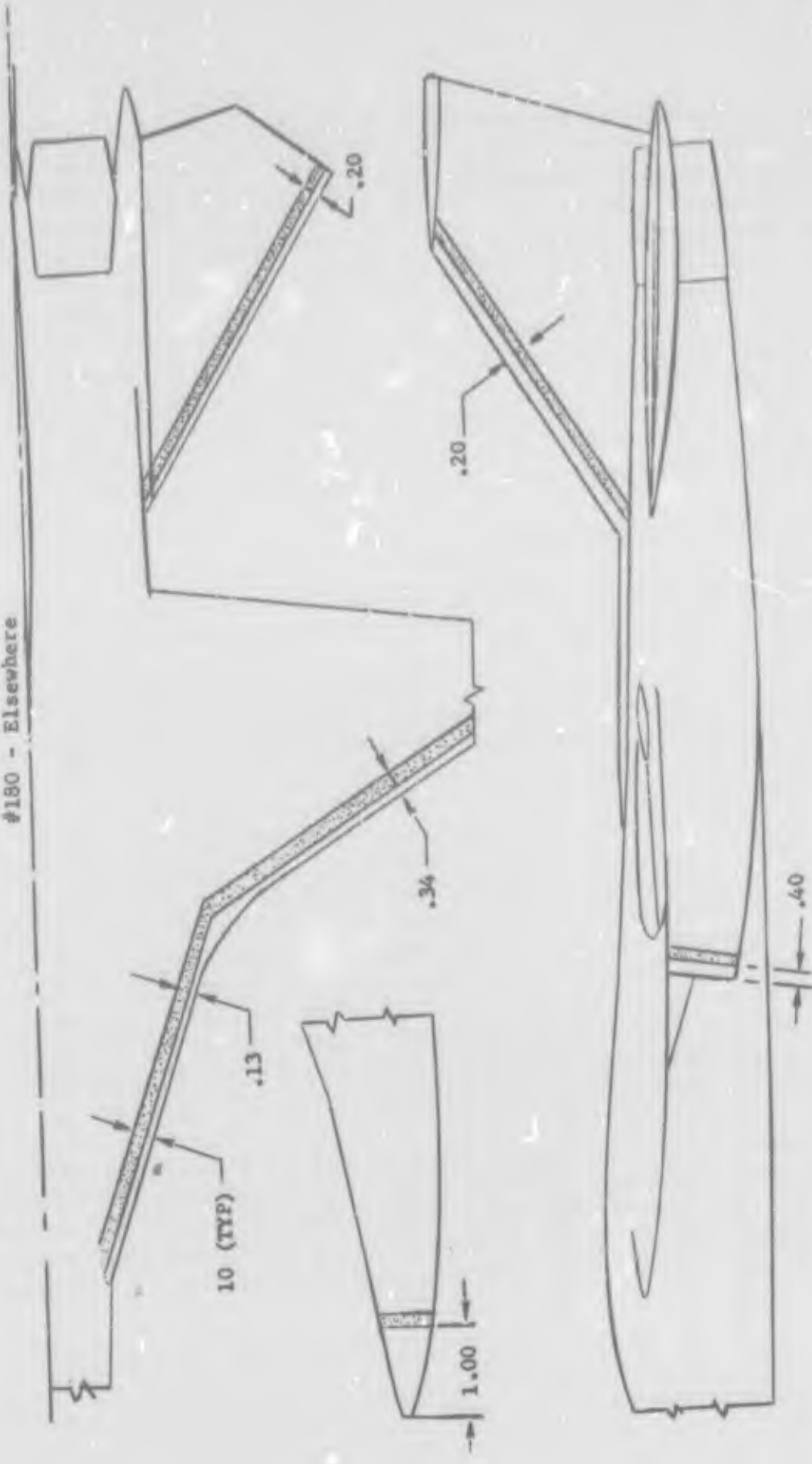


Figure 18 TRANSITION STRIP LOCATIONS  
(LEDE RESEARCH FORCE MODEL)



thoroughly cleaned and sprayed with flat-black acrylic lacquer. It was observed that the indicator would flow successfully for about 15 minutes and then would bake into the lacquer finish. As a consequence, the surface flow data could be obtained at only one Mach number during a run. It was decided to take surface flow data at .9 Mach number in the 4T facility unless a shutdown occurred for operational reasons prior to completion of a series of Mach numbers. It was further decided to take the oil flow data first and then take force data without a shutdown. This test approach was considered feasible and practical since no significant surface irregularities were produced by the surface flow mixture after it had baked into the lacquer finish. Some example photographs are shown in Sections VI and VII.

### c. Basic Test Configuration

One of the most significant problems that occurred in the 4T tests was that angle of attack for the wing-body combination was limited to angles of attack of about 15 degrees. This situation was caused by two factors. First, the force balance was located relatively aft in the existing fuselage so that for transonic conditions, horizontal tail off, almost all of the normal force was carried by the forward normal force gage. Second, high vibrational dynamics were encountered near 15 degrees angle of attack. The dynamics were attributed to two causes - aerodynamic buffet and an adverse flow situation at the support system strut. During the first entry of TC-043 in PWT 4T, a gap existed where the strut extended below the tunnel floor. The gap was sized to allow the sting support boom to extend below the floor for the higher angles of attack. Prior to the second entry of TC-043 (Part No. 400 and on), a strut flapper-door-seal was installed in the tunnel floor to minimize the opening surrounding the strut and the dynamics encountered were reduced by this tunnel modification.

Addition of the horizontal tail to the configuration altered the aerodynamic loading such that less load was carried by the forward gage and more by the rear gage. Maximum angles of attack for the complete model tests ranged from 20 to 30 degrees depending on Mach number and unit Reynolds number conditions. Because

the higher angles of attack were of major interest in the study the complete configuration was used for most of the roll-control device runs.

### 3. FORCE AND MOMENT MEASUREMENTS

Six-component force and moment data were computed in the stability axes system about a reference moment center located at F.S. 20.397 (which corresponds to the 25%  $\bar{c}$  of the LEDE wing), and at W.L. 7.367. However, the tie-in data were reduced about a point located at F.S. 21.951 (which corresponds to the 45%  $\bar{c}$  at wing sweep of 16 degrees) and W.L. 7.367. The stability axis system and sign convention are shown in Figure 19.

The measured data have been reduced to coefficient form and non-dimensionalized by the following:

|  | <u>LEDE</u> | <u>TIE-IN MODEL</u> |
|--|-------------|---------------------|
| b - Wing Reference Span, in.                 | 22.524      | 31.500              |
| $\bar{c}$ - Wing Reference mac, in.          | 6.583       | 4.521               |
| $S_w$ - Wing Reference Area, ft <sup>2</sup> | 0.86512     | 0.91146             |

The model angle of attack is referenced to the wing reference chord which is one degree negative to a waterline plane for the LEDE wing, and one degree positive to a waterline plane for the tie-in model.

The data were corrected for fuselage and nozzle plug base drag and duct internal drag. Fuselage and nozzle plug base drag corrections were determined concurrently with the force data throughout the tests and applied as a drag coefficient correction. Internal drag coefficients were also applied as drag coefficient corrections (to the 4T and 16T data) from the pressure runs obtained at the beginning of TC-043 for Mach numbers of 0.70, 0.80, 0.90, and 1.20. A linear interpolation was utilized to obtain the internal drag corrections for Mach = 0.85. No

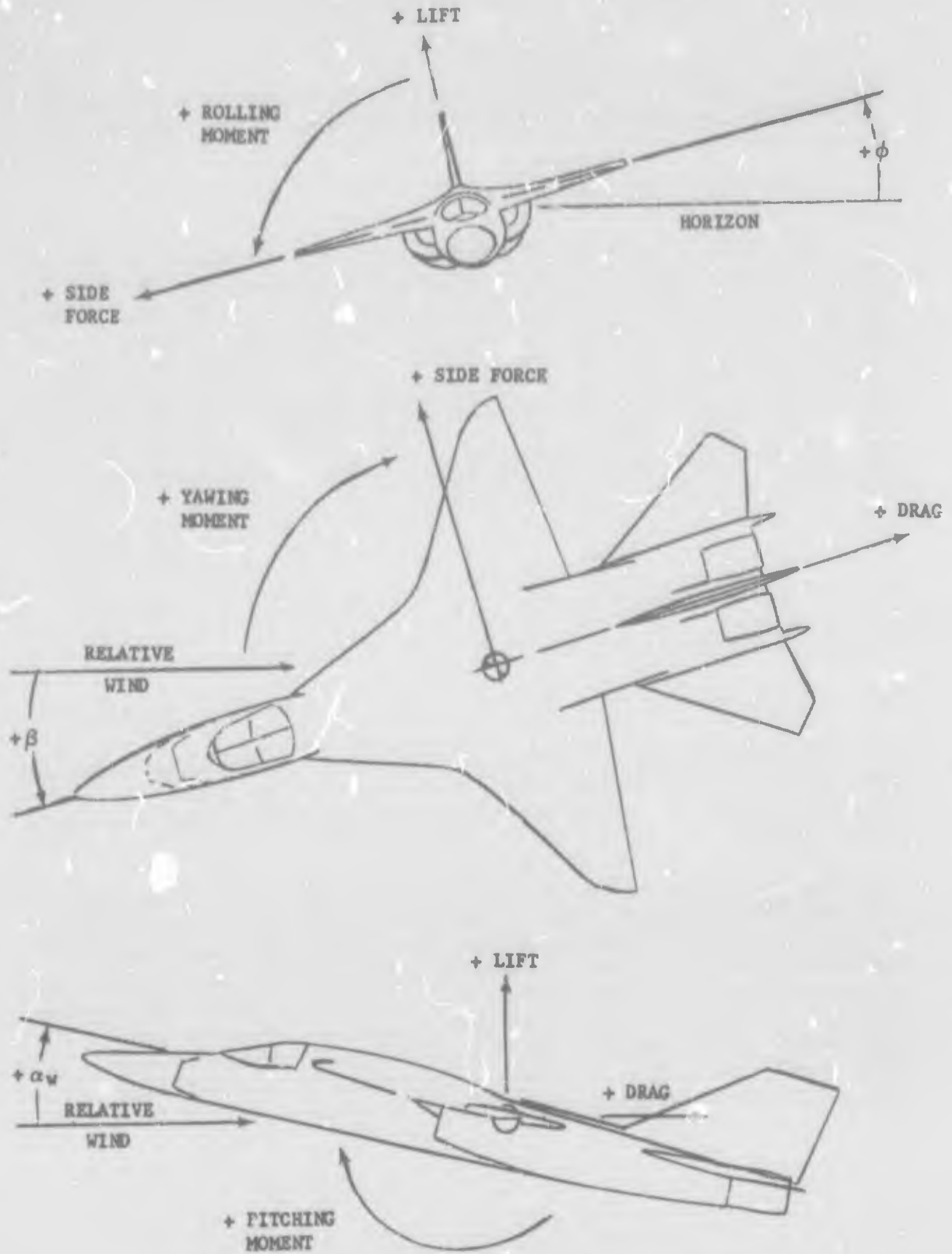


Figure 19 STABILITY AXES SIGN CONVENTION

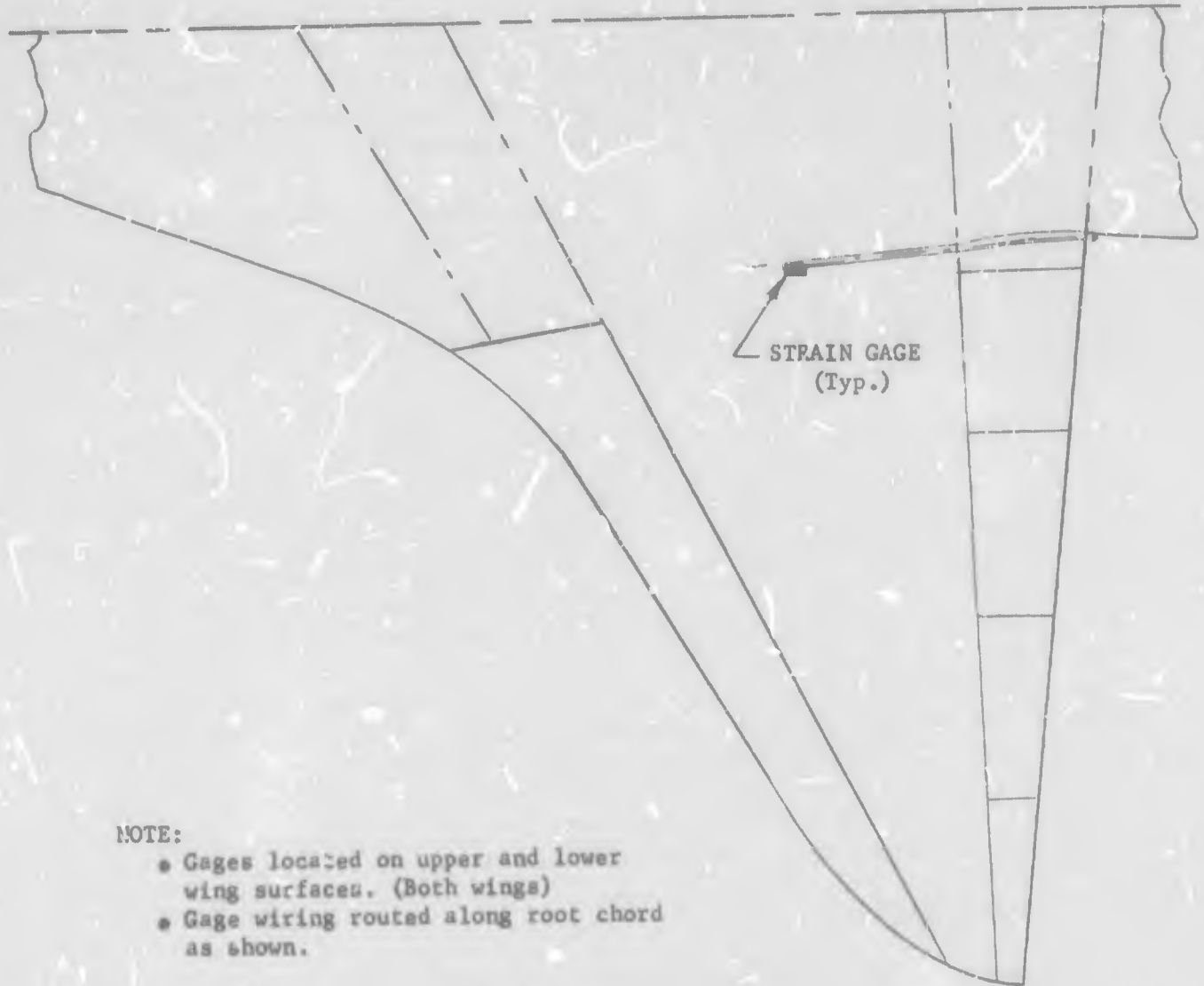
interpolations were attempted for Mach numbers above 0.90; therefore, internal drag corrections for  $M = 0.95$  were those obtained for Mach 0.90. Similarly, the internal drag corrections for  $M = 1.0$  and 1.10 were those values obtained for Mach 1.20.

The 1.50-inch Task MK-VI-A six-component internal strain gage balance was used during the first entry in PWT 4T (Test No. TC-043) until a fatigue failure in the drag linkage occurred during Part No. 316. The second entry into 4T, as well as the test in the 16T facility, were completed with the 1.50-inch Task MK-VI-B balance.

The balance normal, side, and axial forces, as well as rolling moment, were recorded on an oscillograph, along with angle of attack, in order to provide a method for locating the angle of attack at the onset of buffet. Buffet-type data were also recorded from strain gage bridges located just outboard of the nacelle on both the right- and left-hand wings as indicated in Figure 20. The output of the gages was amplified and then fed through an RMS meter and integrated over a short period of time. Considerable difficulty was encountered with the buffet measurements during the course of the tests and reliable data were obtained for only a few configurations. Since this type of data was to be used primarily to aid in the interpretation of the force and moment data and to evaluate the baseline configuration, only selected results are presented in this report.

#### 4. TEST PROGRAMS

Test data for tests TC-043 and TF-216 were obtained at Mach numbers of 0.70, 0.80, 0.90, and 1.20 at a nominal unit Reynolds number of  $5.2 \times 10^6$  per foot. A limited amount of data was obtained at  $M = 0.85$  and 0.95, at the two facilities. In addition to the Mach numbers mentioned above, the "clean" wing configuration was tested at Mach numbers of 1.00 and 1.10 in PWT 16T. A limited amount of data was also obtained at alternate Reynolds numbers of 3.0 and  $6.5 \times 10^6$  per foot as previously mentioned.



**NOTE:**

- Gages located on upper and lower wing surfaces. (Both wings)
- Gage wiring routed along root chord as shown.

**Figure 20 WING STRAIN GAGE LOCATIONS**

The model was pitched through the angle of attack range at 0 degrees sideslip. The pitch range at PWT 4T was obtained by utilizing the normal pitch sector, strut, and sting attachment receptacle (boom). However, an auxiliary pitch mechanism was required in PWT 16T in order to obtain the higher angles of attack, see Figure 21. All the angles of attack were set with the auxiliary pitch mechanism, with the basic sting support system in a fixed position.

The PWT 4T tunnel wall porosity was set at the optimum position of 6 percent for all the Mach numbers tested between 0.70 and 1.20. However, prior to the second entry of TC-043, the optimum porosity setting for Mach = 1.20 was changed from 6 percent to 4.85 percent. No porosity changes were made for Mach numbers less than 1.20. The PWT 16T facility has a fixed wall porosity of 6 percent.

No flow angularity corrections were made to the data presented herein from the 4-foot and 16-foot transonic facilities.

Test conditions and configuration descriptions are listed on the Summary Test Log for each test. (Tables II and III.)

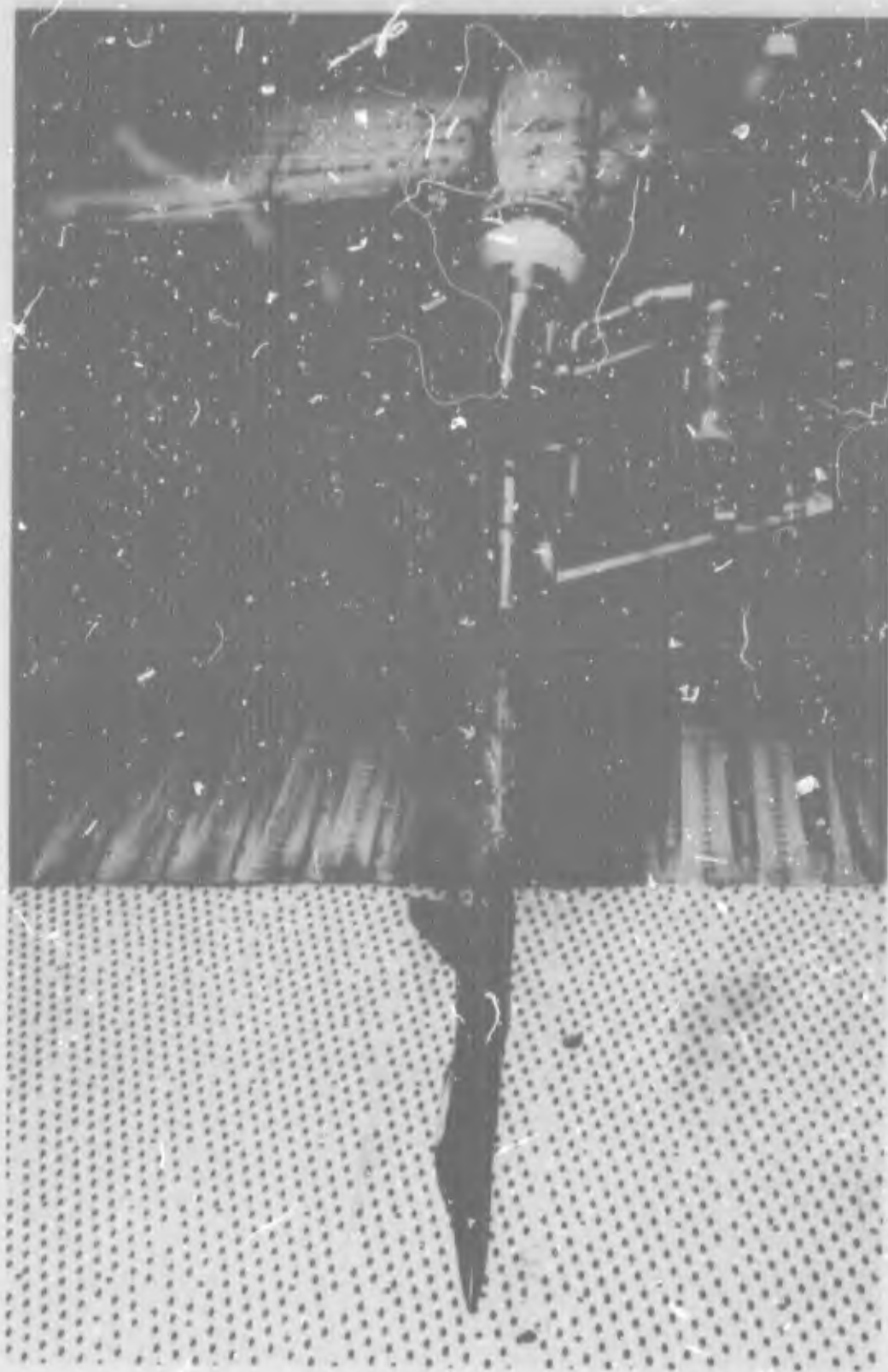


Figure 21 LEDE MODEL IN PWT 16T





Table II (Continued)

| 2<br>3<br>4<br>5 | CONFIGURATION                    | LEADING EDGE |            | TRAINING EDGE |           |               |           |               |           | $\delta_{NT}$ | $\delta_{NT}$ | PART NO. @ MACH NUMBER |      |      | REMARKS                                     |      |
|------------------|----------------------------------|--------------|------------|---------------|-----------|---------------|-----------|---------------|-----------|---------------|---------------|------------------------|------|------|---|------|
|                  |                                  | $\delta_L$   | $\delta_e$ | $\delta_{LE}$ |           | $\delta_{TR}$ |           | $\delta_{TR}$ |           |               |               | 0.70                   | 0.80 | 0.90 |   | 1.20 |
|                  |                                  | $10^\circ$   | $10^\circ$ | $0^\circ$     | $0^\circ$ | $0^\circ$     | $0^\circ$ | $0^\circ$     | $0^\circ$ |               |               |                        |      |      |   |      |
| ✓                | LEDE WING (ROSEN)                | $10^\circ$   | $10^\circ$ | $0^\circ$     | $0^\circ$ | $0^\circ$     | $0^\circ$ | $0^\circ$     | $0^\circ$ | $0^\circ$     | $0^\circ$     | 139                    | 141  | 143  |   |      |
| ✓                | + SPLIT FLAP ( $F_3$ )           |              |            | $0^\circ$     | $0^\circ$ | $0^\circ$     | $0^\circ$ | $0^\circ$     | $0^\circ$ | $0^\circ$     | $0^\circ$     | 140                    | 142  | 143  |   |      |
| ✓                | + SPLIT FLAP ( $F_2$ )           |              |            | $0^\circ$     | $0^\circ$ | $0^\circ$     | $0^\circ$ | $0^\circ$     | $0^\circ$ | $0^\circ$     | $0^\circ$     | 146                    | 148  | 150  |   |      |
| ✓                | + SPLIT FLAP ( $F_1$ )           |              |            | $0^\circ$     | $0^\circ$ | $0^\circ$     | $0^\circ$ | $0^\circ$     | $0^\circ$ | $0^\circ$     | $0^\circ$     | 153                    | 155  | 157  |   |      |
| ✓                | + SPLIT FLAP ( $F_2$ )           |              |            | $0^\circ$     | $0^\circ$ | $0^\circ$     | $0^\circ$ | $0^\circ$     | $0^\circ$ | $0^\circ$     | $0^\circ$     | 160                    | 162  | 161  |   |      |
| ✓                | + SPLIT FLAP ( $F_1$ )           |              |            | $0^\circ$     | $0^\circ$ | $0^\circ$     | $0^\circ$ | $0^\circ$     | $0^\circ$ | $0^\circ$     | $0^\circ$     | 165                    | 167  | 168  |   |      |
| ✓                | + SPOILER @ $-75^\circ$ (WING)   | $15^\circ$   | $0^\circ$  | $0^\circ$     | $0^\circ$ | $0^\circ$     | $0^\circ$ | $0^\circ$     | $0^\circ$ | $0^\circ$     | $0^\circ$     | 172                    | 173  | 174  | Flow $V=0.8M$                               |      |
| ✓                |                                  | $10^\circ$   | $10^\circ$ | $0^\circ$     | $0^\circ$ | $0^\circ$     | $0^\circ$ | $0^\circ$     | $0^\circ$ | $0^\circ$     | $0^\circ$     | 177                    | 179  | 181  |   |      |
| ✓                |                                  |              |            | $0^\circ$     | $0^\circ$ | $0^\circ$     | $0^\circ$ | $0^\circ$     | $0^\circ$ | $0^\circ$     | $0^\circ$     | 184                    | 186  | 185  | Flow Dynamics                               |      |
| ✓                |                                  |              |            | $0^\circ$     | $0^\circ$ | $0^\circ$     | $0^\circ$ | $0^\circ$     | $0^\circ$ | $0^\circ$     | $0^\circ$     | 191                    | 193  | 191  |   |      |
| ✓                |                                  |              |            | $0^\circ$     | $0^\circ$ | $0^\circ$     | $0^\circ$ | $0^\circ$     | $0^\circ$ | $0^\circ$     | $0^\circ$     | 198                    | 200  | 198  |   |      |
| ✓                |                                  |              |            | $0^\circ$     | $0^\circ$ | $0^\circ$     | $0^\circ$ | $0^\circ$     | $0^\circ$ | $0^\circ$     | $0^\circ$     | 205                    | 207  | 205  | $R_{eff}$ curves with<br>Mach 1.0, 1.2, 1.4 |      |
| ✓                | + SPLIT FLAP ( $F_1$ ) INTERCEPT |              |            | $0^\circ$     | $0^\circ$ | $0^\circ$     | $0^\circ$ | $0^\circ$     | $0^\circ$ | $0^\circ$     | $0^\circ$     | 209                    | 209  | 209  |   |      |
| ✓                |                                  |              |            | $0^\circ$     | $0^\circ$ | $0^\circ$     | $0^\circ$ | $0^\circ$     | $0^\circ$ | $0^\circ$     | $0^\circ$     | 212                    | 212  | 212  |   |      |
| ✓                |                                  |              |            | $0^\circ$     | $0^\circ$ | $0^\circ$     | $0^\circ$ | $0^\circ$     | $0^\circ$ | $0^\circ$     | $0^\circ$     | 215                    | 215  | 215  |   |      |
| ✓                |                                  |              |            | $0^\circ$     | $0^\circ$ | $0^\circ$     | $0^\circ$ | $0^\circ$     | $0^\circ$ | $0^\circ$     | $0^\circ$     | 218                    | 218  | 218  |   |      |
| ✓                |                                  |              |            | $0^\circ$     | $0^\circ$ | $0^\circ$     | $0^\circ$ | $0^\circ$     | $0^\circ$ | $0^\circ$     | $0^\circ$     | 220                    | 220  | 220  |   |      |
| ✓                |                                  |              |            | $0^\circ$     | $0^\circ$ | $0^\circ$     | $0^\circ$ | $0^\circ$     | $0^\circ$ | $0^\circ$     | $0^\circ$     | 223                    | 223  | 223  |   |      |
| ✓                | + VORTEX GENERATOR               | $5^\circ$    | $5^\circ$  | $0^\circ$     | $0^\circ$ | $0^\circ$     | $0^\circ$ | $0^\circ$     | $0^\circ$ | $0^\circ$     | $0^\circ$     | 226                    | 226  | 226  |   |      |
| ✓                |                                  |              |            | $0^\circ$     | $0^\circ$ | $0^\circ$     | $0^\circ$ | $0^\circ$     | $0^\circ$ | $0^\circ$     | $0^\circ$     | 229                    | 229  | 229  |   |      |
| ✓                |                                  |              |            | $0^\circ$     | $0^\circ$ | $0^\circ$     | $0^\circ$ | $0^\circ$     | $0^\circ$ | $0^\circ$     | $0^\circ$     | 232                    | 232  | 232  |   |      |
| ✓                |                                  |              |            | $0^\circ$     | $0^\circ$ | $0^\circ$     | $0^\circ$ | $0^\circ$     | $0^\circ$ | $0^\circ$     | $0^\circ$     | 235                    | 235  | 235  |   |      |
| ✓                |                                  |              |            | $0^\circ$     | $0^\circ$ | $0^\circ$     | $0^\circ$ | $0^\circ$     | $0^\circ$ | $0^\circ$     | $0^\circ$     | 238                    | 238  | 238  |   |      |
| ✓                |                                  |              |            | $0^\circ$     | $0^\circ$ | $0^\circ$     | $0^\circ$ | $0^\circ$     | $0^\circ$ | $0^\circ$     | $0^\circ$     | 241                    | 241  | 241  |   |      |
| ✓                |                                  |              |            | $0^\circ$     | $0^\circ$ | $0^\circ$     | $0^\circ$ | $0^\circ$     | $0^\circ$ | $0^\circ$     | $0^\circ$     | 244                    | 244  | 244  |   |      |
| ✓                |                                  |              |            | $0^\circ$     | $0^\circ$ | $0^\circ$     | $0^\circ$ | $0^\circ$     | $0^\circ$ | $0^\circ$     | $0^\circ$     | 247                    | 247  | 247  |   |      |
| ✓                |                                  |              |            | $0^\circ$     | $0^\circ$ | $0^\circ$     | $0^\circ$ | $0^\circ$     | $0^\circ$ | $0^\circ$     | $0^\circ$     | 250                    | 250  | 250  | Flow $V=0.8M$                               |      |
| ✓                |                                  |              |            | $0^\circ$     | $0^\circ$ | $0^\circ$     | $0^\circ$ | $0^\circ$     | $0^\circ$ | $0^\circ$     | $0^\circ$     | 253                    | 253  | 253  |   |      |
| ✓                |                                  |              |            | $0^\circ$     | $0^\circ$ | $0^\circ$     | $0^\circ$ | $0^\circ$     | $0^\circ$ | $0^\circ$     | $0^\circ$     | 256                    | 256  | 256  |   |      |
| ✓                |                                  |              |            | $0^\circ$     | $0^\circ$ | $0^\circ$     | $0^\circ$ | $0^\circ$     | $0^\circ$ | $0^\circ$     | $0^\circ$     | 259                    | 259  | 259  |   |      |
| ✓                |                                  |              |            | $0^\circ$     | $0^\circ$ | $0^\circ$     | $0^\circ$ | $0^\circ$     | $0^\circ$ | $0^\circ$     | $0^\circ$     | 262                    | 262  | 262  |   |      |
| ✓                |                                  |              |            | $0^\circ$     | $0^\circ$ | $0^\circ$     | $0^\circ$ | $0^\circ$     | $0^\circ$ | $0^\circ$     | $0^\circ$     | 265                    | 265  | 265  |   |      |
| ✓                |                                  |              |            | $0^\circ$     | $0^\circ$ | $0^\circ$     | $0^\circ$ | $0^\circ$     | $0^\circ$ | $0^\circ$     | $0^\circ$     | 268                    | 268  | 268  |   |      |
| ✓                |                                  |              |            | $0^\circ$     | $0^\circ$ | $0^\circ$     | $0^\circ$ | $0^\circ$     | $0^\circ$ | $0^\circ$     | $0^\circ$     | 271                    | 271  | 271  |   |      |
| ✓                |                                  |              |            | $0^\circ$     | $0^\circ$ | $0^\circ$     | $0^\circ$ | $0^\circ$     | $0^\circ$ | $0^\circ$     | $0^\circ$     | 274                    | 274  | 274  |   |      |





## SECTION IV

### COMPARISONS BETWEEN WIND TUNNELS

Concern with respect to wind tunnel wall effects at transonic high lift conditions is well founded judging from the results of the present investigation. Fortunately both proposed approaches to investigating possible effects were carried out during the program. The tie-in runs raised questions while the tests in the 16T facility provided some useful answers to those questions.

The general differences between data obtained in the 4T facility and data obtained in the larger facilities can be ascribed to an apparent alteration of the external flow field due to wall constraint at less than sonic speeds. Table IV contains a summary of the test section blockage for the particular model configurations and transonic test facilities used. At all angles of attack other than those for zero lift, the lift is lower and the drag higher in the 4T facility than in the 16T. In general, flow separation is induced at lower lift coefficients in 4T but the effects occur more gradually with increases in angle of attack. Some of the differences presented in the following subsections are attributable to flow angularity which is apparently more severe in the 4T than in the 16T and of opposite sense.

#### 1. TIE-IN RUNS

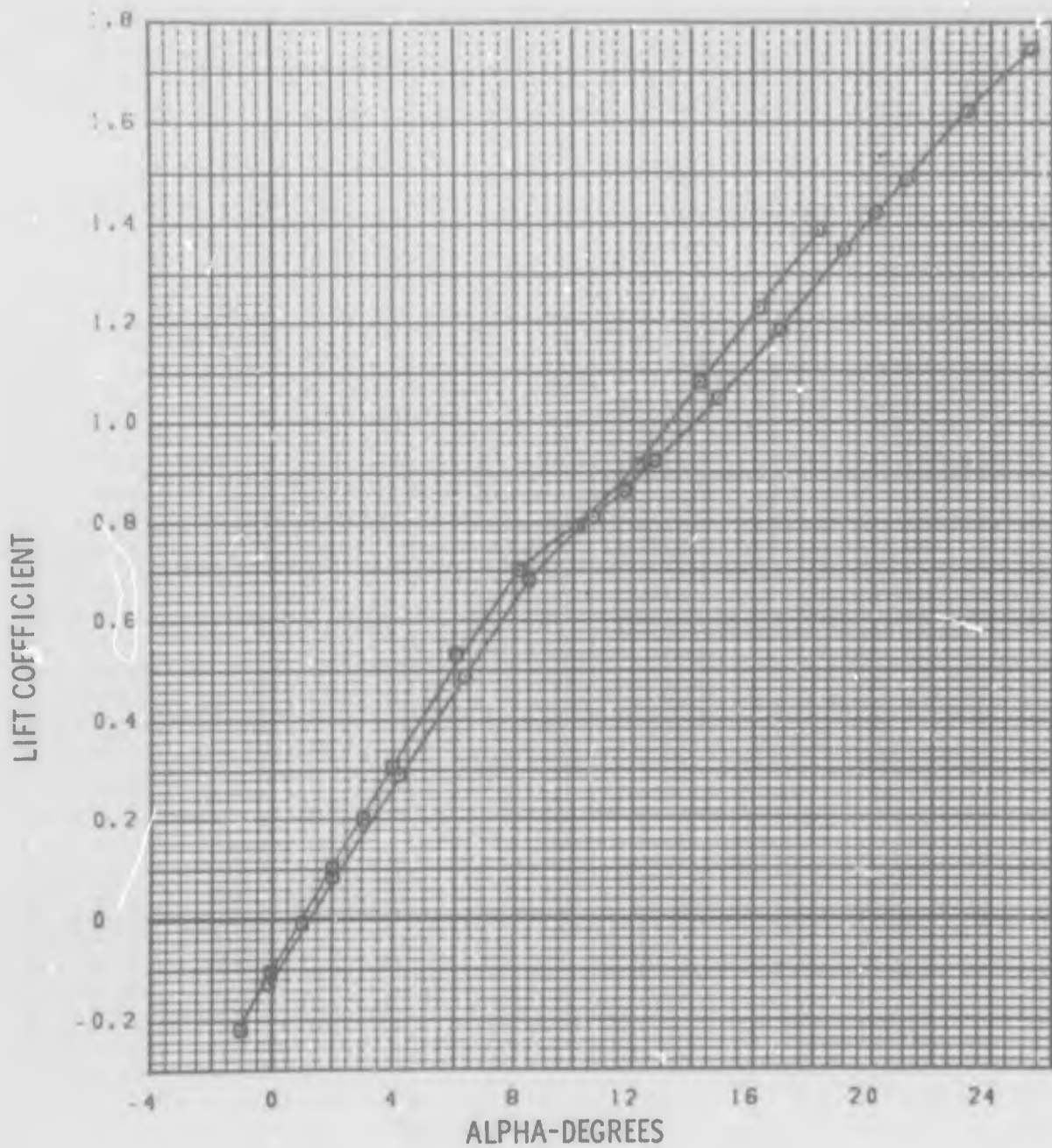
The tie-in configuration tested during the present program was unfortunately not identical to that previously tested in the Cornell Aeronautical Laboratory 8-foot transonic facility; however, the configuration differences are not significant enough to produce the differences in the results which occurred. Comparisons between the two sets of data are shown in Figure 22 for Mach numbers of 0.9 and 1.2.

At 0.9 Mach number, the lift curve slope obtained in the 4T is significantly reduced from that obtained in CAL.

Table IV NOMINAL BLOCKAGE OF TEST CONFIGURATIONS

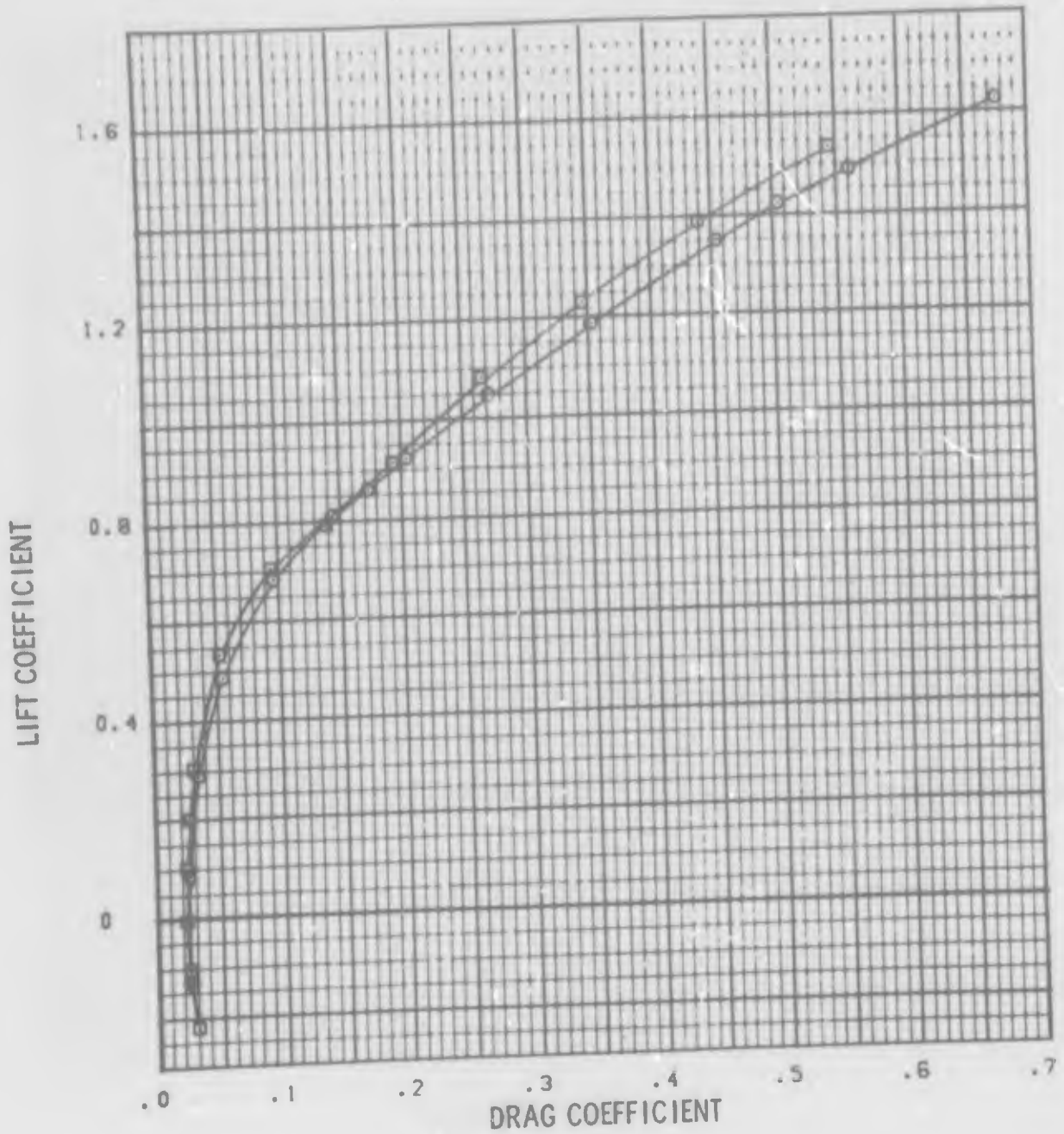
| FACILITY | WIND TUNNEL<br>CROSS SECTION AREA<br>FT <sup>2</sup> | MODEL  | CROSS SECTION AREA<br>FT <sup>2</sup> | MAXIMUM<br>SECTION AREA<br>FT <sup>2</sup> | CAPTIVE AREA<br>(@ 0.9 MACH)<br>FT <sup>2</sup> | NOMINAL BLOCKAGE * |
|----------|--|--|---------------------------------------|--|---|--------------------|
| CAL 8 FT | 64.0   | 1/24 F-111A<br>@ $\Lambda = 45^\circ$              | 0.1244                                | 0.1244                                     | 0.0254  | 0.15%              |
| PWT-4T   | 16.0   | 1/24 LEDE<br>1/24 TIE-IN<br>@ $\Lambda = 45^\circ$ | 0.1228                                | 0.1228                                     | 0.0254  | 0.61%              |
| PWT-16T  | 256.0  | 1/24 LEDE  | 0.1228                                | 0.1228                                     | 0.0254  | 0.62%              |
|          |  |  |                                       |  |   | 0.038%             |

\* Excluding Capture Area of Internal Ducting



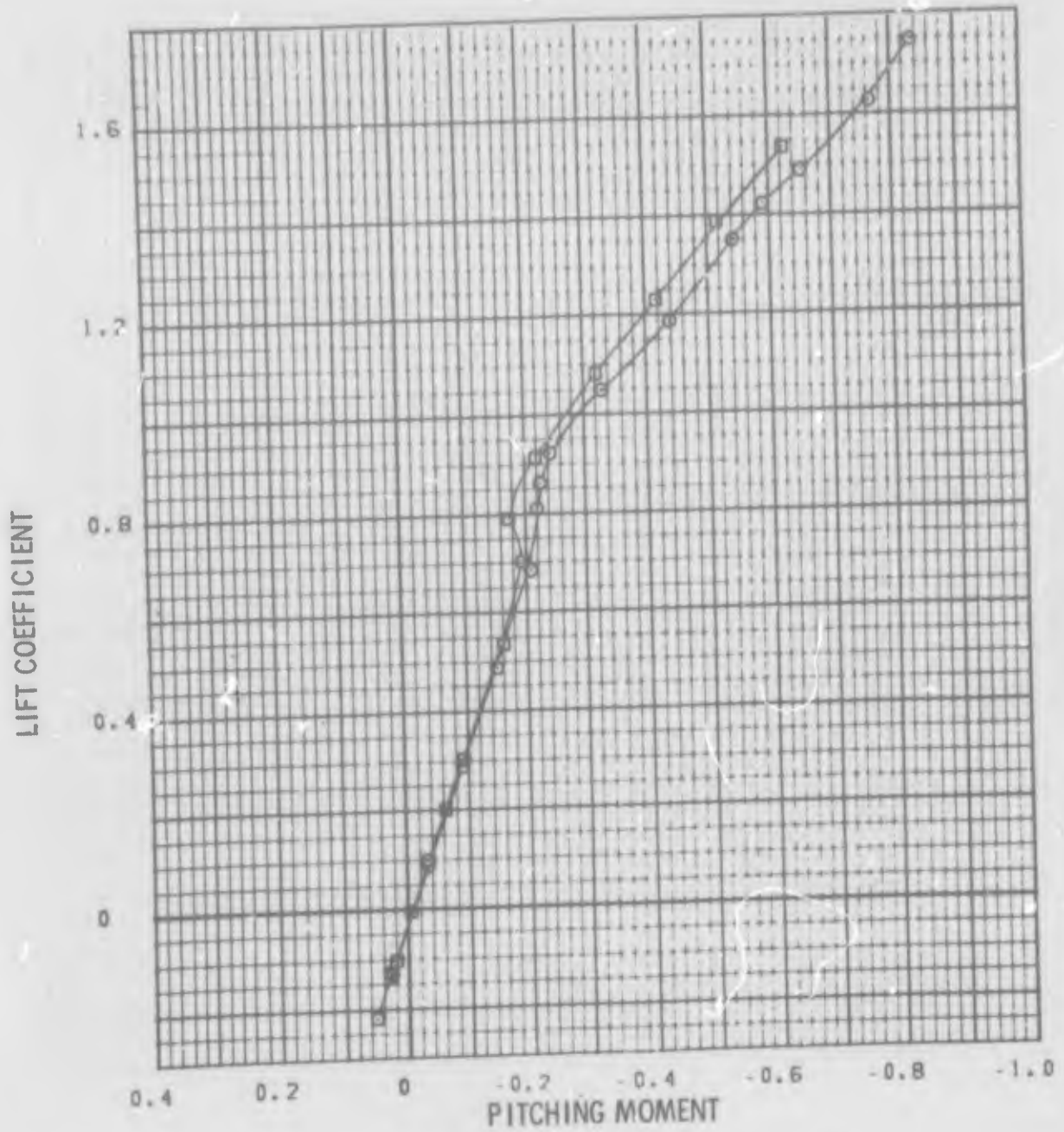
| SYM | TEST            | PAR | RN/FT       |
|-----|-----------------|-----|-------------|
| ⊙   | AEDC PWT 1C 043 | 13  | 3.0 MILLION |
| ⊠   | CAL G52 253     | 269 | 3.0 MILLION |

FIGURE 22a TIE-IN COMPARISON BETWEEN CAL AND PWT 4T  
AT L.E. SWEEP = 45 DEG., M = 0.9



| SYM | TEST            | PART | REMARKS     |
|-----|-----------------|------|-------------|
| ○   | AEDC PWT TC 043 | 13   | 3.0 MILLION |
| □   | CAL G52-253     | 269  | 3.0 MILLION |

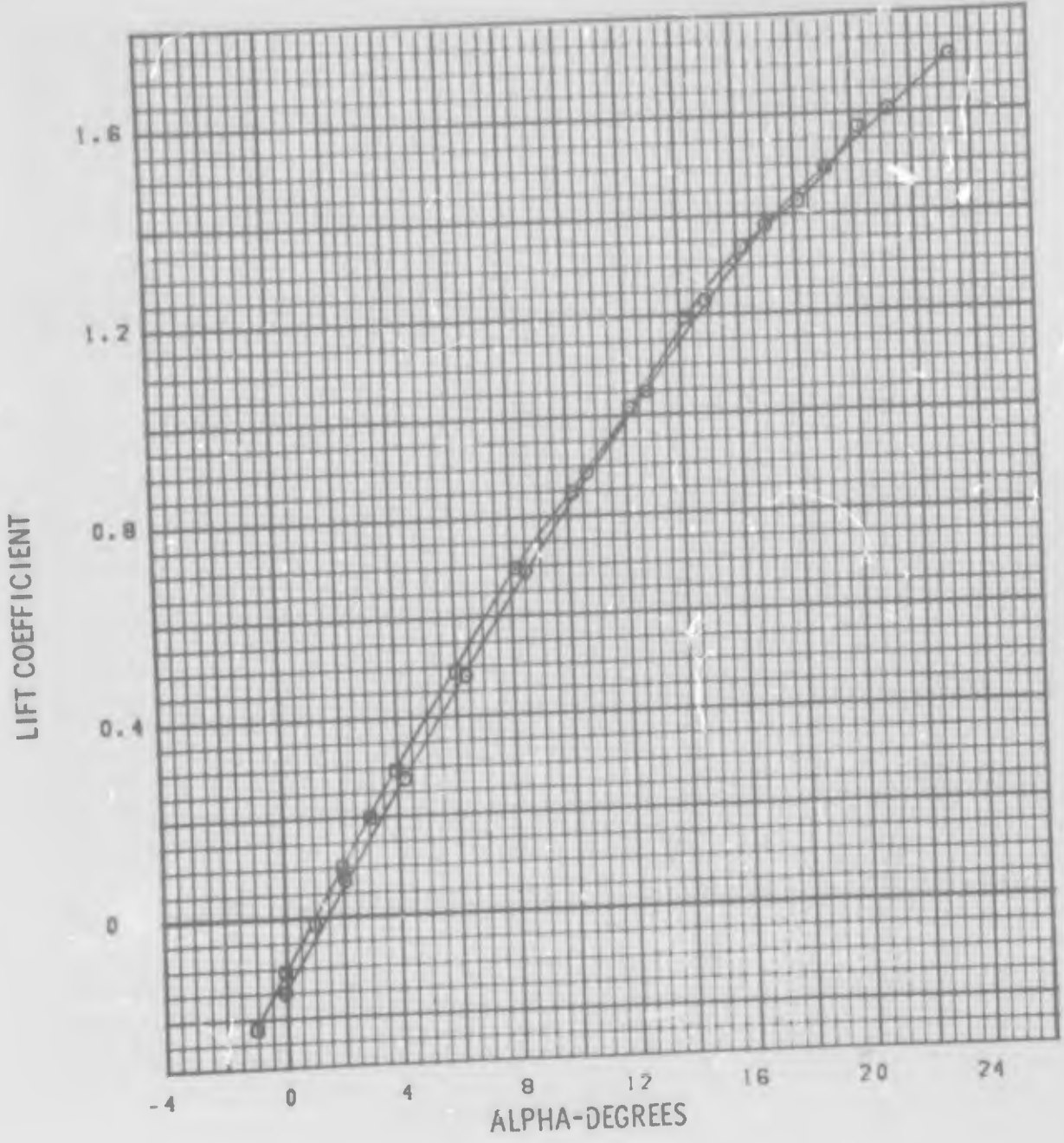
FIGURE 22a TIE-IN COMPARISON BETWEEN CAL AND PWT 4T  
AT L.E. SWEEP = 45 DEG. M = 0.9



| SYM | TEST            | PART | RAVE       |
|-----|-----------------|------|------------|
| ○   | AEDC PWT TC 043 | 13   | 3.0 MI 10N |
| □   | CAL G52 253     | 269  | 3.0 MI 10N |

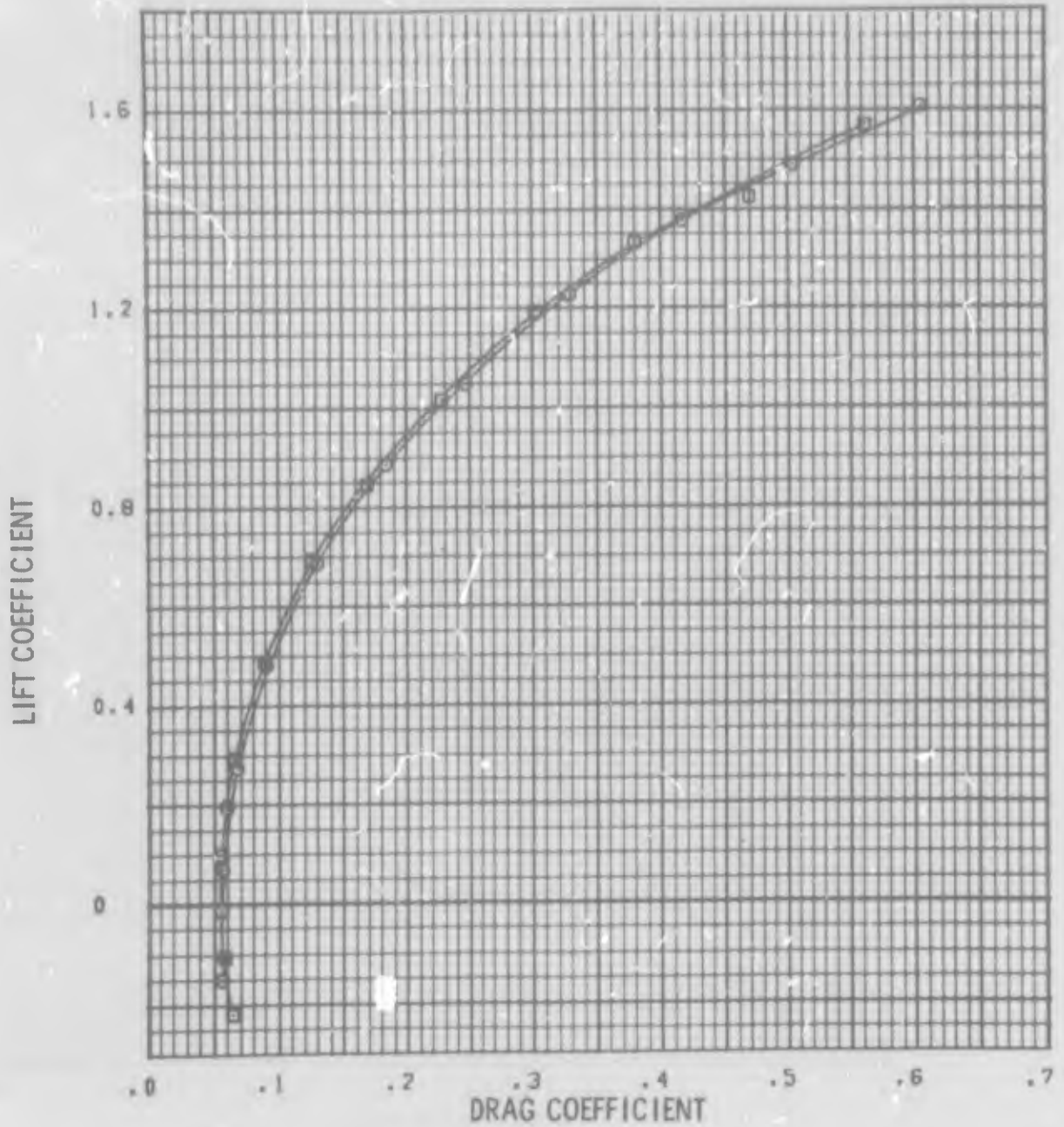
FIGURE 22a TIE-IN COMPARISON BETWEEN CAL AND PWT 4T  
 AT L.E. SWEEP = 45 DEG., M = 0.9





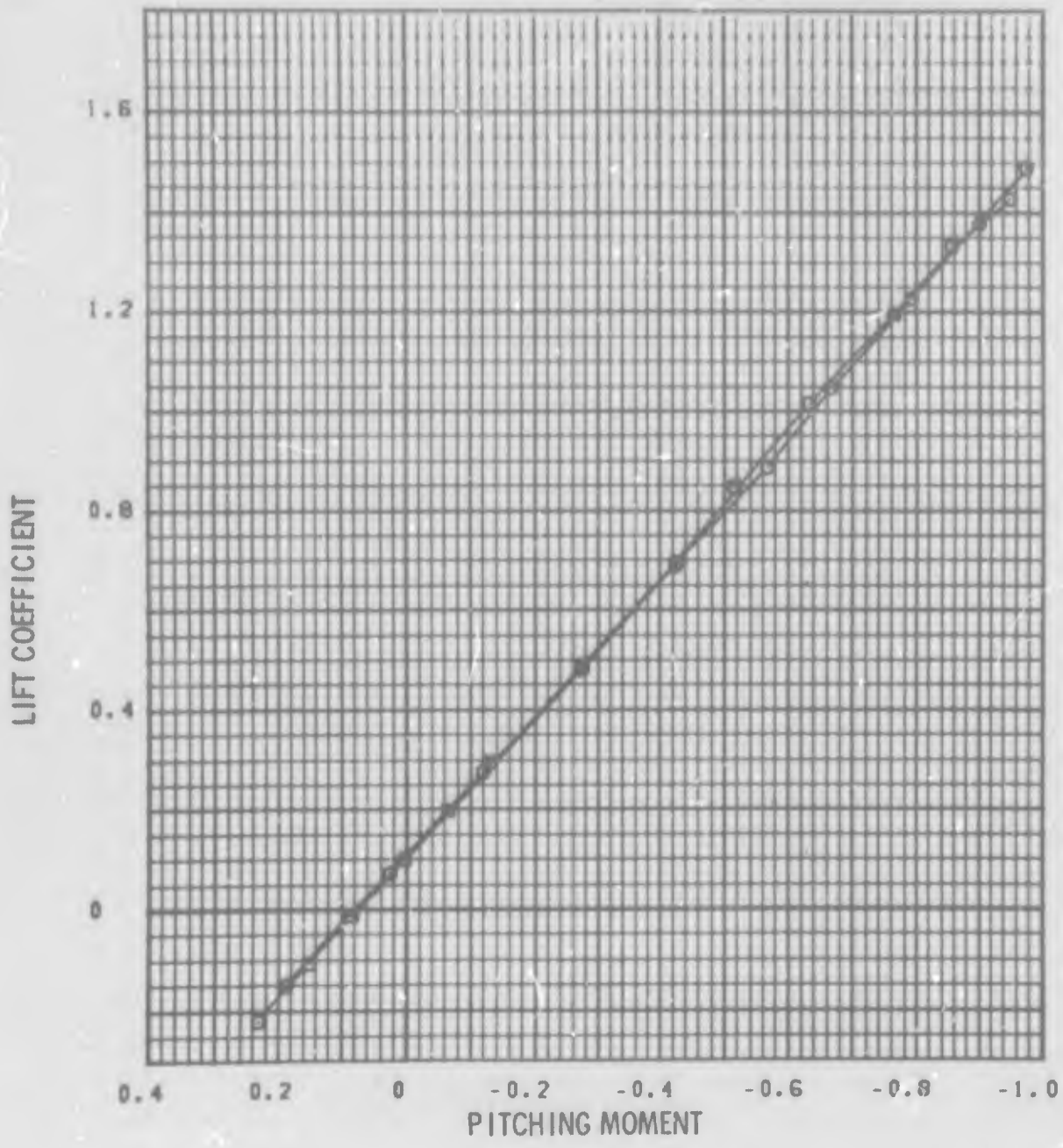
| SYM | TEST            | PART | RV...      |
|-----|-----------------|------|------------|
| ○   | AEDC PWT TC 043 | 14   | 3.0 MI :ON |
| □   | CAL G52 253     | 266  | 3.0 MI :ON |

FIGURE 22b TIE-IN COMPARISON BETWEEN CAL AND PWT 4T  
 AT L.E. SWEEP = 45 DEG. M 1.2



| SYM | TEST            | PART | RV/T        |
|-----|-----------------|------|-------------|
| ⊙   | AEOC PWT TC 043 | 14   | 3.0 MILLION |
| ⊠   | CAL G52-253     | 266  | 3.0 MILLION |

FIGURE 22b TIE-IN COMPARISON BETWEEN CAL AND PWT 4T  
AT L.E. SWEEP = 45 DEG., M = 1.2



| SYM | TEST            | PART | RN/FT       |
|-----|-----------------|------|-------------|
| ⊙   | AEDC PWT TC-043 | 14   | 3.0 MILLION |
| ⊠   | CAL G52-253     | 266  | 3.0 MILLION |

FIGURE 22b TIE-IN COMPARISON BETWEEN CAL AND PWT 4T  
AT L.E. SWEEP = 45 DEG., M = 1.2

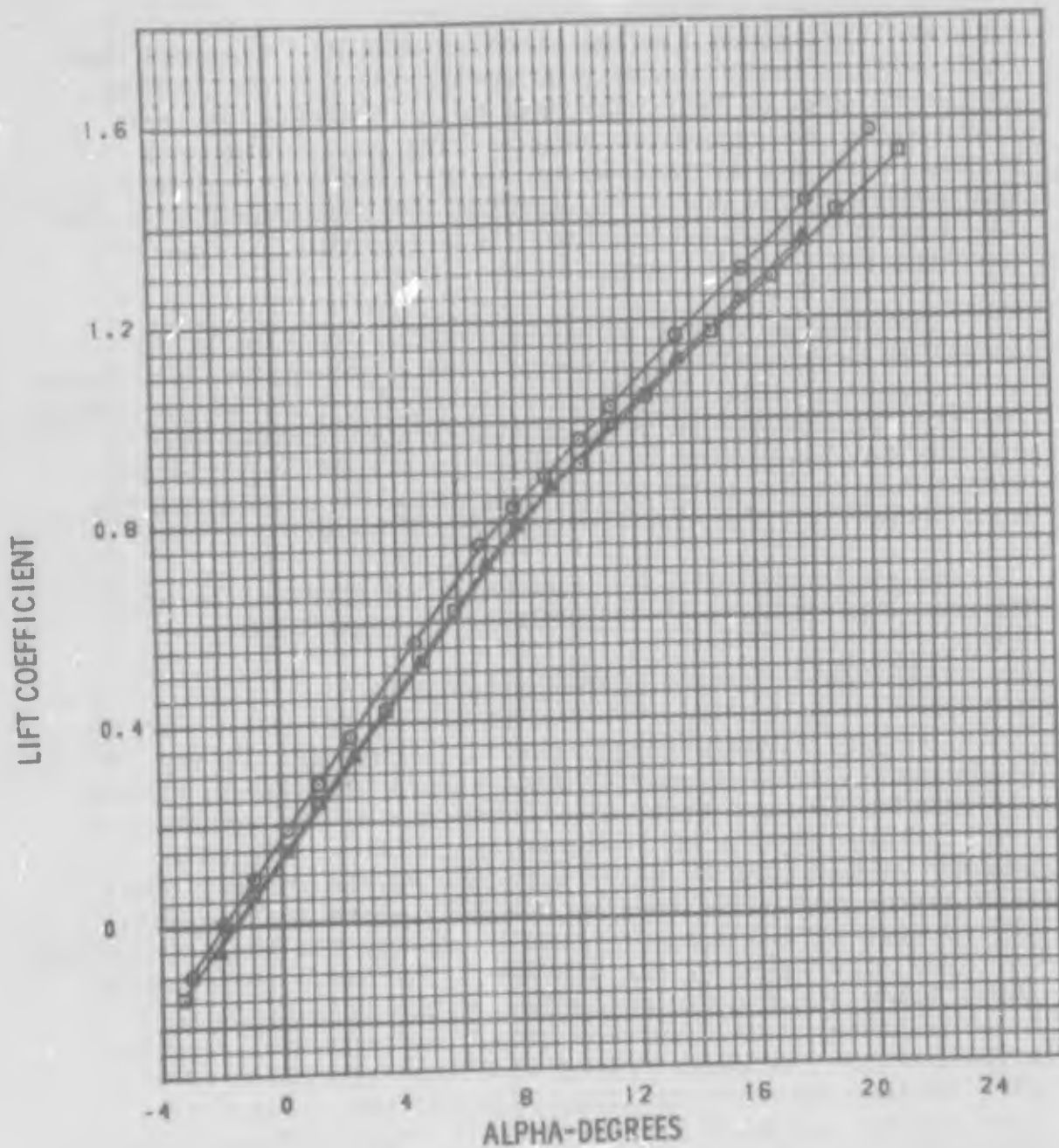
Both the lift curve and the pitching moment curve show that the nonlinearities due to flow separation are less severe in the 4T than in CAL. The drag polar exhibits the most distressing discrepancies because both polar shape and minimum drag are altered in an adverse sense in the 4T. Again the effects due to separation are less pronounced with the significant exception that the drag level at high lift coefficients is much larger in the 4T.

The general trends of these results are similar to anomalies previously obtained in other General Dynamics tests at subsonic speeds. Because of the differences in the models and the differences in wall configurations between the 4T and the CAL facilities, the anomalies cannot be strictly attributed to the relative size between the models and the wind tunnels on the basis of the tie-in data.

At  $M = 1.2$  much better agreement is obtained between the two sets of data as illustrated in Figure 22b.

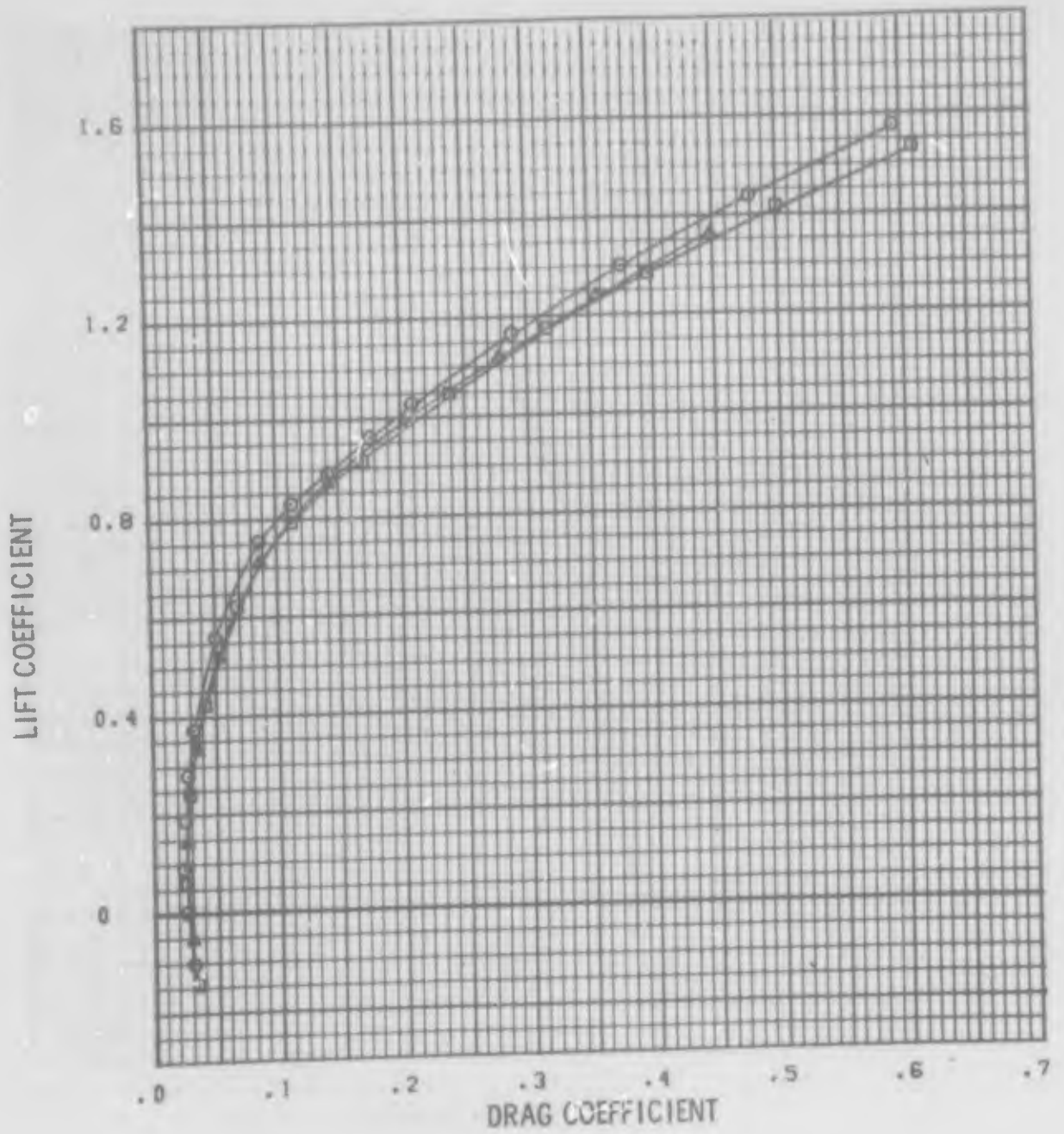
## 2. LEDE CONFIGURATION LONGITUDINAL DATA

The LEDE configurations tested in both the 4T and 16T tests were identical and the wind tunnel wall configurations are similar in that both facilities are of the porous wall type and have the holes inclined to the flow. For the present program the 4T walls were set at six percent porosity except for a few runs at  $M = 1.2$ , where the porosity was changed to 4.8 percent. Wall porosity for the 16T facility is fixed at a value of six percent. Therefore, the results shown below are a good indication of the effects of model size relative to test section size. Longitudinal data are presented for the basic "clean wing" configuration (i.e., wing leading-edge and trailing-edge devices all set at zero degrees deflection) in Figure 23, Mach numbers of 0.7, 0.9 and 1.2. Other comparisons can be made from the available data, but those shown are representative of the general trends.



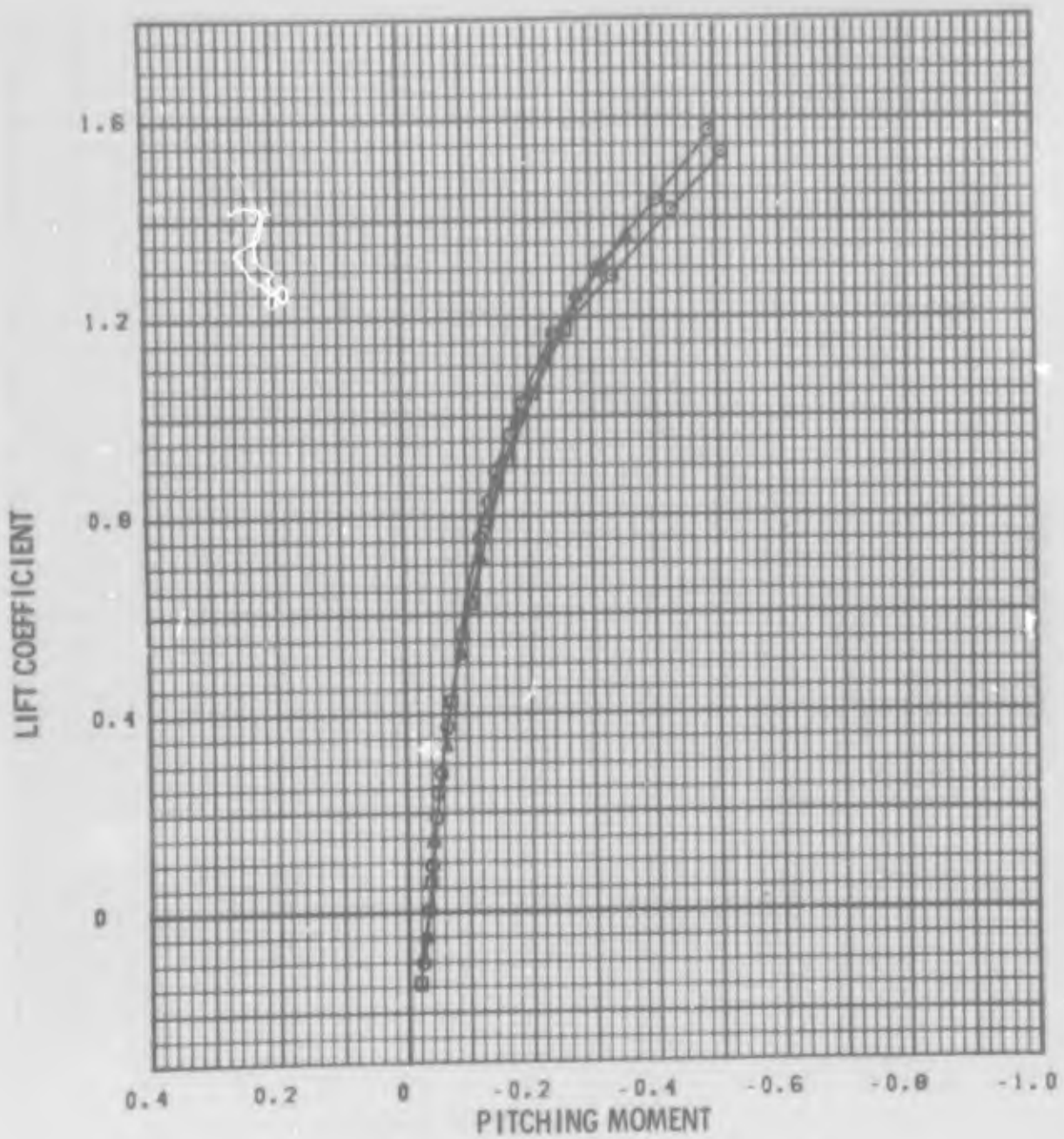
| SYM | TEST           | PART |
|-----|----------------|------|
| ⊙   | PWT 16T TF-216 | 49   |
| ⊠   | PWT 4T TC-043  | 268  |
| ▲   | PWT 4T TC-043  | 438  |

FIGURE 23a LEDE, CLEAN WING COMPARISON BETWEEN PWT 4T AND 16T  
M = 0.7



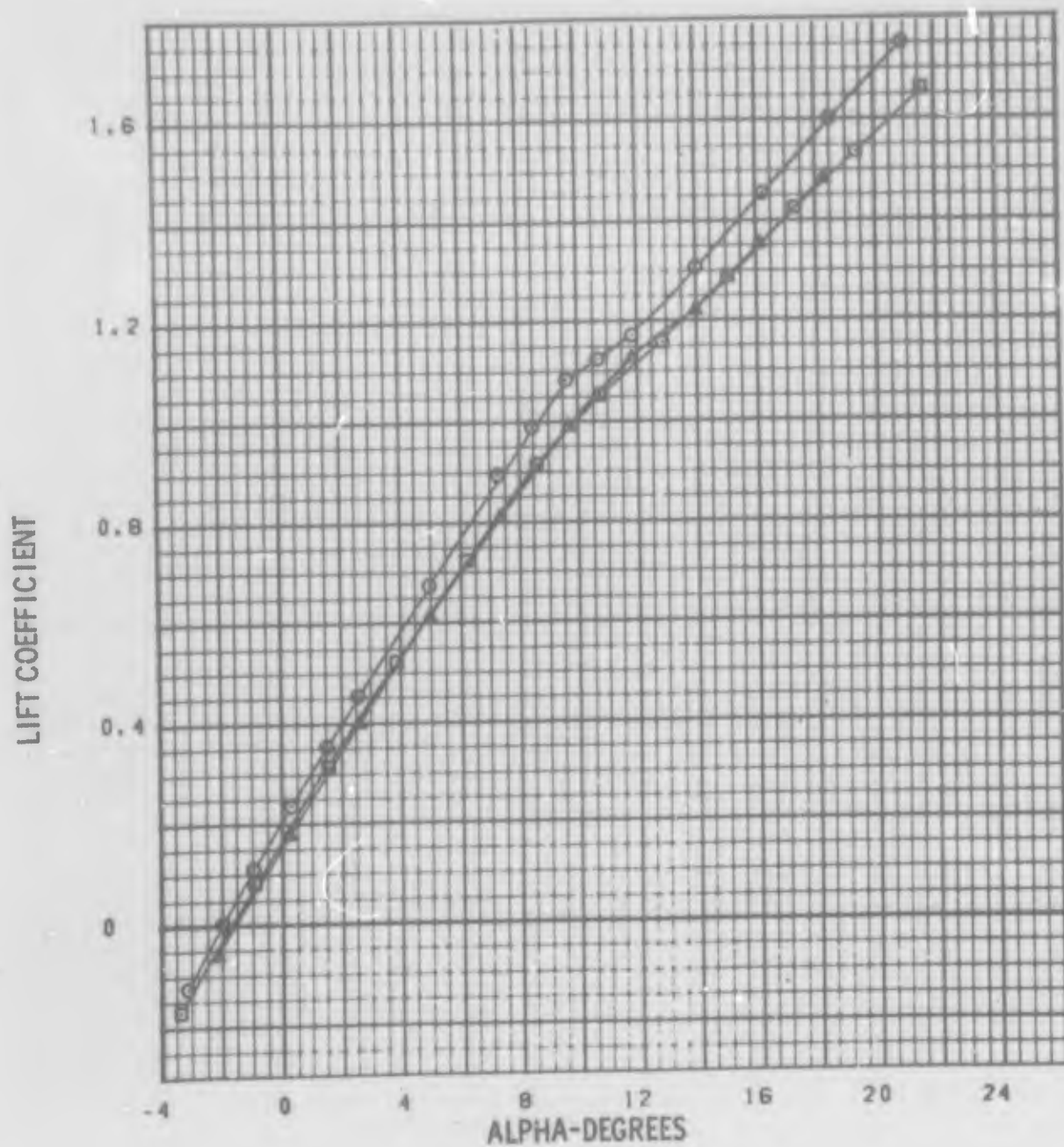
| SYM | TEST           | PART |
|-----|----------------|------|
| ○   | PWT 16T TF-216 | 49   |
| □   | PWT 4T TC-043  | 268  |
| ▲   | PWT 4T TC-043  | 438  |

FIGURE 23a LEDE. CLEAN WING COMPARISON BETWEEN PWT 4T AND 16T  
M = 0.7



| SYM | IFS'           | PART |
|-----|----------------|------|
| ⊙   | PWT 16T IF 216 | 49   |
| ⊠   | PWT 4T IC 043  | 268  |
| ▲   | PWT 4T IC 043  | 438  |

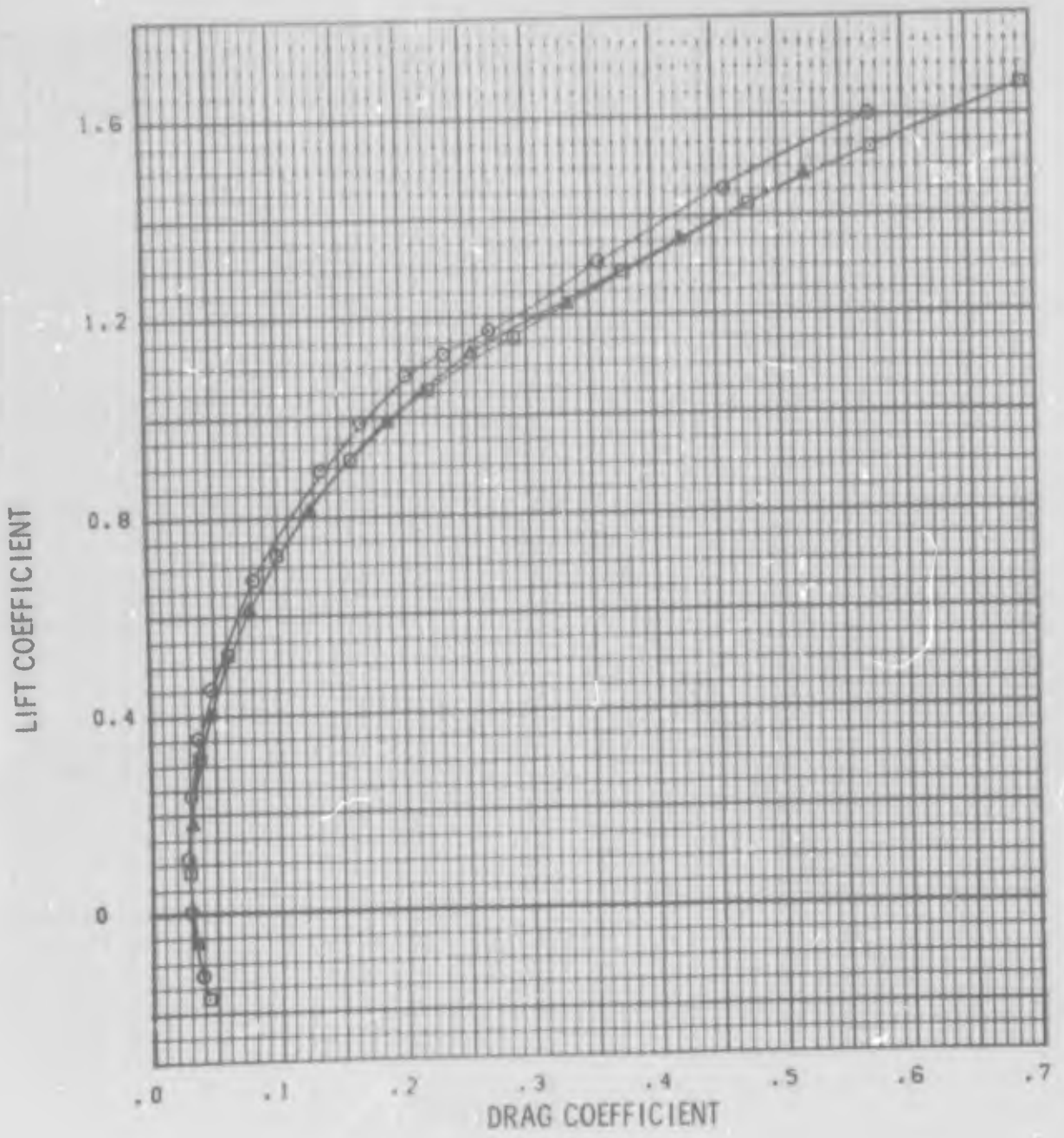
FIGURE 23a LEDE. CLEAN WING COMPARISON BETWEEN PWT 4T AND 16T  
M = 0.7



| SYM | TES            | PART |
|-----|----------------|------|
| ○   | PWI 161 TF 216 | 52   |
| □   | PWI 41 TC 043  | 264  |
| ▲   | PWI 41 TC 043  | 441  |

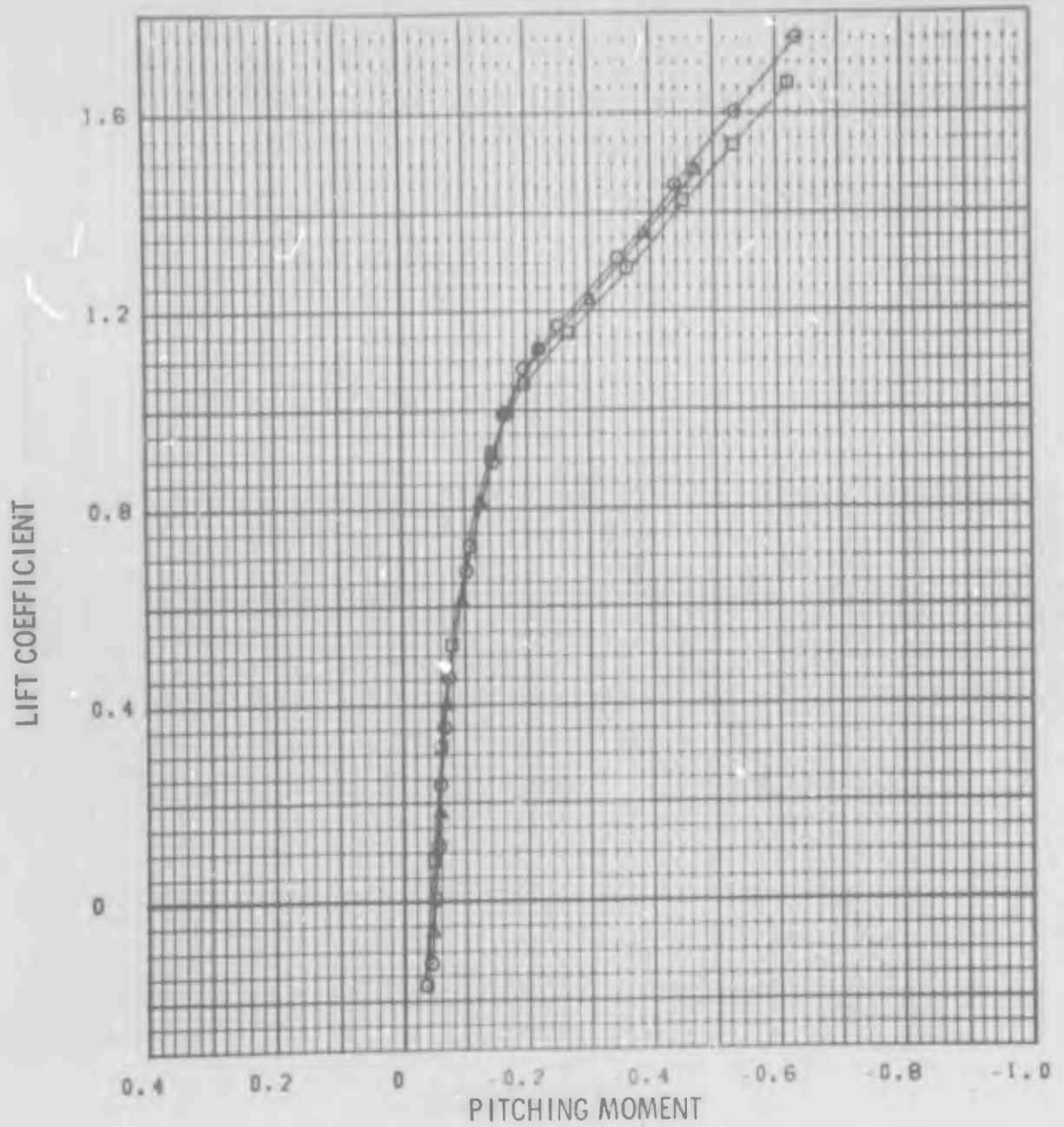
FIGURE 23b LEDE. CLEAN WING COMPARISON BETWEEN PWI 41 AND 161  
M 0.9





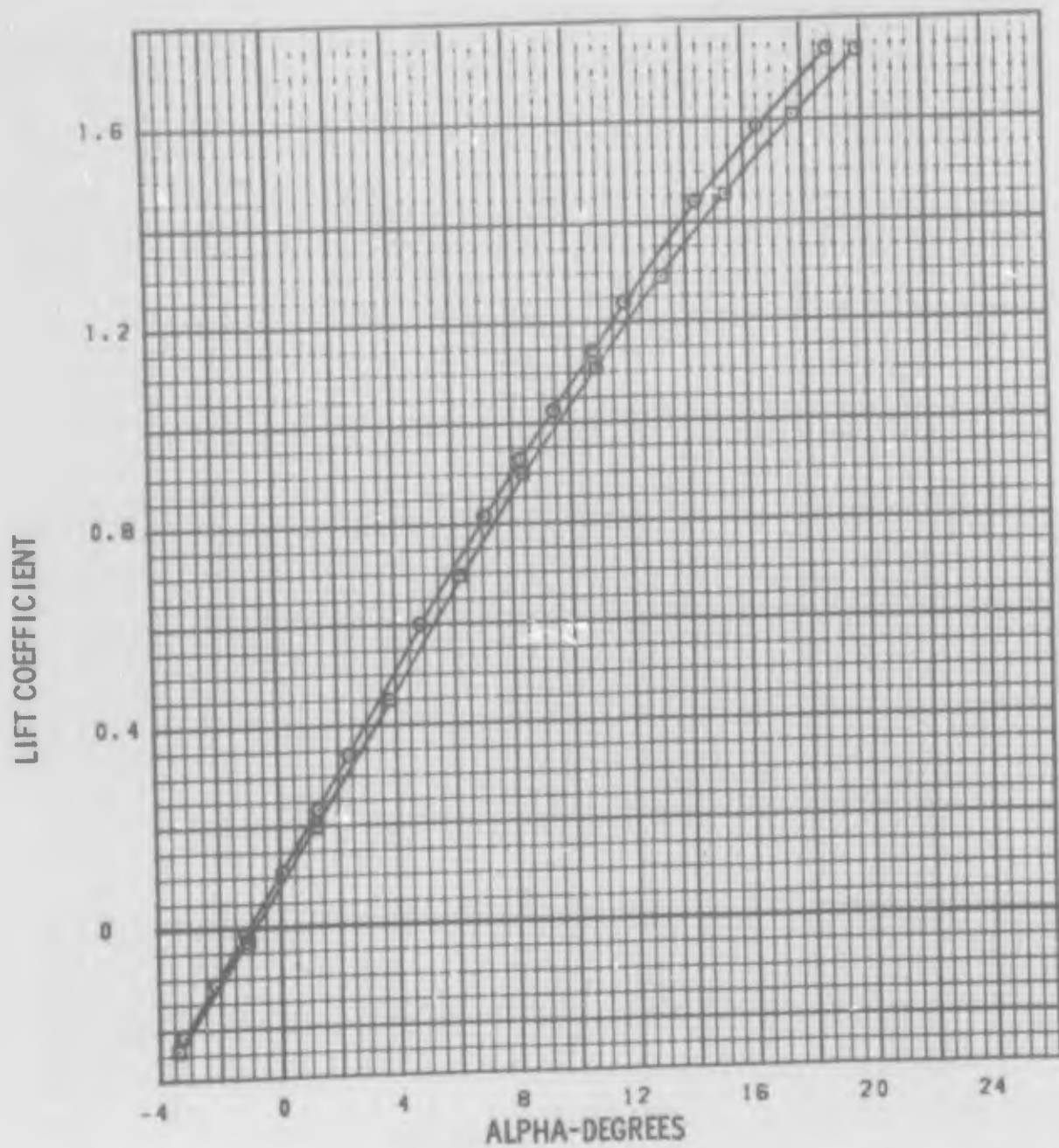
| SYM | TEST           | PART |
|-----|----------------|------|
| ○   | PWT 161 TR 216 | 52   |
| □   | PWT 41 TC 043  | 264  |
| ▲   | PWT 41 TC 043  | 441  |

FIGURE 23b LEDE, CLEAN WING COMPARISON BETWEEN PWT 41 AND 161  
M = 0.9



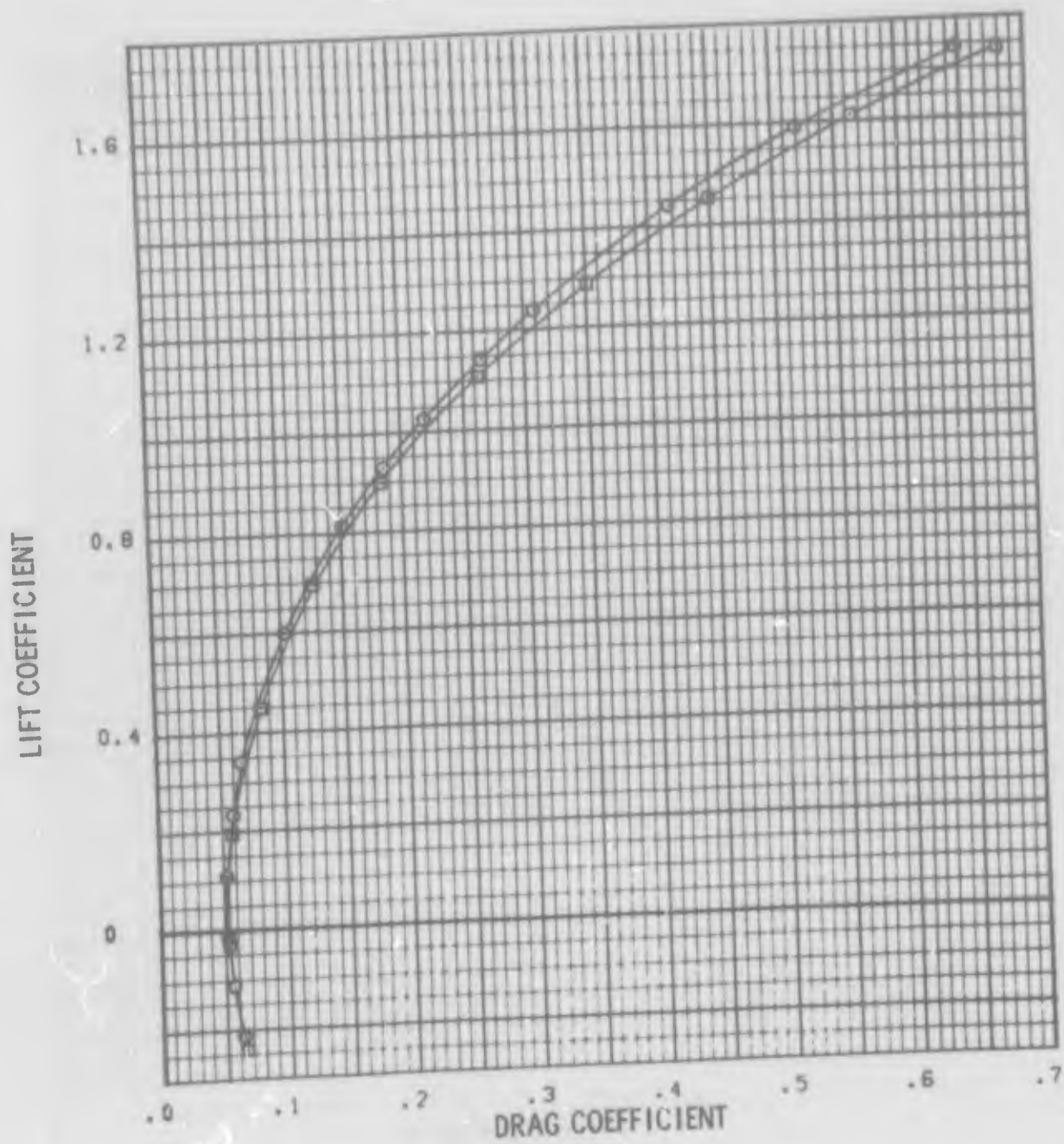
| SYM | TEST           | PART |
|-----|----------------|------|
| ○   | PWT 16T TF 216 | 52   |
| □   | PWT 4T TC 043  | 264  |
| ▲   | PWT 4T TC 043  | 441  |

FIGURE 23b LEDE. CLEAN WING COMPARISON BETWEEN PWT 4T AND 16T  
M = 0.9



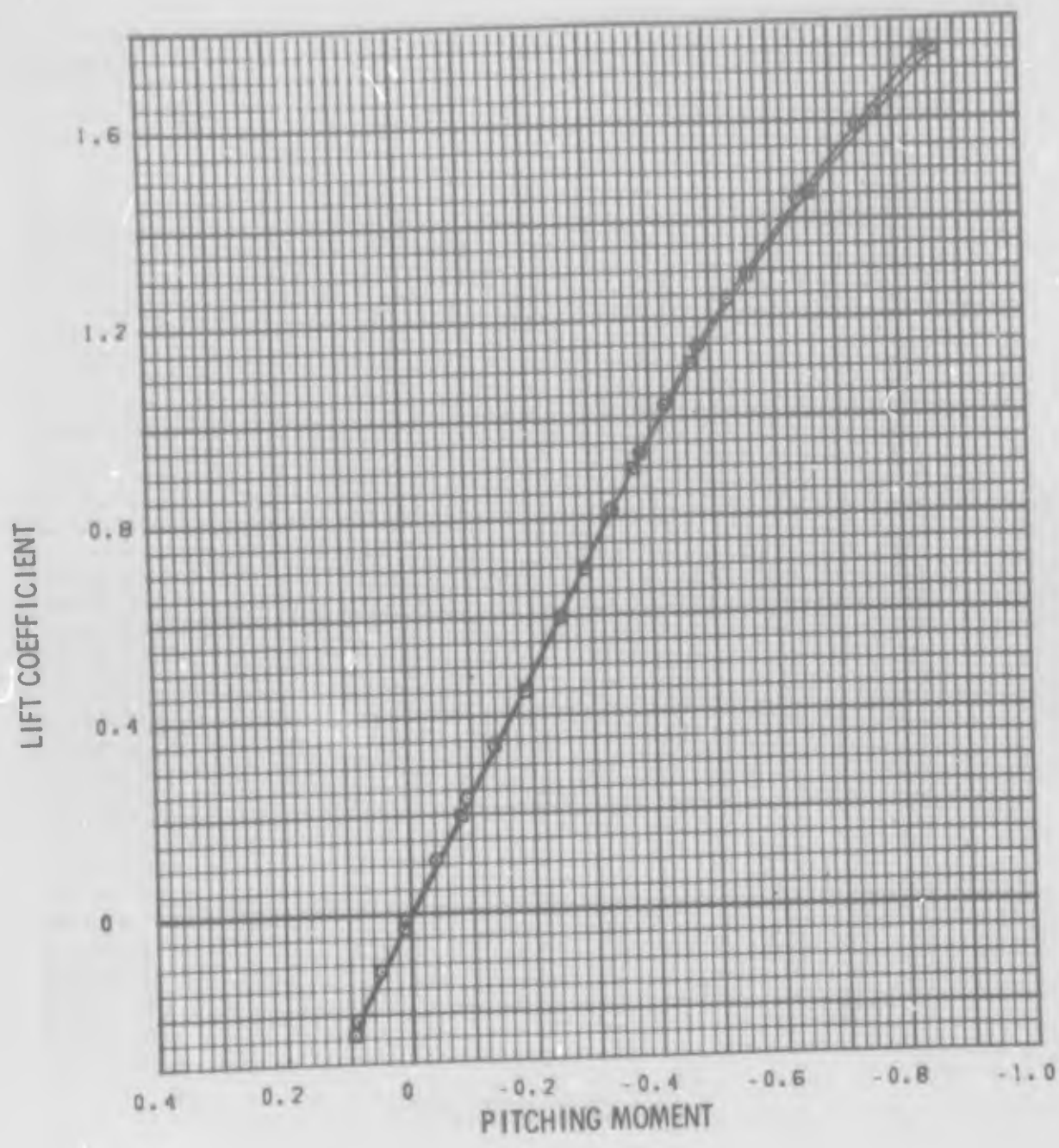
| SYM | TEST           | PART |
|-----|----------------|------|
| ⊙   | PWT 16T TF-216 | 54   |
| ⊠   | PWT 4T TC-043  | 269  |

FIGURE 23c LEDE. CLEAN WING COMPARISON BETWEEN PWT 4T AND 16T  
M = 1.2



|     |               |     |
|-----|---------------|-----|
| SYM | 15'           | 16' |
| ○   | PW 16' IC 216 | 54  |
| □   | PW 4' IC 043  | 269 |

FIGURE 23c LIFT-DRAG WING COMPARISON BETWEEN PW 4' AND 16'  
M = 1.2



| SYM | TEST           | PART |
|-----|----------------|------|
| ⊙   | PWT 161 TC 216 | 54   |
| ⊠   | PWT 41 TC 043  | 269  |

FIGURE 23c LEDE. CLEAN WING COMPARISON BETWEEN PWT 41 AND 161  
M = 1.2

The LEDE configuration results are qualitatively similar to those for the tie-in runs, but the discrepancies in subsonic lift and drag measurements between the two facilities are more pronounced. Some of the differences are caused by significant flow angularity in the 4T facility.

In general, the effects on lift and drag are large while discrepancies in pitching moment are small except at high angles of attack where flow separation exists. Specifically, the effects of flow separation occur at lower lift coefficients in the 4T facility and show less abrupt nonlinearities in the lift and pitching moment data than occur in the 16T. The drag polar shapes in the 4T are degraded both for nonseparated flow and separated flow conditions.

The wall interference problem at transonic speeds is not new and attempts have been made to derive theoretical methods to correct measured data. Reference 20 presents a discussion of methods related to slotted wall facilities and experimental data obtained in two different size tunnels on the same subsonic-transport-type model. Application of the theoretical wall corrections to data from both the smaller facility and the larger facility generally brings the two sets into agreement for unseparated flow conditions. The report points out that no comparable method of correcting data obtained in porous wall facilities exists at the present time.

A preliminary assessment of the calibration test data obtained by ARO on the LEDE model indicates that using different wall-porosity settings in the 4T can improve the degree of agreement between 4T and 16T data. More detailed analysis of that data must be done before any definitive guidelines can be established. The AEDC report will probably be available by the time the present report is distributed (Reference 21).

Data presented in this report have not been corrected for either flow angularity or wall effects. Therefore, the reader is cautioned to use data from the 16T test to establish comparisons between the longitudinal characteristics of the LEDE configuration and a particular configuration of interest.

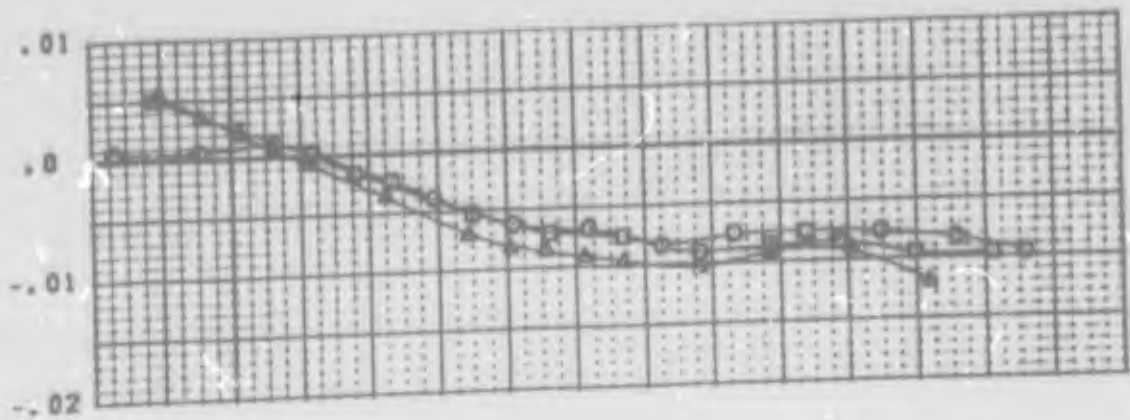
Lift, drag and pitching moment effects caused by control surface deflections may be obtained by using incremental data obtained at fixed angles of attack. However, the differences in angle of zero lift between 4T and 16T data, where appropriate, should be accounted for in applying such incremental data.

### 3. LATERAL-DIRECTIONAL DATA

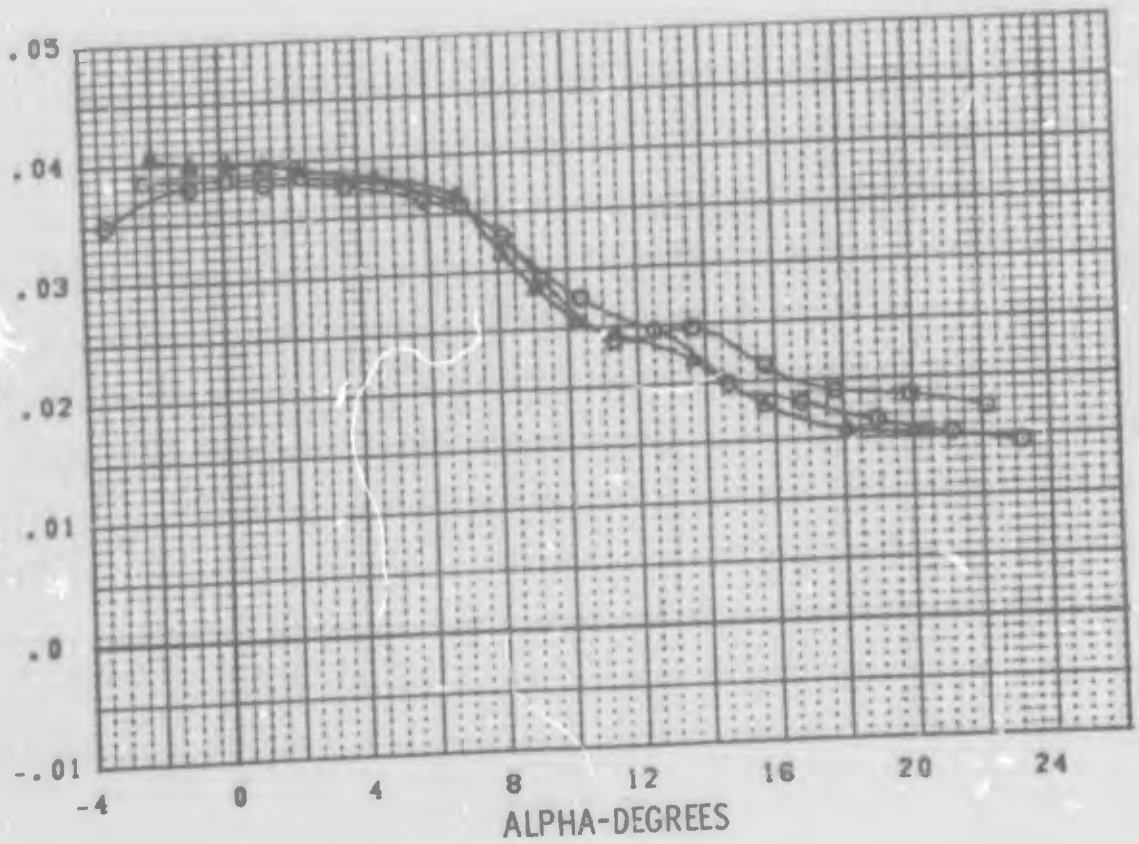
Rolling and yawing moment measurements obtained during each of the three separate tunnel entries are given in Figure 24 for the mid-aileron configuration. The rolling moment data demonstrate that effects due to flow separation are more abrupt for the 16T measurements (note in particular data for 0.9 Mach number). Differences in level are also apparent at high angles of attack, mainly for the 16T data at 0.9 Mach number, although some differences are evident for other conditions and also between the two entries in PWT 4T. Yawing moment differences are most pronounced for the low angle of attack transonic conditions between the two sets of data from 4T. It is believed, these differences resulted from installing the strut flapper-door-seal prior to the second entry to minimize the floor cavity near the strut. During the first entry, considerable lateral motion of the model was observed visually that was not present in the later 4T test. In general, it is quite evident that the repeatability between entries and facilities is much better at supersonic conditions than at transonic conditions.

Comparisons between PWT 4T and 16T data for differential leading edge deflection in combination with the mid- and extended-span ailerons are shown in Figures 25 and 26. This data, for 0.9 Mach number, exhibits variations between facilities similar to those noted previously for the mid aileron configuration. Note particularly the more abrupt variations in rolling moment with angle of attack for the 16T data.

YAWING MOMENT



ROLLING MOMENT

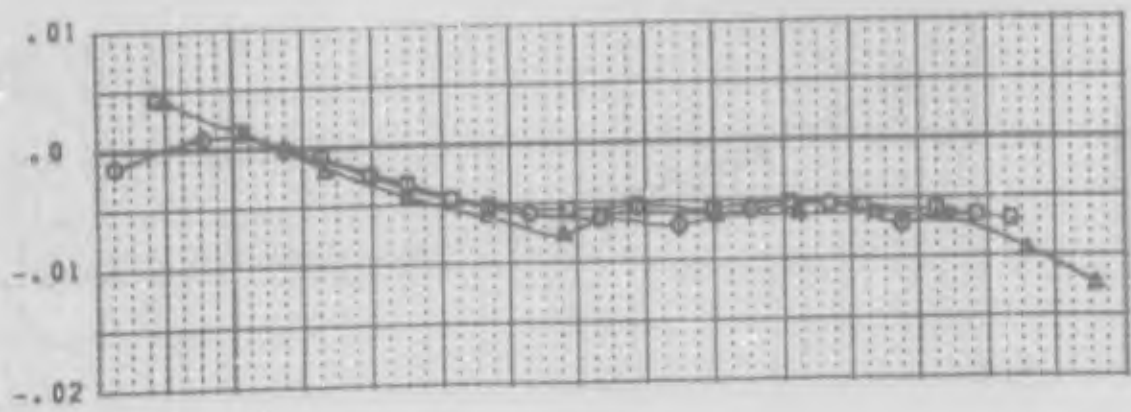


| SYM | TEST           | PART | L.E. (L/R) | AILERON (L/R) |
|-----|----------------|------|------------|---------------|
| ○   | PWT 4T TC-043  | 215  | K1 0/0     | MID 20/-20    |
| □   | PWT 4T TC-043  | 410  | K1 0/0     | MID 20/-20    |
| △   | PWT 16T TF-216 | 13   | K1 0/0     | MID 20/-20    |

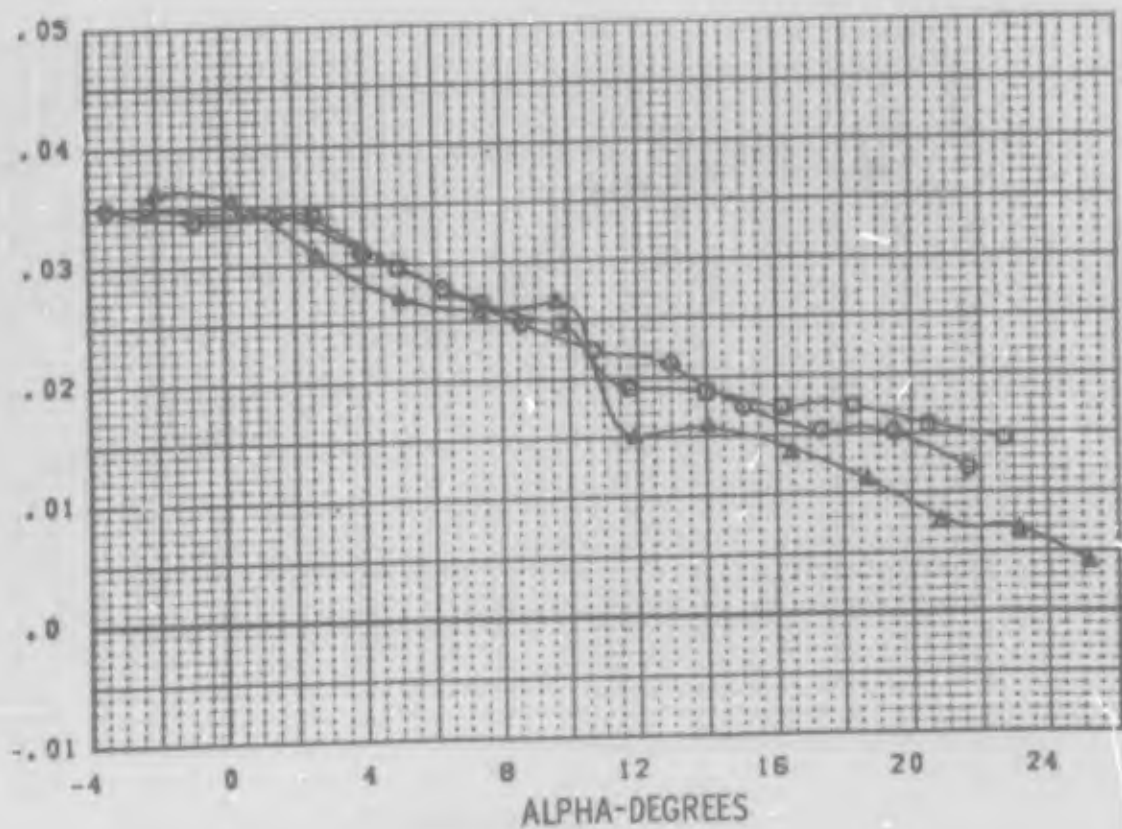
FIGURE 24a LEDE, MID AILERONS. COMPARISONS BETWEEN PWT 4T AND 16T. M = 0.7



YAWING MOMENT

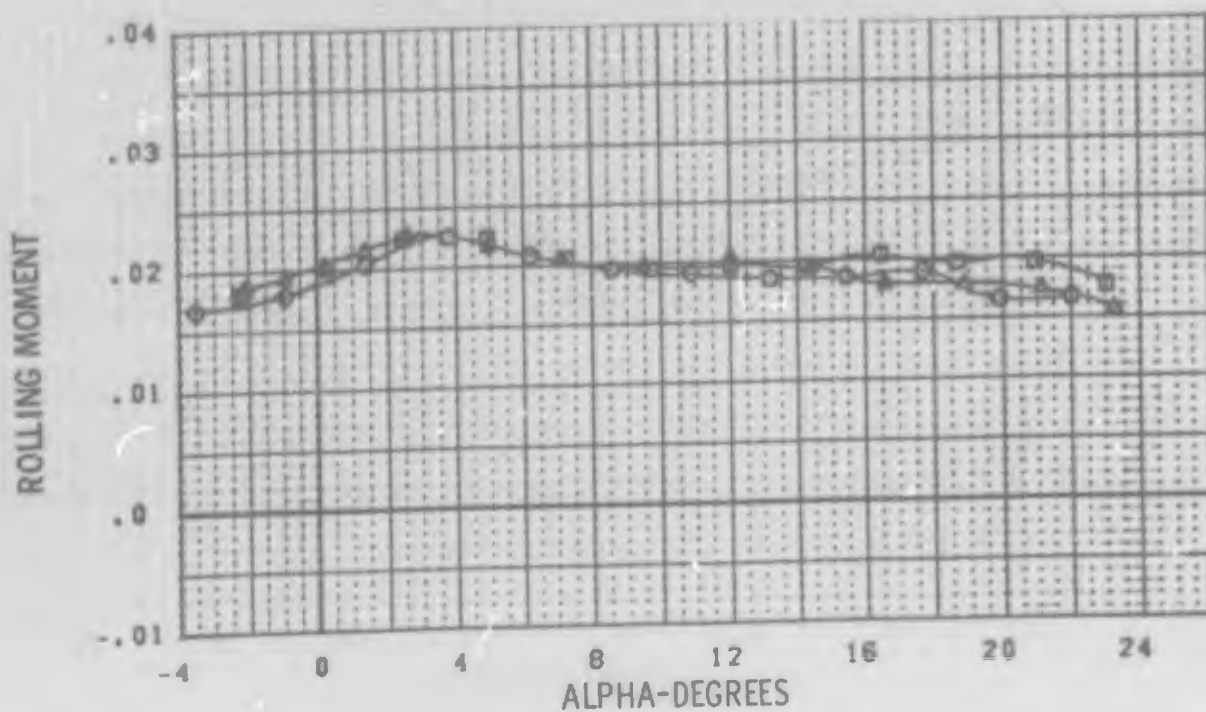
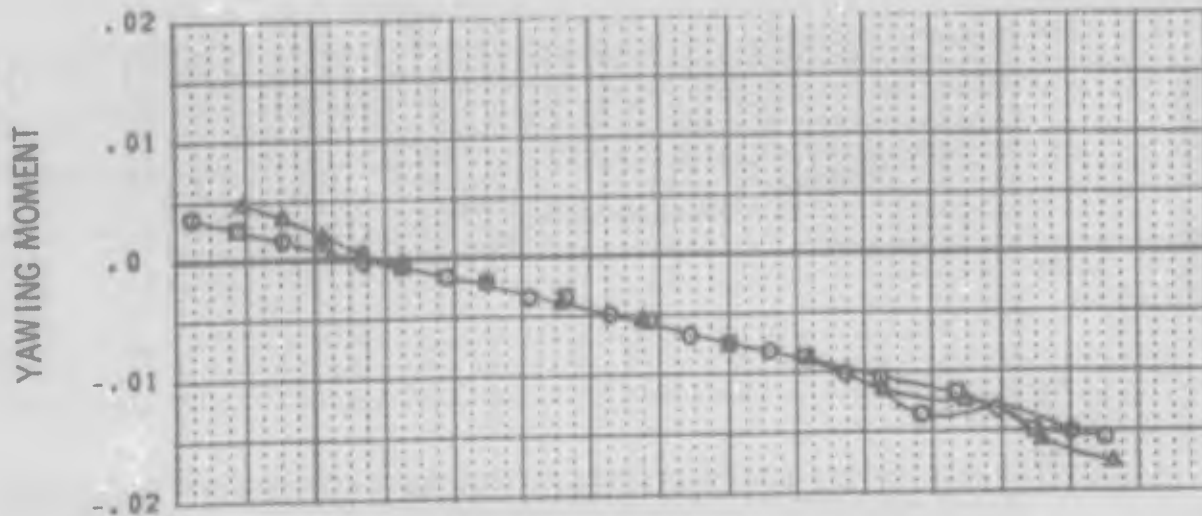


ROLLING MOMENT



| SYM | TEST           | PART | L.E. (L/R) | AILERON (L/R) |
|-----|----------------|------|------------|---------------|
| ○   | PWT 4T TC-043  | 213  | K1 0/0     | MID 20/-20    |
| □   | PWT 4T TC-043  | 412  | K1 0/0     | MID 20/-20    |
| ▲   | PWT 16T TF-216 | 8    | K1 0/0     | MID 20/-20    |

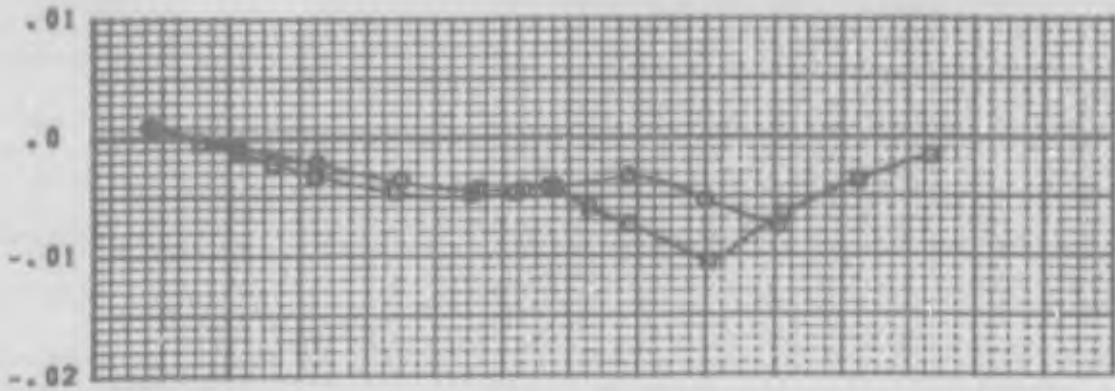
FIGURE 24b LEDE, MID AILERONS. COMPARISONS BETWEEN PWT 4T AND 16T. M = 0.9



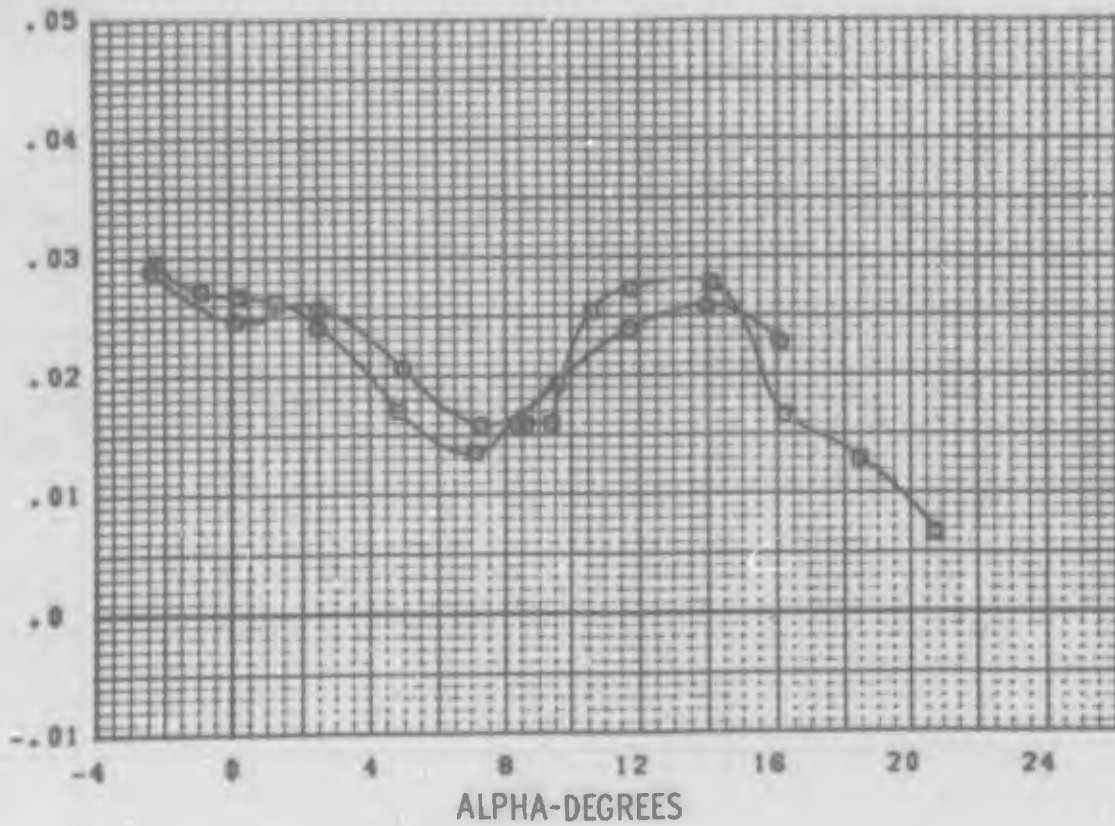
| SYM | TEST           | PART | L.E. (L/R) | AILERON (L/R) |
|-----|----------------|------|------------|---------------|
| ○   | PWT 4T TC-043  | 216  | K1 0/0     | MID 20/-20    |
| □   | PWT 4T TC-043  | 414  | K1 0/0     | MID 20/-20    |
| ▲   | PWT 16T TF-216 | 10   | K1 0/0     | MID 20/-20    |

FIGURE 24c LEDE, MID AILERONS. COMPARISONS BETWEEN PWT 4T AND 16T. M = 1.2

YAWING MOMENT



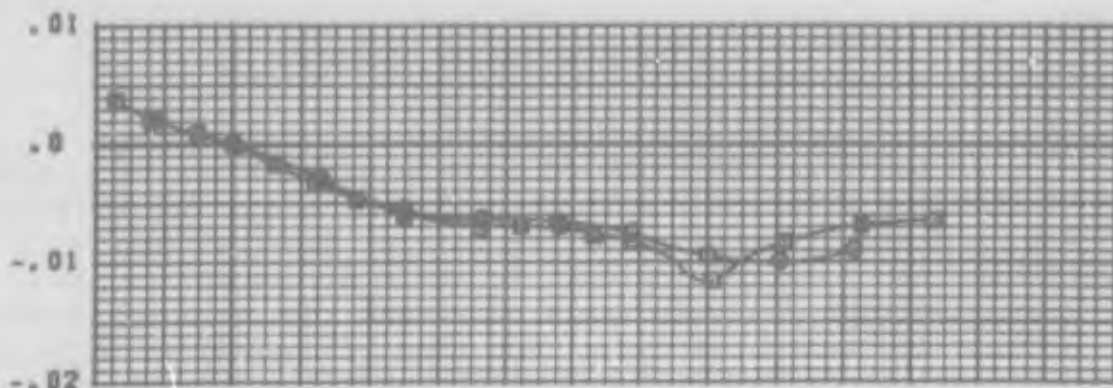
ROLLING MOMENT



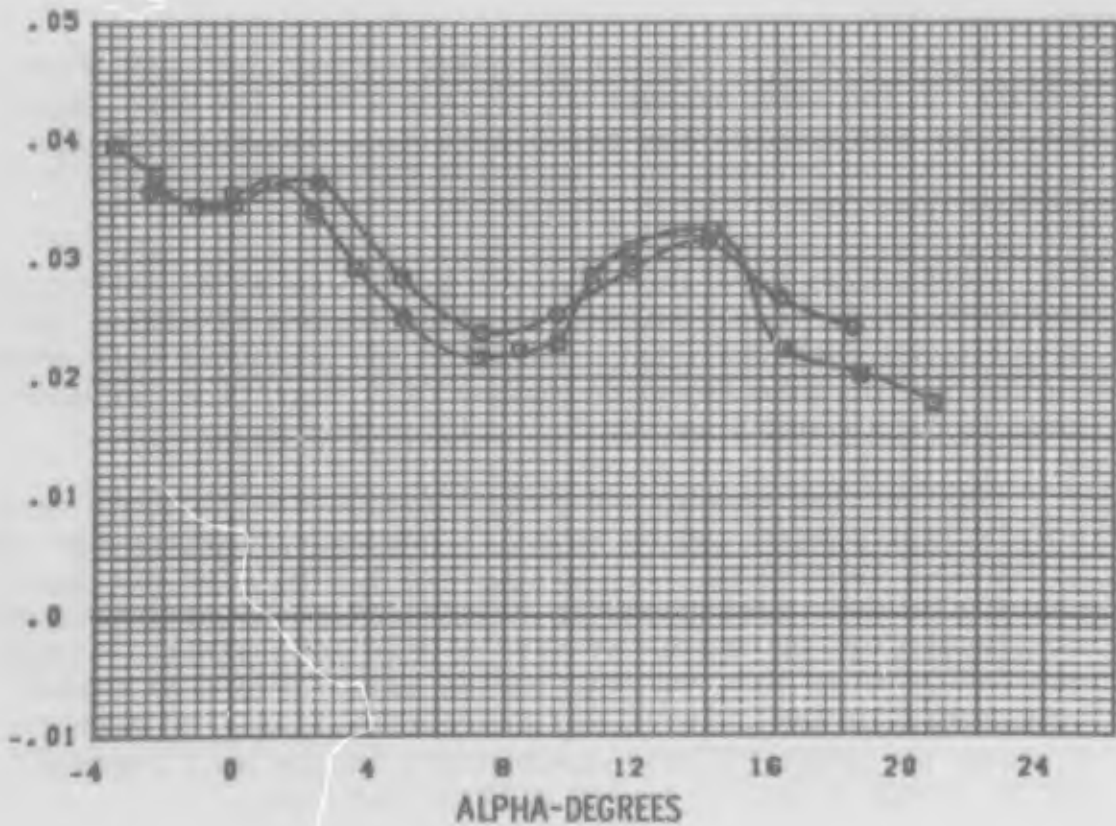
| SYM | TEST           | PART | L.E. (L/R) | AILERON (L/R) |
|-----|----------------|------|------------|---------------|
| ⊙   | PWT 4T TC-043  | 425  | K1 10/0    | MID 20/-20    |
| ⊠   | PWT 16T TF-216 | 31   | K1 10/0    | MID 20/-20    |

FIGURE 25 LEDE, DIFFERENTIAL L.E.FLAP AND MID AILERONS  
COMPARISON BETWEEN PWT 4T AND 16T M = 0.9

YAWING MOMENT



ROLLING MOMENT



| SYM | TEST           | PART | L.E. (L/R) | AILERON (L/R)  |
|-----|----------------|------|------------|----------------|
| G   | PWT 4T TC-043  | 513  | K1 10/0    | 3 SEGM. 20/-20 |
| Q   | PWT 16T TF-216 | 60   | K1 10/0    | 3 SEGM. 20/-20 |

FIGURE 26 LEDE. DIFFERENTIAL L.E. FLAP AND EXTENDED AILERONS  
COMPARISON BETWEEN PWT 4T AND 16T M = 0.9

## SECTION V

### REYNOLDS NUMBER EFFECTS

In general, the Reynolds numbers effects are very similar to previous experience with thin wing models. The significant effects discerned from the data as Reynolds number increases are a slight increase in angle of attack for zero lift, a slight delay in angle of attack for onset of separation effects and an accompanying reduction of separation effects at high angles of attack, and a slight positive increment in the pitching moments.

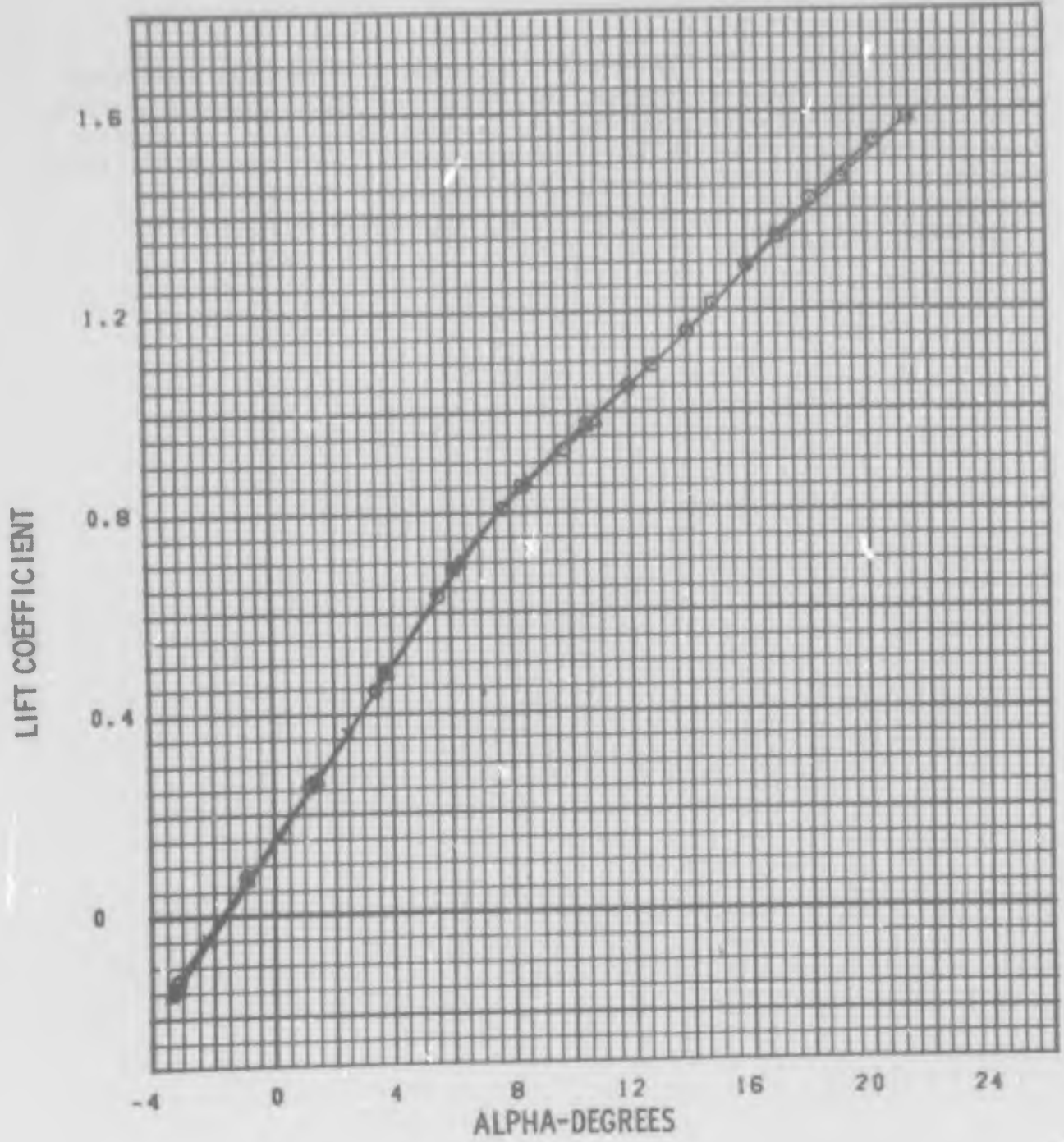
Typical lift, drag and pitching moment data are shown in Figure 27 for Mach numbers of .80 and .90. The data merely serve to corroborate the statements made above. The major effects occur between unit Reynolds numbers of 3.0 and 5.2 million per foot.

Comparison data from the 16T tests are shown in Figure 28. The effects are qualitatively similar to the 4T data. The nonlinearities obtained upon separation are slightly more severe in the 16T at unit Reynolds number of 3.0 million per foot but tend to be smoothed out at 5.2 million per foot.

The rolling moment and yawing moment coefficients were only slightly effected by Reynolds number variations over the attainable test range, 3.0 million to 6.4 million per foot, see Figure 29. Variations in aileron effectiveness were primarily limited to angles of attack near wing stall. Larger percentage-wise changes over a wide angle-of-attack range were noted in the aileron yaw characteristics. In both instances the major effects again occur in the unit Reynolds number range from 3.0 to 5.2 million per foot.

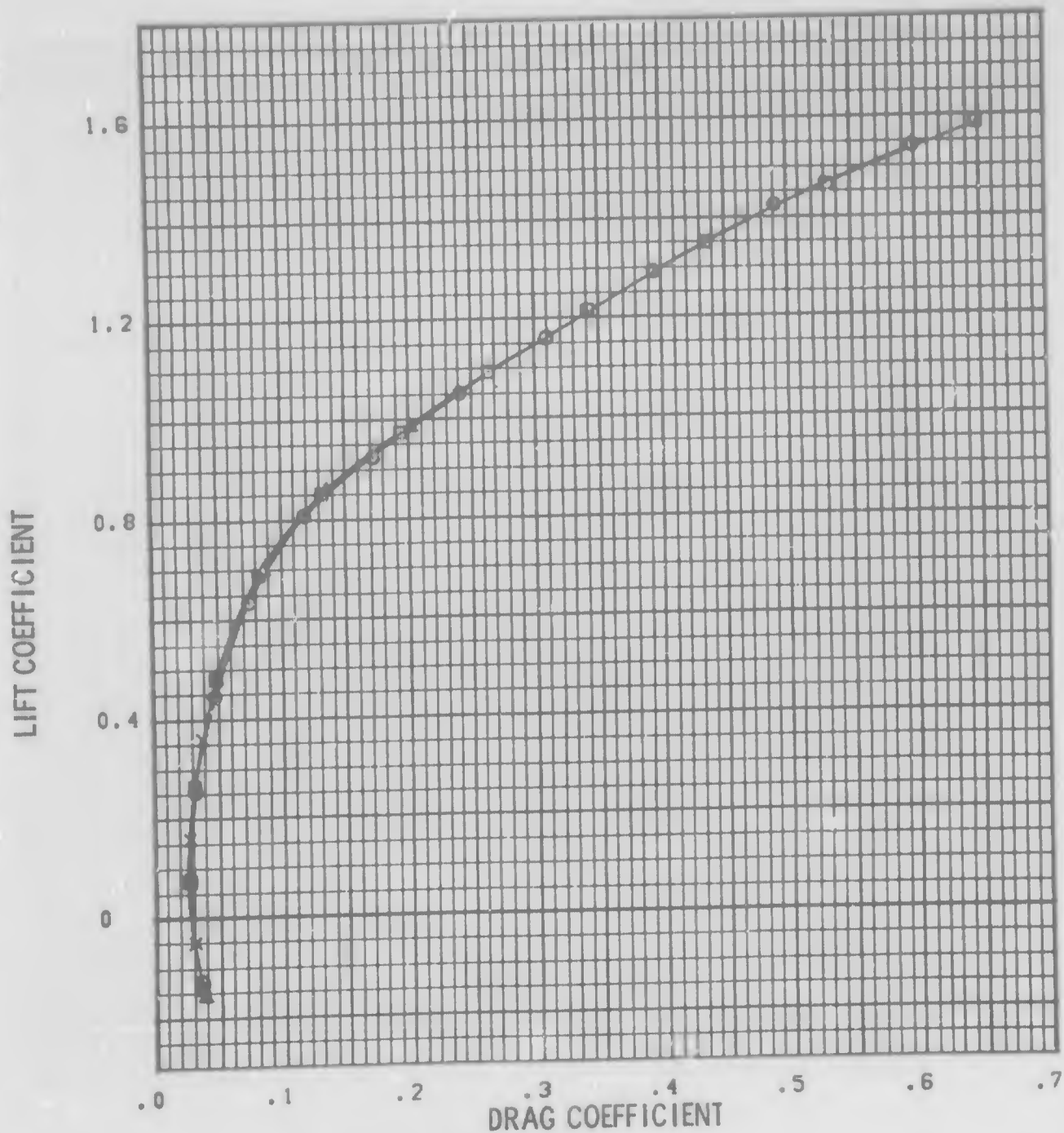
On the basis of these results we can conclude only that scaling effects will not significantly alter the qualitative conclusions drawn from comparisons of the different roll

control devices. The quantitative results should be used with some caution pending further investigation which hopefully will be accomplished either during the second phase of this program or within that time period in other studies of transonic scaling effects. It is probable that data obtained at unit Reynolds number of 5.2 million will provide reasonable estimates of incremental effects.



| SYM | TEST          | PART | RN/FT       |
|-----|---------------|------|-------------|
| ⊙   | PWT 4T TC-043 | 273  | 3.0 MILLION |
| ⊠   | PWT 4T TC-043 | 267  | 5.2 MILLION |
| ▲   | PWT 4T TC-043 | 263  | 6.2 MILLION |
| x   | PWT 4T TC-043 | 439  | 4.9 MILLION |

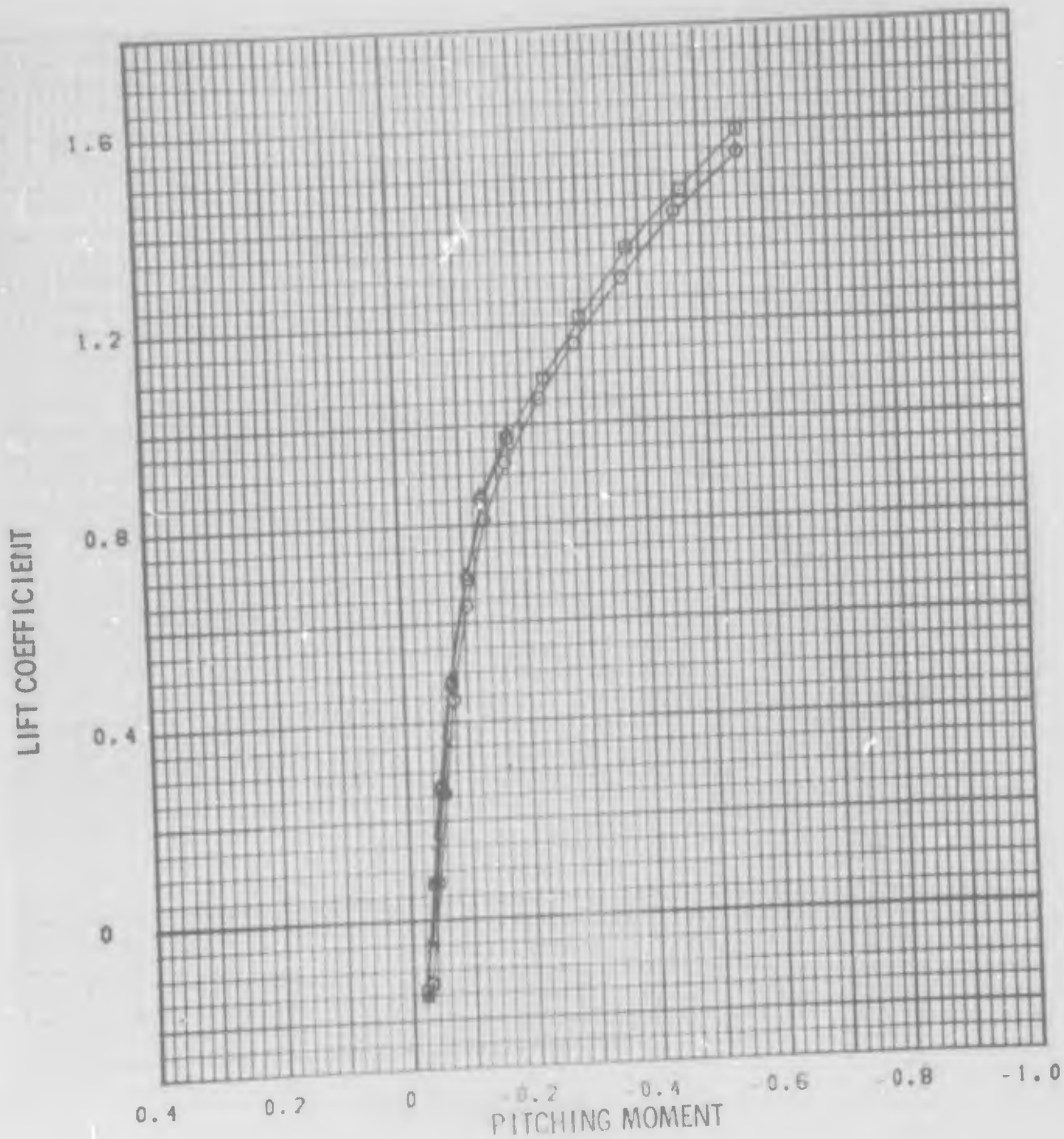
FIGURE 27a REYNOLDS NUMBER EFFECT ON LEDE CLEAN WING PWT 4T  
M = 0.8



| SYM | TEST          | PART | RN/FT       |
|-----|---------------|------|-------------|
| ⊙   | PWT 4T TC-043 | 273  | 3.0 MILLION |
| ⊠   | PWT 4T TC-043 | 267  | 5.2 MILLION |
| ▲   | PWT 4T TC-043 | 263  | 6.2 MILLION |
| x   | PWT 4T TC-043 | 439  | 4.9 MILLION |

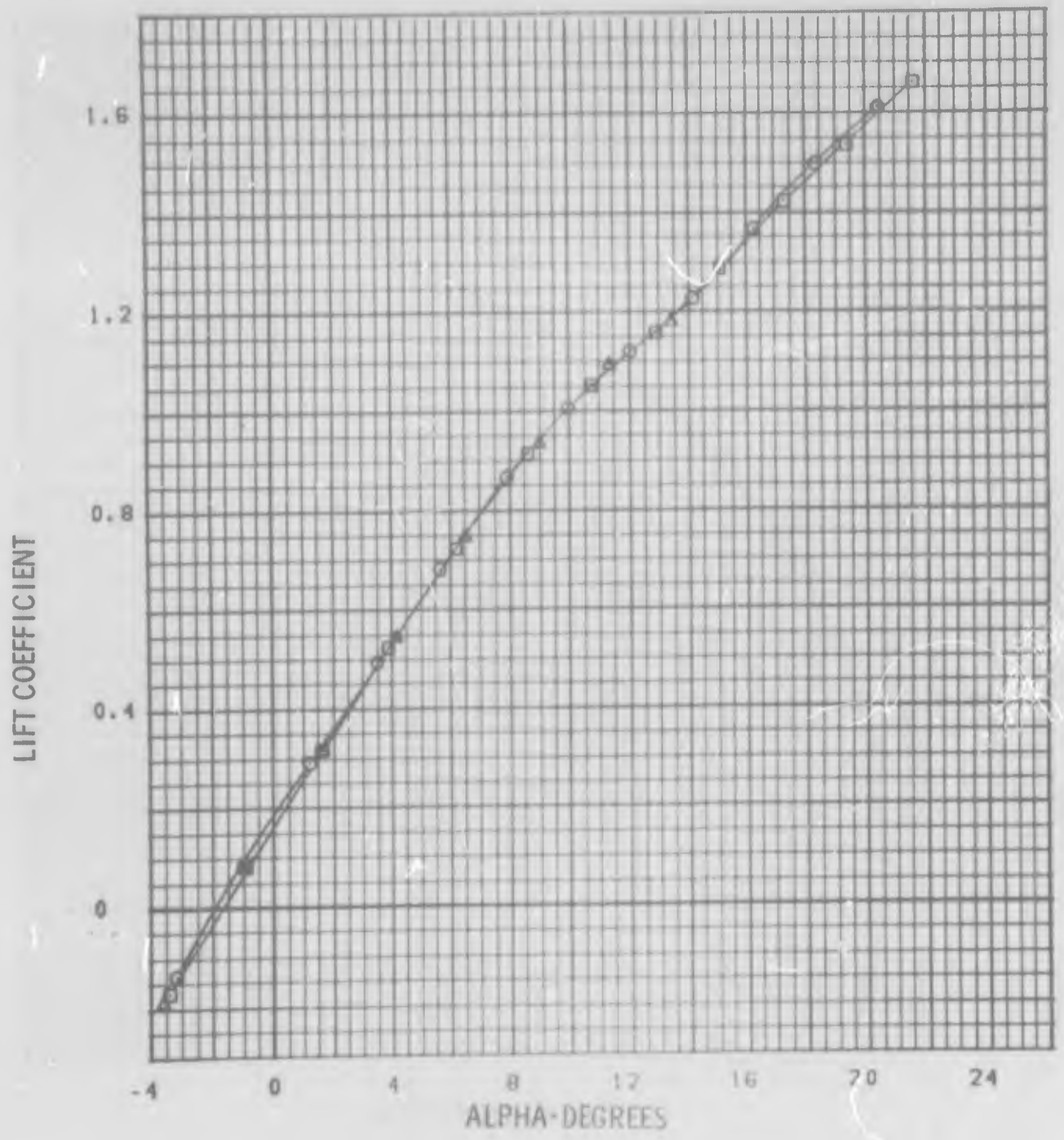
FIGURE 27a REYNOLDS NUMBER EFFECT ON LEDE CLEAN WING PWT 4T  
M = 0.8





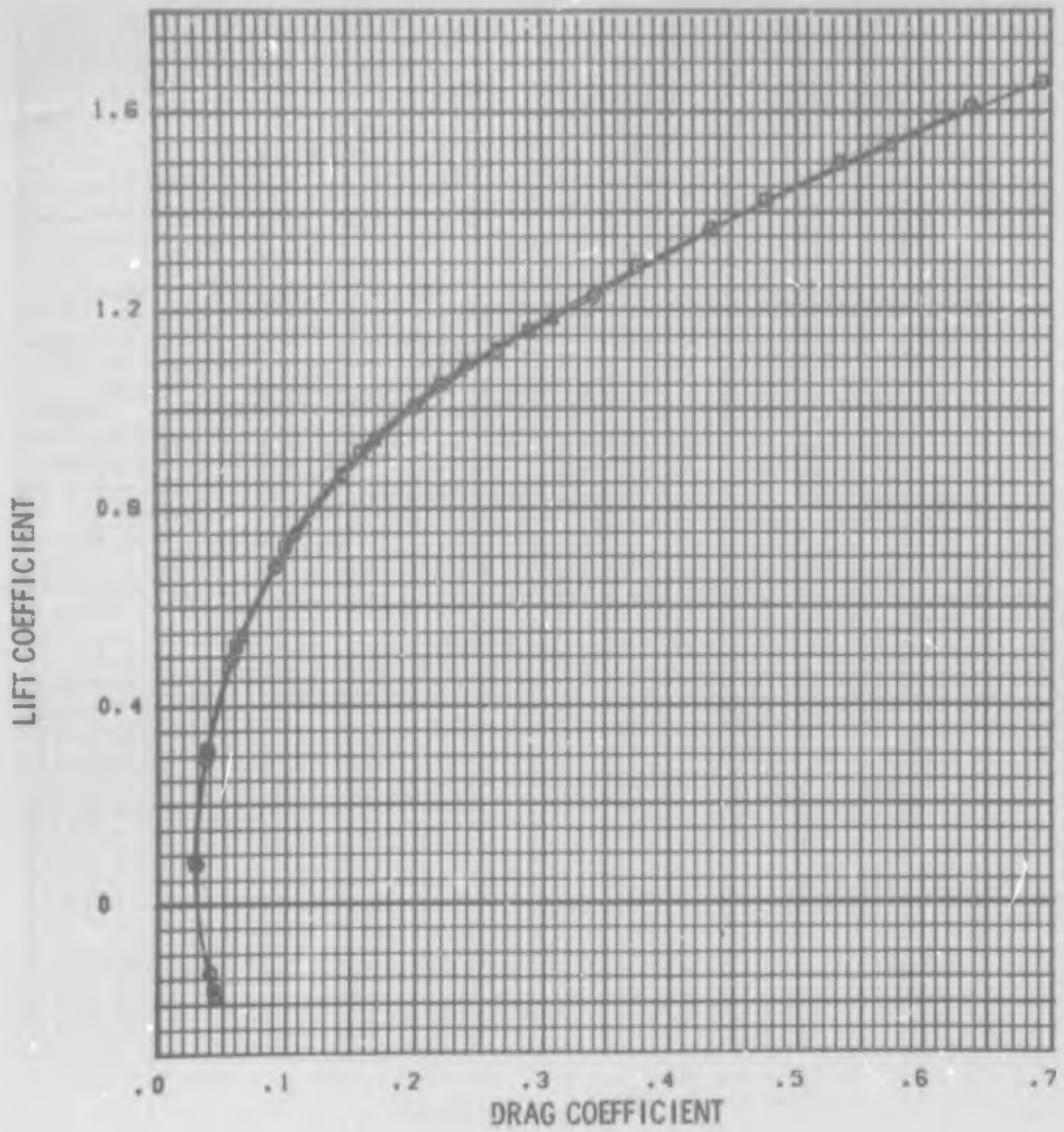
| SYM | TEST          | REYN | REYN        |
|-----|---------------|------|-------------|
| ○   | PWT 41 IC-043 | 273  | 3.0 MILLION |
| □   | PWT 41 IC-043 | 267  | 5.2 MILLION |
| △   | PWT 41 IC-043 | 263  | 6.7 MILLION |
| x   | PWT 41 IC-043 | 435  | 4.9 MILLION |

FIGURE 274 REYNOLDS NUMBER EFFECT ON LIFT CLEAN WING PWT 41



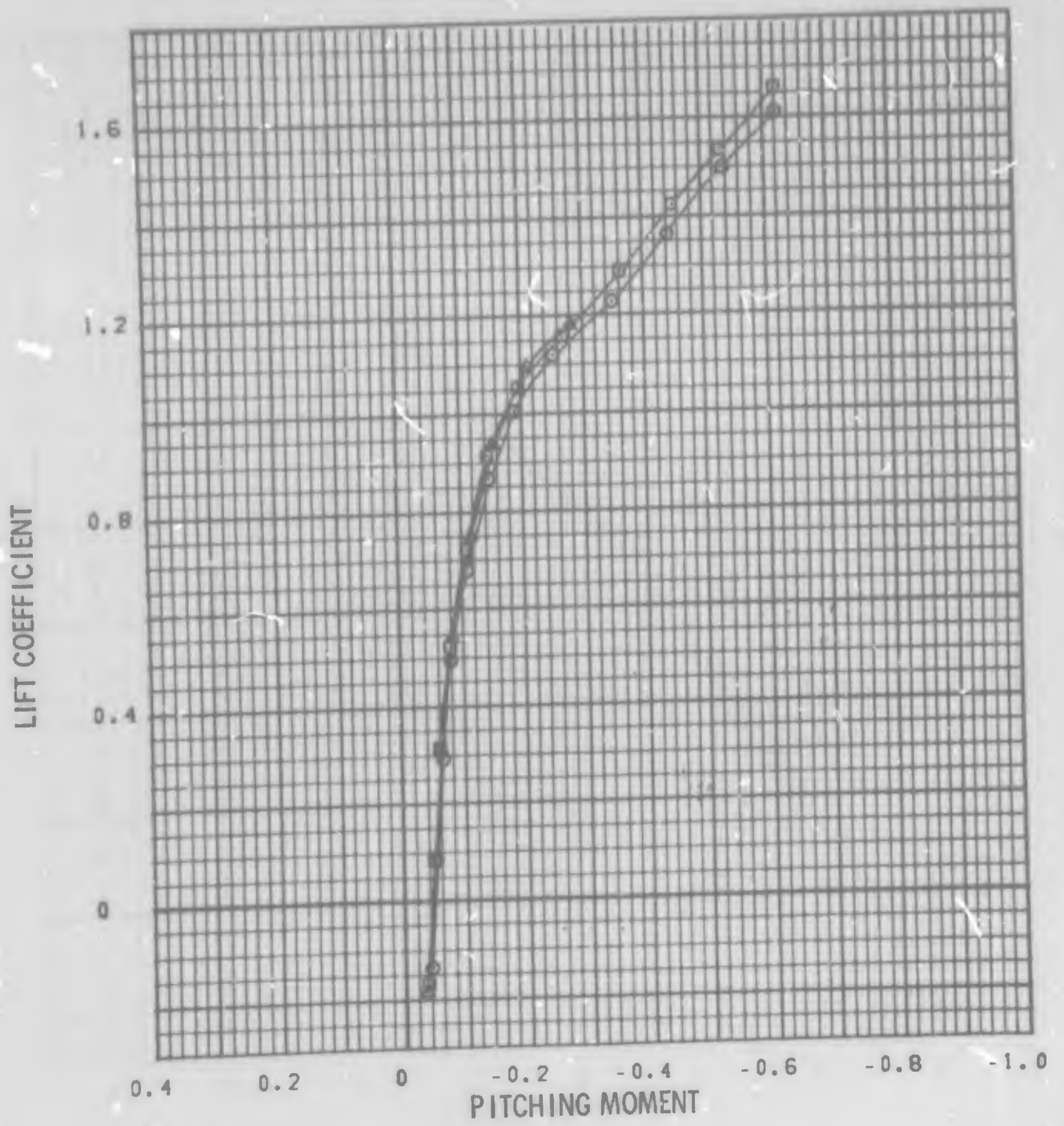
| SYM | TEST          | PART | REYNOLD     |
|-----|---------------|------|-------------|
| ○   | PWT 4T IC-043 | 272  | 3.0 MILLION |
| □   | PWT 4T IC-043 | 264  | 3.2 MILLION |
| △   | PWT 4T IC-043 | 267  | 5.5 MILLION |

FIGURE 27b REYNOLDS NUMBER EFFECT ON LEDE CLEAN WING PWT 4T  
 $M = 0.9$



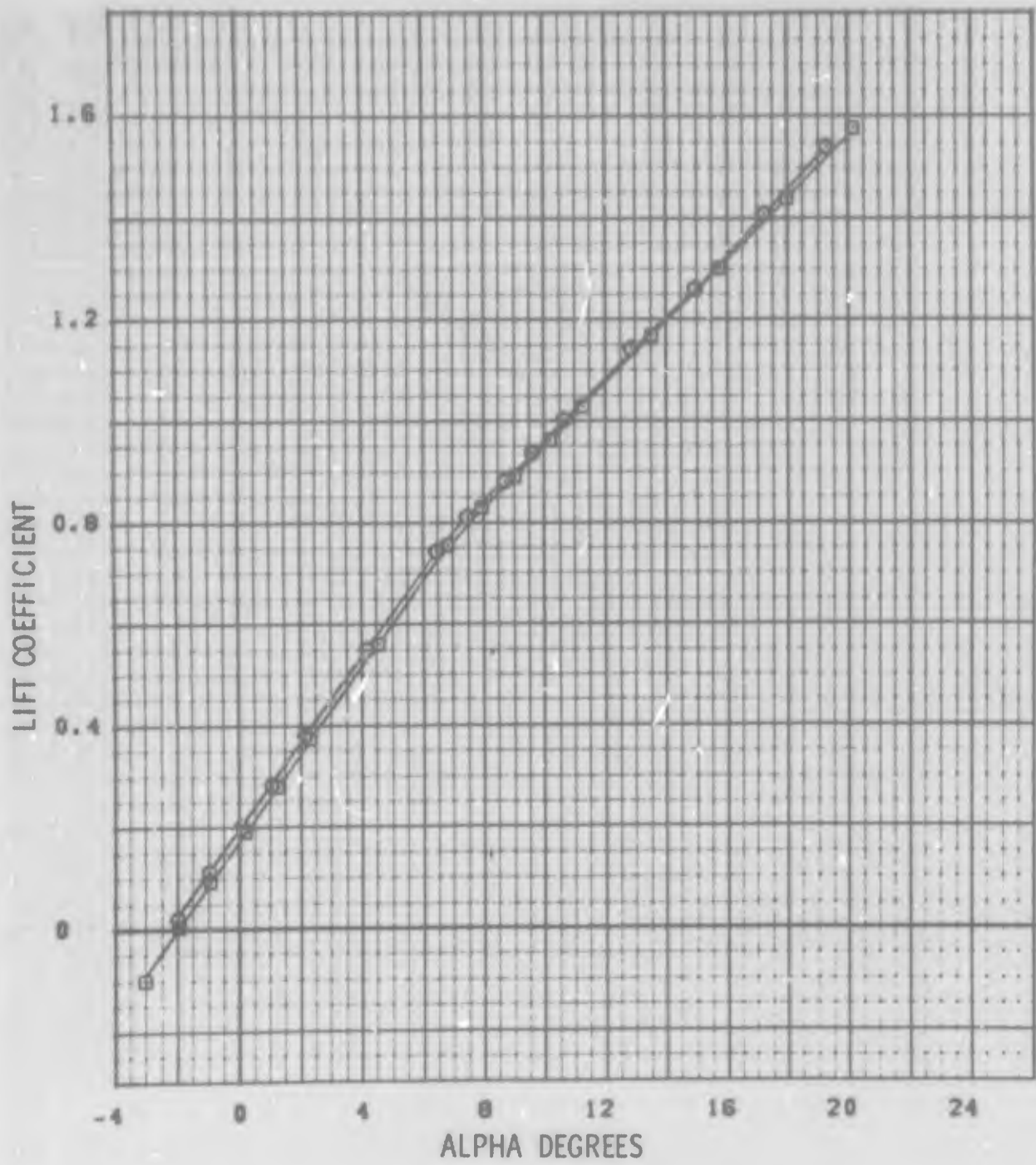
| SYM | TEST          | PART | RN/FT       |
|-----|---------------|------|-------------|
| ○   | PWT 4T TC-043 | 272  | 3.0 MILLION |
| □   | PWT 4T TC-043 | 264  | 5.2 MILLION |
| △   | PWT 4T TC-043 | 262  | 6.5 MILLION |

FIGURE 27b REYNOLDS NUMBER EFFECT ON LEDE CLEAN WING PWT 4T  
M = 0.9



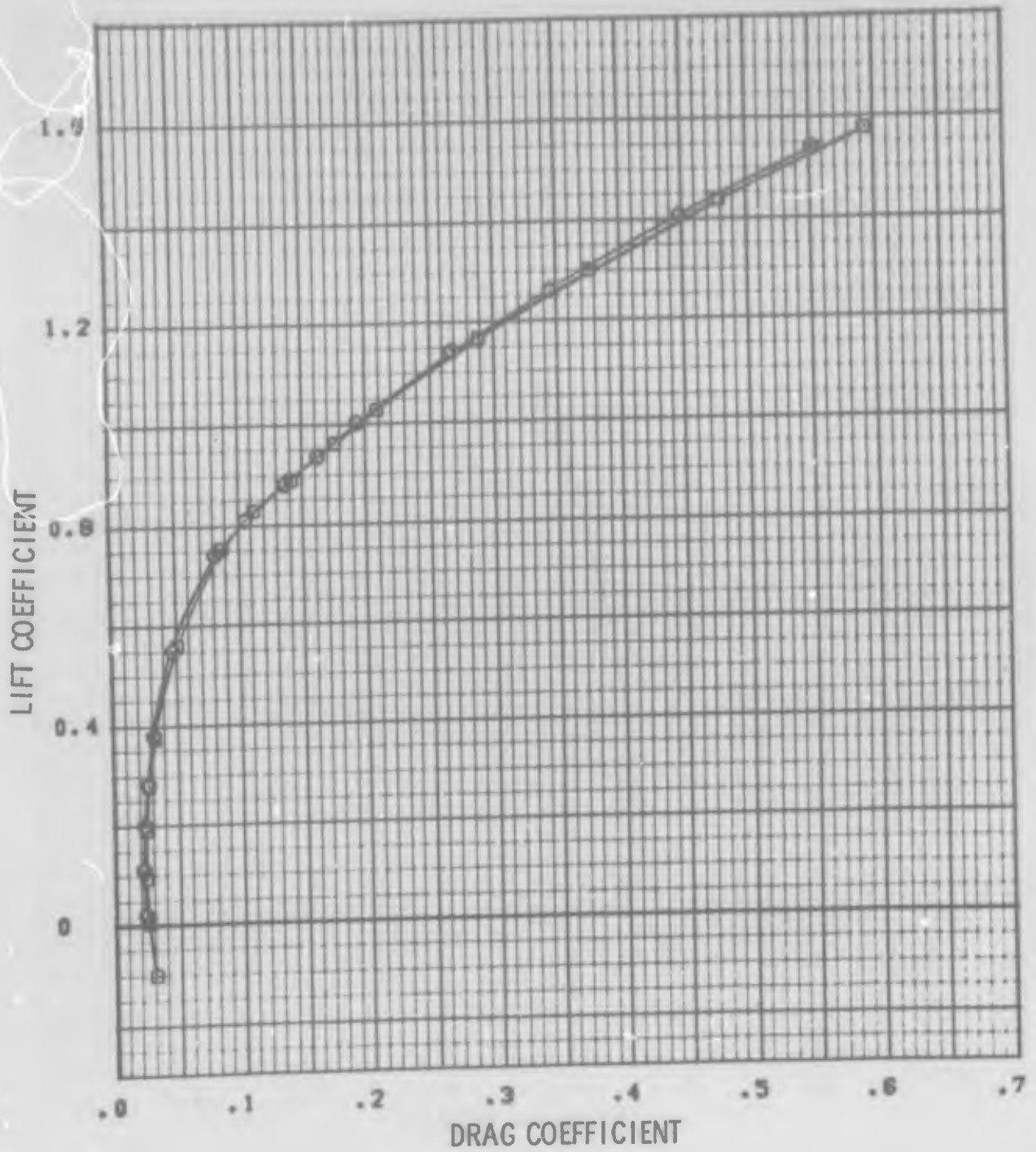
| SYM | TEST          | PART | RN/FT       |
|-----|---------------|------|-------------|
| ⊙   | PWT 4T TC-043 | 272  | 3.0 MILLION |
| ⊠   | PWT 4T TC-043 | 264  | 5.2 MILLION |
| ▲   | PWT 4T TC-043 | 262  | 6.5 MILLION |

FIGURE 27b REYNOLDS NUMBER EFFECT ON LEDE CLEAN WING PWT 4T  
M = 0.9



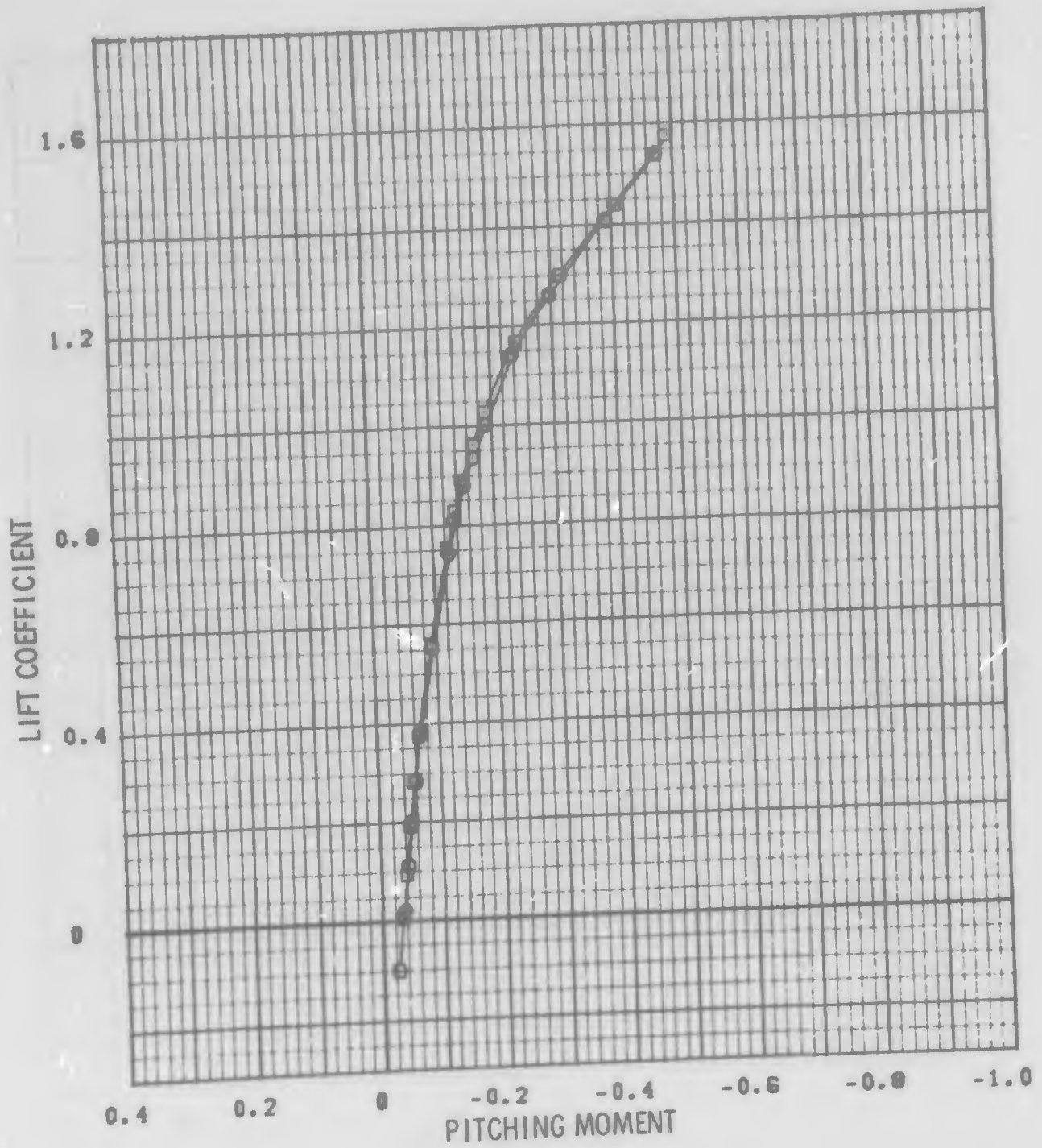
| SYM | TEST           | PART | RN/FT       |
|-----|----------------|------|-------------|
| ○   | PWT 16T TF-216 | 39   | 3.0 MILLION |
| □   | PWT 16T TF-216 | 49   | 5.2 MILLION |

FIGURE 28a REYNOLDS NUMBER EFFECT ON LEDE CLEAN WING PWT 16T  
M = 0.7



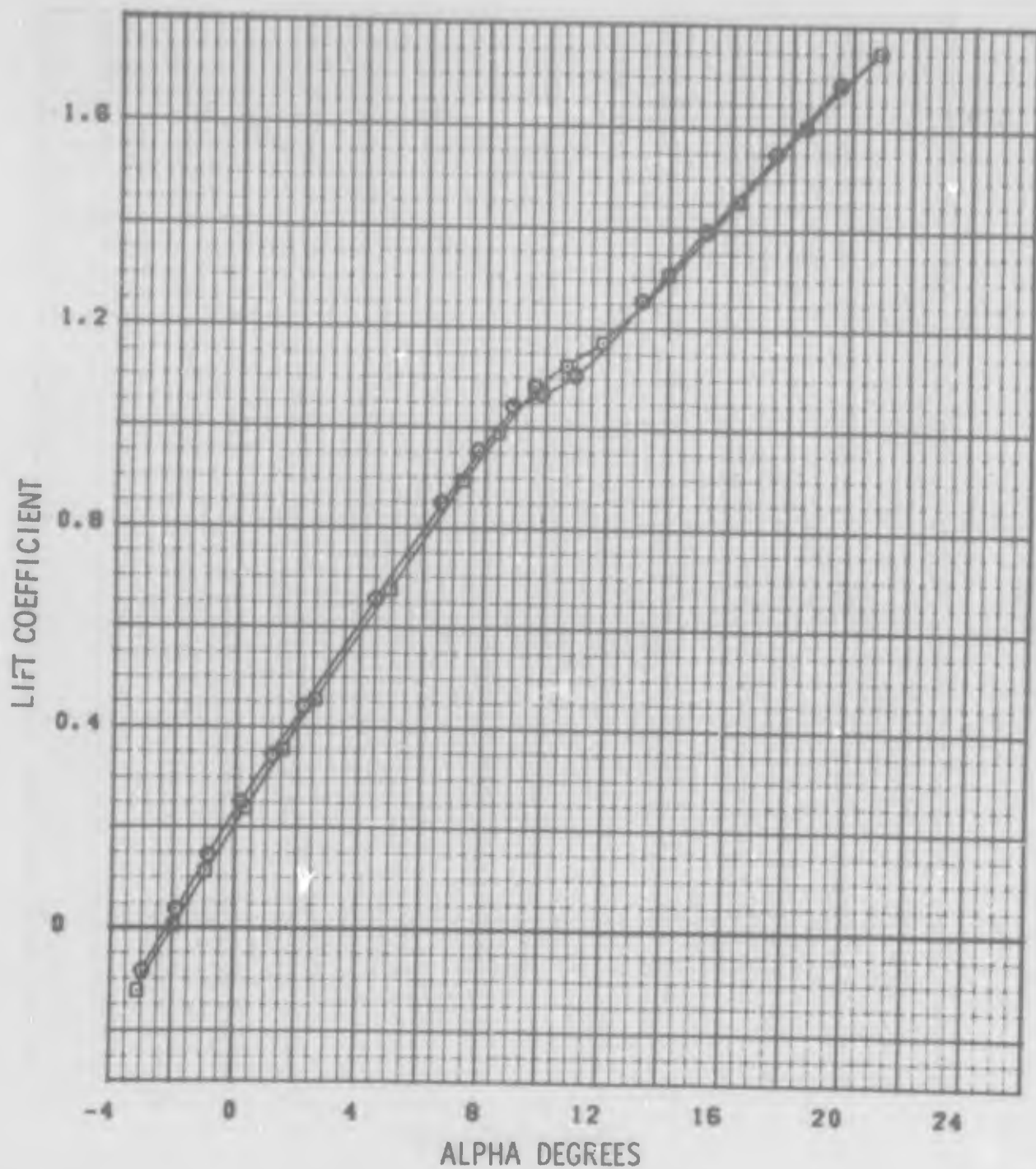
| SYM | TEST           | PART | RN/FT       |
|-----|----------------|------|-------------|
| ○   | PWT 16T TF-216 | 39   | 3.0 MILLION |
| □   | PWT 16T TF-216 | 49   | 5.2 MILLION |

FIGURE 28a REYNOLDS NUMBER EFFECT ON LEDE CLEAN WING PWT 16T  
M = 0.7



| SYM | TEST           | PART | RN/FT       |
|-----|----------------|------|-------------|
| ○   | PWT 16T TF-216 | 39   | 3.0 MILLION |
| □   | PWT 16T TF-216 | 49   | 5.2 MILLION |

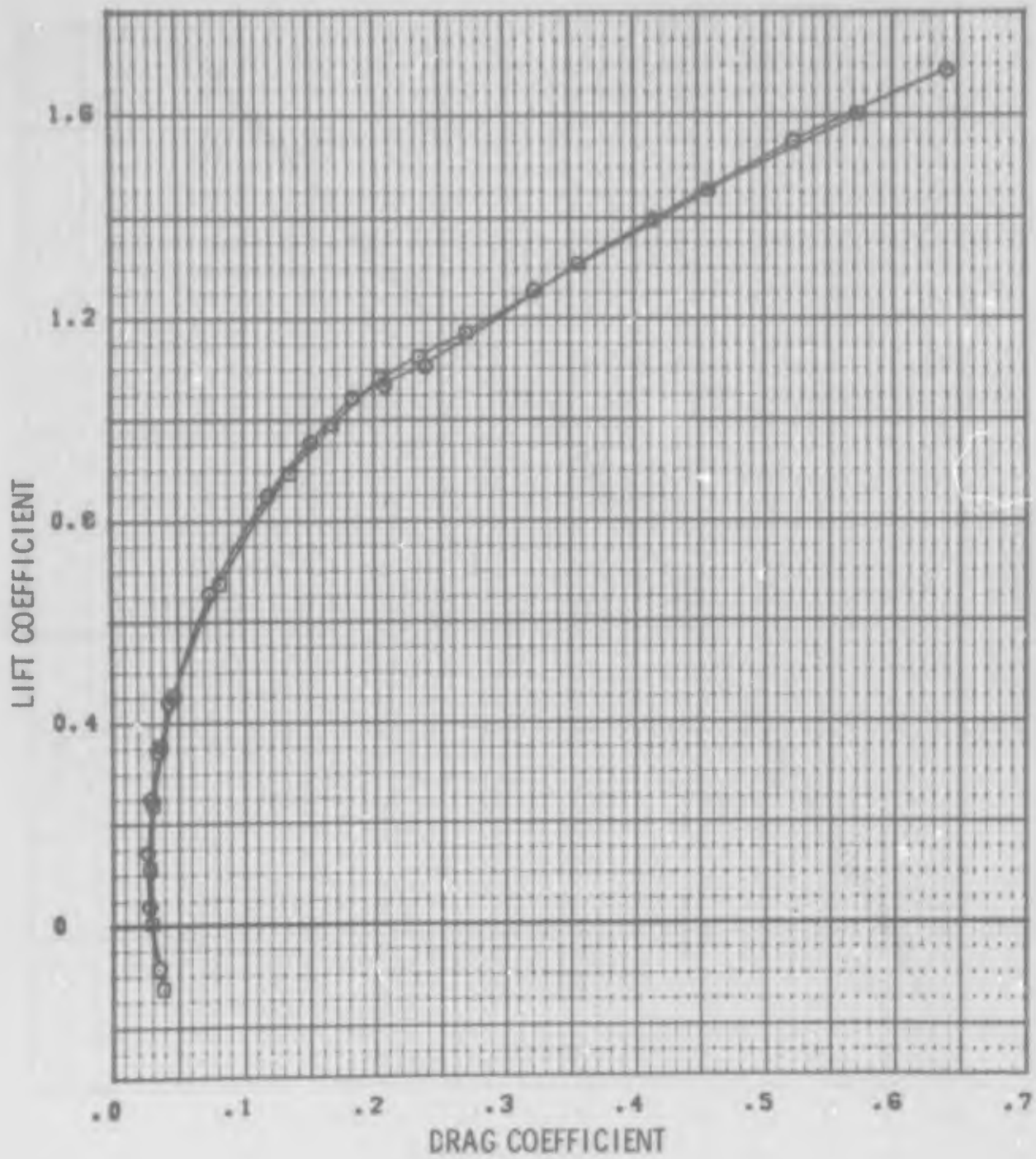
FIGURE 28a REYNOLDS NUMBER EFFECT ON LEDE CLEAN WING PWT 16T  
M = 0.7



| SYM | TEST           | PART | RN/FT       |
|-----|----------------|------|-------------|
| ⊙   | PWT 16T TF-216 | 41   | 3.0 MILLION |
| ⊠   | PWT 16T TF-216 | 52   | 5.2 MILLION |

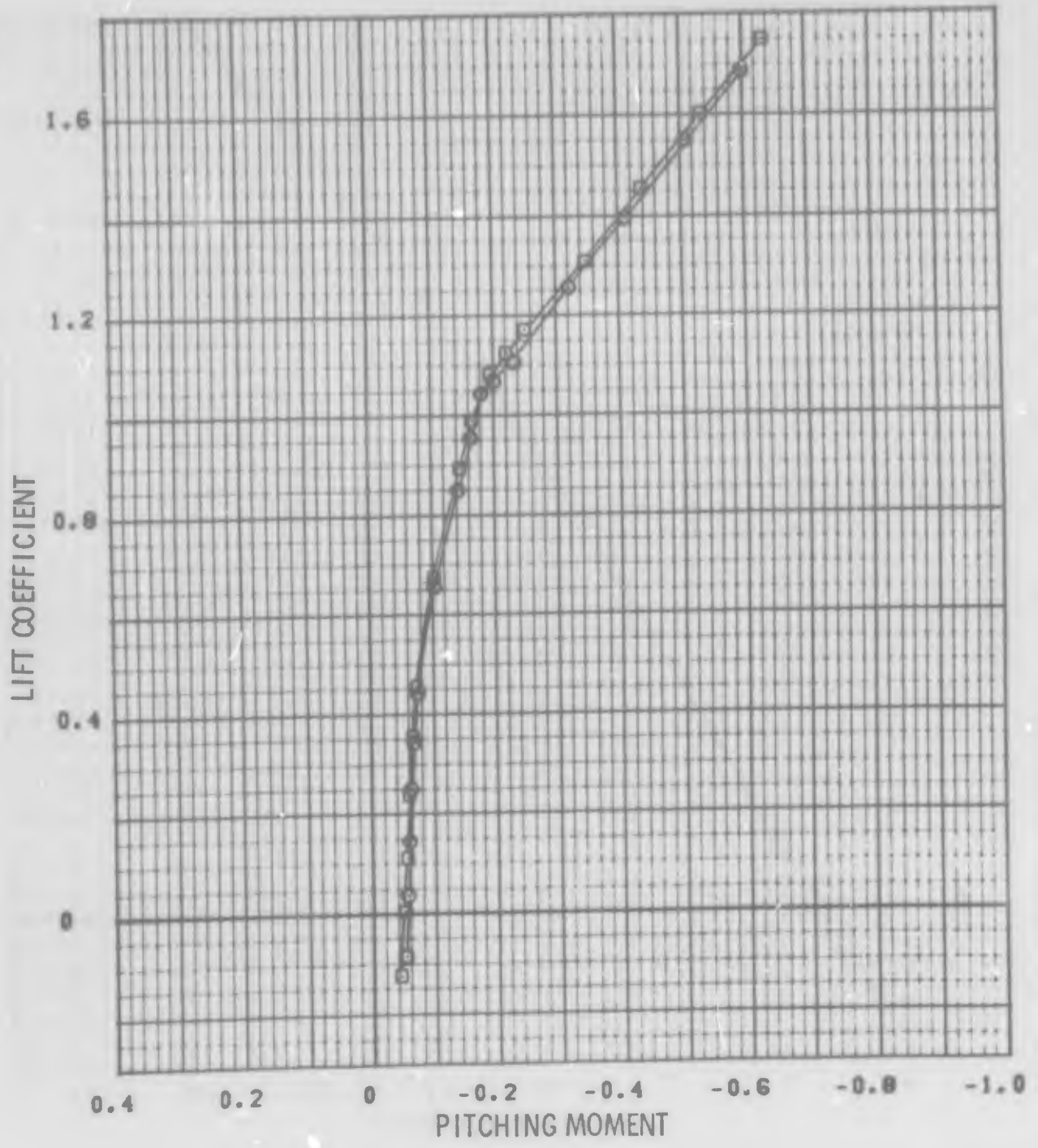
FIGURE 28b REYNOLDS NUMBER EFFECT ON LEDE CLEAN WING PWT 16T  
M = 0.9





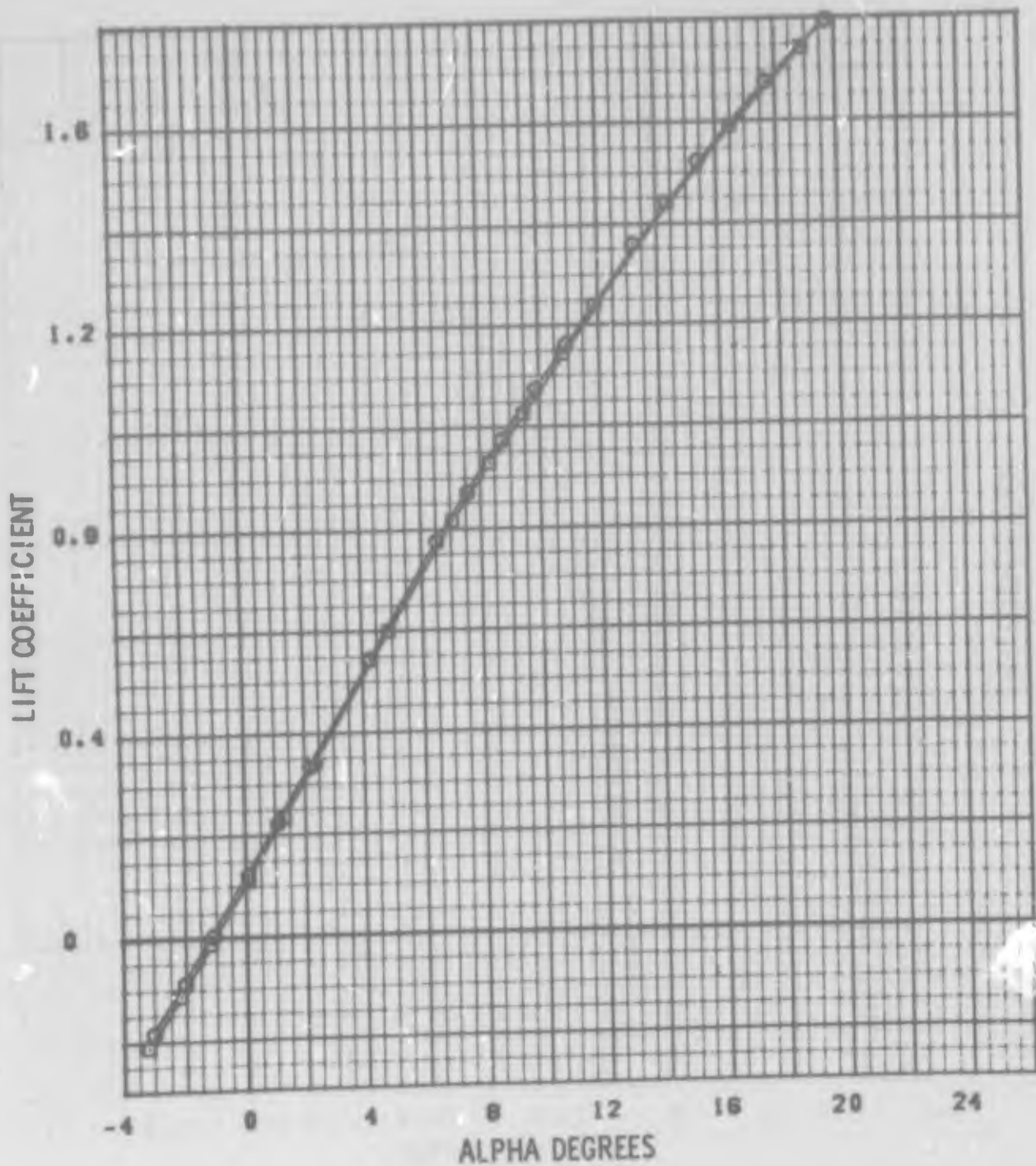
| SYM | TEST           | PART | RN/FT       |
|-----|----------------|------|-------------|
| ○   | PWT 16T TF-216 | 41   | 3.0 MILLION |
| □   | PWT 16T TF-216 | 52   | 5.2 MILLION |

FIGURE 28b REYNOLDS NUMBER EFFECT ON LEDE CLEAN WING PWT 16T  
M = 0.9



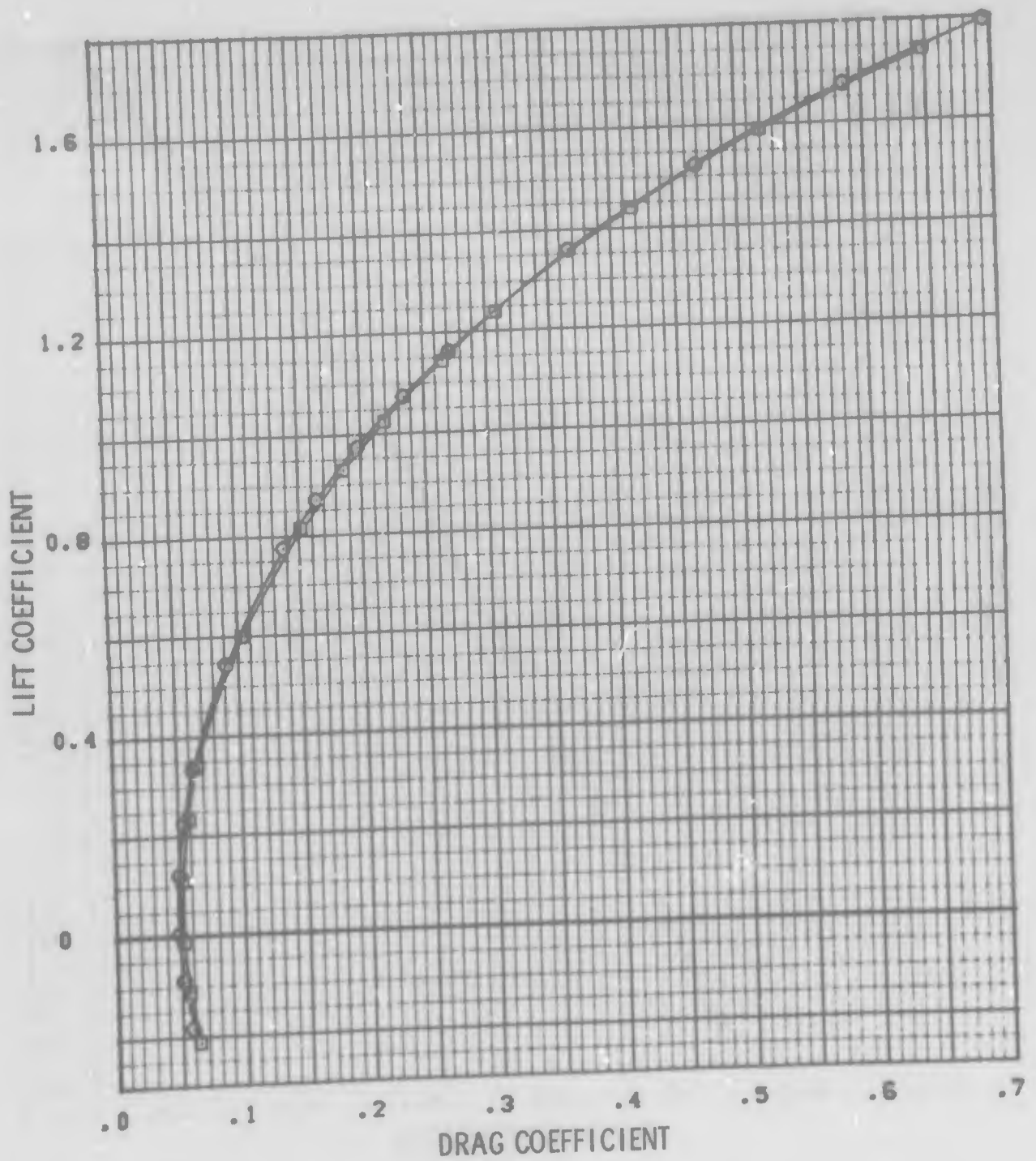
| SYM | TEST           | PART | RN/FT       |
|-----|----------------|------|-------------|
| ⊙   | PWT 16T TF-216 | 41   | 3.0 MILLION |
| ⊠   | PWT 16T TF-216 | 52   | 5.2 MILLION |

FIGURE 28b REYNOLDS NUMBER EFFECT ON LEDE CLEAN WING PWT 16T  
M = 0.9



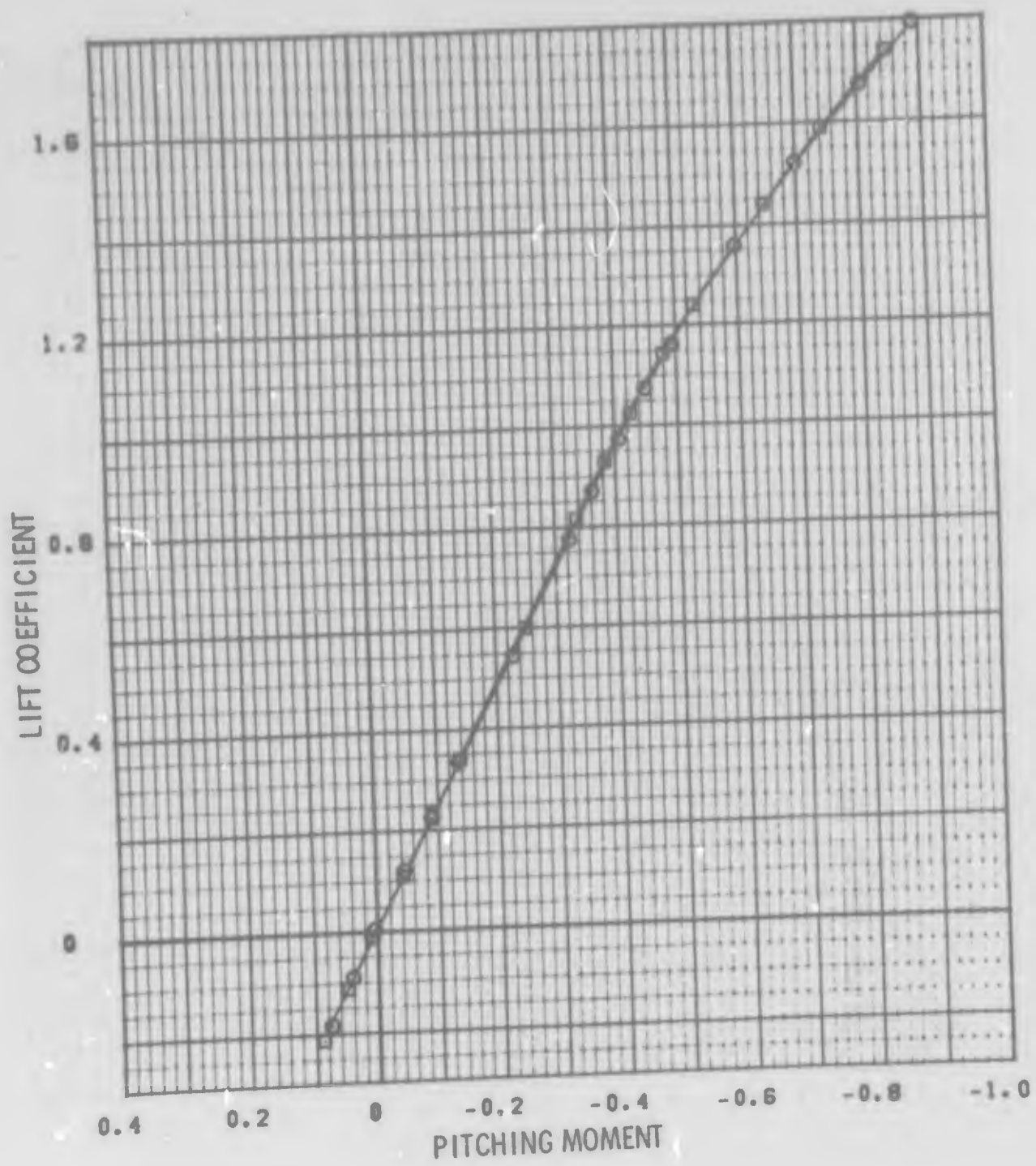
| SYM | TEST           | PART | RN/FT       |
|-----|----------------|------|-------------|
| ⊙   | PWT 16T TF-216 | 45   | 3.0 MILLION |
| ⊠   | PWT 16T TF-218 | 54   | 5.2 MILLION |

FIGURE 28c REYNOLDS NUMBER EFFECT ON LEDE CLEAN WING PWT 16T  
M = 1.2



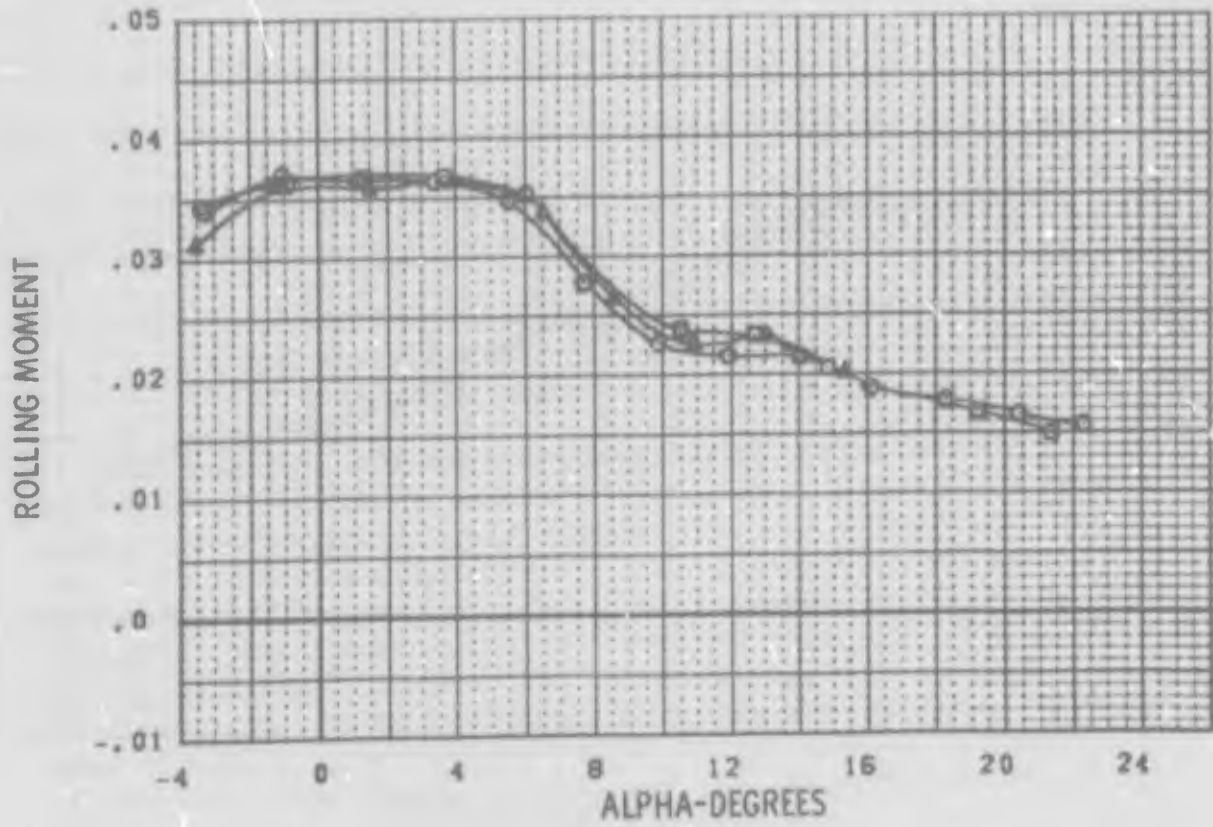
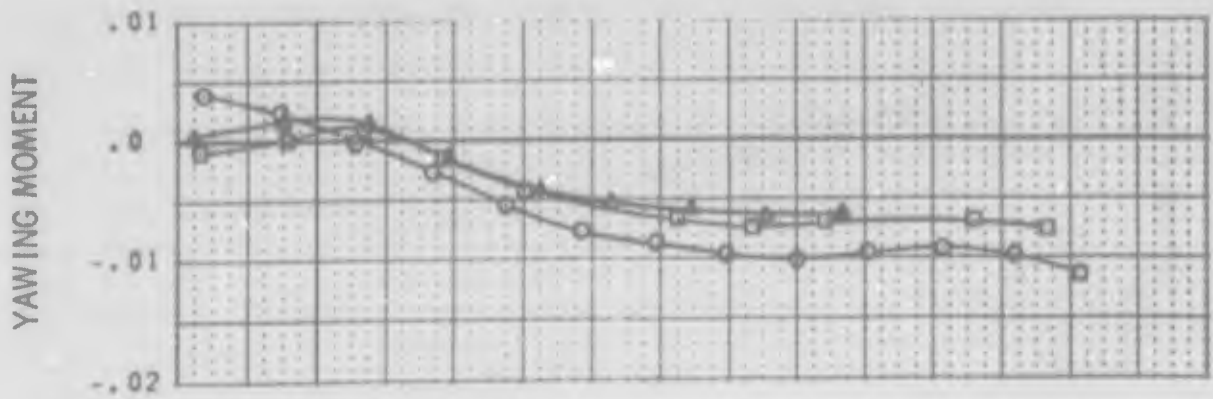
| SYM | TEST           | PART | RN/FT       |
|-----|----------------|------|-------------|
| ○   | PWT 16T TF-216 | 45   | 3.0 MILLION |
| □   | PWT 16T TF-216 | 54   | 5.2 MILLION |

FIGURE 28c REYNOLDS NUMBER EFFECT ON LEDE CLEAN WING PWT 16T  
M = 1.2



| SYM | TEST           | PART | RN/FT       |
|-----|----------------|------|-------------|
| ○   | PWT 16T TF-216 | 45   | 3.0 MILLION |
| □   | PWT 16T TF-216 | 54   | 5.2 MILLION |

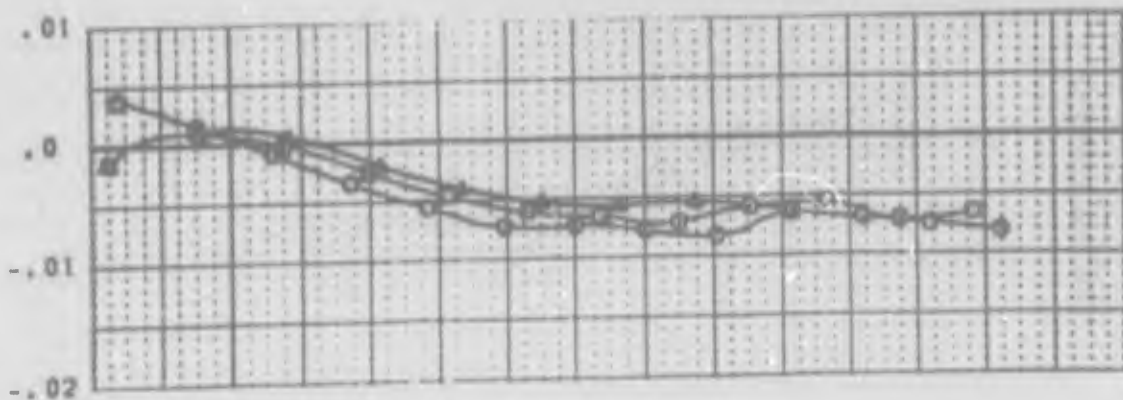
FIGURE 28c REYNOLDS NUMBER EFFECT ON LEDE CLEAN WING PWT 16T  
M = 1.2



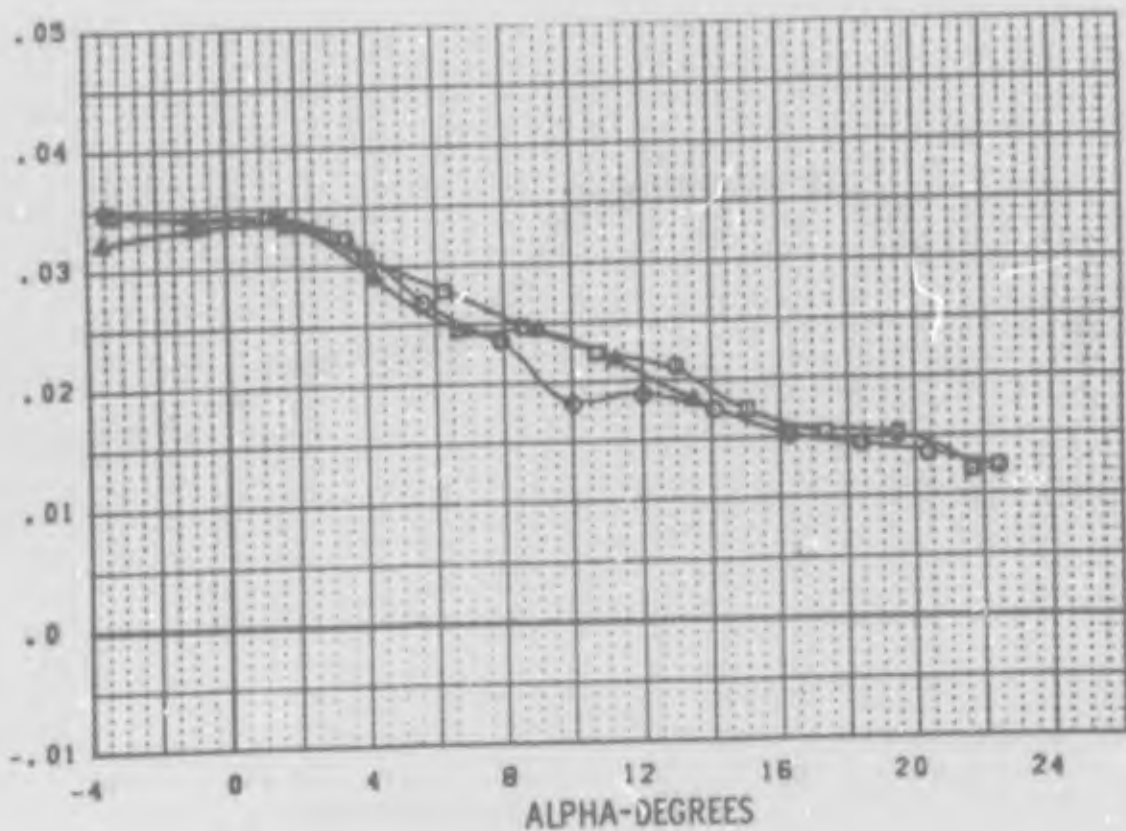
| SYM | TEST          | PART | L.E. (L/R) | AILERON (L/R) | RN/FT.      |
|-----|---------------|------|------------|---------------|-------------|
| ○   | PWT 4T TC-043 | 284  | K1 0/0     | MID 20/-20    | 3.9 MILLION |
| □   | PWT 4T TC-043 | 214  | K1 0/0     | MID 20/-20    | 5.2 MILLION |
| ▲   | PWT 4T TC-043 | 279  | K1 0/0     | MID 20/-20    | 6.2 MILLION |

FIGURE 29a REYNOLDS NUMBER EFFECT ON MID AILERONS  
M = 0.8

YAWING MOMENT



ROLLING MOMENT



| SYM | TEST          | PART | L.E. (L/R) | AILERON (L/R) | RN/FT.      |
|-----|---------------|------|------------|---------------|-------------|
| ○   | PWT 4T TC-043 | 203  | K1 0/0     | MID 20/-20    | 3.0 MILLION |
| □   | FWT 4T TC-043 | 213  | K1 0/0     | MID 20/-20    | 5.2 MILLION |
| ▲   | PWT 4T TC-043 | 270  | K1 0/0     | MID 20/-20    | 6.4 MILLION |

FIGURE 29b REYNOLDS NUMBER EFFECT ON MID AILERONS  
M = 0.9

## SECTION VI

### SYMMETRICAL CONFIGURATION EFFECTS

Considerable data for the LEDE configuration with symmetrical deflections of both the leading- and trailing-edge devices, including clean-wing data, were obtained during the two wind tunnel tests. The principal purpose of these data was to provide a means of assessing the characteristics of the asymmetrical deflection of the control devices, however, they also reveal much useful and significant information about the longitudinal characteristics of this configuration. Accordingly, detailed attention is now devoted to analysis of the symmetrical configuration results.

The objectives of this section are:

- 1) To verify the test configuration design approach;
- 2) To establish the basic longitudinal aerodynamic characteristics of the LEDE configuration; and
- 3) To present typical results for effects on longitudinal characteristics caused by symmetric configuration test variables.

In general, the test configuration design approach was successful. While we cannot claim to have eliminated shock-induced separation effects completely, it is apparent from the data that the significant effects have been delayed to quite high lift coefficients. The transonic performance characteristics are competitive with current aircraft configurations at low lift coefficients and markedly superior at high lift coefficients. No significant stability problems are apparent from the data. Maximum lift will be set either by the ability of the horizontal tail to trim out the pitching moment or by buffet intensity since the tail-on lift curves show continuously increasing lift with angle of attack up to the maximum angles of attack tested.

The effects of leading- and trailing-edge devices are qualitatively as expected. The leading-edge devices improve the flow over the outer wing panel at high angles of attack and provide positive lift increments in that region at subsonic speeds. The trailing-edge devices produce significant lift increments at low angles of attack but the effectiveness diminishes as angle of attack is increased.



The vortex generator pattern improved the linearity of the lift and pitching moment curves but the effects are small. A slight drag reduction was obtained at 0.9 Mach number.

## 1. TEST CONFIGURATION VERIFICATION

Two indicators of the success of the test configuration design approach are the lift/drag and buffet onset characteristics. Figure 30 presents a comparison for 0.9 Mach number between measured lift/drag ratio variations with lift coefficients for the LEDE configuration and the F-111A at leading edge sweep of 45 degrees. The values of L/D up to the maximum are comparable for both configurations; however, at high lift coefficients, the LEDE configuration L/D ratio is up to 33 percent higher than that of the F-111A. The improvement holds up to a lift coefficient of 1.05.

The buffet onset lift coefficient variation with Mach number for the LEDE configuration is presented in Figure 31 along with flight values for several operational thin wing aircraft. Definitive buffet data were obtained in the 16T facility at a unit Reynolds number of 3.0 million per foot and are represented at Figure 31 by the lower bound of the cross-hatched area. The upper bound was determined from data obtained at Reynolds number of 5.2 million per foot. The variations of wing-root-bending moment obtained at the higher Reynolds number were somewhat erratic and an accurate definition of buffet onset was hard to determine. The comparisons with data from other aircraft again indicate that the LEDE configuration wing design has improved flow characteristics at transonic high-lift conditions.

## 2. LEDE CONFIGURATION LONGITUDINAL CHARACTERISTICS

The lift, drag, and pitching moment characteristics of the basic LEDE configuration with the tail are presented in Figure 32 for Mach numbers from 0.7 to 1.2. All data in these figures were obtained in the 16T facility at a unit Reynolds number of 3.0 million per foot and thus represent a conservative baseline for evaluating the general characteristics.

The data are presented in formats which emphasize the strong influence of increasing free stream Mach number in suppressing flow separation effects at high lift coefficients. For example, Figure 32 shows that from Mach 0.7 to 0.85 the lift curve slope at  $C_L$  of 1.0 changes only very slightly, but between Mach 0.85 and 0.9 a transition takes place and the lift curve slope is only very slightly reduced from that at lower lift coefficients. By

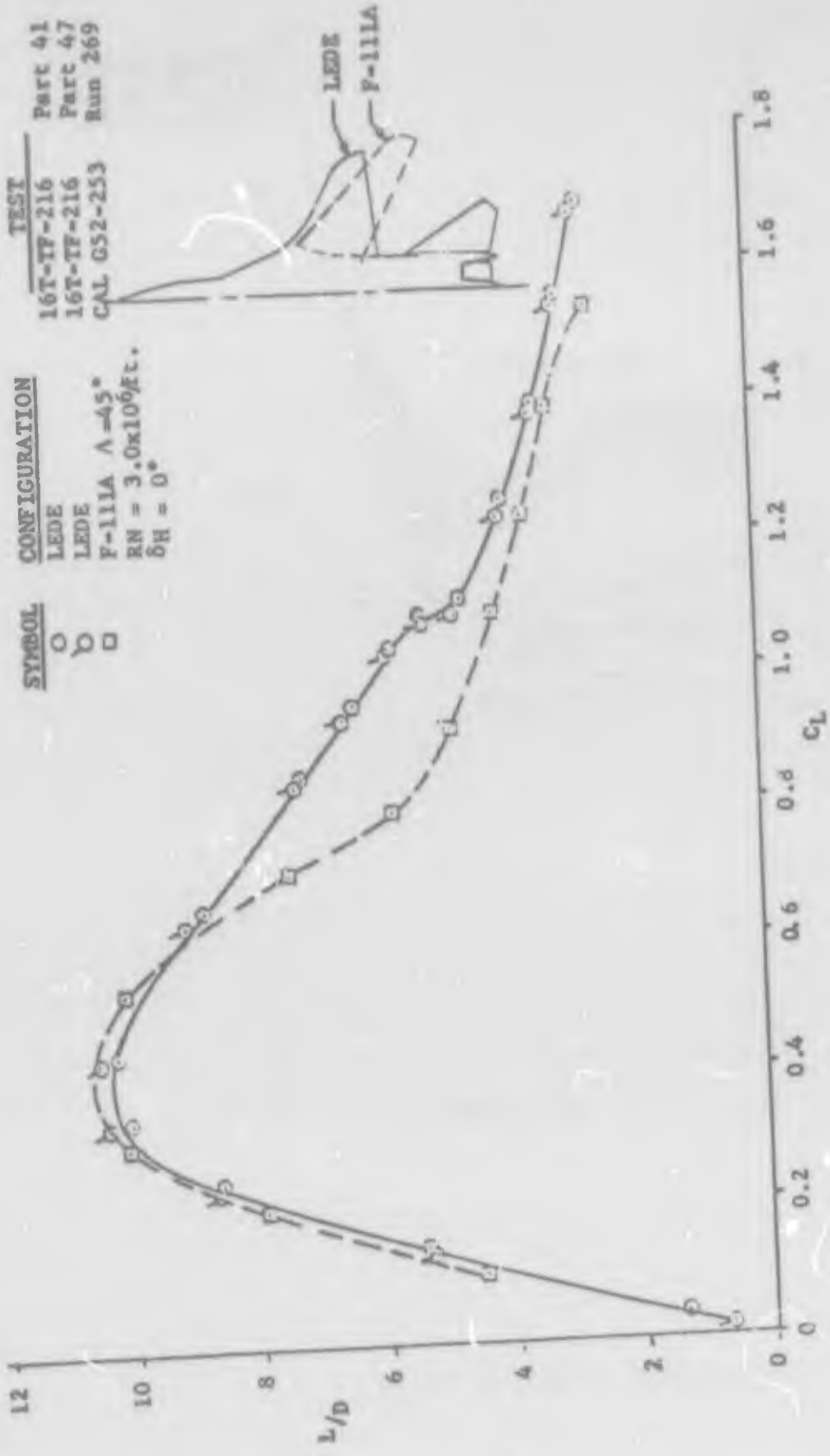


Figure 30 COMPARISON OF LIFT/DRAGE RATIOS  
 MACH = 0.9

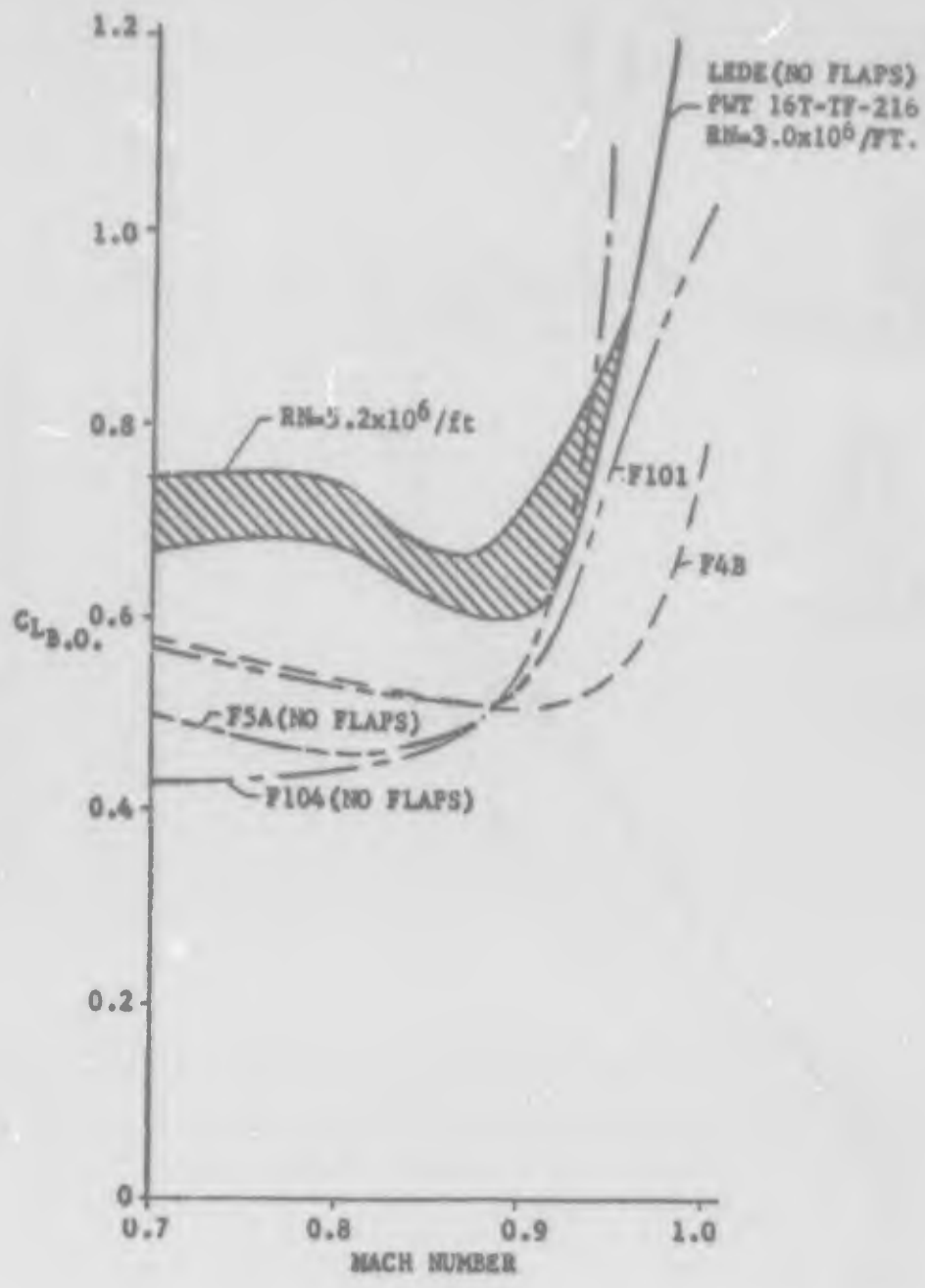
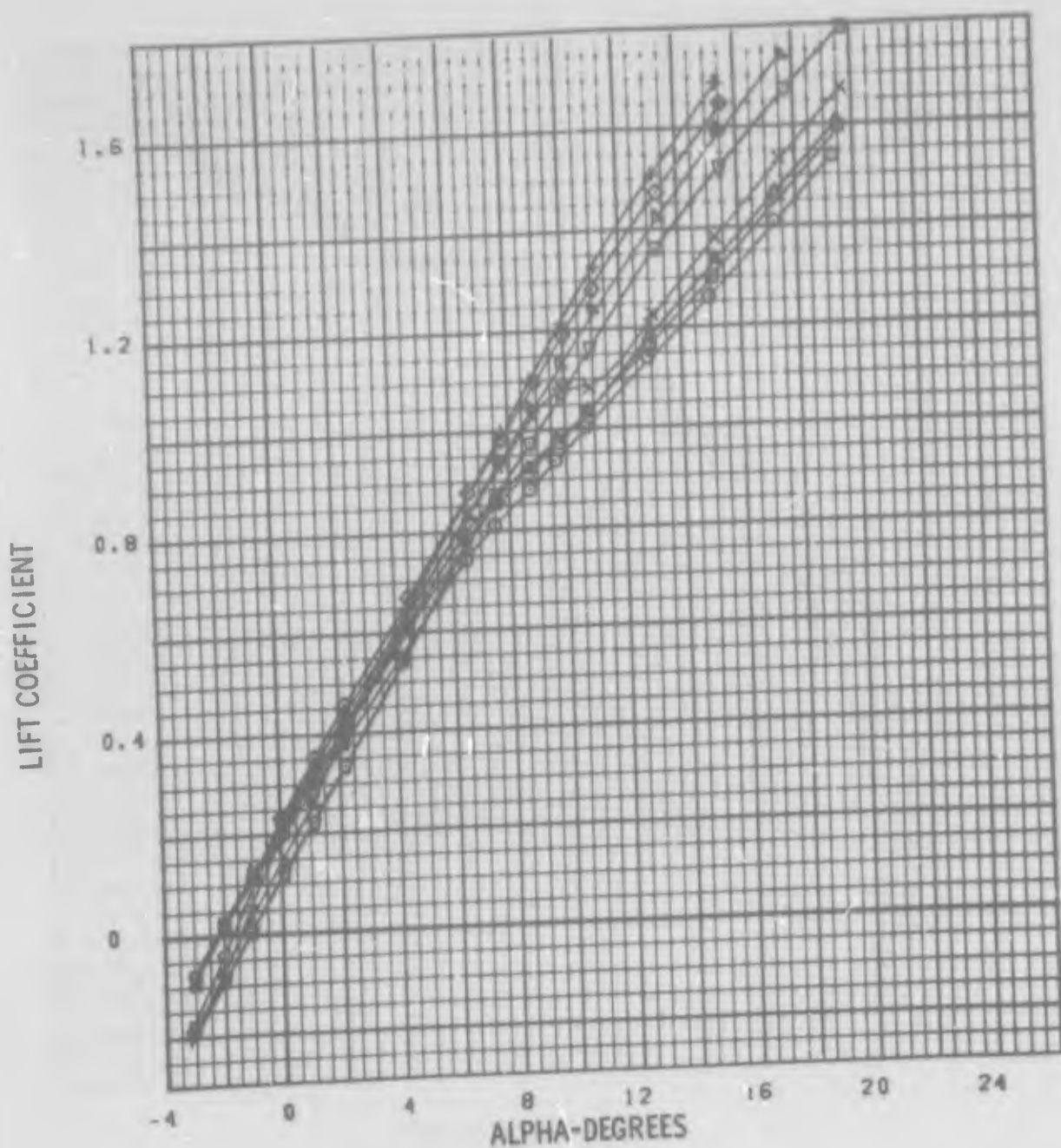
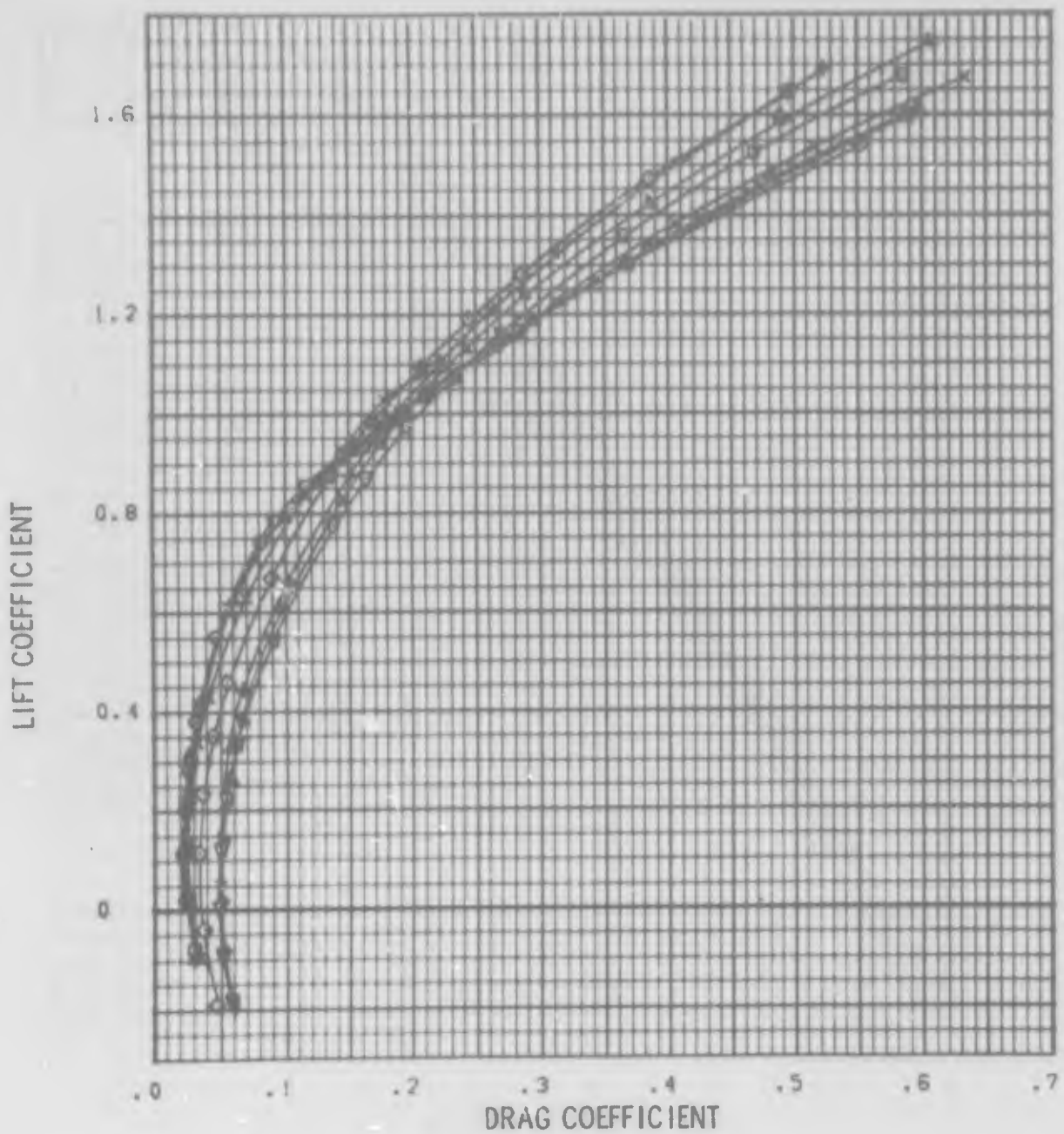


Figure 31 COMPARISON OF BUFFET ONSET



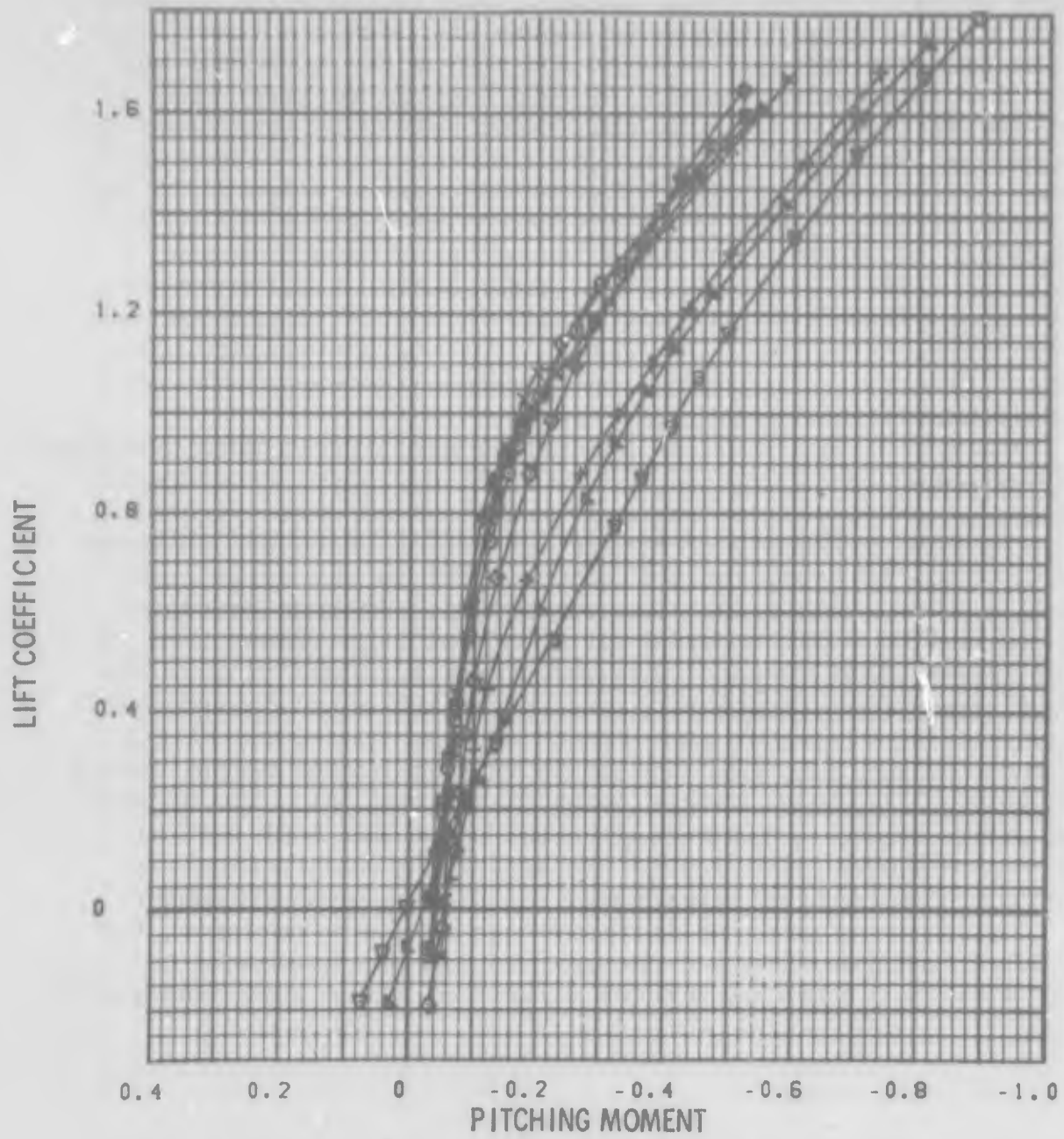
| SYM | TEST           | PART | MACH NO. |
|-----|----------------|------|----------|
| ⊙   | PWT 16T TF-216 | 39   | 0.70     |
| ⊠   | PWT 16T TF-216 | 40   | 0.80     |
| ▲   | PWT 16T TF-216 | 46   | 0.85     |
| ×   | PWT 16T TF-216 | 47   | 0.90     |
| ◇   | PWT 16T TF-216 | 42   | 0.95     |
| +   | PWT 16T TF-216 | 43   | 1.00     |
| ▴   | PWT 16T TF-216 | 44   | 1.10     |
| ▽   | PWT 16T TF-216 | 45   | 1.20     |

FIGURE 32 MACH NUMBER EFFECTS ON LEDE CLEAN WING  
 RN/FT = 3.0 MILLION



| SYM | TEST           | PART | MACH NO. |
|-----|----------------|------|----------|
| ○   | PWT 16T 1K 216 | 39   | 0.70     |
| □   | PWT 16T 1K 216 | 40   | 0.80     |
| △   | PWT 16T 1K 216 | 46   | 0.85     |
| x   | PWT 16T 1K 216 | 47   | 0.90     |
| ◇   | PWT 16T 1K 216 | 42   | 0.95     |
| +   | PWT 16T 1K 216 | 43   | 1.00     |
| ▲   | PWT 16T 1K 216 | 44   | 1.10     |
| ▽   | PWT 16T 1K 216 | 45   | 1.20     |

FIGURE 32 MACH NUMBER EFFECTS ON LIFT OF CLEAN WING  
 RN/FT = 3.0 MILLION



| SYM | TEST           | PART | MACH NO. |
|-----|----------------|------|----------|
| ⊙   | PWT 16T TF-216 | 39   | 0.70     |
| ⊠   | PWT 16T TF-216 | 40   | 0.80     |
| ▲   | PWT 16T TF-216 | 46   | 0.85     |
| x   | PWT 16T TF-216 | 47   | 0.90     |
| ◇   | PWT 16T TF-216 | 42   | 0.95     |
| +   | PWT 16T TF-216 | 43   | 1.00     |
| ▴   | PWT 16T TF-216 | 44   | 1.10     |
| ▽   | PWT 16T TF-216 | 45   | 1.20     |

FIGURE 32 MACH NUMBER EFFECTS ON LEDE CLEAN WING  
 RN/FT = 3.0 MILLION

Mach 0.95 the lift curve is very nearly linear throughout the entire angle of attack range tested. Similar behavior is noted in the drag polars presented in Figure 32. Again a transition in character is apparent between the curves for Mach 0.35 and 0.9. One interesting feature of this plot is the fact that at lift coefficients above 1.05 the lowest untrimmed drag level is achieved at Mach 0.95. The pitching moment curves presented in Figure 32 indicate how well behaved the configuration is in the subsonic regime. There is no indication of pitchup due to flow separation on the wing; instead the pitching moment breaks stable at lift coefficients above about 0.80. For the supersonic conditions, the pitching moment is nearly linear over the entire range of lift coefficients. It is interesting to note that at high lift conditions the transonic and supersonic data exhibit nearly equal stability levels.

The data from which the buffet characteristics were evaluated are presented in Figures 33 and 34 which are plots of wing-root-bending moment and axial force as functions of angle of attack. In each case, the angle of attack for buffet onset was conservatively selected using the inflection point in the axial force curve as the criteria for flow separation. In some instances the inflection point occurred prior to any significant rise in wing root-bending moment. In other cases a slight rise in the buffet moment occurs prior to the inflection point in the axial force curves. Previous comparisons of wind-tunnel and flight buffet data indicate that the early rise in buffet moment is not a valid indication of buffet onset (Reference 22). The slight peak which occurs in the buffet moment curve for Mach 0.95 at a Reynolds number of  $3.0 \times 10^6$  is apparently due to wing tip separation which is eliminated at the higher Reynolds number.

Detailed analysis of lift and drag data was performed for the LEDE configuration and the results are now presented to form a basis for evaluating the effects of other test configurations.

#### a. Lift Curve Slope

The variation of lift curve slope with Mach number determined near zero lift is shown in Figure 35. Data are shown for the complete configuration as obtained in both the 16T and 4T facilities. Comparison of these data confirms the point made earlier that the measured lift-curve slopes are higher in the larger facility. The effect of supercritical flow over the wing is evident in the inflections which occur in the 16T data variation between Mach 0.8 and 1.0.

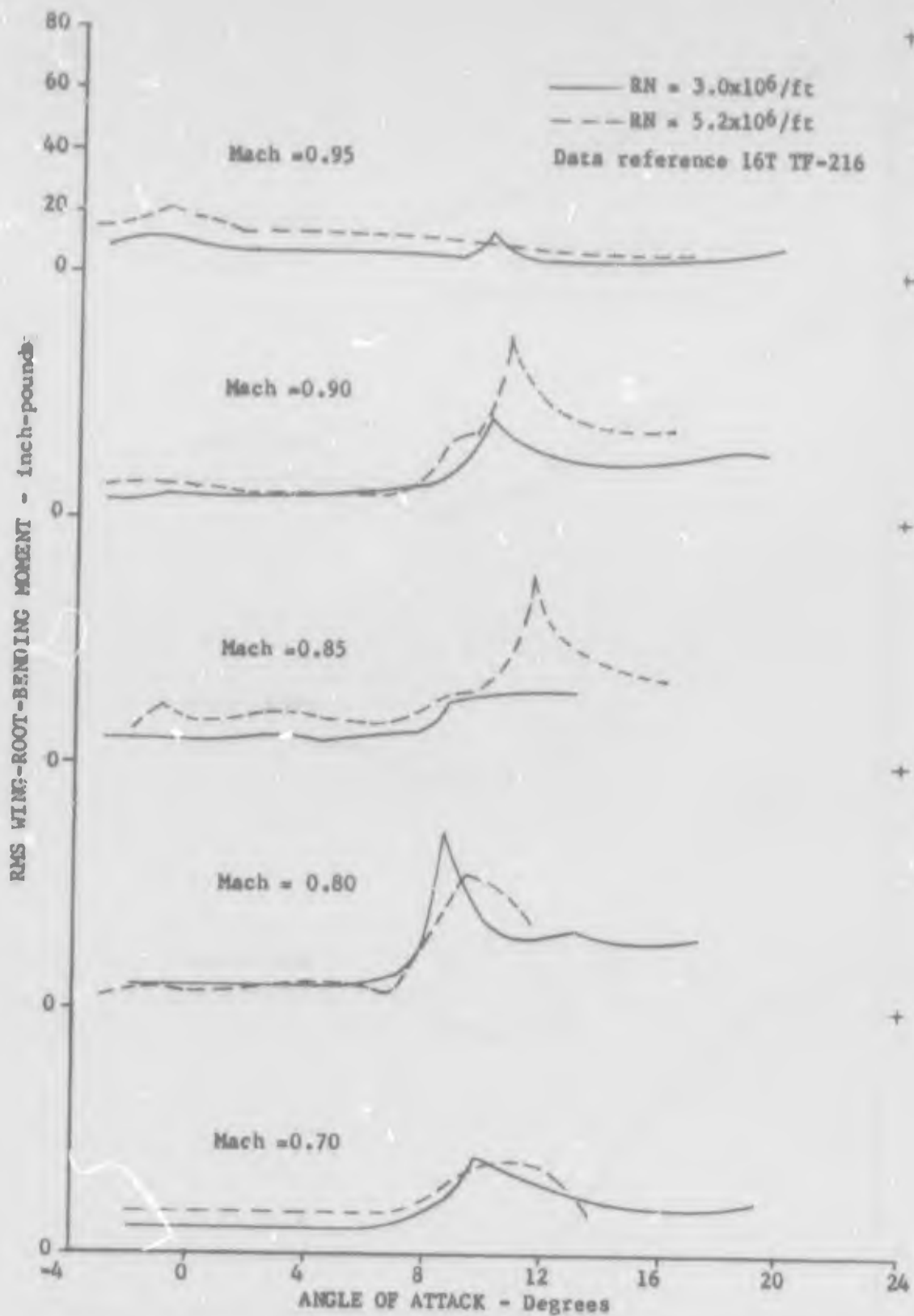


Figure 33 LEDE CONFIGURATION BUFFET CHARACTERISTICS, WING-ROOT-BENDING MOMENT



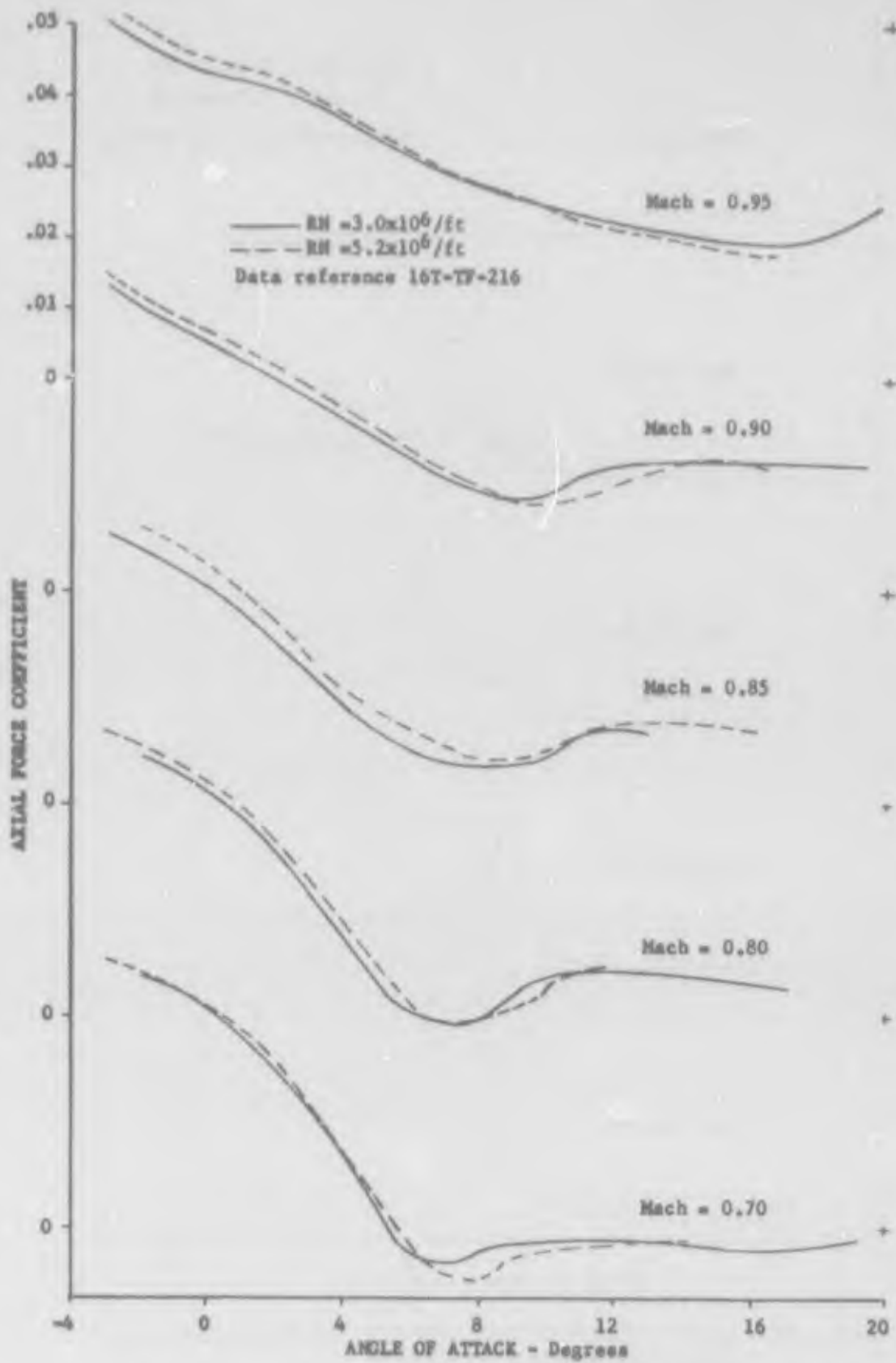


Figure 34 LEDE CONFIGURATION BUFFET CHARACTERISTICS, AXIAL FORCE COEFFICIENT

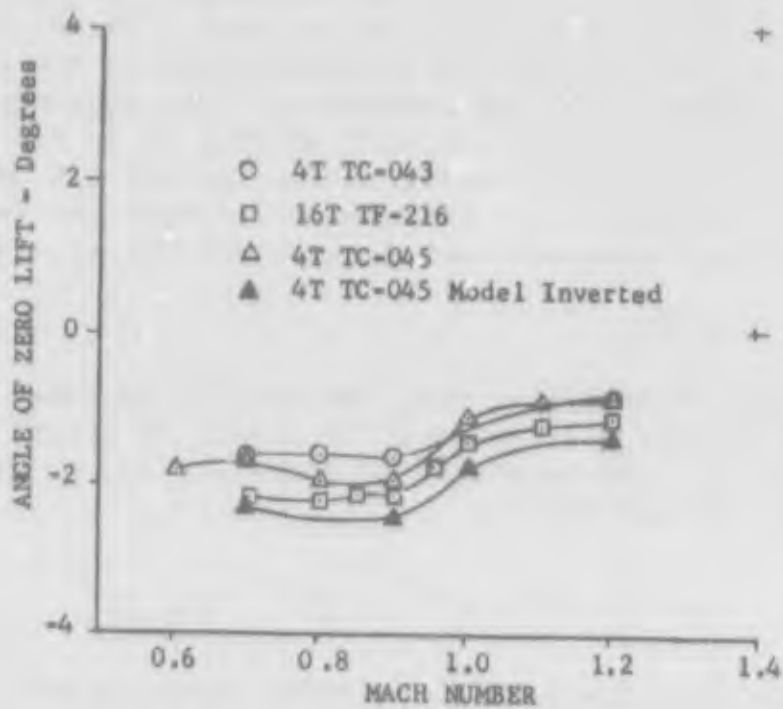
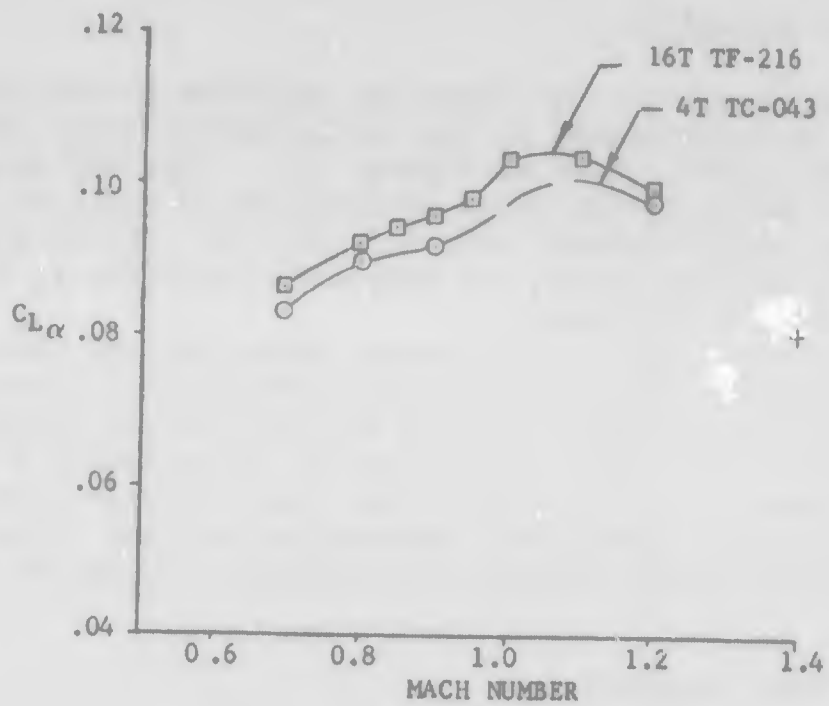


Figure 35 LIFT CURVE PARAMETERS, LEDE CLEAN WING HORIZONTAL TAIL ON

## b. Angle of Zero Lift

Wing camber effects are generally modified in the transonic flow regime as is indicated in the variations of angle of zero lift with Mach number shown in Figure 35 . The 16T data for the complete configuration shows an increase in angle of zero lift of nearly one degree between Mach 0.8 and 1.2. The 4T data show a similar trend but the levels are somewhat higher due to flow inclination as previously mentioned.

Angle of zero lift data obtained during the ARO calibration test in the 4T facility (PWT-4T TC-045) are presented in Figure 35 . Data are presented for the model in both the upright and inverted positions. The data indicated a flow inclination of approximately 0.3 degrees at all Mach numbers. The 16T values fall approximately midway between the ARO calibration test data. Accounting for flow inclination makes the degree of agreement between data obtained in the two facilities quite good.

## c. Minimum Drag Coefficient

The variation of minimum drag coefficient with Mach number shows a very slight drag creep below 0.9 Mach number and then the typical drag rise associated with fixed wing aircraft of relatively high aspect ratio. Comparison data between the LEDE configuration and the F-111A (  $\Lambda = 45^\circ$  ) are presented in Figure 36 for a unit Reynolds number of 3.0 million per foot. The F-111A data are taken from CAL test G52-253 and are referenced to the LEDE wing area to provide a common basis for comparison. The subsonic drag level variations with Mach number are very similar up to 0.9 Mach number. The drag rise for the LEDE configuration between 0.9 Mach number and supersonic speeds is moderate which reflects the fact that the configuration was "tailored" using the transonic area rule.

## d. Drag Due to Lift

The method of analyzing drag due to lift is based on the assumption that over a large range of angles of attack the drag polar (Figure 37 ) is parabolic in shape and can be represented by an equation of the form:

$$C_D = C_{D_{min}} + K [C_L - C_{L(C_{D_{min}})}]^2 \quad (1)$$

where K is the drag-due-to-lift or polar shape factor.

For a cambered configuration the minimum drag coefficient,  $C_{D_{min}}$ , occurs generally at a non-zero value of lift coefficient,  $C_{L(C_{D_{min}})}$ . Above a critical value of lift coefficient,  $C_{L_c}$ , flow separation occurs and the drag values are no longer represented by the value of K applicable to the parabolic region.

- △ LEDE PWT 16T-TF-216
- F-111A  $\Lambda=45^\circ$  CAL G52-253
- ◊ TIE-IN  $\Lambda=45^\circ$  PWT 4T-TC-043

$RN \approx 3.0 \times 10^6$  Ft.

$S_{REF} = 498.3$  Sq.Ft.

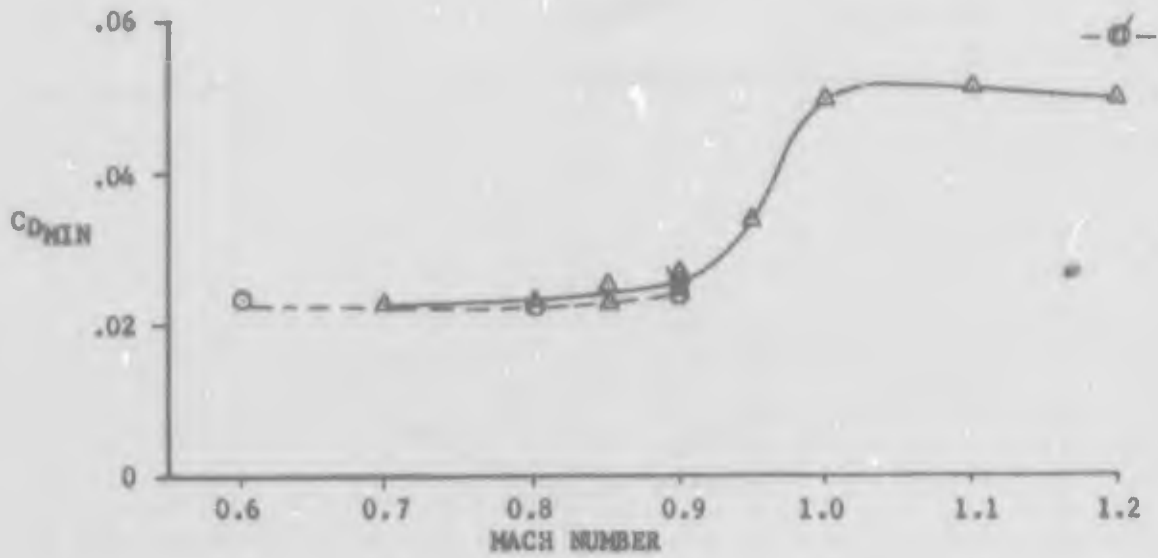


Figure 36 COMPARISON OF  $C_{D_{MIN}}$  VARIATION WITH MACH NUMBER  
HORIZONTAL TAIL ON

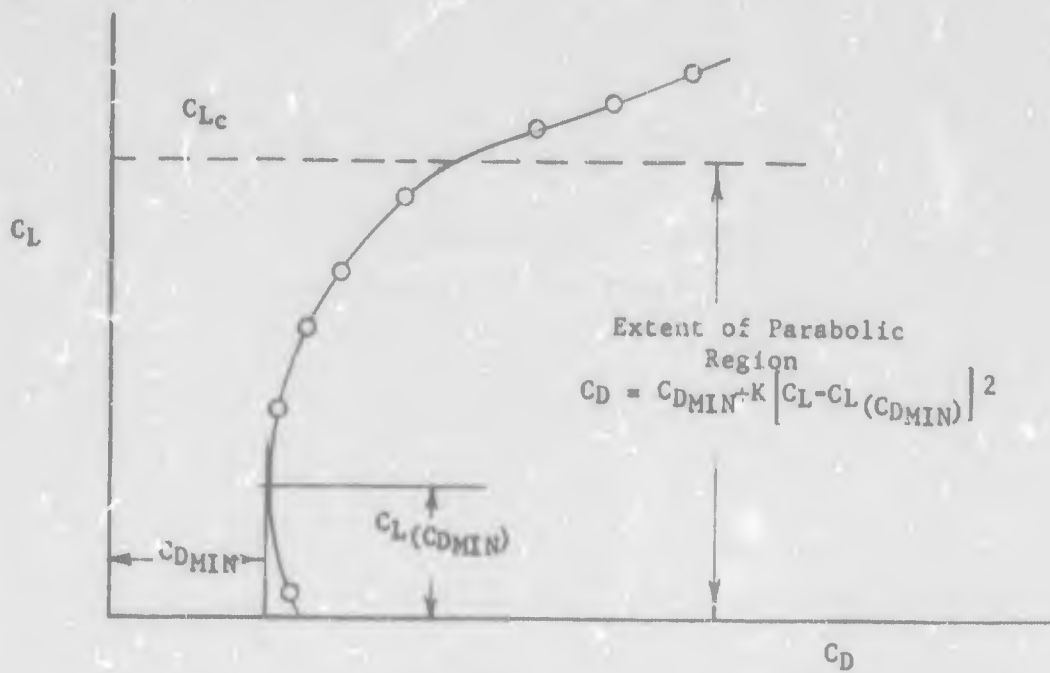


Figure 37 SQUARE ROOT PLOT FOR DRAG-DUE-TO-LIFT ANALYSIS OF CAMBERED CONFIGURATIONS

A very effective method of analyzing drag polars uses the square-root plot illustrated schematically in Figure 37. The ordinate is the lift coefficient and the abscissa is the square-root of the drag-due-to-lift term in the basic equation which is equal to  $(C_D - C_{D_{MIN}})$ . When a parabolic region exists, a straight line can be drawn through the data and the intercept on the ordinate axis is the value of lift coefficient at  $C_{D_{MIN}}$ . The slope of the straight line is the inverse square root of the drag-due-to-lift factor. The critical lift coefficient can be defined as the value at which the measured data deviates from the straight line fairing. A more readily determined value for  $C_{L_c}$  is that obtained at the intersection of two straight line fairings, one for data in the parabolic region and one for data just above the parabolic region. The latter definition of  $C_{L_c}$  is used in this report.

The Mach number variations of  $C_{L(C_{D_{MIN}})}$ ,  $K$ , and  $C_{L_c}$  determined from square-root plots of the 16T data for unit keynolds number of 3.0 million per foot are presented in Figure 38. Values for the lift coefficient for minimum drag show that the effective camber of the configuration reaches a peak at about 0.8 Mach number and then decreases. The reduction is associated with the increase in angle of attack for zero lift with Mach number previously shown in Figure 35. Figure 38 shows that the drag-due-to-lift factor increases (by 26 percent) between Mach 0.7 and 1.0 and then dips back down at supersonic speeds. The variation shown in Figure 38 is smooth, which indicates that no severe adverse effects will be encountered in the transition from subsonic to supersonic speeds. Figure 38 shows that  $C_{L_c}$  increases rapidly between Mach 0.85 and 0.90 and again illustrates the powerful effect of Mach number in delaying flow separation effects at high lift coefficients.

#### e. Aerodynamic Center

The basic LEDE pitching moment characteristics, shown previously in Figure 32, demonstrate the high degree of linearity for the complete configuration. The results of corresponding tests in PWT 4T, given in Appendix IV, confirm that pitching moment linearity is also good without the horizontal tail. However, as might be expected, the transonic data, tail off, have a gentle break unstable at lift coefficients near unity. This undesirable effect is more than offset by the increased horizontal tail effectiveness at high angles of attack so that the complete configuration exhibits smooth stable changes in stability as lift coefficient is increased. These characteristics afford a meaningful summary of longitudinal stability in terms of aerodynamic center as given below.

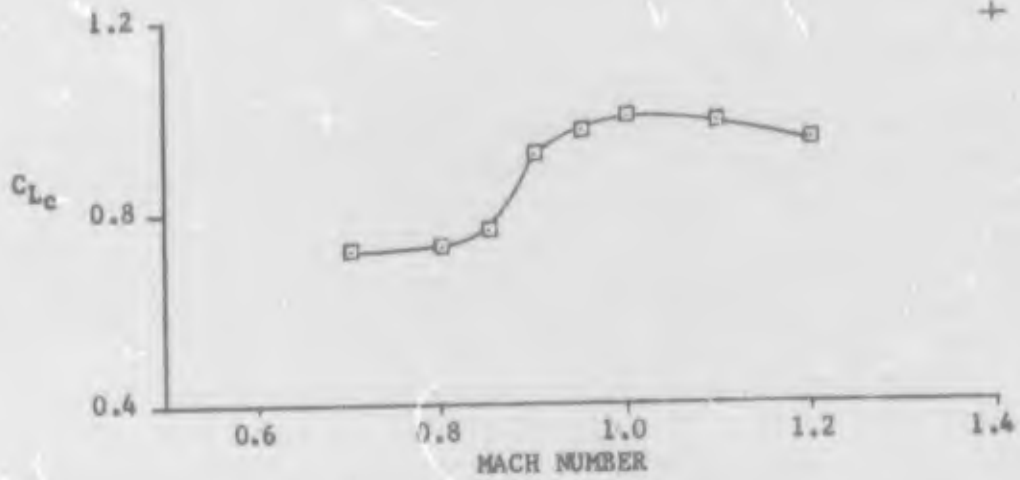
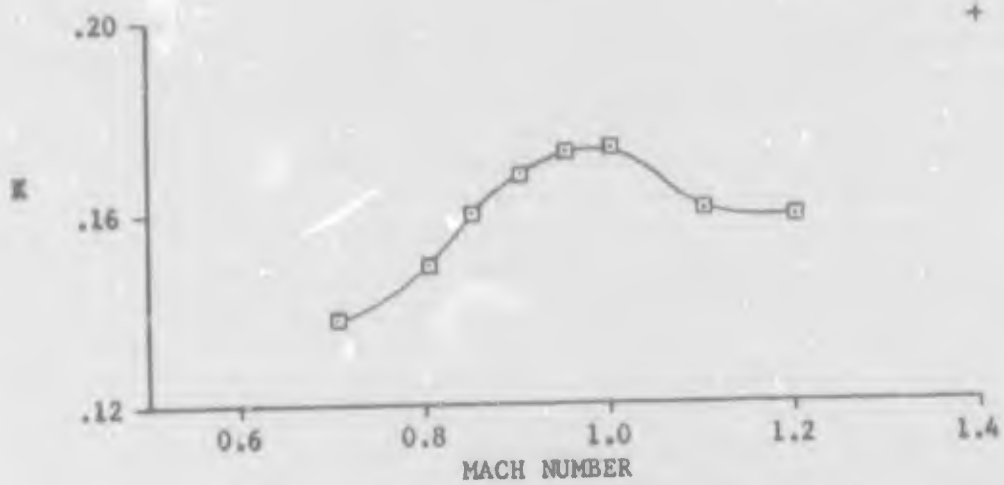
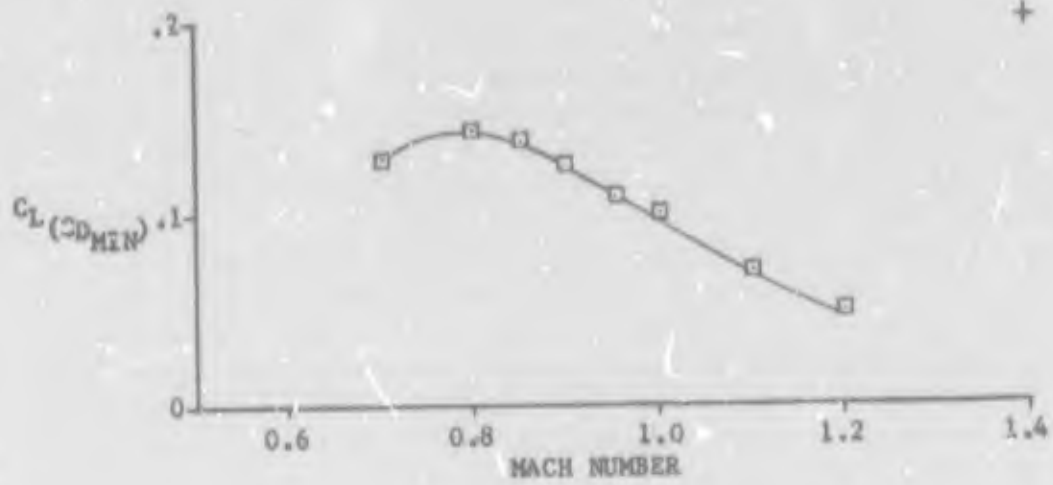


Figure 38 DRAG-DUE-TO-LIFT PARAMETERS, LEDE CLEAN WING HORIZONTAL TAIL ON

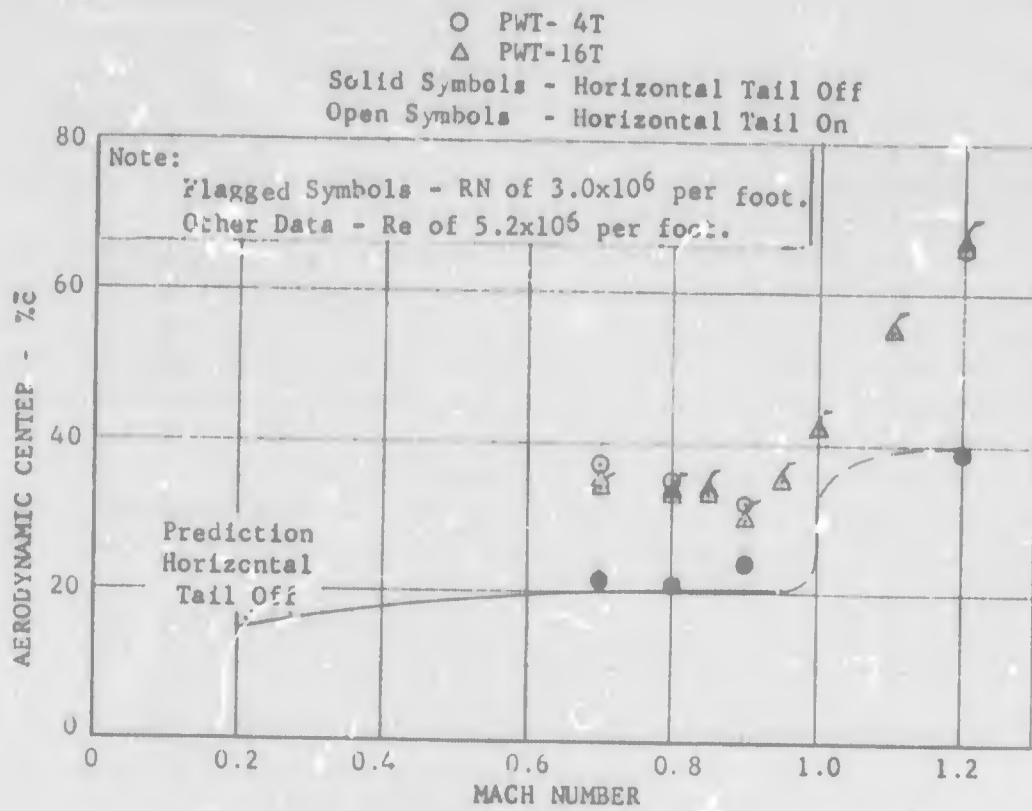


Figure 39 AERODYNAMIC CENTER



Aerodynamic center data extracted from wind tunnel measurements are shown in Figure 39. The stability levels shown are for the low to moderate lift coefficient ranges. The test data for configurations without horizontal tail are in good agreement with predictions based on the method of Reference 5. No predictions were made for the configuration with horizontal tails since plans were to accomplish almost all of the LEDE wind tunnel program tail-off. Data for the complete configuration demonstrate good agreement between results obtained in PWT 4T and PWT 16T. Also, the data from 16T indicate small effects due to Reynolds number. This maximum variation of one percent MAC is about the level of accuracy in determining aerodynamic center from plotted wind tunnel data. One other item of interest is the marked loss in tail contribution (at low angles of attack) near 0.9 Mach number that results in a significant forward shift in aerodynamic center for the complete configuration.

### 3. LEADING EDGE FLAP EFFECTS

In general the leading edge flaps improve the flow over the outer wing panel at moderate-to-high angles of attack. The angle of attack at which a given flap deflection provides a positive increment in lift increases with Mach number in the subsonic range. The basic reason for this behavior is that, for the thin cambered wing of the LEDE configuration, the primary type of flow separation is a leading-edge separation. Drooping the leading-edge flaps delays the angle of attack at which leading-edge separation occurs. As Mach number is increased, leading-edge separation for the basic wing is suppressed by the transonic attachment phenomenon, and thus is delayed until higher angles of attack are attained (see Reference 23 for further discussion).

At transonic speeds (which can be defined as Mach numbers above the minimum value for leading-edge attachment) a shock system develops on the wing. The thin wing produces relatively weak shock waves and thus shock-induced separation occurs only over a limited angle of attack and Mach region. Within that range of Mach numbers, leading-edge flap deflection at low angles of attack is detrimental rather than beneficial because shock-induced separation occurs.

Figures 40 and 41 illustrate the point made above. Figure 40 is a set of surface oil-flow photographs which are unfortunately of poor quality. Figure 41 is sketches of the flow patterns which depict schematically the major flow phenomena observed in the

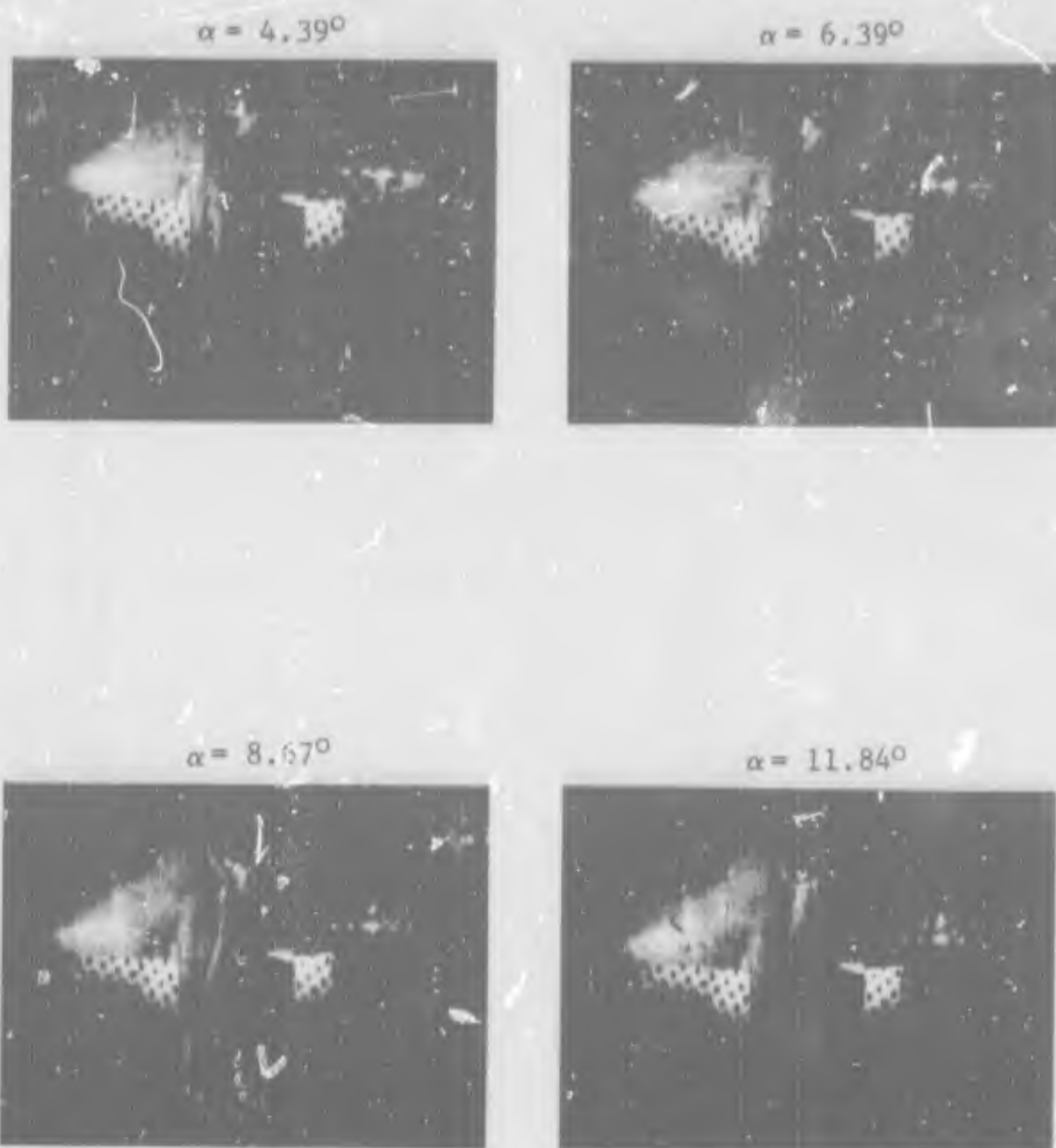


Figure 40 FLOW VISUALIZATION LEADING EDGE EFFECTS  
LEFT 10, RIGHT 0 MACH = 0.9

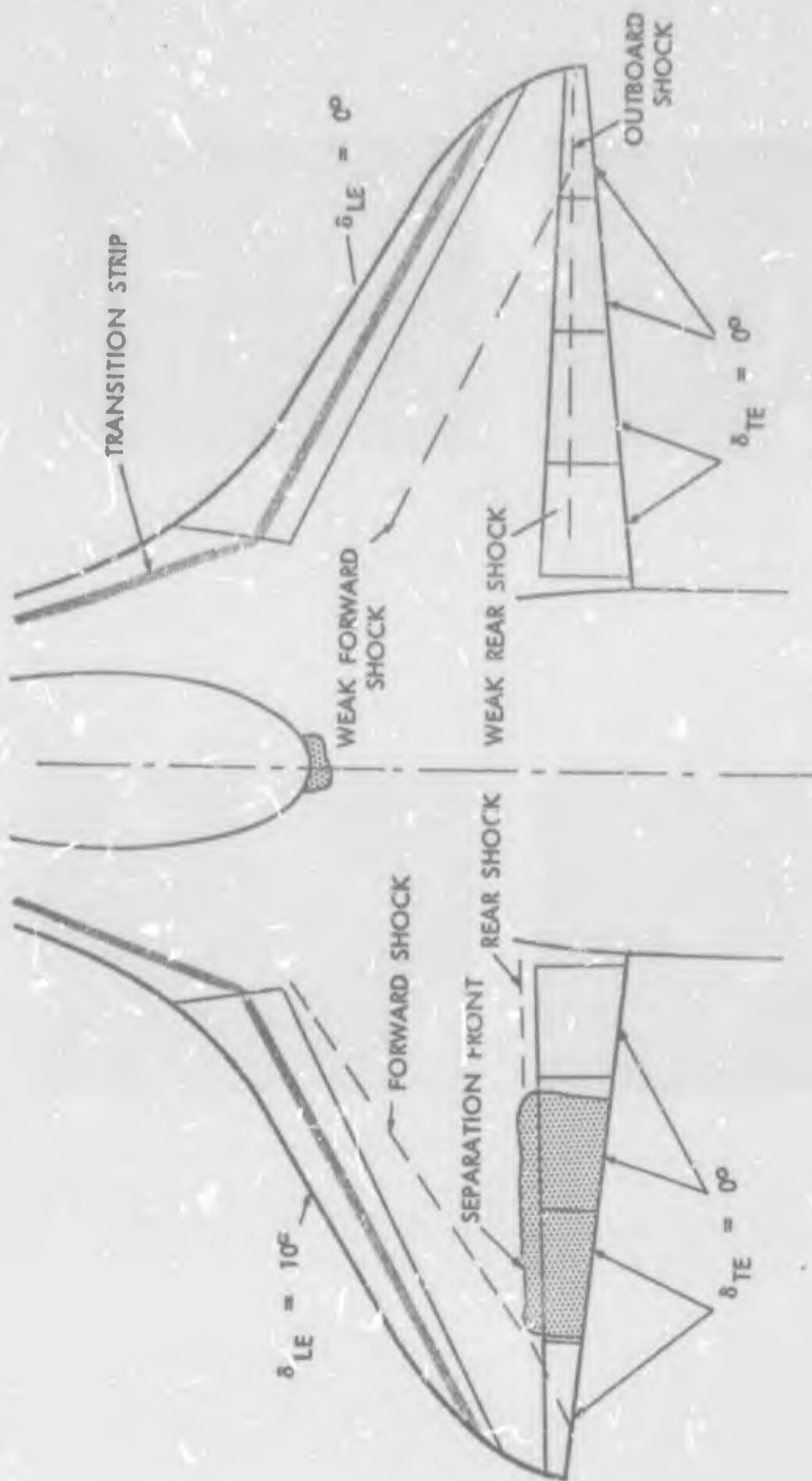


Figure 4.1a SKETCH OF FLOW PATTERNS FOR DIFFERENTIAL LEADING EDGE DEFLECTION  
 $\alpha = 4.39^\circ$ , MACH = 0.90

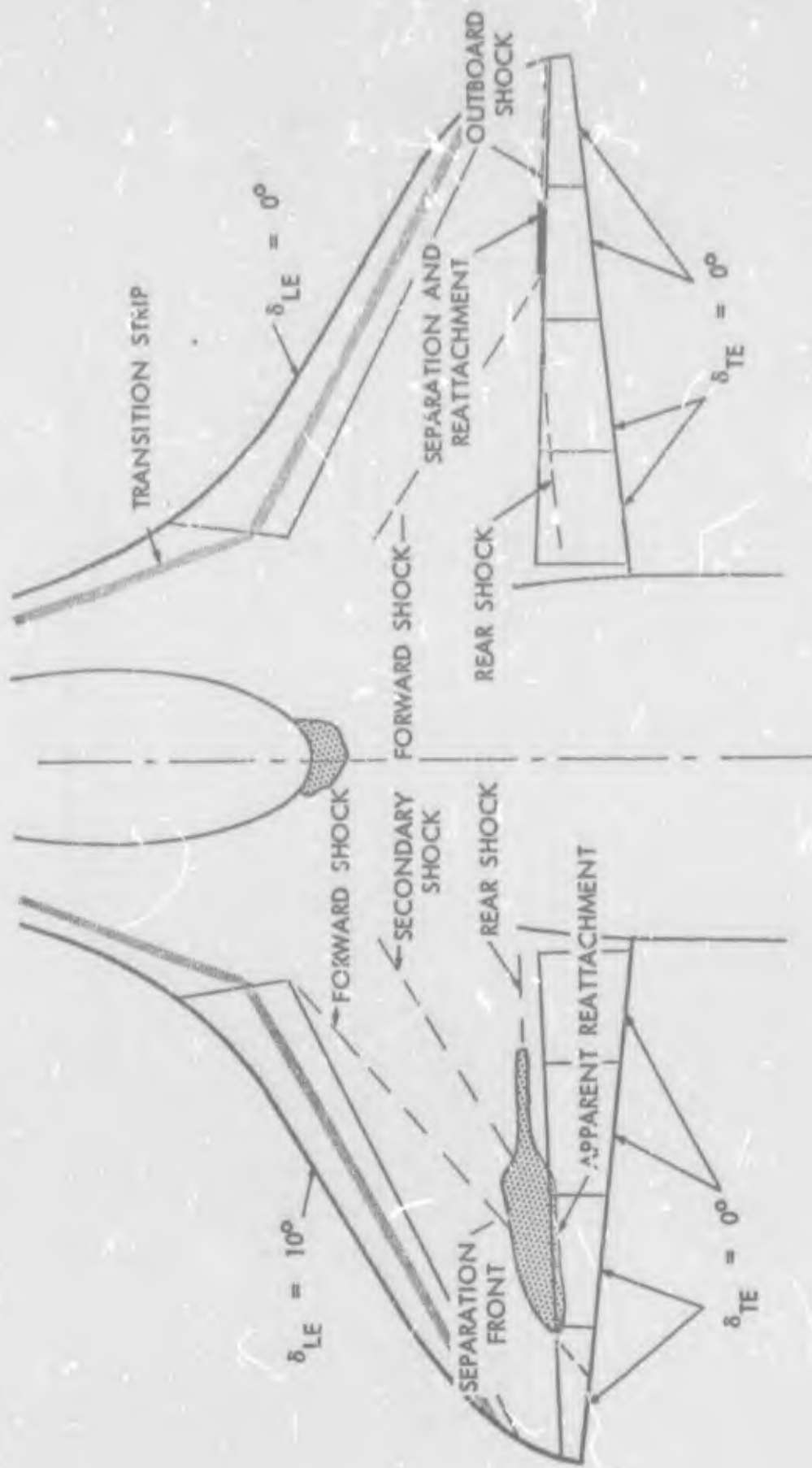


Figure 41b SKETCH OF FLOW PATTERNS FOR DIFFERENTIAL LEADING EDGE DEFLECTION  $\alpha = 6.39^\circ$ , MACH = 0.90

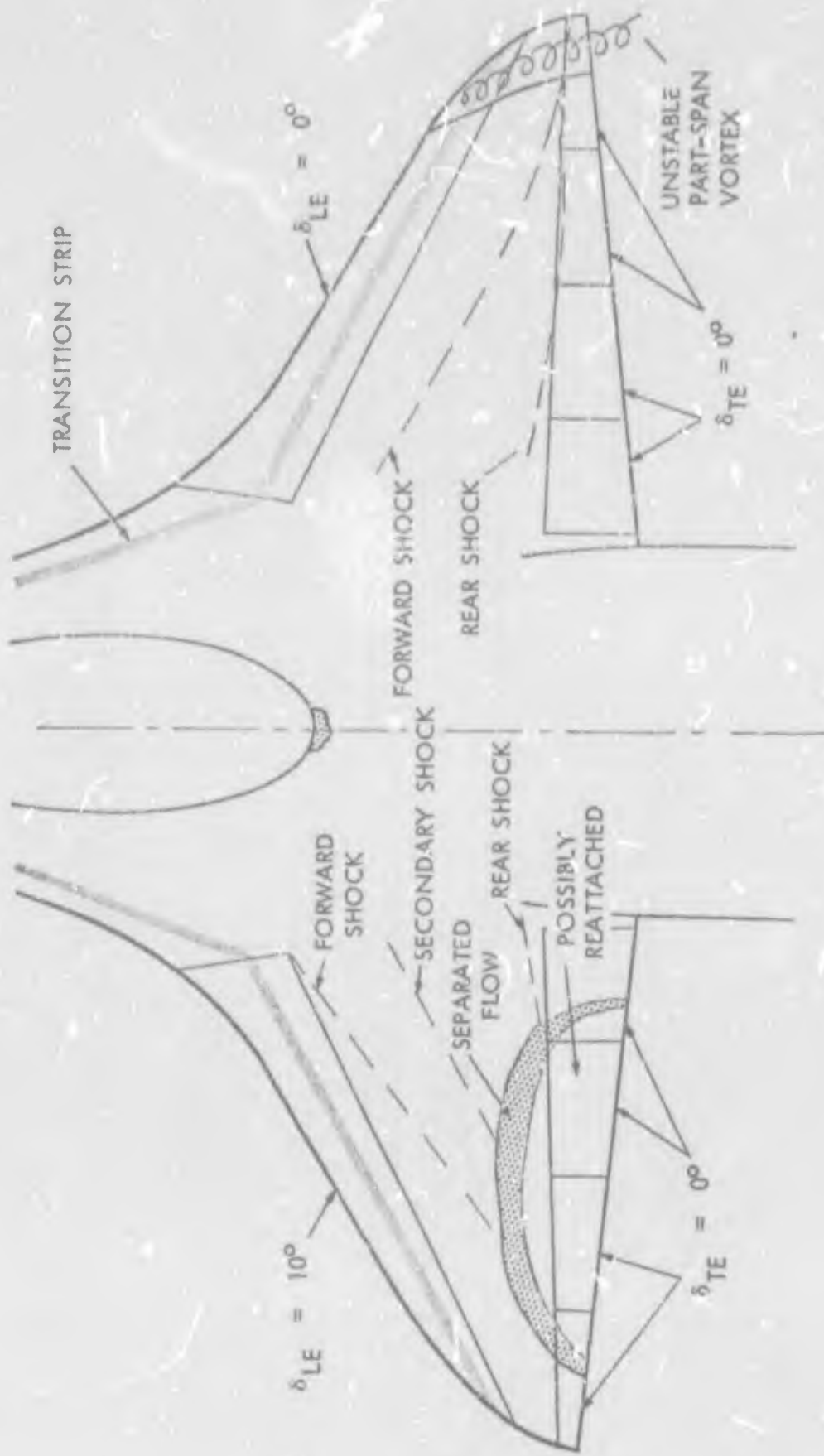


Figure 41c SKETCH OF FLOW PATTERNS FOR  
 DIFFERENTIAL LEADING EDGE DEFLECTION  
 $\alpha = 8.67^\circ$ , MACH = 0.90

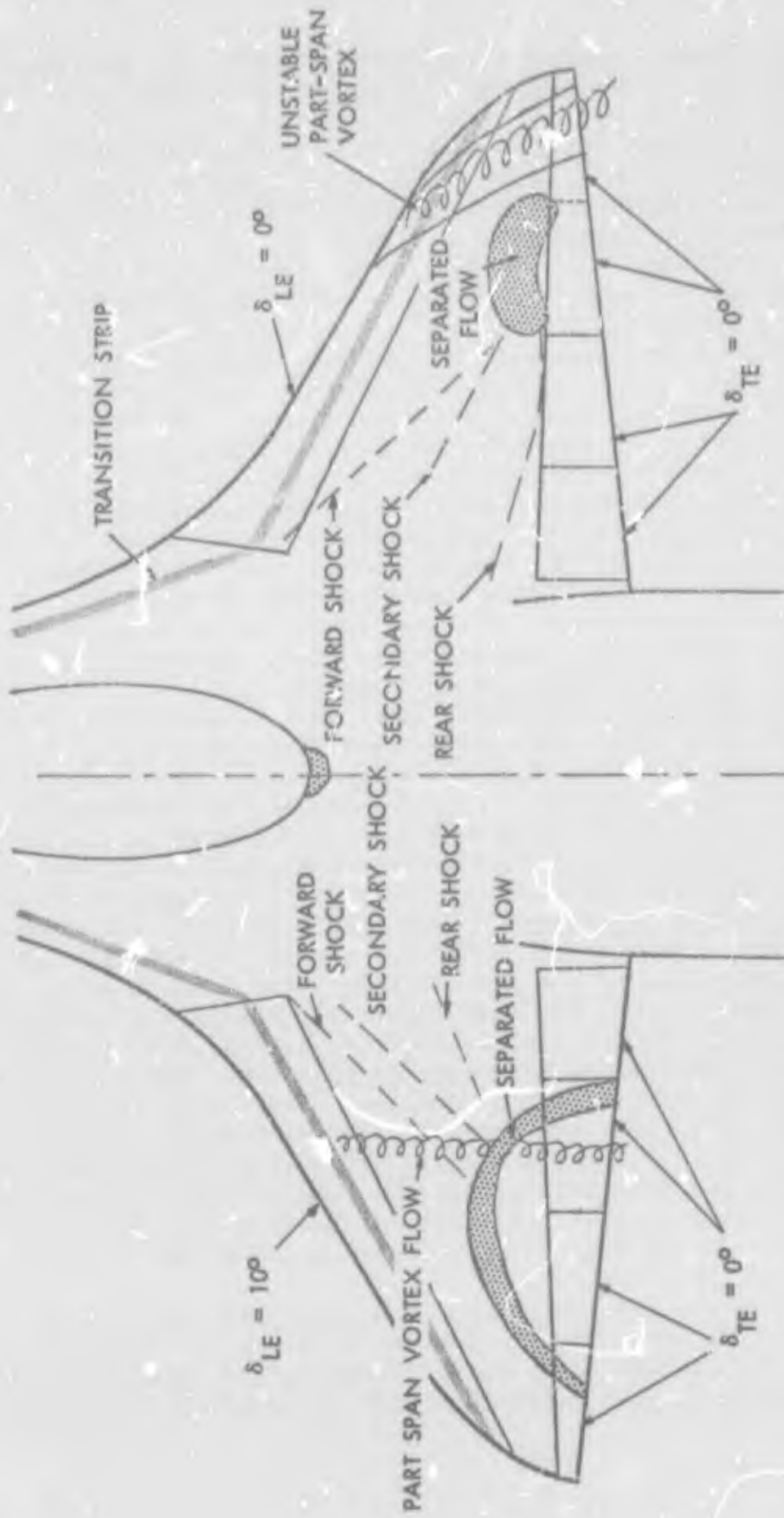


Figure 41d SKETCH OF FLOW PATTERNS FOR DIFFERENTIAL LEADING EDGE DEFLECTION  
 $\alpha = 11.84^\circ$ , MACH = 0.90

original data films. The test configuration has the left leading-edge flap set at 10 degrees deflection, the right wing has no deflection.

On the right wing a three-shock pattern is present at an angle of attack of 4.39 degrees. The forward shock occurs well aft on the wing and apparently all three shocks are relatively weak for there is no indication of separated flow. At 6.39 degrees angle of attack, the forward shock is more highly swept and there is a small region of separated flow where the forward shock and rear shock merge to form the outboard shock. The flow reattaches almost immediately. At 8.67 degrees angle of attack, the flow separates at the leading edge just inboard of the tip and an unsteady part-span vortex occurs. The vortex flow modifies the shock pattern such that no distinct outboard shock can be observed. Finally at 11.84 degrees angle of attack, the origin of the part-span vortex has moved inboard on the leading-edge. Another forward shock occurs which originates just ahead of the flap hinge-line and sweeps back sharply to intersect the previous shock system at about 50 percent of the exposed span. A region of separated flow exists just outboard of the shock intersection. This separated flow interacts strongly with the part span vortex.

The flow patterns on the left wing are different from those on the right wing. At 4.39 degrees angle of attack, a forward shock originates from the hinge line at the inboard end of the leading-edge flap. This forward shock is caused by the very rapid expansion over the highly curved surface at the hinge line. The rear shock occurs farther forward on the left wing than on the right wing and is apparently stronger for a well defined region of separated flow occurs over the two middle control surface segments. At 6.4 degrees angle of attack, the separation moves forward and its front is altered in shape by a secondary shock wave. The flow apparently reattaches on the control surfaces. At 8.4 degrees angle of attack, the separation front is highly curved and has expanded spanwise. There is no indication of leading edge separation. Finally at 11.84 degrees angle of attack, the shock-induced separation front has moved forward still further and again there is no indication of flow separation from the leading edge near the tip. However, a part-span vortex streams back from the leading-edge near midspan. This vortex apparently has its origin at the inboard leading-edge of the flap.

From the above discussions one can infer that the use of leading edge flap deflection to prevent or delay the onset of flow separation effects (e.g. buffet onset) would require complex programming of flap deflection with angle of attack and

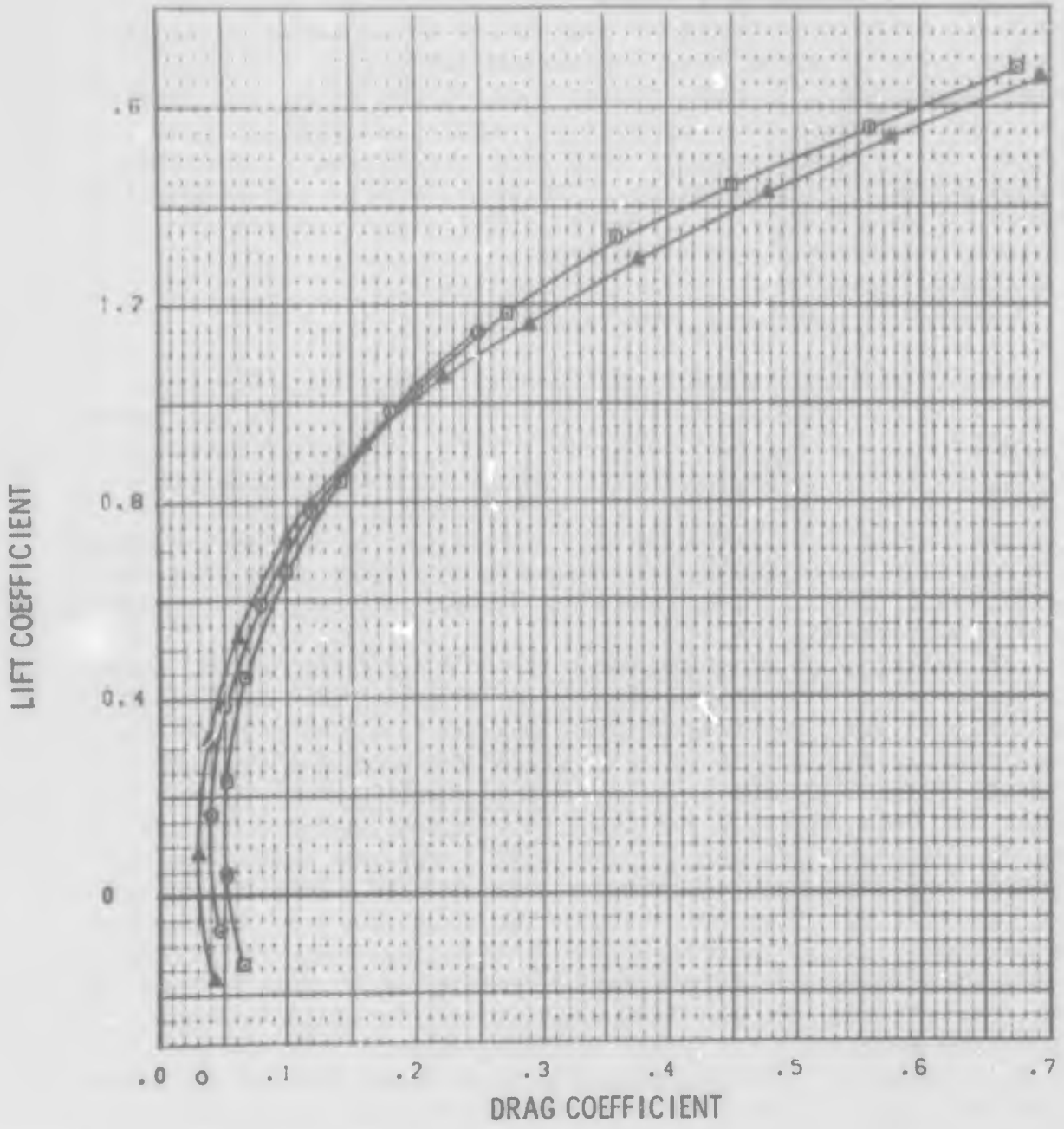
Mach number. Such use would not appear to be practical in application. A more realistic and practical use of leading-edge flaps would employ a simple two-position control such that zero deflection would be used below about seven or eight degrees angle of attack and a selected deflection for higher angles of attack. In this design concept the flaps are used primarily to reduce the severity of separation effects (for example the drag increase at high lift coefficients) and thus enhance transonic maneuvering. The test results and discussions thereof presented in the following subsections support the simple two-positions design concept.

#### a. Test Results for Basic Leading Edge

The effects of symmetrical leading edge flap deflection on the lift and drag characteristics of the LEDE test configuration with and without the horizontal tail are illustrated by Figures 42 and 43, respectively. These figures present comparisons of the drag polars at 0.9 Mach number for each leading edge deflection. Data for the additional Mach numbers tested are presented in Appendix IV. These drag polars show that the leading-edge flaps improve the drag levels at high lift coefficients for subsonic speeds.

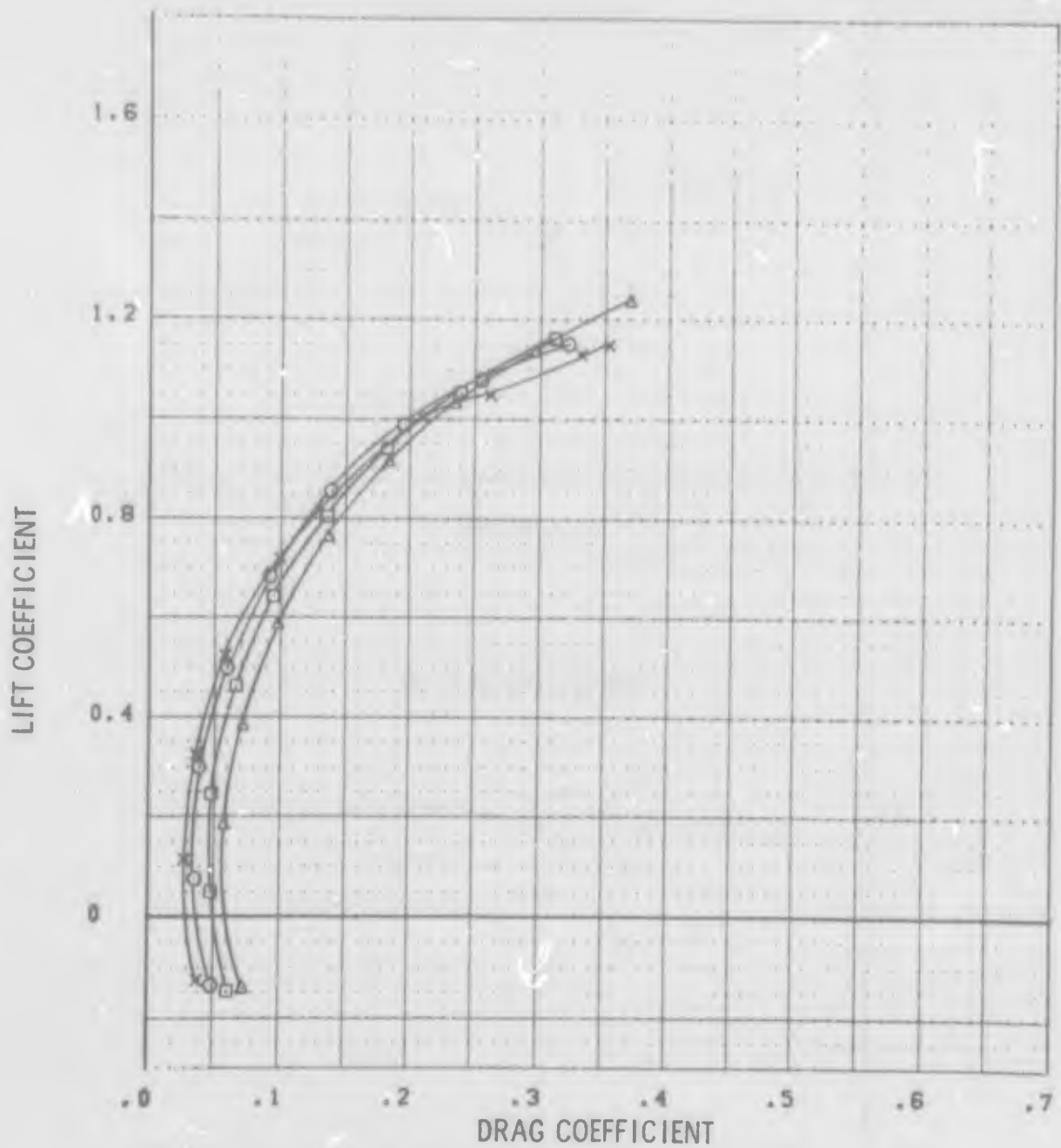
An analysis of drag-due-to-lift data from the 4-foot tunnel was performed by the square-root plot method. The results of the analysis for the various leading-edge flap deflections are summarized in Figures 44 thru 46 where the drag-due-to-lift parameters,  $C_{Lc}$ ,  $K$ , and  $C_{L(CD_{MIN})}$  are plotted against Mach number for constant flap deflections. These analysis curves provide evidence that the leading-edge flaps are efficient in reducing upper surface separation. It is noted from Figure 44 that the lift coefficient at which the drag-due-to-lift becomes non-parabolic,  $C_{Lc}$ , increases with increasing flap deflection at all Mach numbers. Furthermore, leading edge flap deflection causes an increase in the lift coefficient for minimum drag, but at the same time increases the drag-due-to-lift factor at all Mach numbers. The overall effect of these factors is beneficial at high lift coefficients as illustrated by the improvement in the drag polars at high angles of attack. However, as Mach number increases, the beneficial effects of deflecting the leading edge are delayed to higher lift coefficients, and the lift and drag penalties incurred at low angles of attack increase markedly. For example, the large deflection angles of 10 and 15 degrees improve the drag polars considerably at 0.7 Mach number, but at 1.2 Mach number even the 5-degree deflection does not offer any improvement in the drag levels until values of  $C_L$  are greater than 1.0. The increases in minimum drag due to leading-edge flap deflection are shown in Figure 47.





| SYM | WING   | FLAP   | PAR. | ... ( / R) |
|-----|--------|--------|------|------------|
| ○   | PWT 4' | TC 043 | 445  | K: 5/5     |
| □   | PWT 4' | TC 043 | 176  | K: 10/10   |
| ▲   | PWT 4' | TC 043 | 264  | K: 0/0     |

FIGURE 42 SYMMETRIC LEADING EDGE FLAP EFFECTS H.T. ON  
M 0.9



| SYM | TEST          | PART | L.E. (L/R) |
|-----|---------------|------|------------|
| ○   | PWT 4T TC-043 | 37   | K1 5/5     |
| □   | PWT 4T TC-043 | 47   | K1 10/10   |
| △   | PWT 4T TC-043 | 54   | K1 15/15   |
| x   | PWT 4T TC-043 | 30   | K1 0/0     |

FIGURE 43 SYMMETRIC LEADING EDGE FLAP EFFECTS. H.T. OFF  
M = 0.9

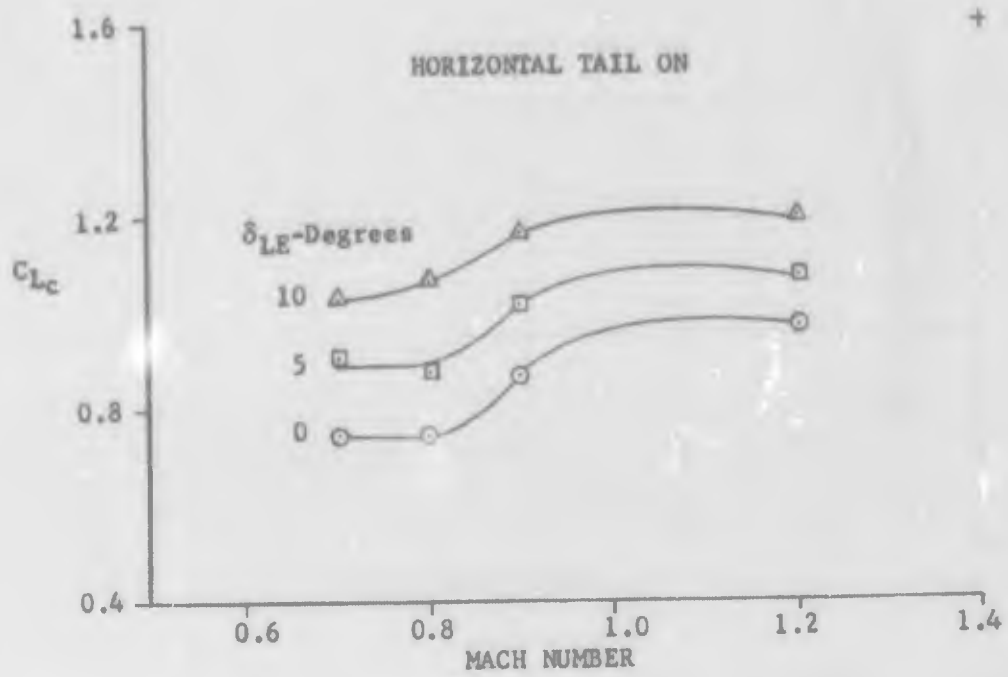
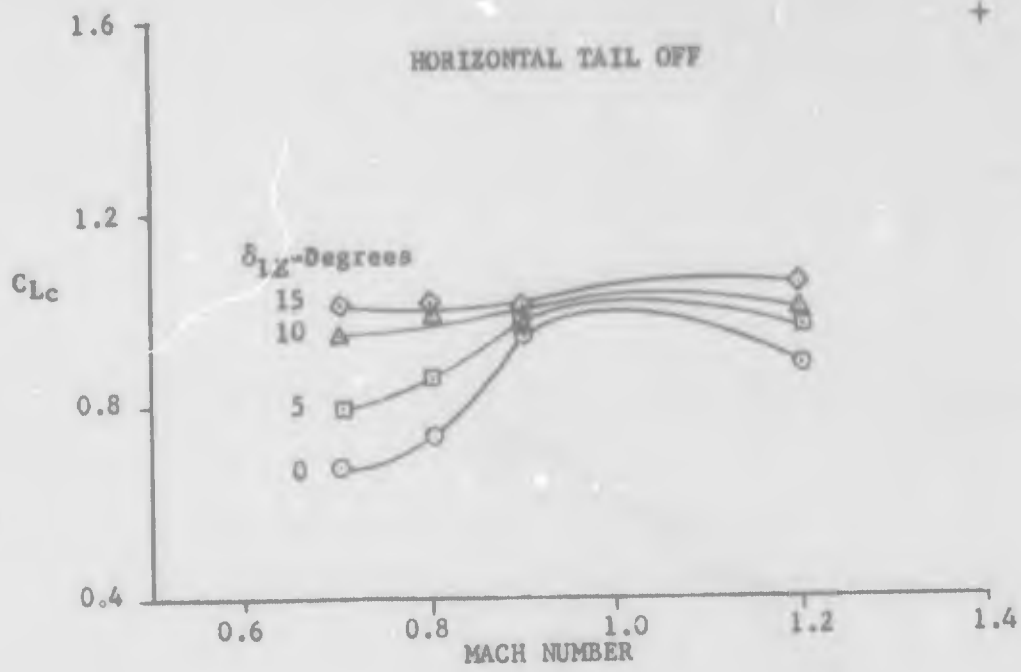


Figure 44 EFFECT OF LEADING EDGE FLAP DEFLECTION ON CRITICAL LIFT COEFFICIENT

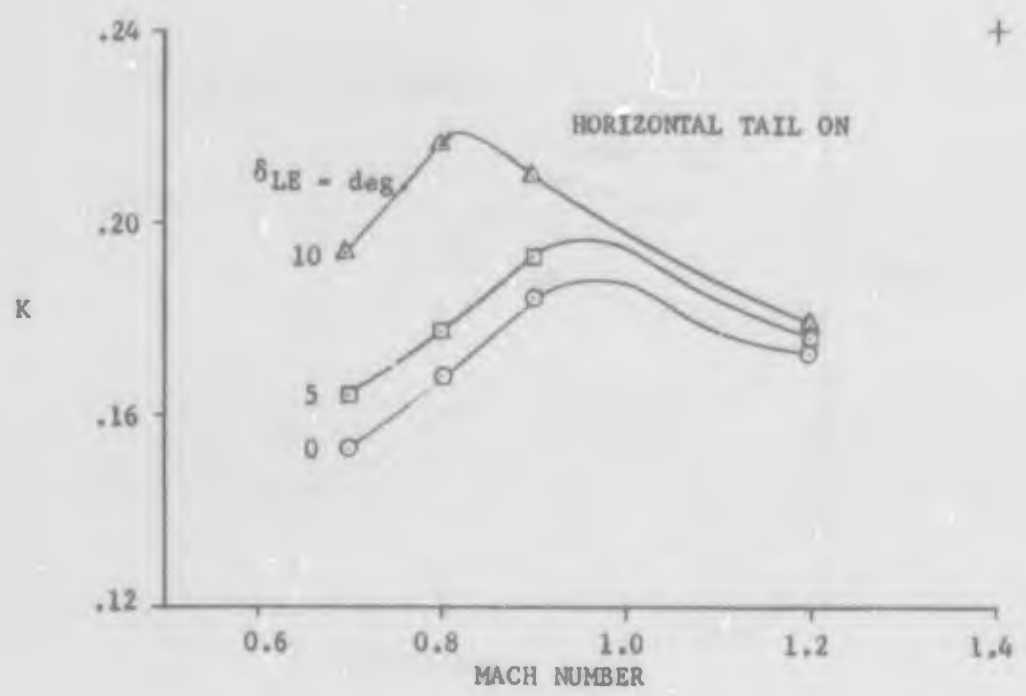
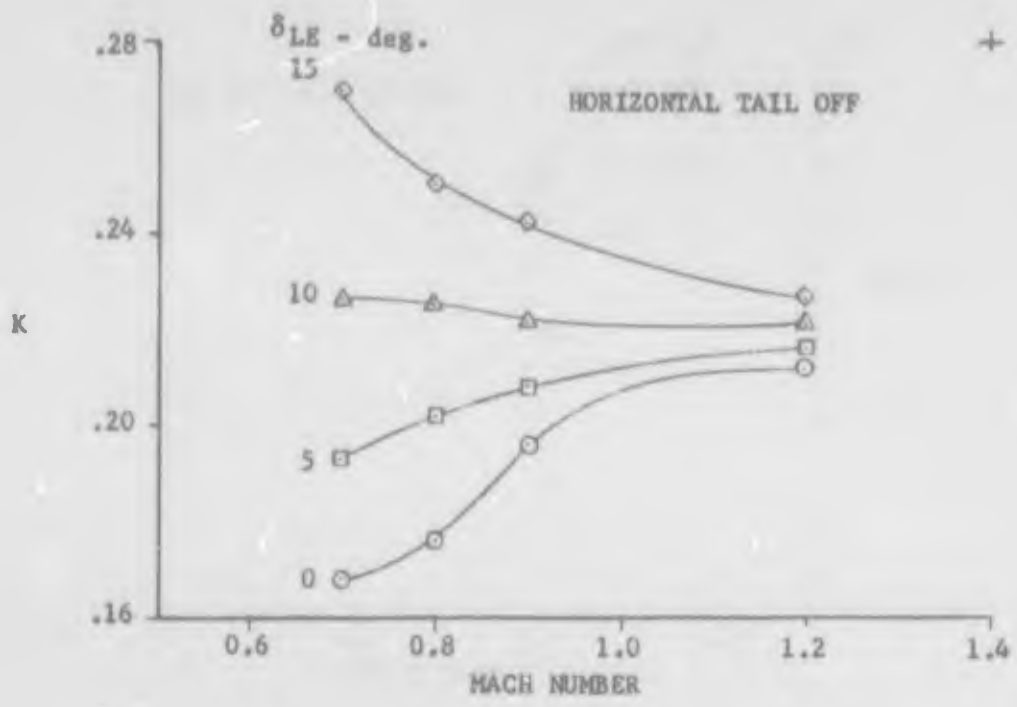


Figure 45 EFFECT OF LEADING EDGE FLAP DEFLECTION ON DRAG-DUE-TO-LIFT FACTOR

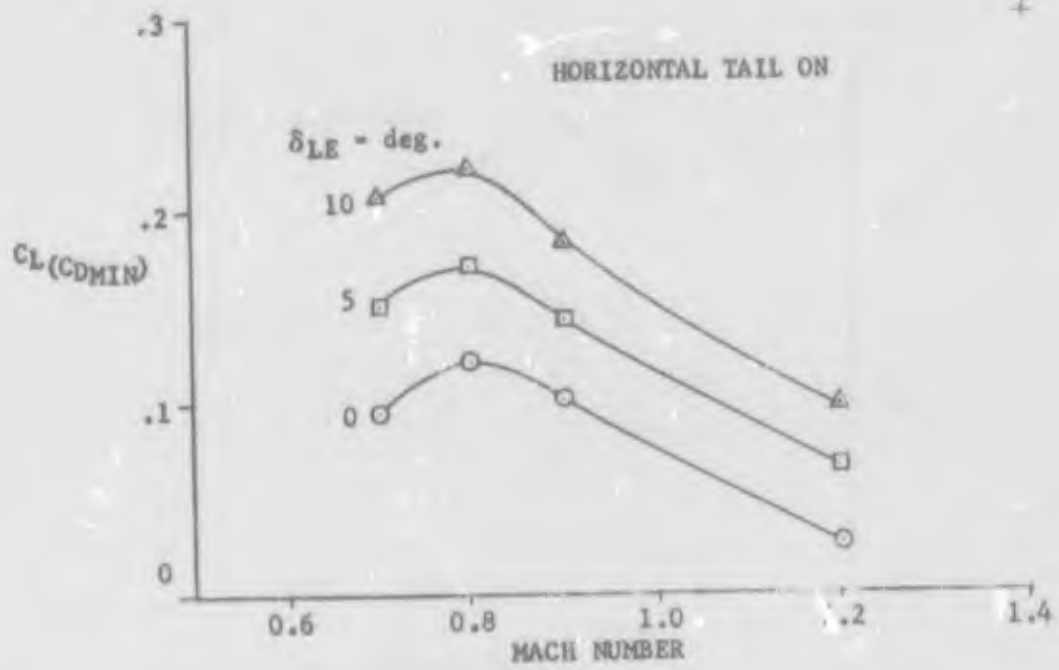
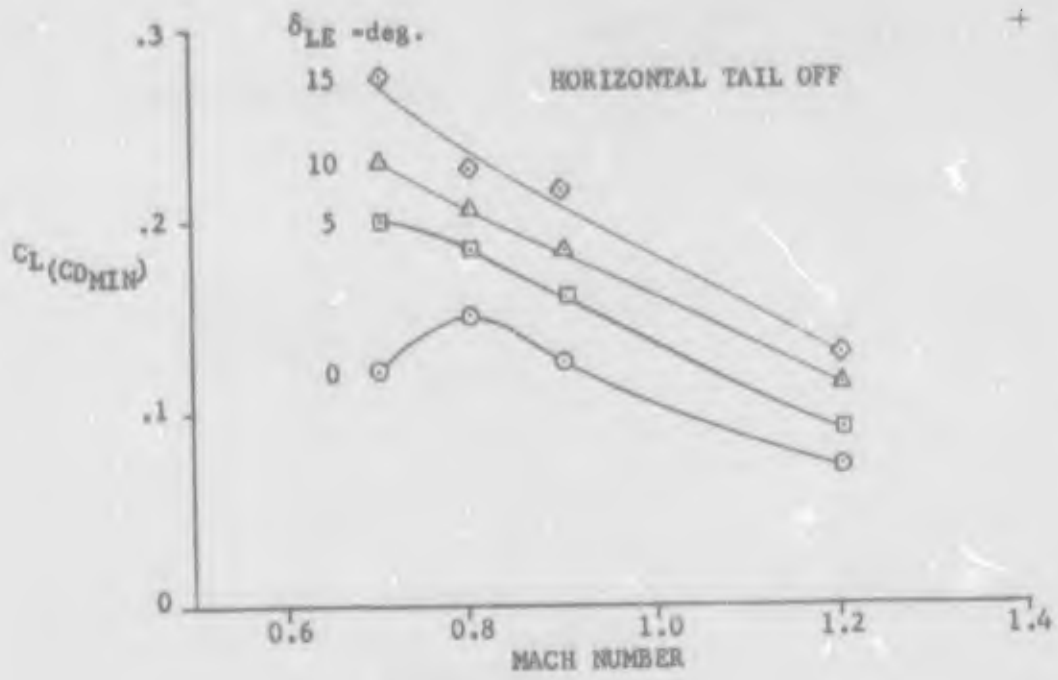


Figure 46 EFFECT OF LEADING EDGE FLAP DEFLECTION ON LIFT COEFFICIENT FOR MINIMUM DRAG

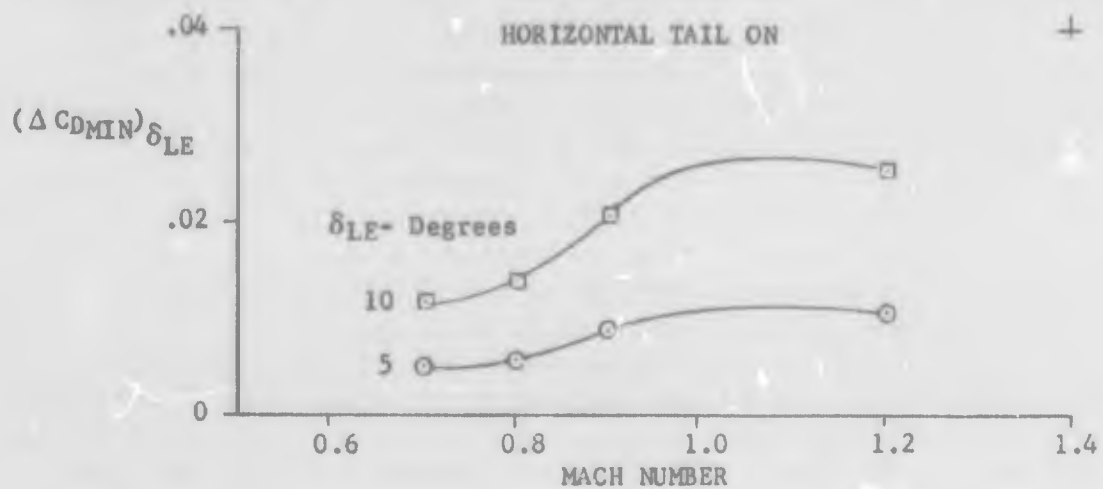
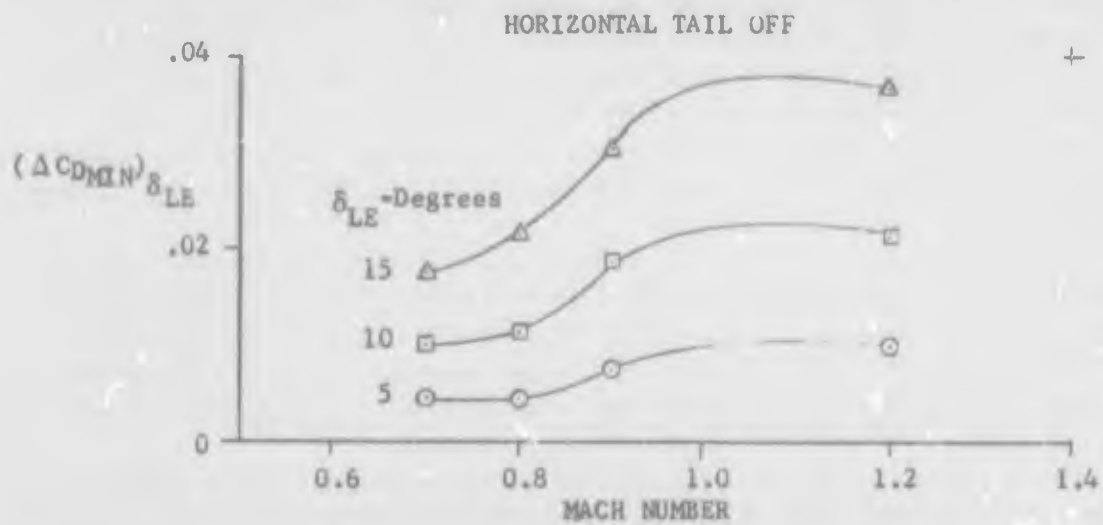


Figure 47 EFFECT OF LEADING EDGE FLAP DEFLECTION ON MINIMUM DRAG COEFFICIENT

Comparison of the drag-due-to-lift parameters, for the tail-off and tail-on cases, Figures 44 thru 46, show that these curves are generally similar but that there are noticeable differences in the trends with Mach number, and in the values themselves. The polar shape factor is improved by addition of the horizontal tail at all flap deflections tested at each Mach number, the lift coefficient for minimum drag generally decreases, and the critical lift coefficient is increased somewhat.

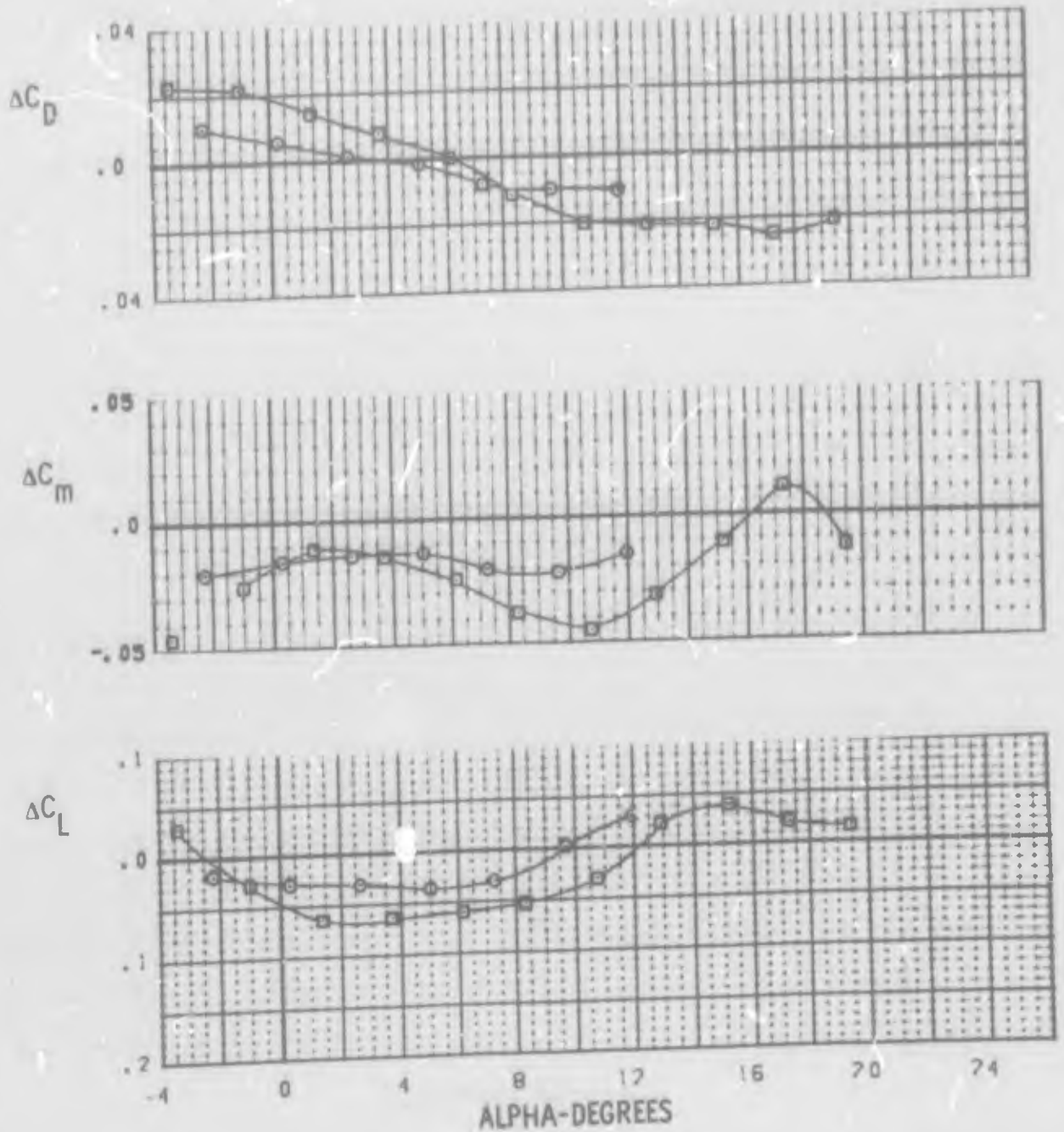
The variation in the increments for lift, drag and pitching moment due to leading edge flap deflection with angle of attack are presented in Figures 48 and 49 for 0.9 Mach number for both the tail-off and the tail-on cases. The increments for the 10-degree deflection are summarized in Figures 50 and 51 to illustrate the effects of Mach number.

The data in Figures 48 and 49 show three typical effects. First, as leading-edge flap deflection is increased, the angles of attack for obtaining reduced drag and increased lift both increase. Second, the drag reduction is obtained at a lower angle of attack than is an increase in lift. The net effect on the drag polars is such that overall drag reduction occurs at relatively high lift coefficients. Third, the lift increments due to flap deflection are somewhat more positive with tail-on than with tail-off which indicates favorable wing/horizontal-tail interference with respect to lift.

Figures 50 and 51 show, for a given flap deflection, that the angles of attack for lift increase and those for drag reduction increase with Mach number, but again are different in value, drag reduction occurring at smaller angles. In the high lift region, the amount of additional lift obtained with a given flap deflection decreases with Mach number.

The variations of the incremental drag with angle of attack, Figures 50 and 51 and Appendix IV, show that all leading-edge flap deflections produce reductions in drag at moderate-to-high angles of attack for all Mach numbers. Both the drag penalties incurred at low angles of attack and the drag savings gained at high angles of attack are appreciable increments. The maximum values of these increments may be as much as  $+0.0300$  and  $-0.0400$ , respectively, depending on the flap deflection and Mach number.

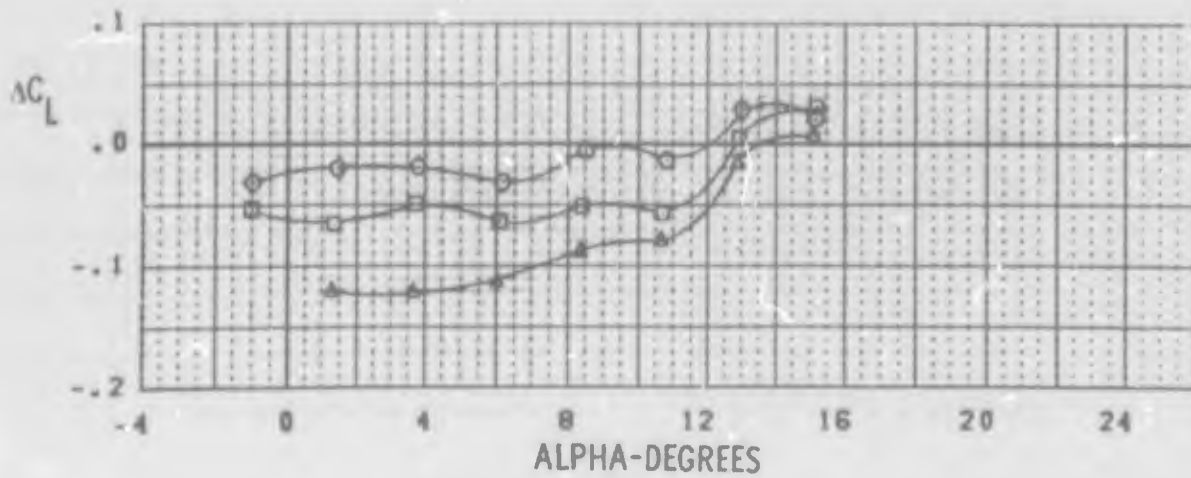
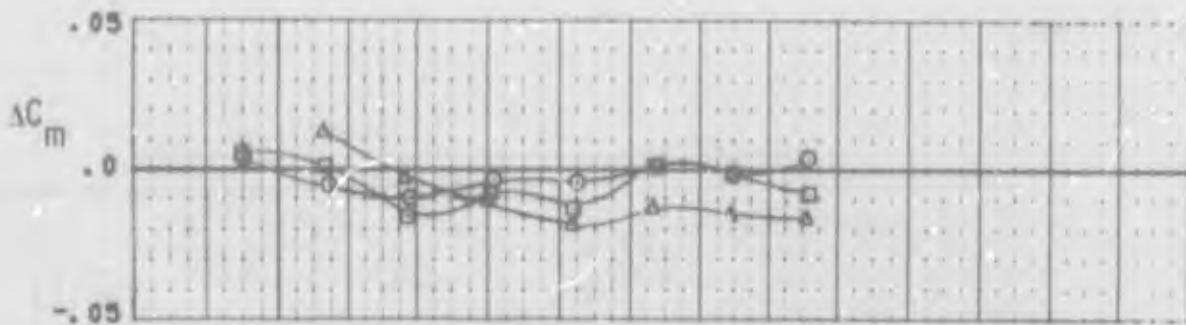
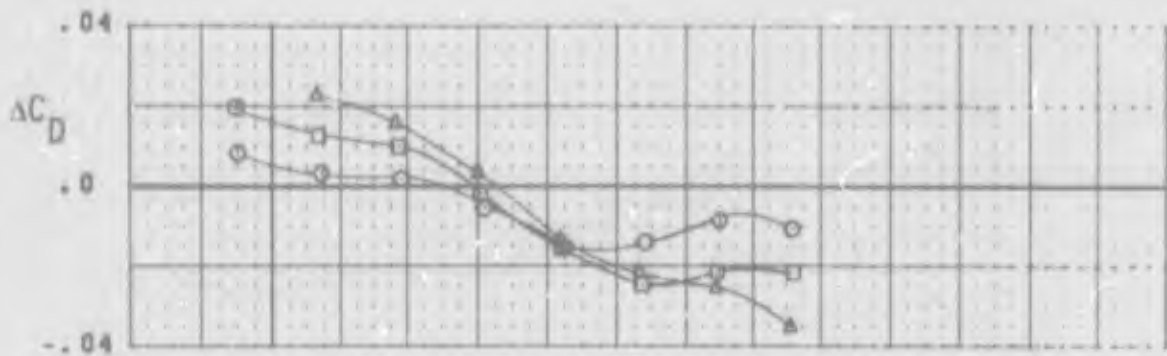
The tail-on and tail-off incremental drag curves are very similar, indicating that adding the horizontal tail does not appreciably affect the drag increment due to leading edge flap deflection.



| SYM | TEST          | INCREMENT       | L.E. (L/R) |
|-----|---------------|-----------------|------------|
| ○   | PWT 4T TC-043 | PN 445 - PN 264 | K1 5/5     |
| □   | PWT 4T TC-043 | PN 126 - PN 264 | K1 10/10   |

Figure 48 SYMMETRIC LEADING EDGE FLAP EFFECTS, H.T. ON  
M = 0.9





| SYM | TEST          | INCREMENT     | L.E. (L/R) |
|-----|---------------|---------------|------------|
| ○   | PWT 4T TC-043 | PN 37 - PN 30 | K1 5/5     |
| □   | PWT 4T TC-043 | PN 47 - PN 30 | K1 10/10   |
| △   | PWT 4T TC-043 | PN 54 - PN 30 | K1 15/15   |

FIGURE 49 SYMMETRIC LEADING EDGE FLAP EFFECTS, H.T. OFF  
M = 0.9

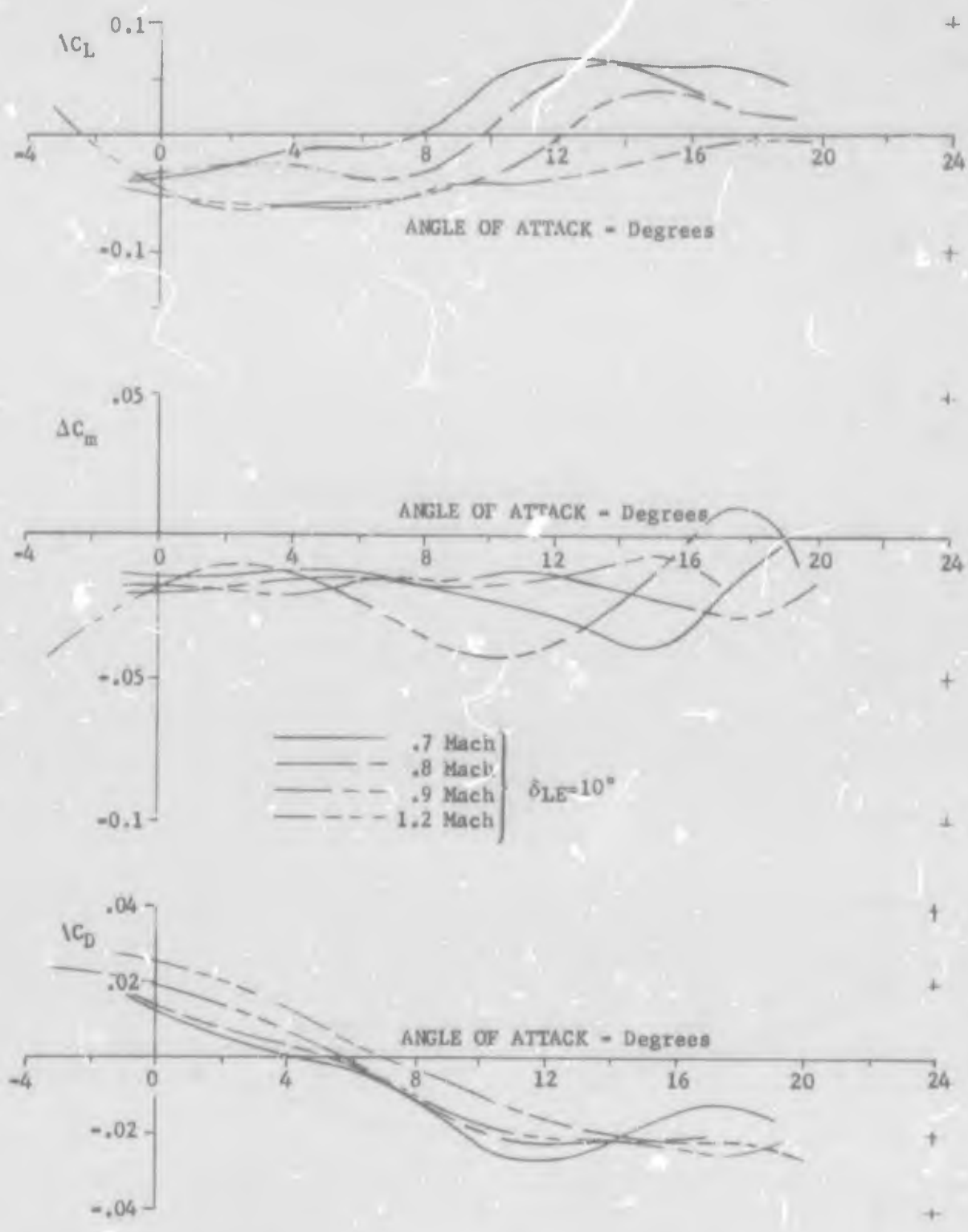


Figure 50 VARIATION OF LEADING EDGE FLAP INCREMENTS WITH MACH NUMBER, HORIZONTAL TAIL ON

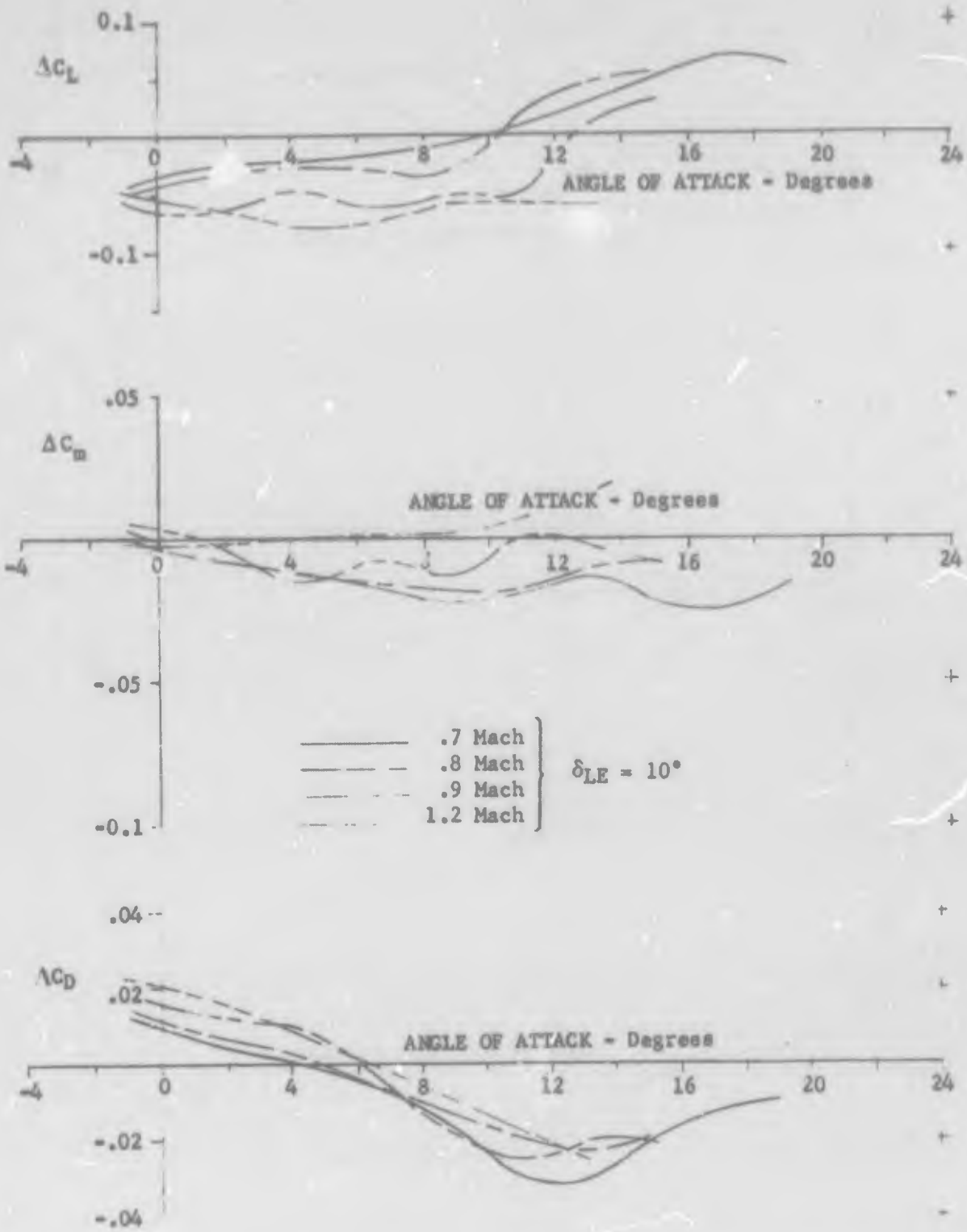


Figure 51 VARIATION OF LEADING EDGE FLAP INCREMENTS WITH MACH NUMBER, HORIZONTAL TAIL OFF

The variation of the incremental pitching moment due to leading edge flap deflection, Figures 50, 51, and Appendix IV show that the trim changes required due to leading-edge flap deflection are not significantly large, with the greatest differences occurring at higher angles of attack. Note that these increments are plotted to a large scale to show the small effects of configuration changes. Variations in stability levels for the various configurations should be evaluated using the basic  $C_m$  versus  $C_L$  plots of Appendix IV.

b. Comparison of Test Results with Predictions

The lift and drag characteristics of the LEDE configuration were estimated at Mach numbers of 0.7, 0.9 and 1.2 for each leading-edge flap deflection prior to testing. The predictions were made for the wing-body configuration since it was originally planned to test without a horizontal tail. The predicted lift curves and drag polars are compared with the measured test data from the 4T facility at Mach 0.9 and 1.2 in Figures 52 and 53.

A comparison between the lift-curve slope measured in the 4T facility and the predicted lift-curve slope is shown in Figure 54. Two different methods of predicting the lift curve slope were used. They are the double-delta method and the cranked-wing method taken from Reference 5. The prediction methods were empirically derived from data primarily for simple wing-body combinations. Apparently the very complex wing geometry of the LEDE configuration enhances the lift curve slope in the subsonic Mach number regime. The cranked wing method provides the better of the two sets of predictions but still underestimates the measured values by about 10 percent at subsonic speeds. The lift curves shown in Figure 52 are based on the double-delta method.

An analysis of the wind tunnel test data previously mentioned was used to account for effects of wing camber, incidence, flow separation, and leading edge flap effects. These incremental effects agree fairly well except at high lift coefficients and at low Mach numbers where separation was predicted too early.

Pretest predictions of the angle of zero lift are presented in Figure 54. These estimates are not good, which reflects the difficulty of predicting this particular characteristic on the basis of data for a different configuration.

Estimated drag polars were obtained by combining minimum drag and drag-due-to-lift predictions. The minimum drag levels

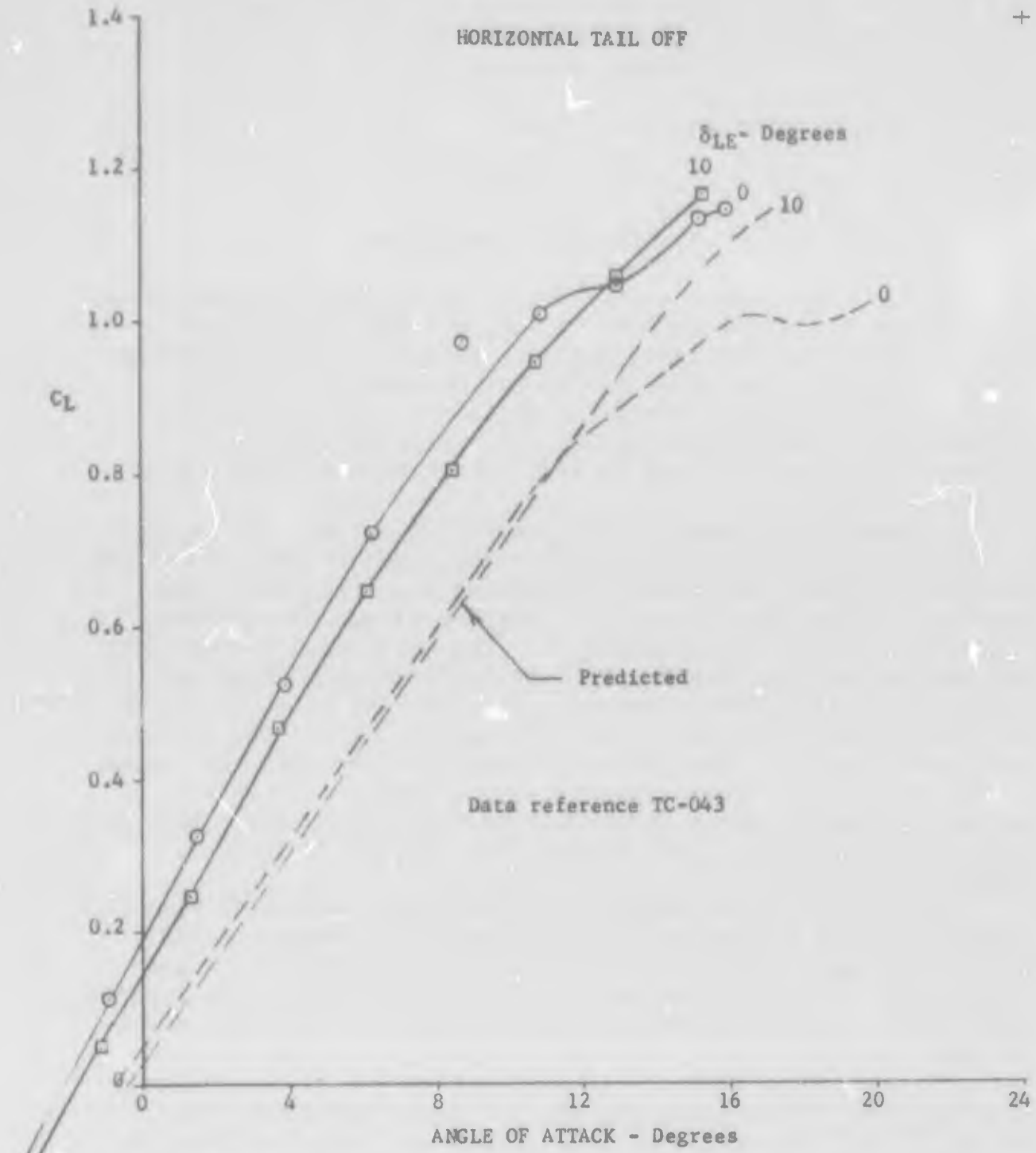
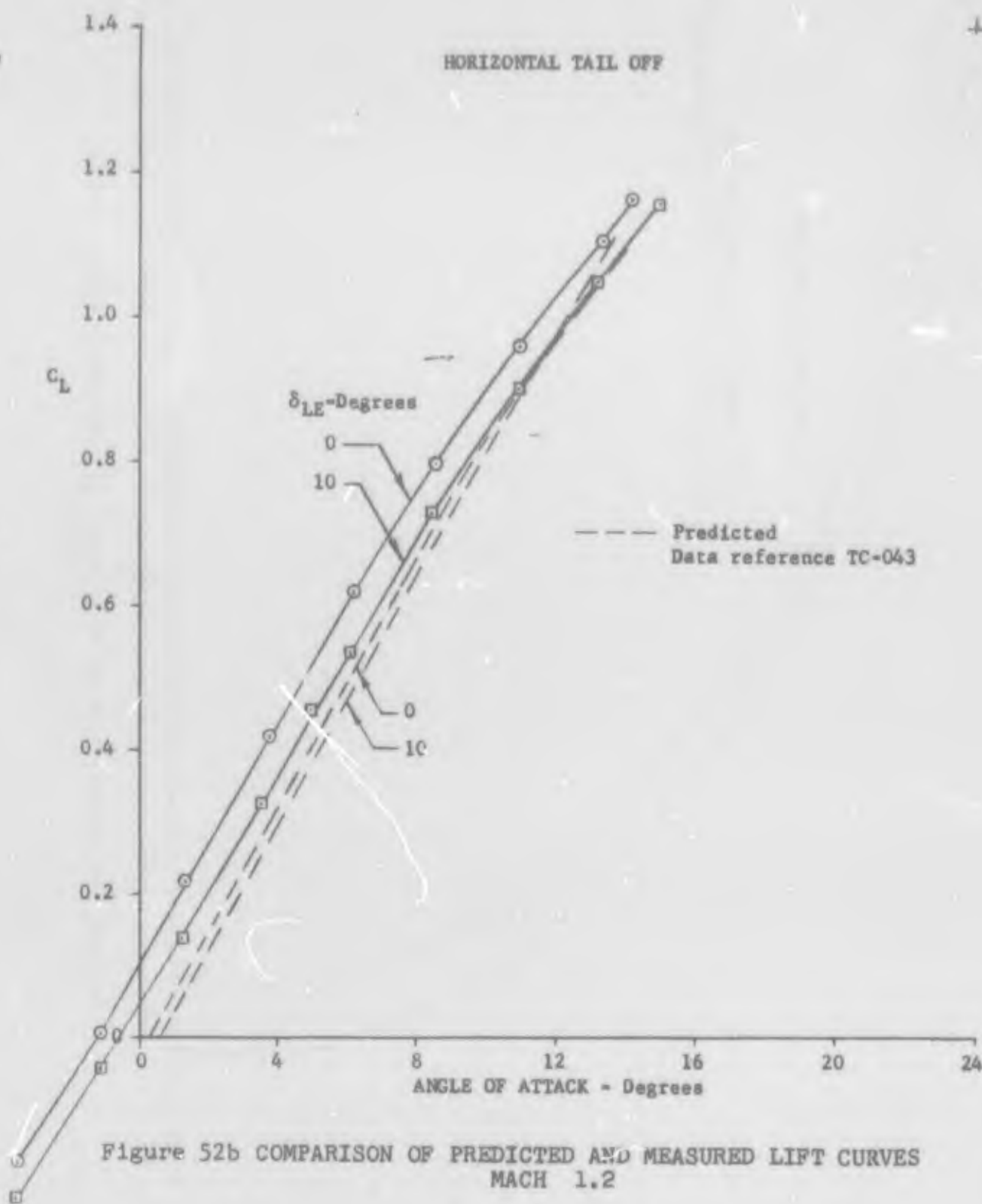


Figure 52a COMPARISON OF PREDICTED AND MEASURED LIFT CURVES  
MACH 0.9



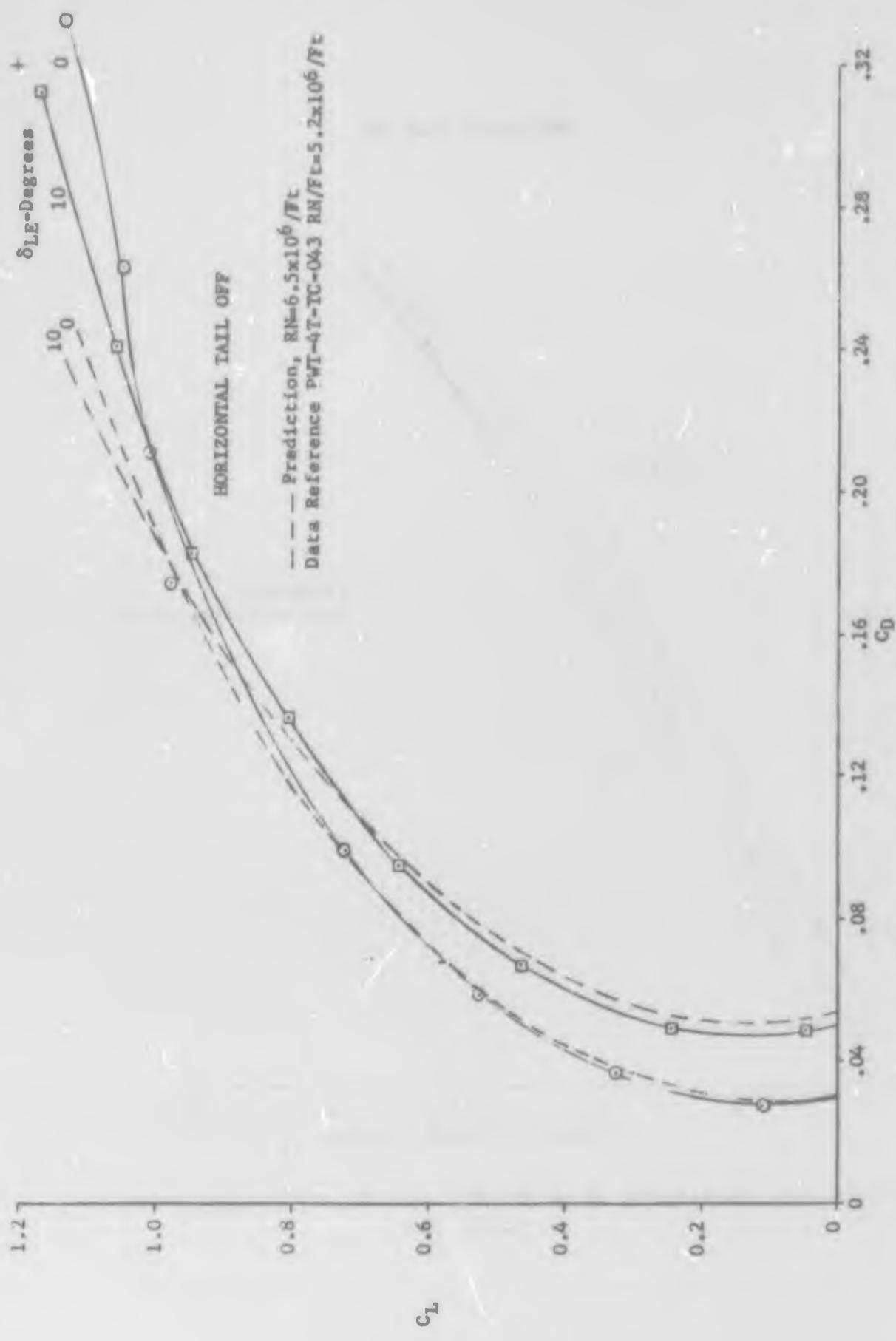


Figure 53a COMPARISON OF PREDICTED AND MEASURED DRAG POLARS  
MACH 0.9

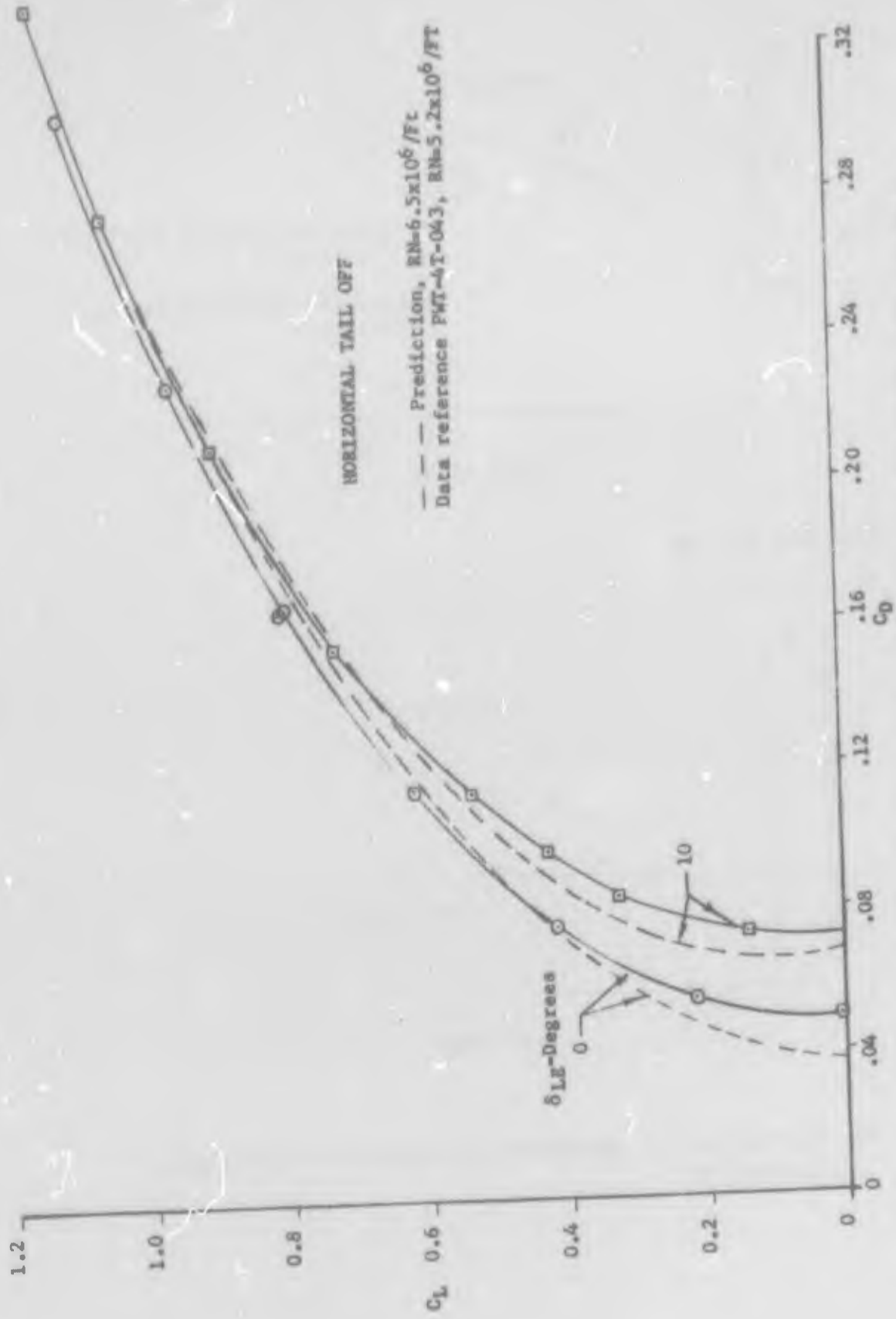
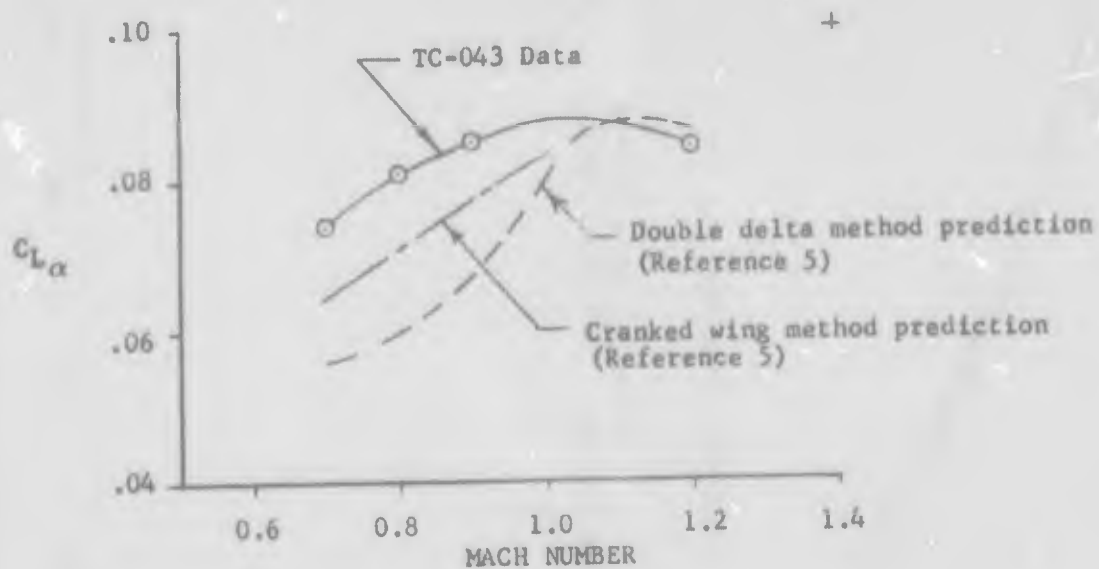


Figure 53b COMPARISON OF PREDICTED AND MEASURED DRAG POLARS  
 MACH 1.2





HORIZONTAL TAIL OFF

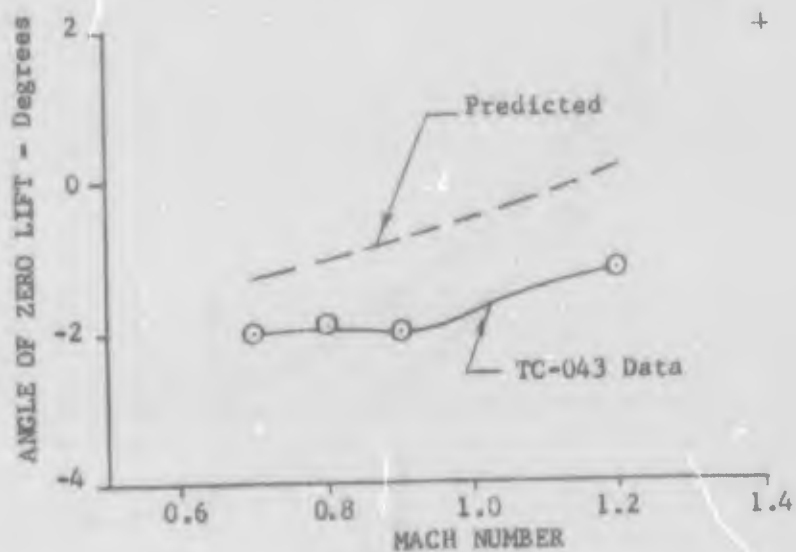


Figure 54 COMPARISON OF PREDICTED AND MEASURED LIFT-CURVE PARAMETERS

were obtained by a buildup of friction, form, wave, compressibility and drag rise, and camber drag increments. These predictions were made using standard General Dynamics techniques described in Reference 24. The drag due to lift predictions were based on semi-empirical methods derived from correlations of wind tunnel and flight test data recently developed at the Fort Worth Division. These predictions were also modified to account for the effects of flow separation and leading edge flap deflection by adding increments determined from analysis of previous test results.

The predicted and measured variations of the minimum drag coefficient with Mach number for the model without the horizontal tails are compared in Figure 55. It is observed that the subsonic predictions agree fairly well with the data, but that the supersonic prediction was considerably off. Several factors certainly influenced the agreement of the two curves. First, the model was tested at a Reynolds number of 5.2 million per foot and with the vertical tail, but predictions were made for the wing-body only at a Reynolds number of 6.5 million per foot. Further, the predicted values contain no attempt to account for the drag penalties associated with the inlet flow field. Finally, the wave drag predictions were made for a non-lifting condition, which is not the case.

The estimated increase in minimum drag for the various leading edge flap deflections is compared with test data from PWT 4T in Figure 56. Good agreement is obtained only for the smallest flap deflection at the low subsonic Mach numbers. In general the test drag increments are lower than the predicted values.

The comparisons of predicted drag polars with 4T test data in Figure 53 show that at subsonic speeds the predictions were optimistic at high lift coefficients. Considering the differences between the 4T and 16T drag polar data for the complete configuration, the predictions are probably better than the comparisons with the 4T data indicate. At supersonic speed, the agreement between prediction and test is reasonably good at high lift coefficients, but is poor at low lift coefficients for the configuration with zero flap deflection.

In summary, significant improvement in prediction techniques is needed to adequately estimate the effects of leading-edge flaps on the aerodynamic characteristics of a specific configuration at transonic and supersonic speeds.

#### 4. ALTERNATE LEADING EDGE

Typical effects of the alternate leading edge airfoil geometry are presented in Figures 57 and 58. These Figures

HORIZONTAL TAIL OFF

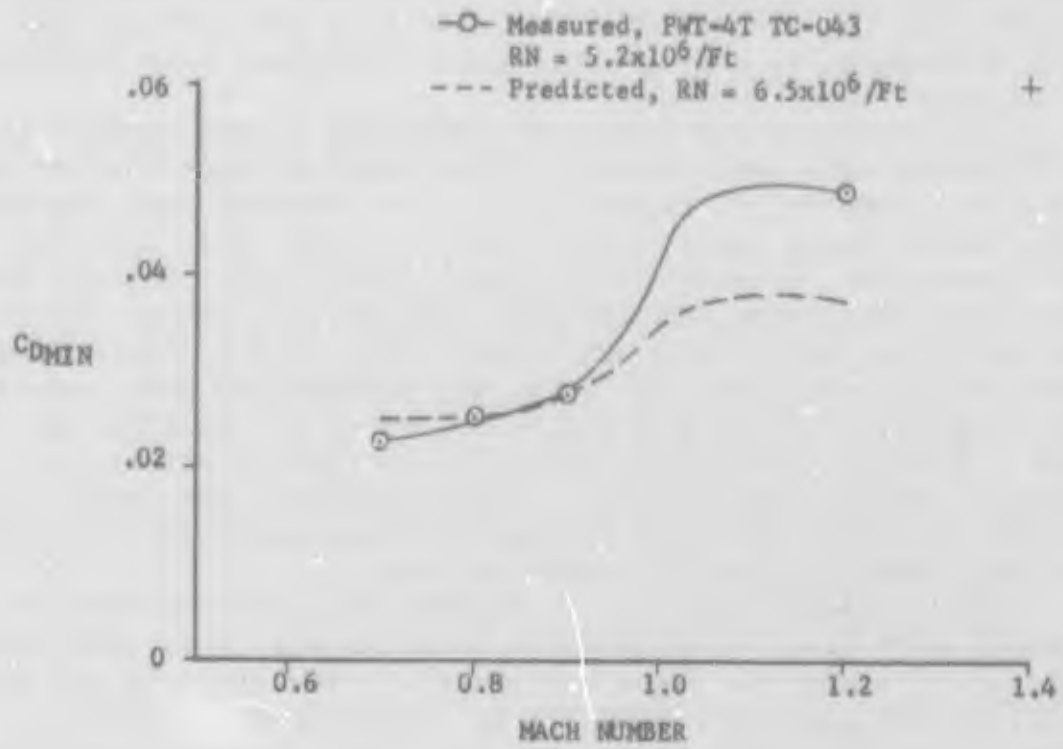


Figure 55 COMPARISON OF PREDICTED AND MEASURED MODEL MINIMUM DRAG LEVELS

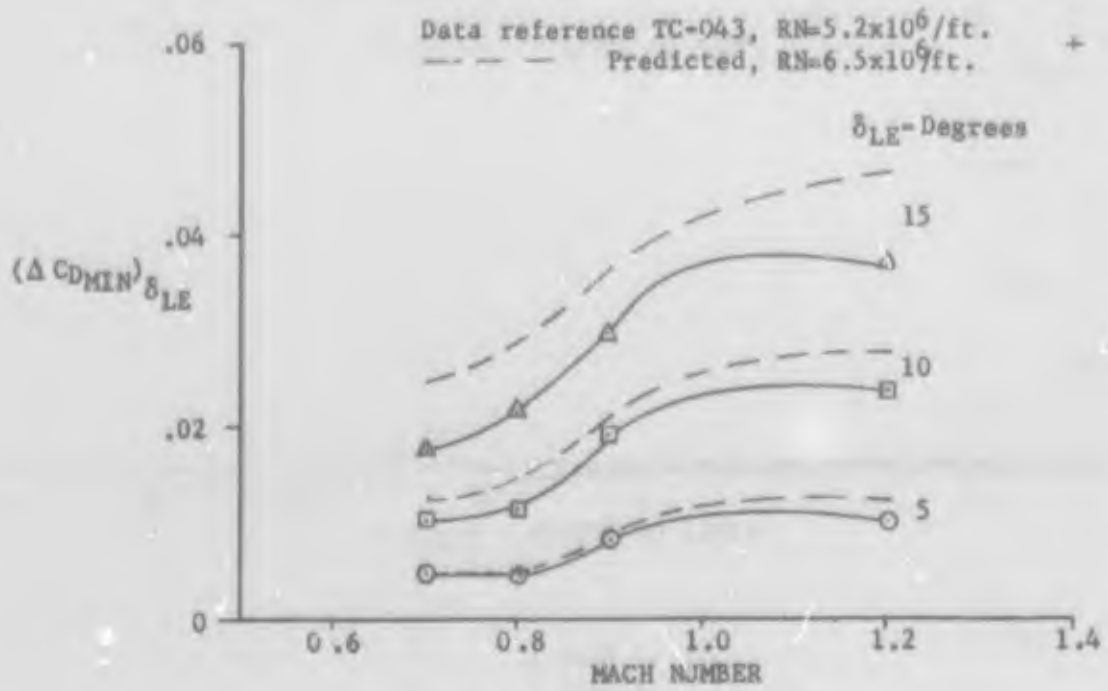


Figure 56 COMPARISON OF PREDICTED AND MEASURED MINIMUM DRAG INCREMENTS DUE TO LEADING EDGE FLAP DEFLECTION

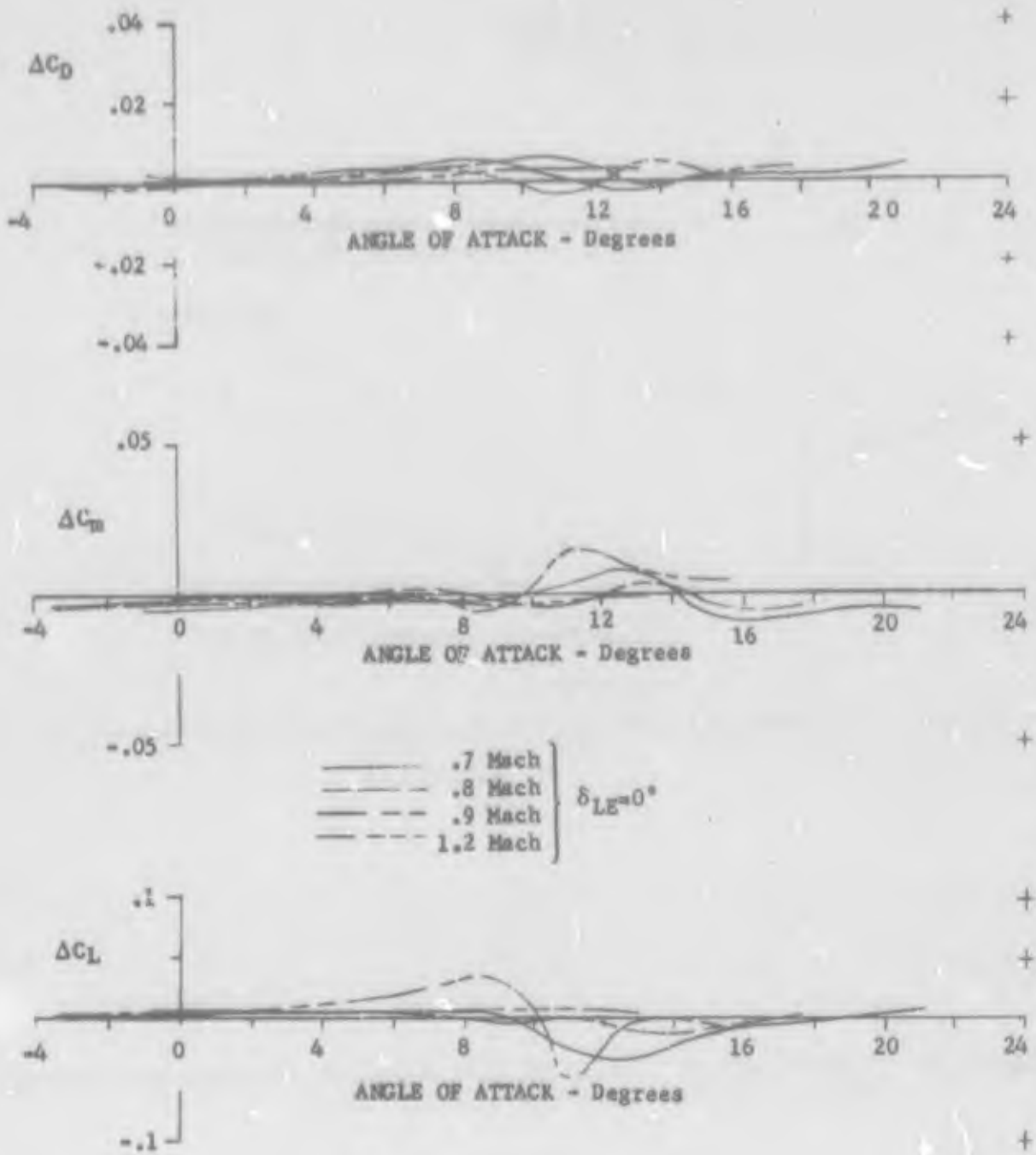


Figure 57 EFFECT OF ALTERNATE LEADING EDGE,  $\delta_{LE} = 0^\circ$

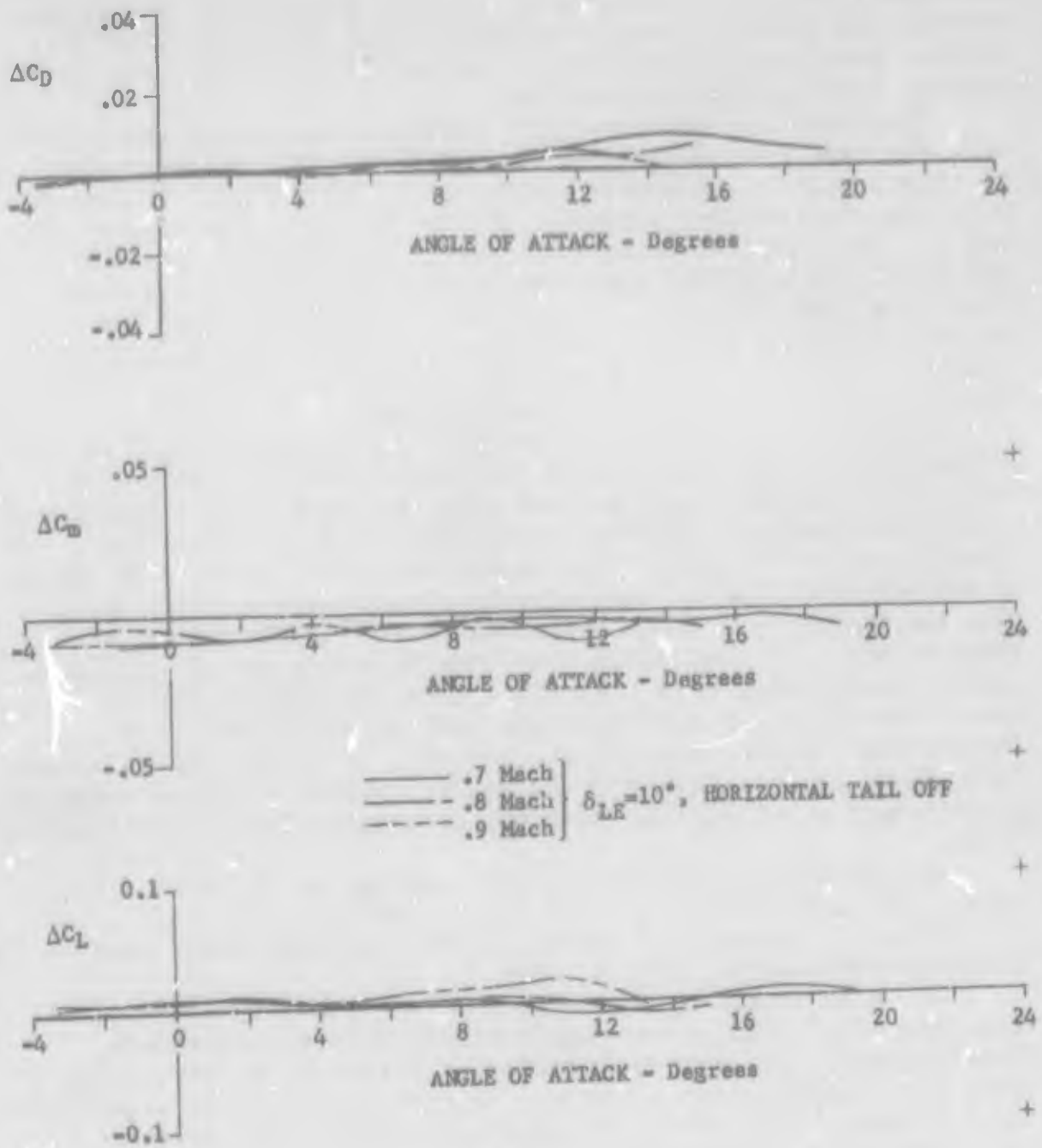


Figure 58 EFFECT OF ALTERNATE LEADING EDGE,  $\delta_{LE} = 10^\circ$

show the incremental lift, drag, and pitching moment differences between the modified wing section (K2) and the basic wing (K1) airfoil section as a function of angle of attack for 0 to 10-degree leading edge deflections.

The intent of the alternate leading edge design was to obtain the favorable effects of a "peaky" airfoil at low angles of attack with no flap deflection and at high angles of attack with flap deflection. However, as can be seen from Figures 57 and 58, the larger leading edge radius and slightly reduced camber of the modified wing section did not improve the flow conditions over the wing as desired. Specifically, at low angles of attack the alternate leading edge has a negligible effect on all three increments for all Mach numbers tested for both the deflected and clean leading edges.

At high angles of attack the K2 leading edges generate a slight increase in incremental lift force but also produce a definite increase in incremental drag for both the deflected and undeflected cases. Whereas these lift and drag variations effectively cancel each other at low angles of attack, at angles of attack beginning at approximately 6 to 8 degrees they do not. The net result is a slight but noticeable degradation of the drag polars. One deviation from this behavior is the Mach 0.9, clean-leading-edge data. For this case the lift increment rises rapidly above 2 degrees angle of attack creating an improvement in the drag polar. However, this improvement is not maintained as the added lift falls off rapidly at about 8 degrees angle of attack and does not compensate for the increased drag.

An important exception to this pattern is the Mach 1.2 case. Here, the lift and drag increments are relatively small and appear to cancel each other so that the drag polar remains unchanged for the K2 leading edge.

It is encouraging, however, that while the hoped-for lift and drag improvements were not realized with the alternate leading edge, the efficient characteristics of the basic wing were not significantly altered. This is particularly significant at 1.2 Mach number where the drag levels were not increased by the more blunt leading edge.

## 5. AUXILIARY DEVICES

Three types of auxiliary devices were tested during the 4T entries consisting of the vortex generator pattern, the drooped trailing edge and the split flaps. Typical results for

these devices as they affect the longitudinal characteristics are presented in this subsection; additional comparison data are presented in Appendix IV.

#### a. Vortex Generators

The design goal for the vortex generator pattern was to alleviate shock-induced separation effects at moderate-to-high angles of attack. Data was obtained with and without vortex generators on the LEDE configuration with 5-degree leading edge flap deflection at Mach numbers of 0.7, 0.8, 0.9 and 1.2. Only the 0.9 Mach number data show any benefits from the vortex generators. Direct comparisons between the data for the configurations with and without the generators are not advisable because one configuration was run during the first entry and the other during the second entry into the 4T. As a consequence incremental effects have been determined using the "clean wing" runs for each entry to obtain a common baseline. Thus, the net effects of the vortex generators have been obtained. Variations in the net increments for lift, drag and pitching moment with angle of attack are presented in Figure 59. The results show modest increases in lift coefficient in the region from 4 to 12 degrees angle of attack. A slight reduction in drag coefficients occurs at angles of attack from zero to about 11 degrees which reaches a maximum  $\Delta C_D$  of -0.003 at 9 degrees. The pitching moment increments show that the vortex generators tend to maintain the basic stability level to higher angles of attack. These results are not completely definitive; however, in conjunction with the rolling moment results presented in the next section, they do indicate that the vortex generators reduce shock-induced separation effects over a limited angle of attack range. In retrospect, it would probably have been better to use the vortex generators with zero degrees leading edge deflection, and to test also at Mach 0.85 where shock induced effects may be more pronounced with the LEDE configuration.

#### b. Drooped Trailing Edge

The effects of 10-degrees full-span trailing edge flap deflection (drooped trailing edge) on the aerodynamic characteristics of the LEDE configuration are summarized in Figure 60 for each Mach number tested. These data show that the trailing edge flaps were very effective at producing additional lift at all angles of attack investigated at each Mach number. The maximum effectiveness occurred at low angles of attack and Mach



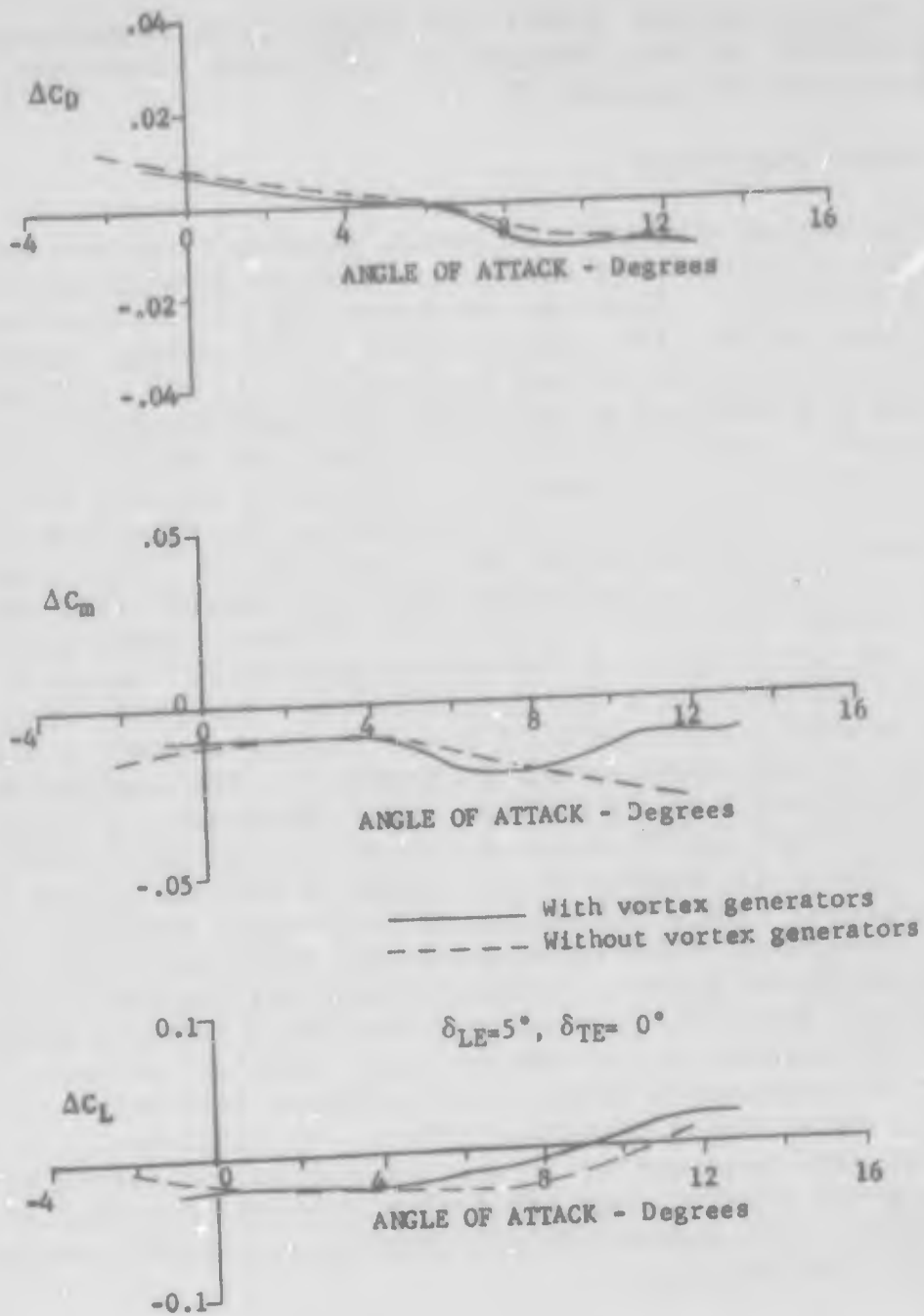


Figure 59 EFFECT OF VORTEX GENERATORS, MACH = 0.9

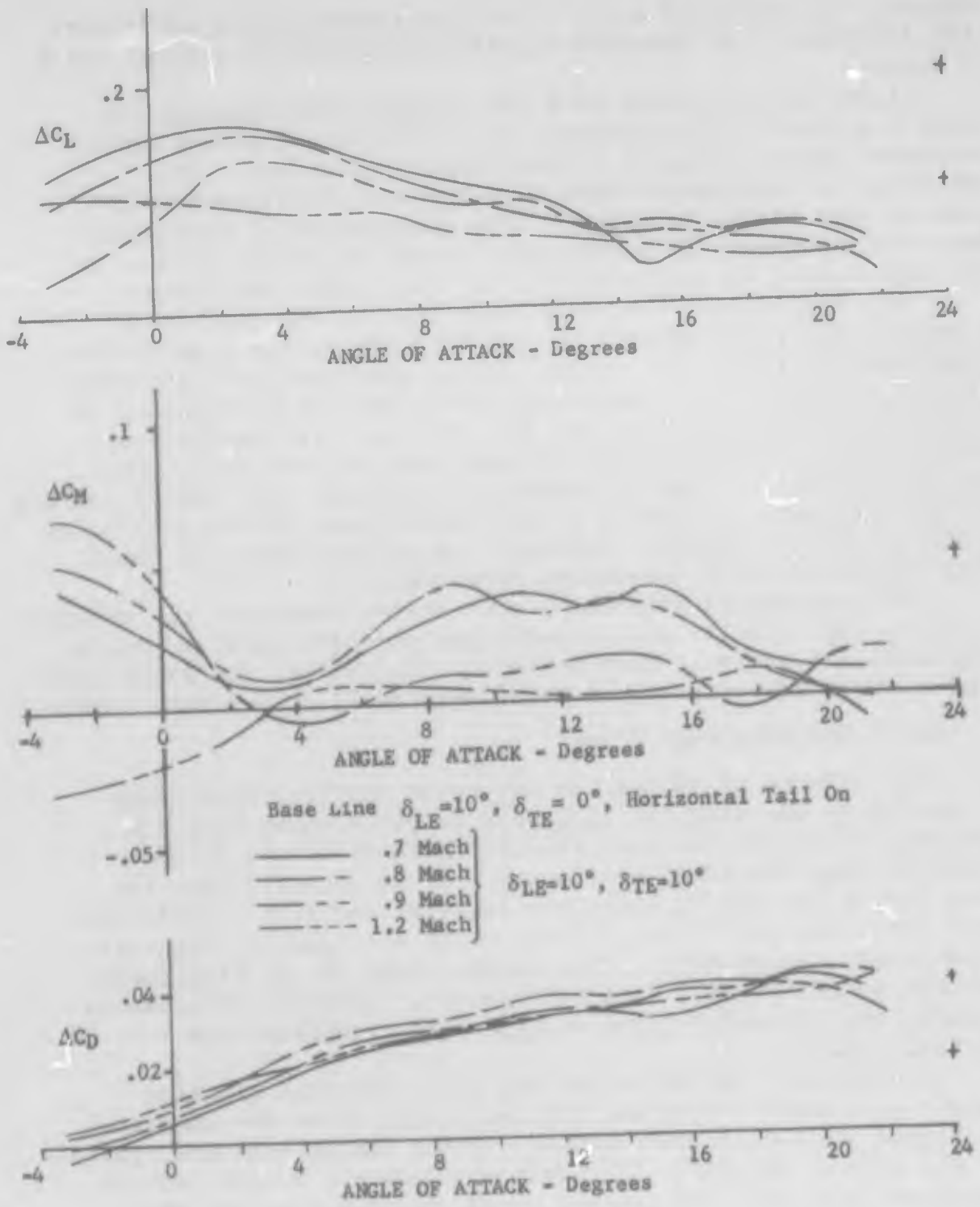


Figure 60 VARIATIONS OF DROOPED TRAILING EDGE FLAP INCREMENTS WITH MACH NUMBER

numbers. As speed and angle of attack increased the additional lift decreased, but remained significant beyond 20 degrees angle of attack.

Figure 60 also shows that the drooped trailing edge produces a positive drag increment at low angles of attack which increases almost linearly to high angles of attack. The variation of incremental drag also appears to be essentially constant for all Mach numbers. The combination of these lift and drag increments at a particular angle of attack produce a net improvement in the drag polar at high lift coefficients.

This conclusion is further supported by the results of a square-root plot analysis of the drag due to lift, which are summarized in Figure 61. These curves show that trailing edge flaps are beneficial in improving the high-lift performance of the wing in that they increase the critical lift coefficient and the lift coefficient for minimum drag at each Mach number, however the polar shape is adversely affected. The overall effect of these factors is again a slight improvement in the drag polar in the high-lift region. However, the effectiveness of these flaps decreases with increasing Mach number.

The incremental pitching moment curves show that the drooped trailing edge results in a significant positive shift in pitching moment at subsonic Mach numbers. This effect decreases with Mach number, however, and is relatively small at 1.2 Mach number.

### c. Split Trailing Edge Flaps

The effects of adding the two split trailing edge flaps F<sub>2</sub> and F<sub>3</sub> to the wing trailing edge in the midspan position (segments 2 and 3) are very similar to those of the drooped trailing edge described previously. It is observed that the drag levels for the F<sub>2</sub> flaps are lower at low lift coefficients than those for the F<sub>3</sub> split flap, which are lower at high-lift conditions, except at 0.9 Mach number where the F<sub>2</sub> flap demonstrates better overall drag performance. However, differences between the two split flaps at high-lift conditions are relatively small.

Incremental variations of the lift, drag and pitching moment with angle of attack for both split flaps are compared in Figure 62 for 0.9 Mach number. These comparisons are typical of the effects of the split flaps at transonic speeds, and as mentioned show the same trends as the drooped trailing edge. It is observed that split flap F<sub>2</sub> produces almost as much lift as F<sub>3</sub> for all subsonic Mach numbers, and the more blunt flap, (F<sub>3</sub>), shows the highest incremental drag values. The similarity of characteristics for the three trailing edge flaps tested indicates that the effects are typical of trailing edge devices. The data obtained in this program is not sufficient to permit a clear decision to be made among the different flaps in terms of overall efficiency.

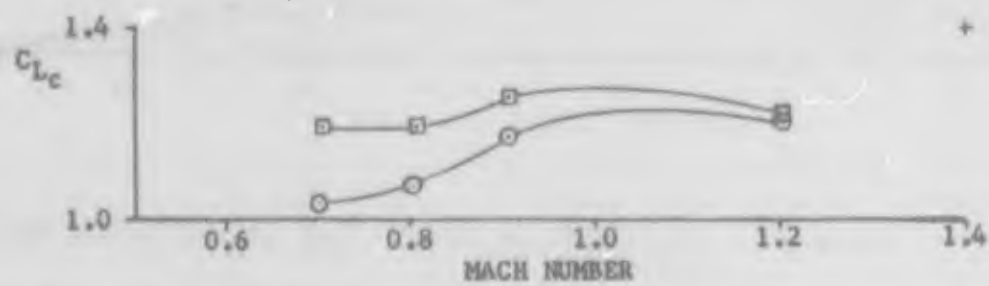
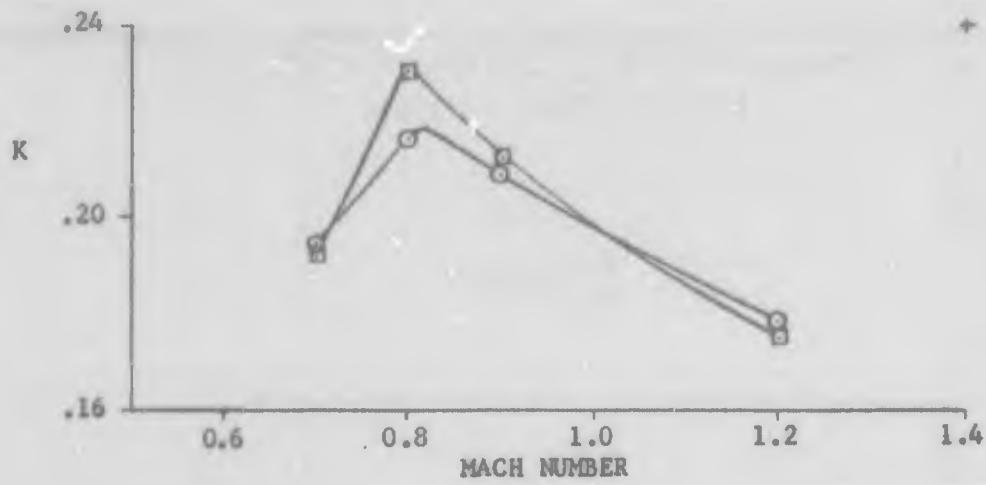
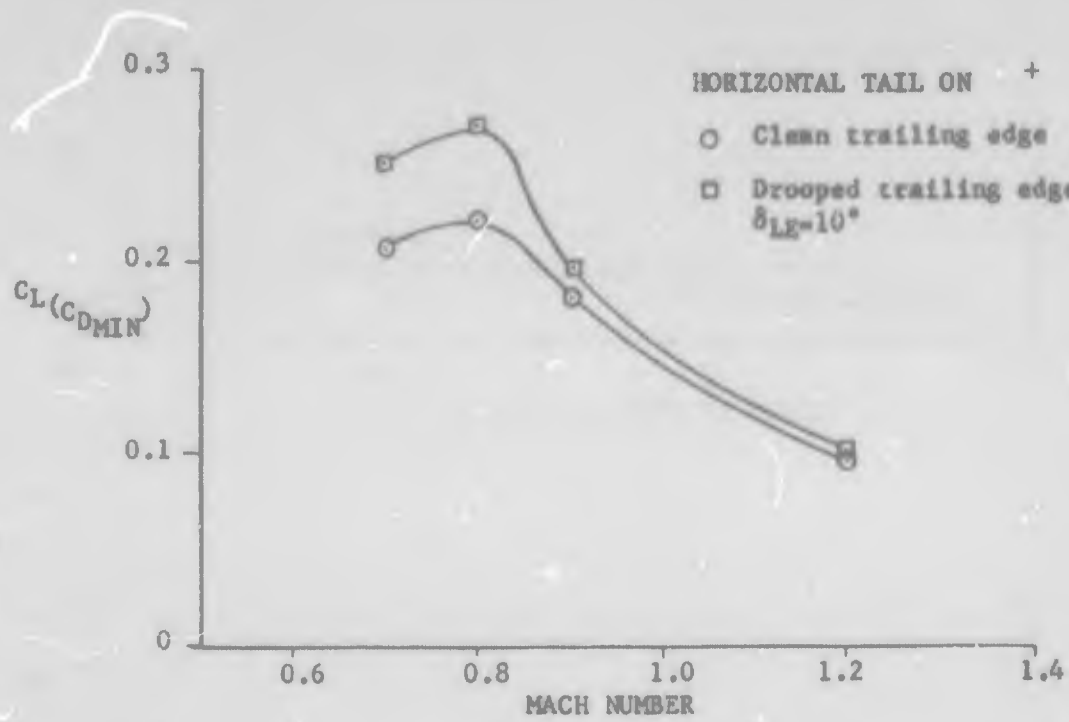


Figure 61 EFFECT OF DROOPED TRAILING EDGE ON DRAG-DUE-TO-LIFT PARAMETERS

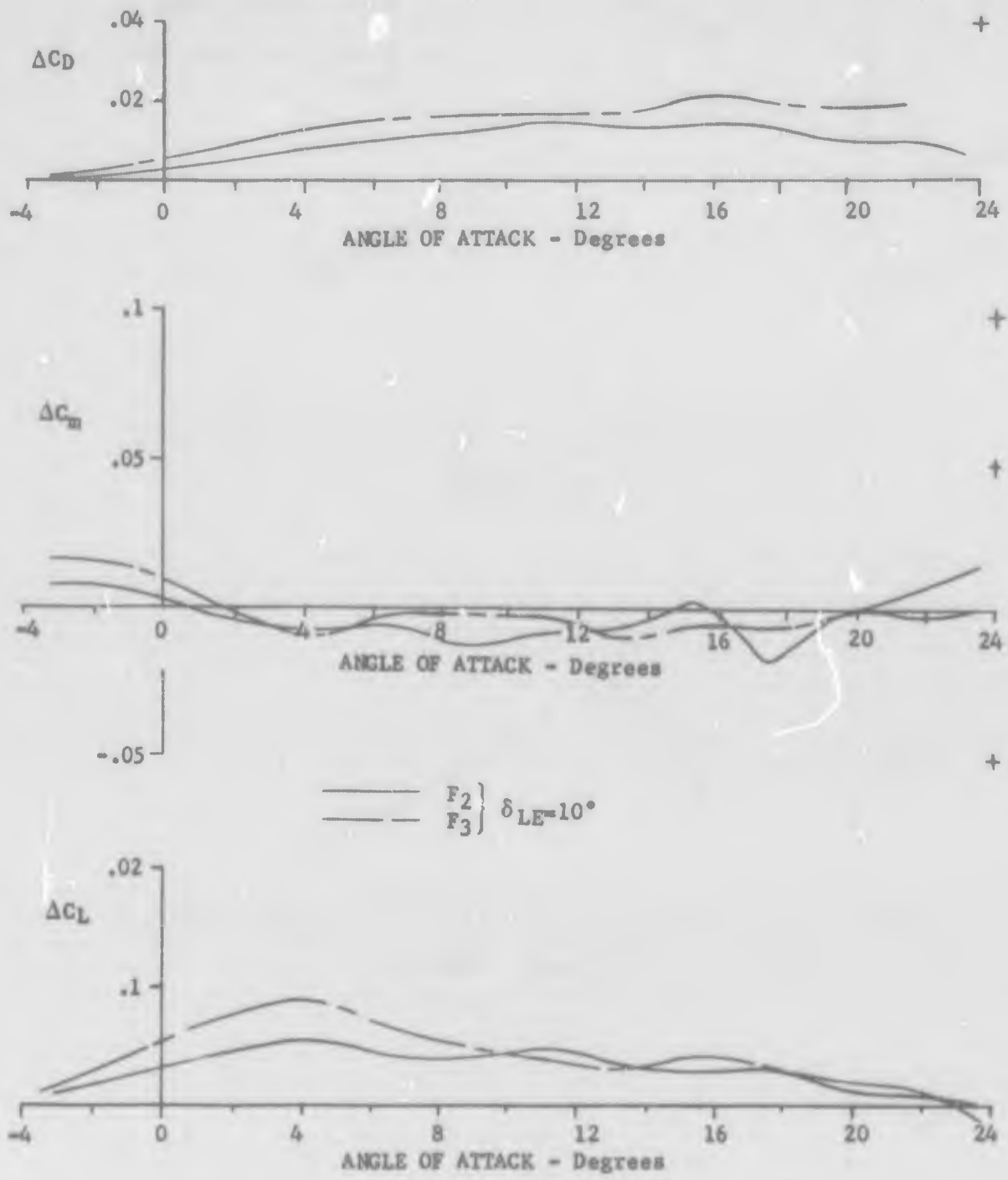


Figure 62 VARIATION OF SPLIT FLAP INCREMENTAL EFFECTS  
MACH 0.9

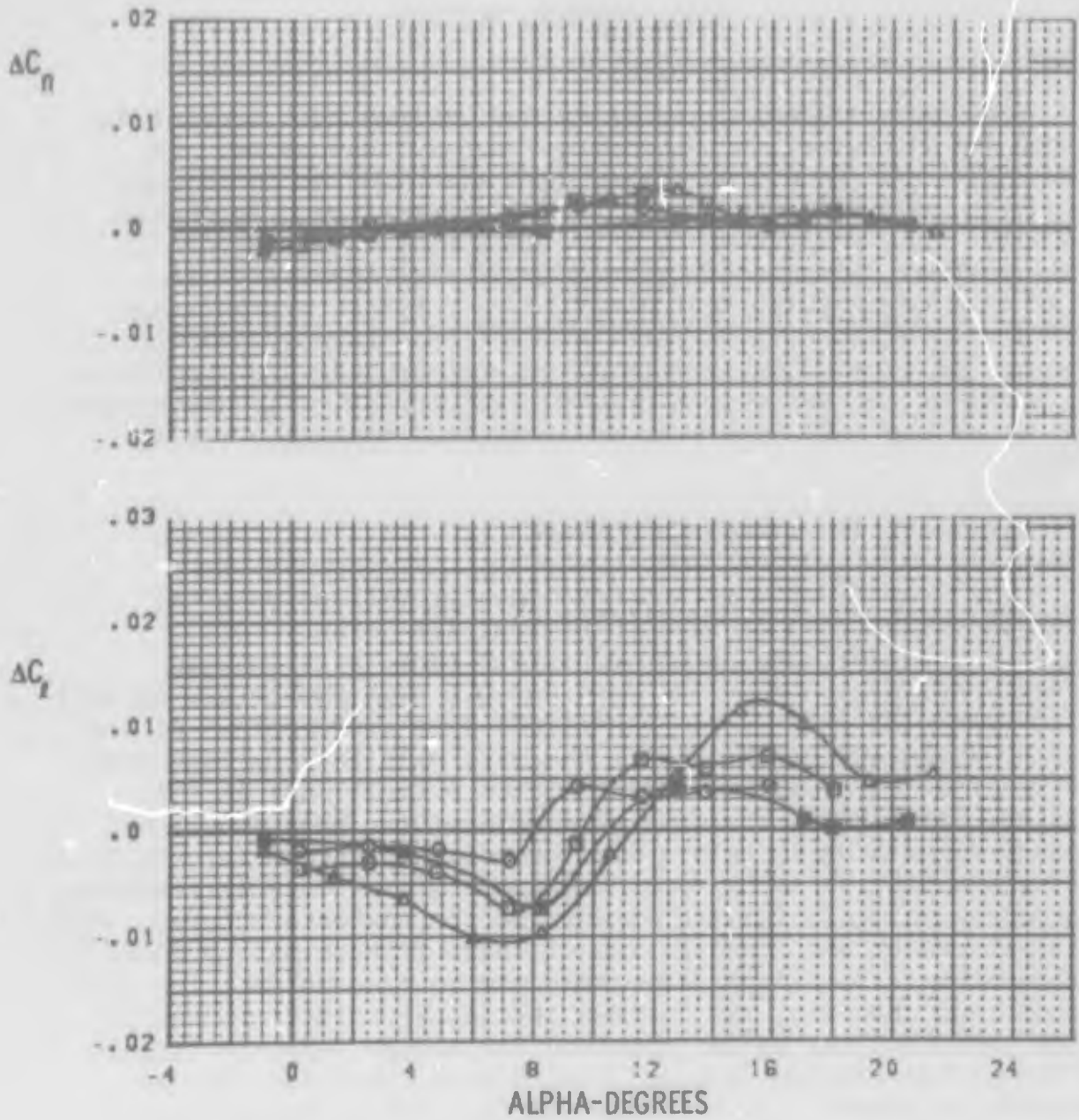
## SECTION VII

### ROLL CONTROL DEVICES

The basic characteristics of the various roll control devices are presented in the several sub-sections below. In each case, the force and moment data are given as increments from the corresponding symmetrical configuration. It should be noted that only representative data plots are included in this section, because of the volume of data involved. The reader is referred to Appendix V for a complete presentation of this material. In the last subsection, the coordination characteristics of the promising control devices are considered in terms of the yawing moment - rolling moment ratio and nominal values of the roll numerator to dutch roll frequency ratio,  $\omega_r/\omega_d$ .

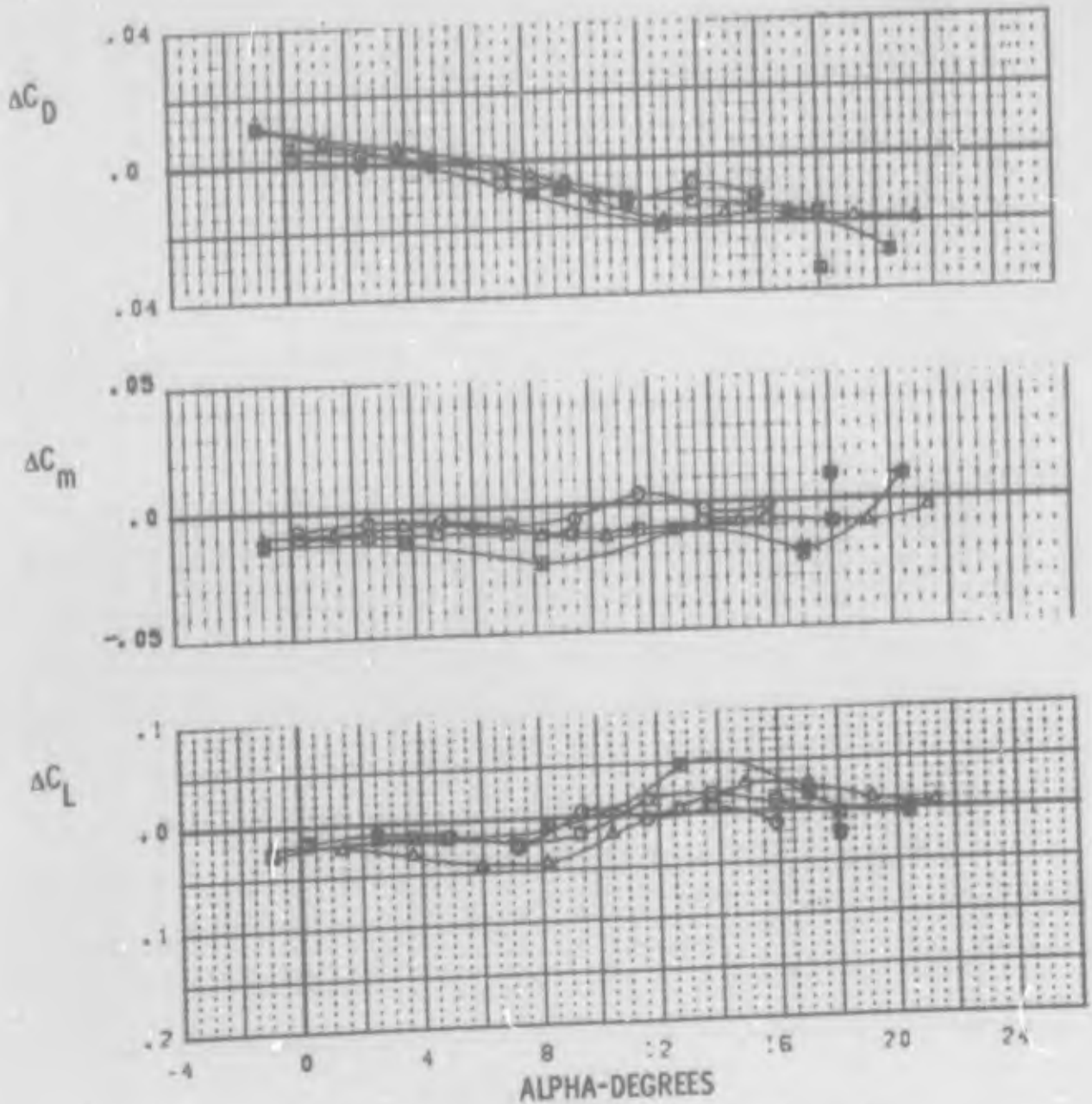
#### 1. DIFFERENTIAL LEADING EDGE FLAPS

The use of differential leading edge deflection alone was generally found to be insufficient for primary roll control over any large angle of attack range at transonic speeds, see Figure 63. The data for 0.8 Mach number are typical of results for free stream conditions less than sonic. At low and moderate angles of attack, the wing with leading edge down deflection (left wing always) exhibits a small loss in lift and attendant small negative rolling moment. This additional camber significantly delays leading-edge separation (starting on the clean wing at about eight degrees angle of attack) resulting in modest positive rolling moments at the higher attitudes, additional comment and illustration of these effects may be found in subsection VI 3. Slight favorable yaw is also evident for this condition. However, the maximum attainable rolling moment is much less than the amount required for modern fighter aircraft. A direct correlation between longitudinal force and lateral moments is evident in the data; rolling moments follow the lift trends while yawing moments are associated with drag effects of leading edge deflection. This correspondance of lift increments for differential leading edge deflection is illustrated in Figure 64. Note the presence of aileron deflection does not change the basic trends.



| SYM | TEST          | INCREMENT       | L.E. (L/R) |
|-----|---------------|-----------------|------------|
| ○   | PWT 4T TC-043 | PN 455 - PN 440 | K1 5/0     |
| □   | PWT 4T TC-043 | PN 434 - PN 440 | K1 10/0    |
| △   | PWT 4T TC-043 | PN 186 - PN 267 | K1 15/0    |
| ■   | PWT 4T TC-043 | PN 254 - PN 267 | K1 10/5    |

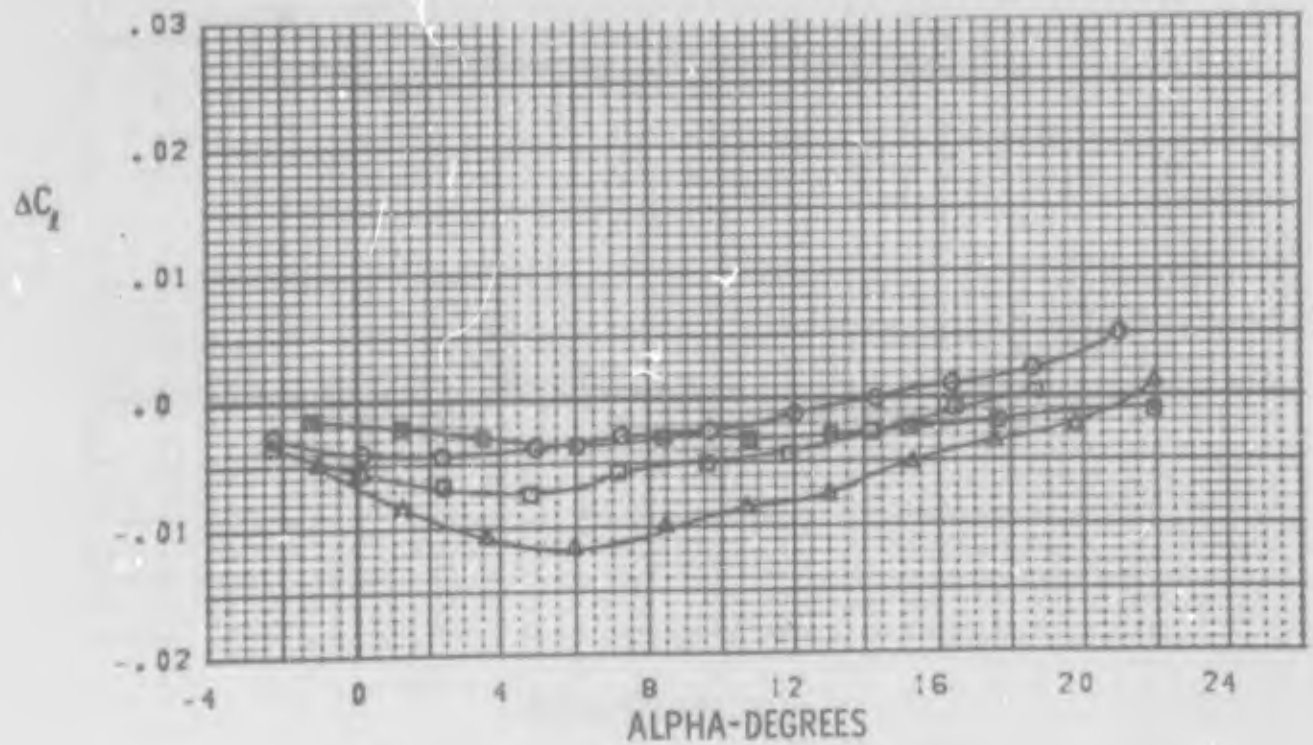
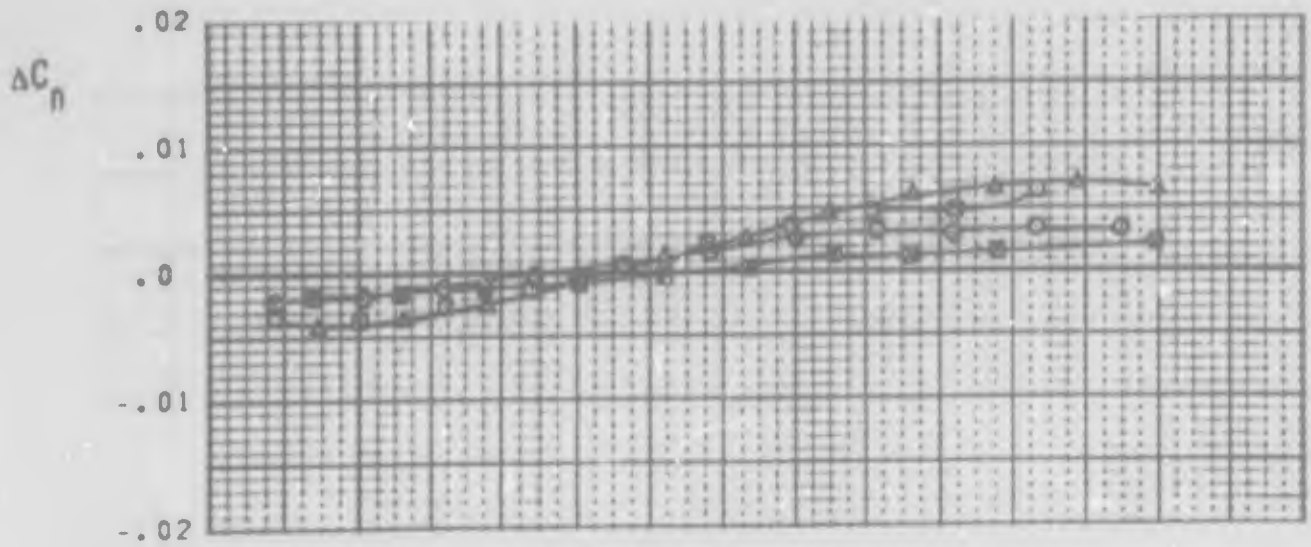
Figure 63a DIFFERENTIAL L.E. FLAP EFFECTS  
M = 0.8



| SYM | TEST          | INCREMENT       | L.E. (L/R) |
|-----|---------------|-----------------|------------|
| ○   | PWT 4T TC-043 | PN 455 - PN 440 | K1 5/0     |
| □   | PWT 4T TC-043 | PN 434 - PN 440 | K1 10/0    |
| △   | PWT 4T TC-043 | PN 186 - PN 267 | K1 15/0    |
| ■   | PWT 4T TC-043 | PN 254 - PN 267 | K1 10/5    |

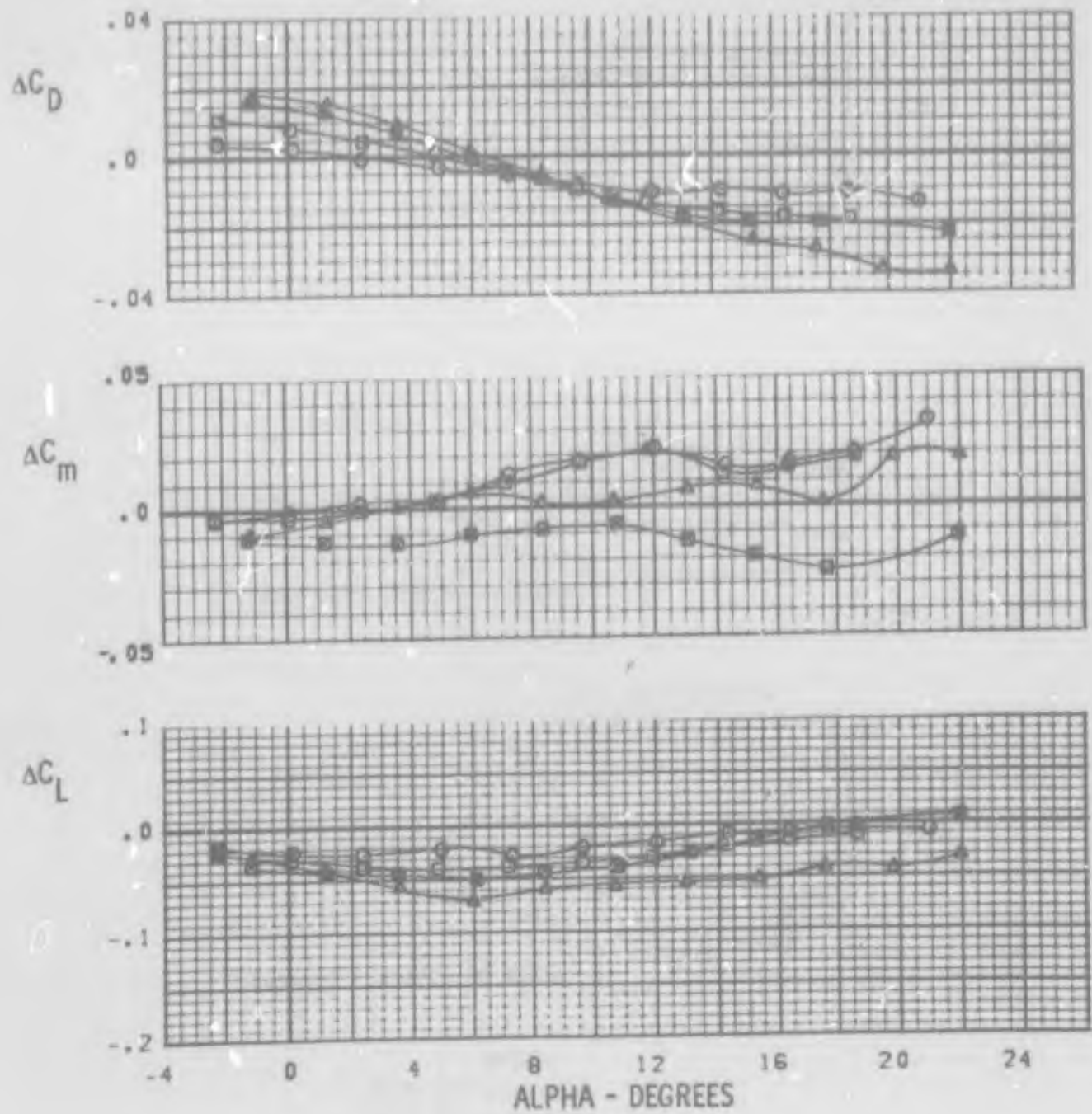
Figure 63a DIFFERENTIAL L.E. FLAP EFFECTS  
M = 0.8





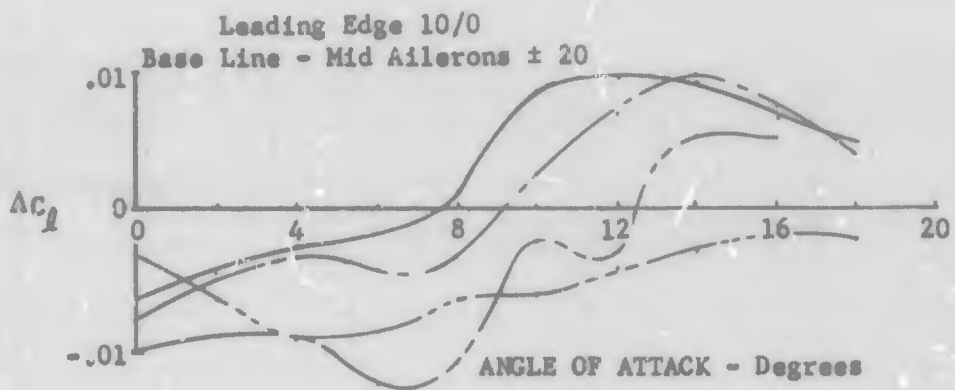
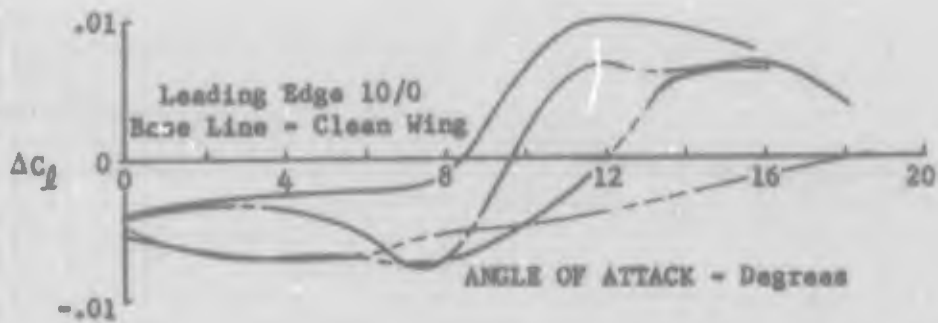
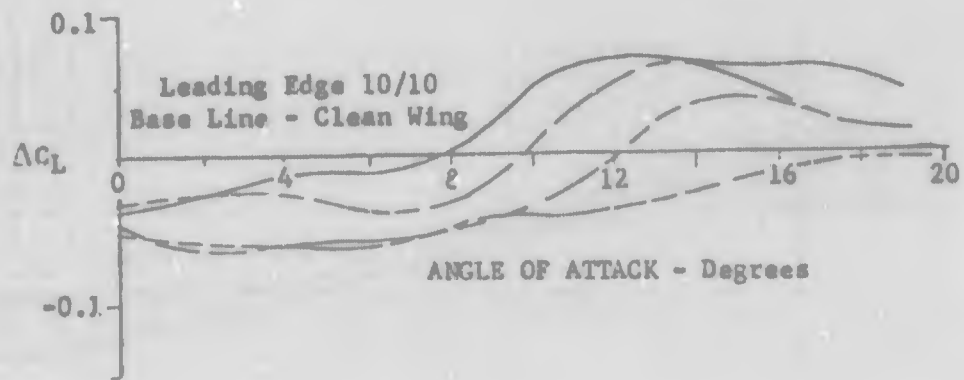
| SYM | TEST          | INCREMENT       | L.E. (R) |
|-----|---------------|-----------------|----------|
| ○   | PWT 4T TC-043 | PN 456 - PN 269 | K: 5 0   |
| □   | PWT 4T TC-043 | PN 435 - PN 269 | K: 10 0  |
| △   | PWT 4T TC-043 | PN 188 - PN 269 | K: 15 0  |
| ■   | PWT 4T TC-043 | PN 258 - PN 269 | K: 10 5  |

FIGURE 63b DIFFERENTIAL EFFECTS  
 150



| SYM | TEST          | INCREMENT       | INC. (L/R) |
|-----|---------------|-----------------|------------|
| ○   | PWT 4T TC-043 | PN 456 - PN 269 | K1 5/0     |
| □   | PWT 4T TC-043 | PN 435 - PN 269 | K1 10/0    |
| △   | PWT 4T TC-043 | PN 188 - PN 269 | K1 15/0    |
| ■   | PWT 4T TC-043 | PN 258 - PN 269 | K1 10/5    |

FIGURE 63b DIFFERENTIAL FLAP EFFECTS  
M = 1.2



LEGEND

- 0.7 Mach
- 0.8 Mach
- - - 0.9 Mach
- · - · 1.2 Mach

Figure 64 COMPARISON OF LEADING EDGE FLAP EFFECTS  
HORIZONTAL TAIL ON

For conditions with established supersonic flow over the wing at all angles of attack (see Figure 63b, 1.2 Mach number) the decrease in lift with nose down deflection is the significant effect producing modest negative rolling moments (left wing down for left leading edge down deflection) over a wide angle of attack range. It is important to note that the effects of angle of attack on the control rolling moment are quite different for the supersonic and transonic cases. For the former case, the gradual changes with angle of attack suggest that leading edge flaps may be useful as a primary roll control at supersonic speeds on configurations with highly swept wing planforms. On the other hand, rapid reversals in the sign of the rolling moment occur with angle of attack change at transonic speeds. This effect limits the usefulness of differential leading edge flaps to a restricted angle of attack range at transonic speeds. For these conditions, the best application appears to be as an auxiliary device to improve roll control at the higher angles of attack.

## 2. AILERONS

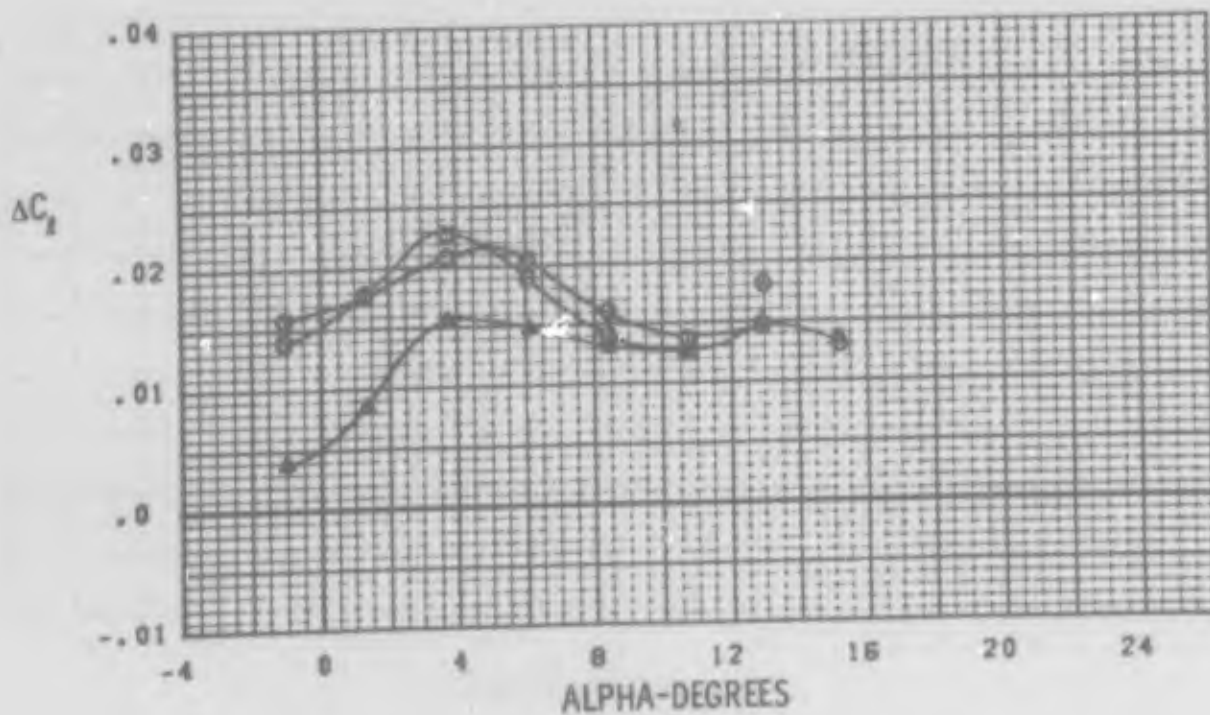
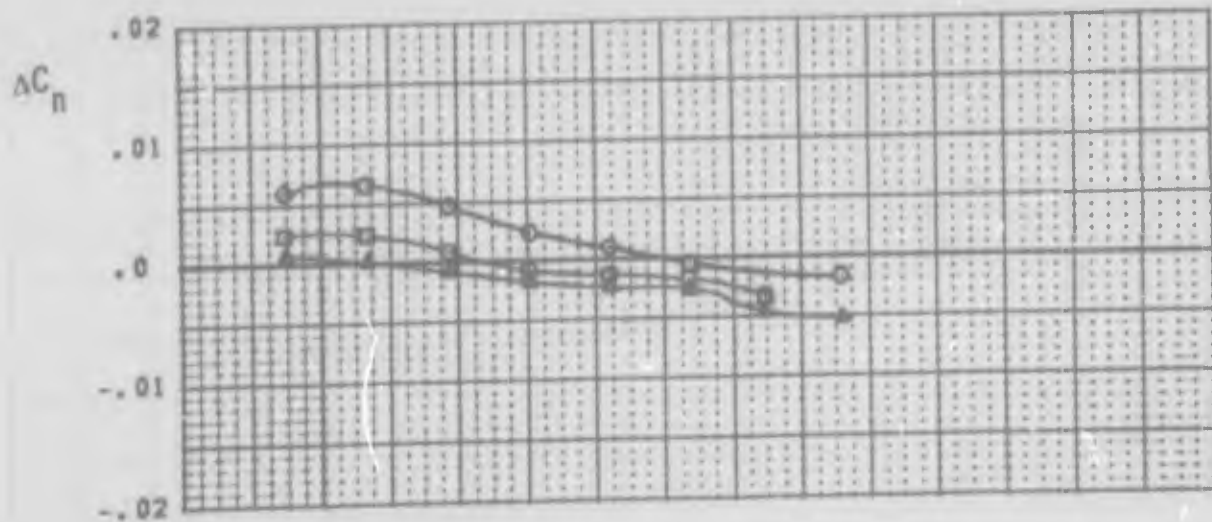
### a. Basic Geometric Effects

Several different factors may strongly influence location of ailerons for control at transonic high lift conditions. The fundamental geometric parameter is the moment area of the surface planform, more outboard surfaces having a given moment area with significantly less surface area. On the other hand, the strength of shock waves and general tendencies for premature flow separation are greater for mid to outboard spanwise positions. Another factor is the vertical location of the horizontal tail. If the asymmetric portion of the wing wake (produced by roll control deflection) comes in close proximity to the horizontal tail, serious interference effects can occur. In view of these several general effects, no attempt was made to have exactly equal control effectiveness for the several aileron geometries tested. The ailerons were only intended to have the same order of magnitude in effectiveness. Key geometric parameters for these surfaces are tabulated below.

| AILERON   | $S_f/S_w$ | $S_f\gamma/S_w b$ |
|-----------|-----------|-------------------|
| Inboard   | .0735     | .0164             |
| Mid-Span  | .0624     | .0190             |
| Outboard  | .0415     | .0163             |
| 3 Segment | .0779     | .0260             |

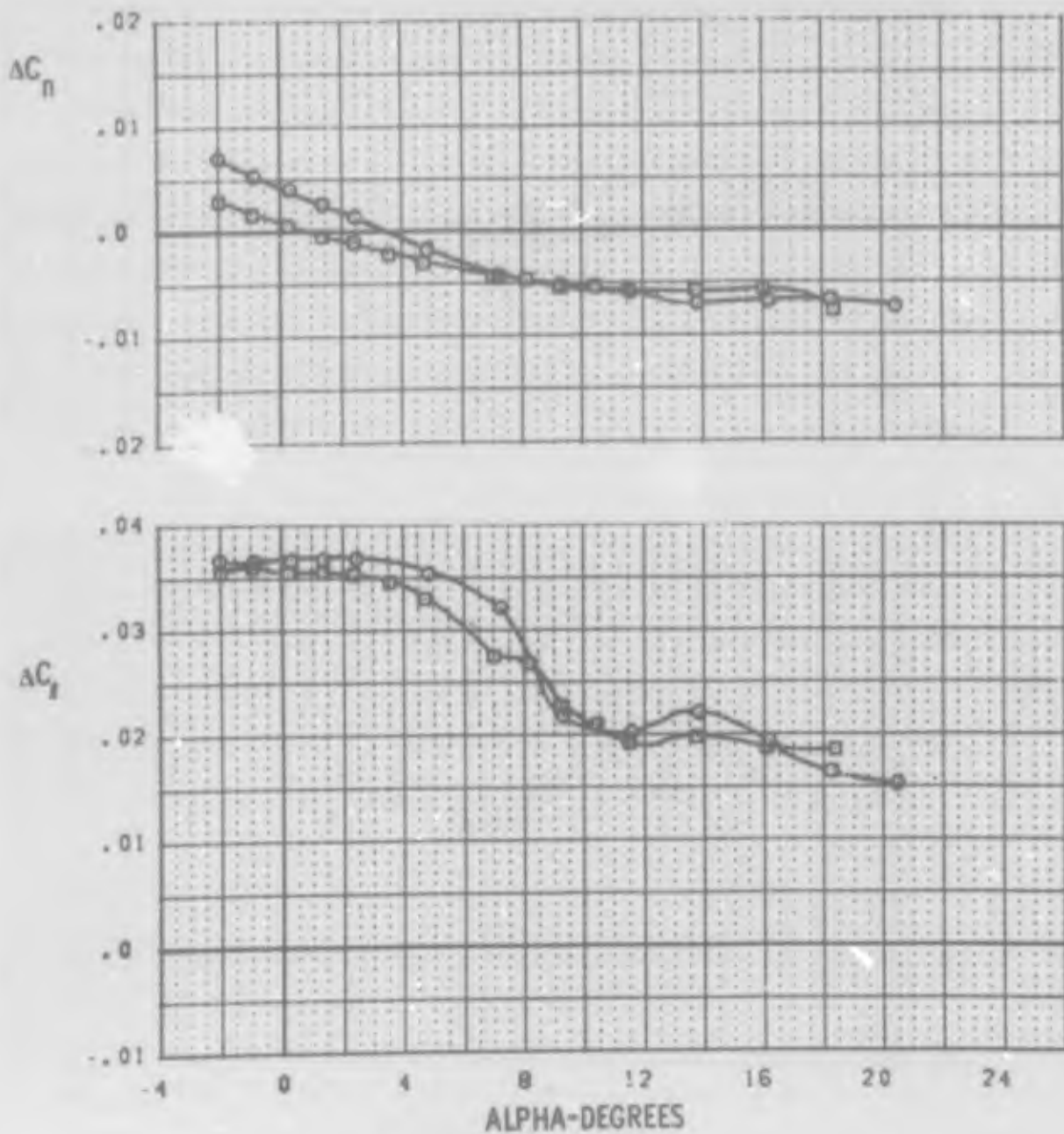
The comparison of effectiveness for the three basic spanwise positions shown in Figure 65 indicates that for small deflections at 0.9 Mach number the inboard and mid-span ailerons have about equal effectiveness, horizontal tail off. However, it will subsequently be shown that the inboard aileron has large interference losses due to the horizontal tail, hence only limited testing was accomplished with this aileron configuration. For the larger deflections, horizontal tail on, the mid-span aileron is slightly better than the outboard aileron, see Figure 66, since significant horizontal tail interference occurs with a mid span location. The general effects of various aileron geometries are indicated in Figure 67 in terms of the aileron control derivative,  $C_{l\delta_a}$ , for low angles of attack. Pre-test predictions based upon the USAF DATCOM, Reference 12, (corresponding to measurements horizontal tail off) are also included on each plot. The horizontal tail interference is very evident for the inboard aileron data. The mid-span aileron was less effective than predicted in the transonic region and also experienced significant interference losses. The combination of these effects results in control effectiveness of only two thirds the predicted level. The outboard aileron experienced no interference losses, as might be expected, however here again the transonic control effectiveness is less than predicted.

Although the extended span aileron (mid ailerons plus tip segment) is the most effective device, the control power is much less than predicted. Comparisons between mid and extended span aileron data indicate the most outboard aileron segment contributes only  $-.0005$  to  $C_{l\delta_a}$  over the Mach range, about one half the estimate for Mach numbers of 0.7 to 0.9. This is attributed to a local reduction in wing loading caused by the increased local leading edge sweep of the curved tip.



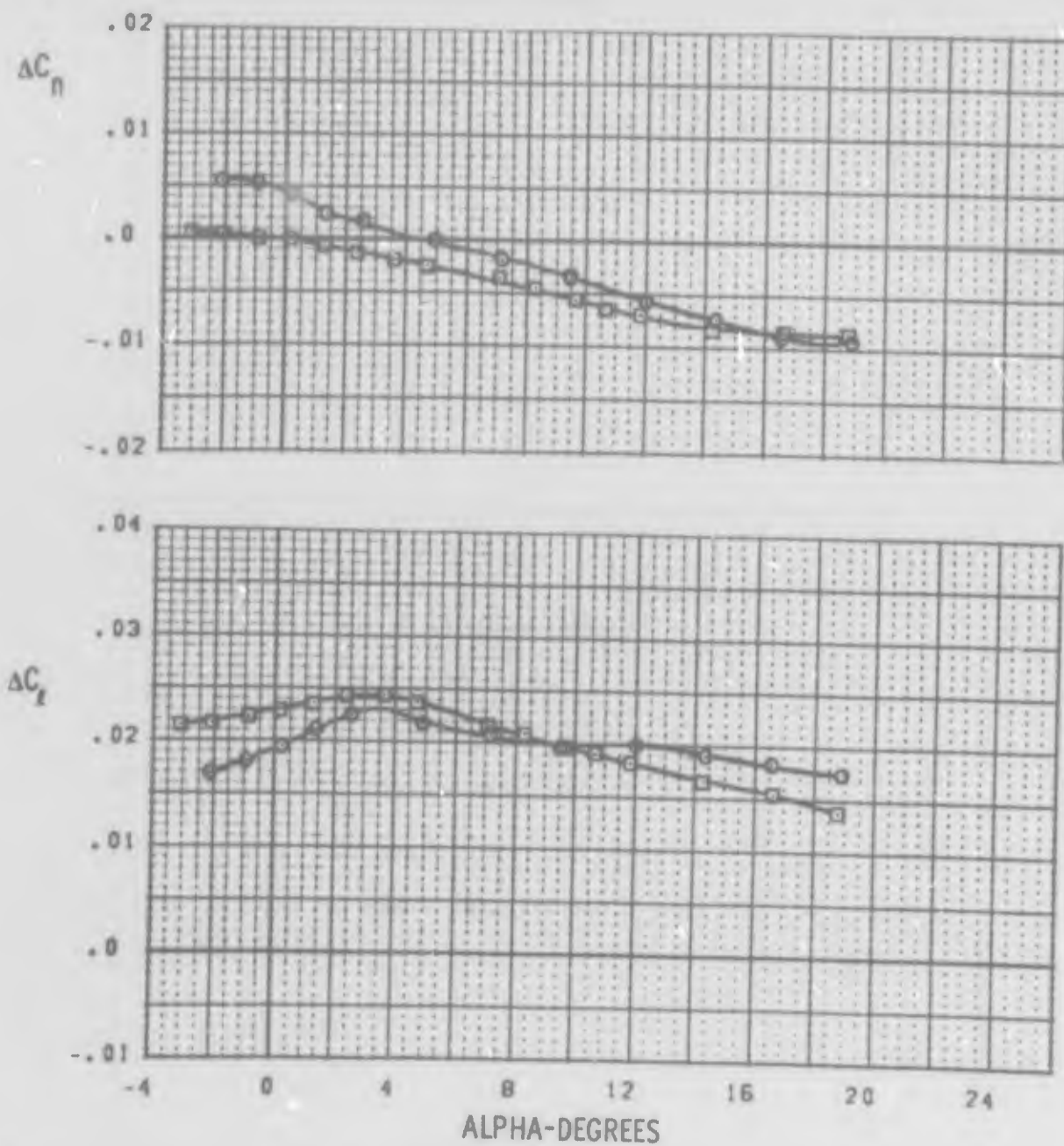
| SYM | TEST          | INCREMENT     | L.E. (L/R) | AILERON (L/R) |
|-----|---------------|---------------|------------|---------------|
| ○   | PWT 4T TC-043 | PN 112 -PN 47 | K1 10/10   | INBD 10/-10   |
| □   | PWT 4T TC-043 | PN 108 -PN 47 | K1 10/10   | MID 10/-10    |
| △   | PWT 4T TC-043 | PN 104 -PN 47 | K1 10/10   | OUTBD 10/-10  |

FIGURE 65 AILERON SPANWISE POSITION EFFECTS  
HORIZONTAL TAIL OFF M = 0.9



| SYM | TEST           | INCREMENT    | L.E. (L/R) | AILERON (L/R) |
|-----|----------------|--------------|------------|---------------|
| ○   | PWT 16T TF-216 | PN 12 -PN 50 | K1 0/0     | MID 20/-20    |
| □   | PWT 16T TF-216 | PN 04 -PN 50 | K1 0/0     | OUTBD 20/-20  |

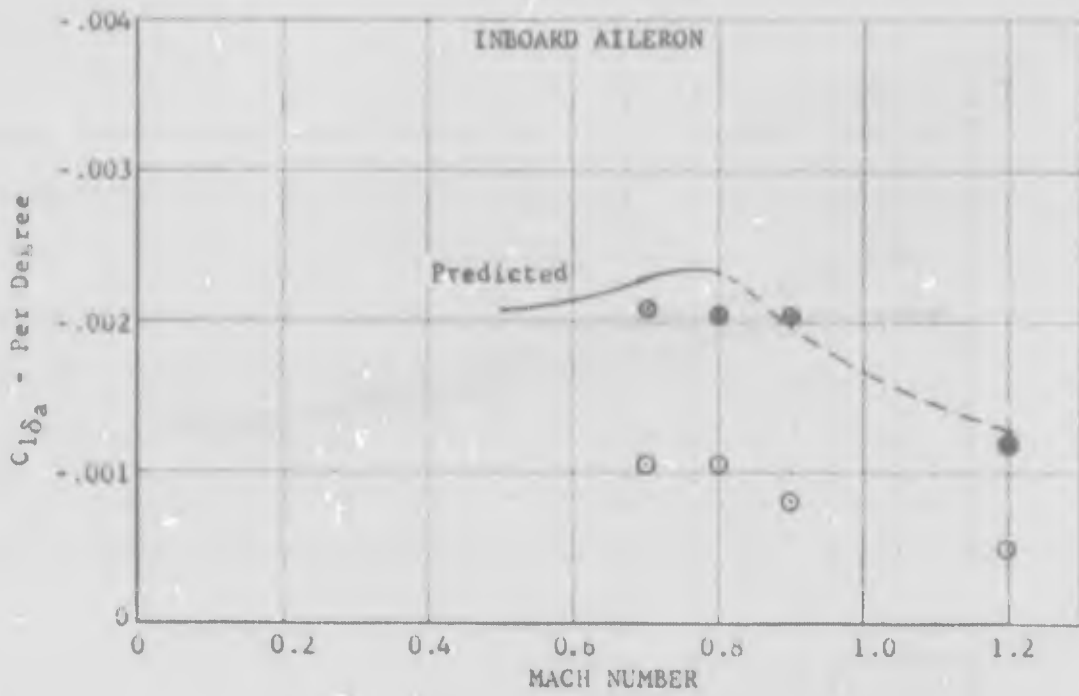
FIGURE 66a AILERON SPANWISE POSITION EFFECTS  
HORIZONTAL TAIL ON M = 0.8



| SYM | TEST           | INCREMENT    | L.E. (L/R) | AILERON (L/R) |
|-----|----------------|--------------|------------|---------------|
| ○   | PWT 16T TF-216 | PN 10 -PN 54 | K1 0/0     | IN 20/-20     |
| □   | PWT 16T TF-216 | PN 82 -PN 54 | K1 0/0     | OUT 20/20     |

FIGURE 66b AILERON SPANWISE POSITION EFFECTS  
HORIZONTAL TAIL ON M = 1.2





Symbol Horizontal Tail  
 ● Off  
 ○ On

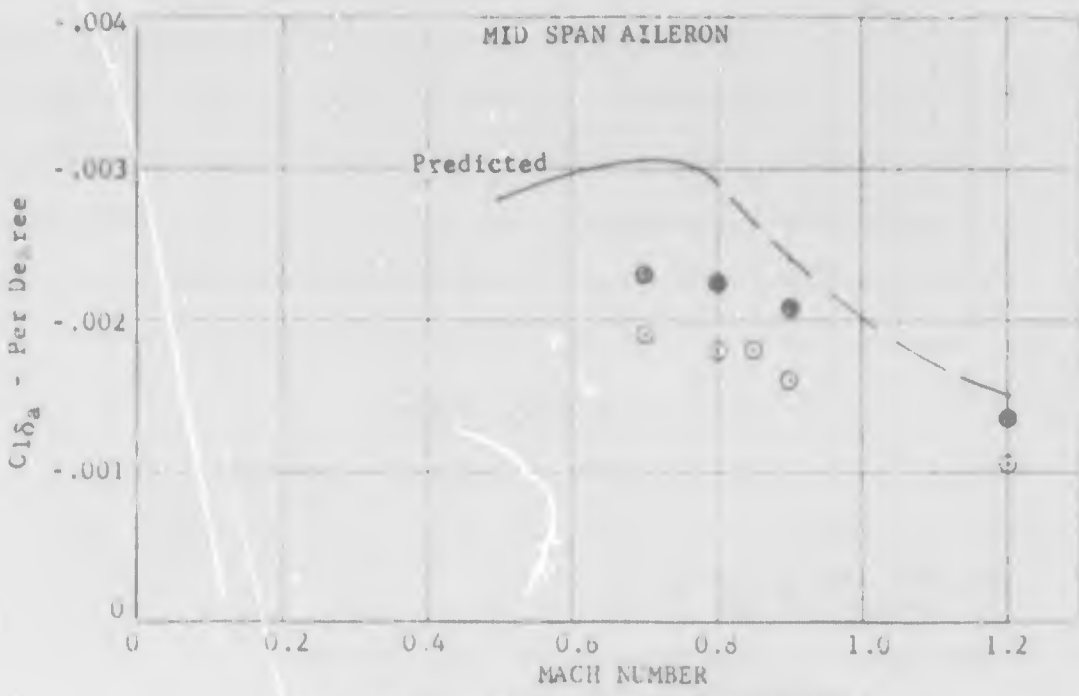
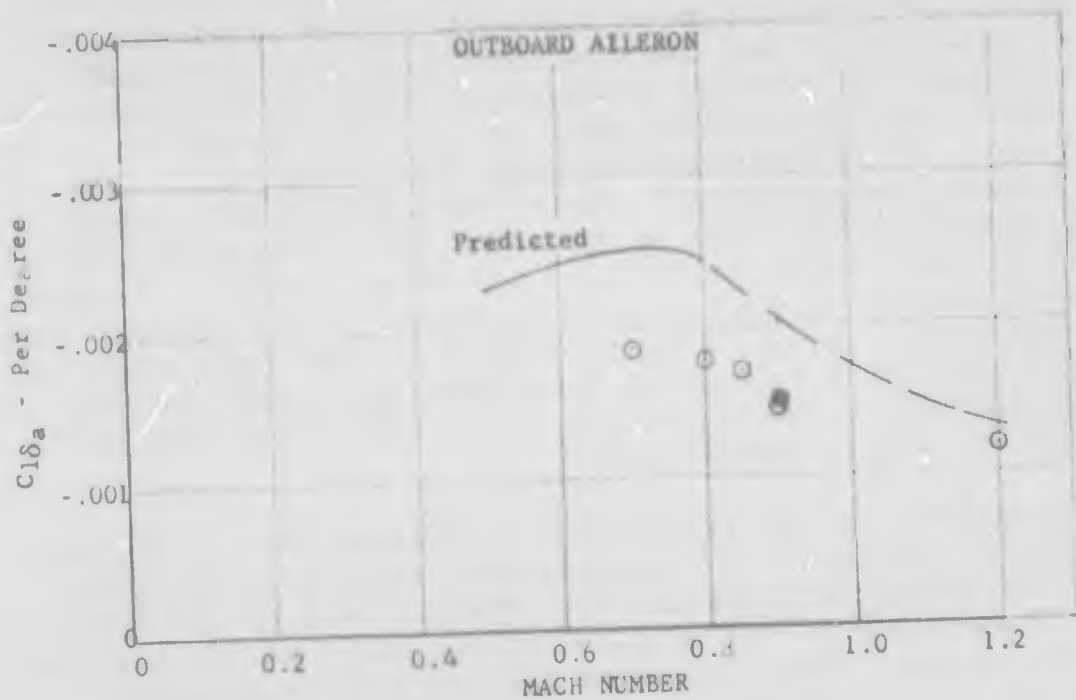


Figure 67 AILERON EFFECTIVENESS  
 LOW ANGLES OF ATTACK



Symbol Horizontal Tail  
 ● Off  
 ○ On

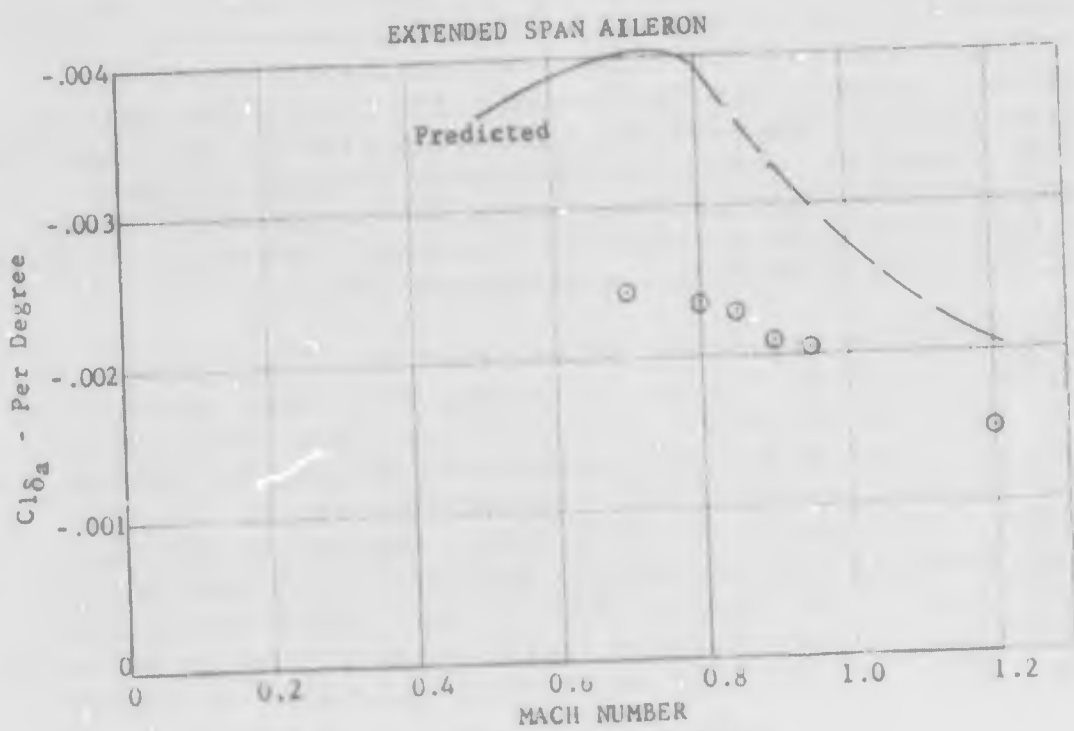


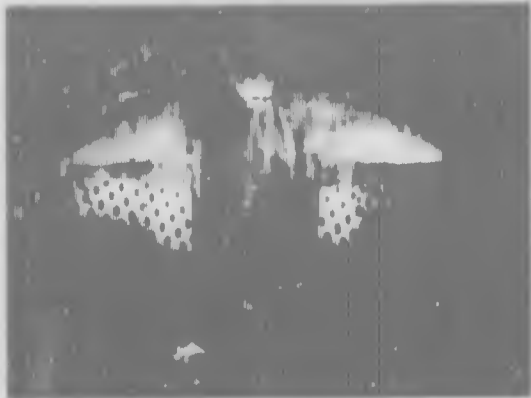
Figure 67 AILERON EFFECTIVENESS  
 LOW ANGLES OF ATTACK

The degree to which measured values of control effectiveness agree with predictions at transonic speeds provides some general knowledge of how the flow conditions vary with spanwise position. In general, these predictions are only intended to be valid for the subsonic range up to a Mach number of about 0.7 to 0.8. It is therefore expected that losses in control effectiveness associated with shock induced separation ahead of the aileron surfaces would be one major contribution to discrepancies between predicted and measured effectiveness. The good agreement for the inboard aileron illustrates that the high swept glove and smooth leading edge transition to the lower sweep angle outboard were quite successful in minimizing forward and aft shock waves on the inboard wing portions. This was also confirmed by oil flow visualization.

Photographs of oil flow patterns obtained with 20 degrees differential deflection of the mid-span ailerons at 0.9 Mach number are presented in Figure 68. However much of the flow detail discernible in the original motion pictures was lost in the still prints. Thus, sketches derived from observation of the original films are given in Figure 69 to illustrate key effects. The most significant fact to be drawn from the flow patterns is that the controlling geometric item is different depending on whether the trailing edge is deflected up or down. Comparison of Figure 69 with Figure 41 reveals that for trailing-edge down deflections (left wing), the shock wave and/or separation patterns ahead of the hinge line are determined by the leading edge geometry and deflection. For the surface with up-deflected aileron, the trailing edge deflection is the controlling geometric variable. Note that the strong adverse pressure gradient and forward shock wave causes separation well forward of the hinge line with an imbedded secondary flow region analogous to that for a two-dimensional compression corner.

The sketch in Figure 69a illustrates the flow patterns at low angles of attack. On the left wing, weak shock waves occur ahead of the down deflected aileron in a pattern identical to that for the clean wing. The forward and aft shocks combine outboard of the aileron to form the outboard shock. No flow separation is evident on the left wing. However on the right wing with trailing-edge up aileron deflection, the pattern is quite different. The forward shock is more highly swept and terminates in a large separated region ahead of the up-deflected aileron. Also, a moderately swept secondary shock is present

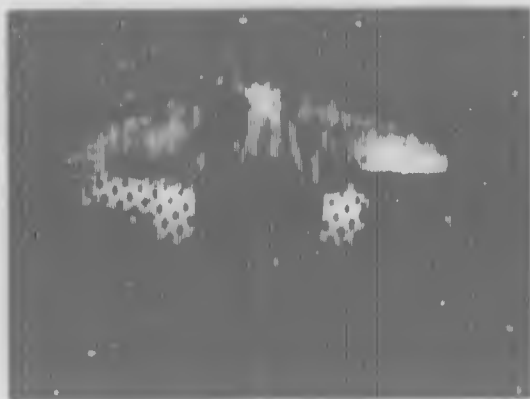
$\alpha = 4.44^\circ$



$\alpha = 6.46^\circ$



$\alpha = 8.75^\circ$



$\alpha = 11.82^\circ$

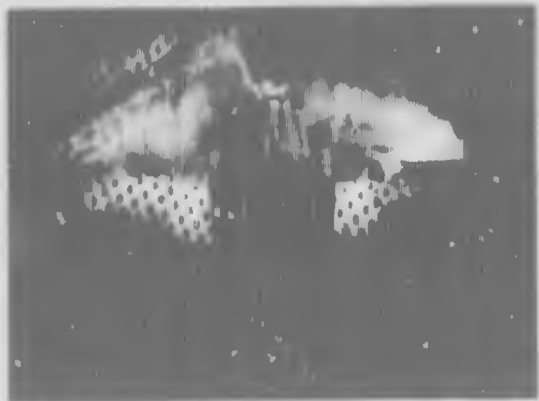


Figure 68 FLOW VISUALIZATION MID AILERON 20/-20  
K1 L.E. 0/0, MACH = 0.9

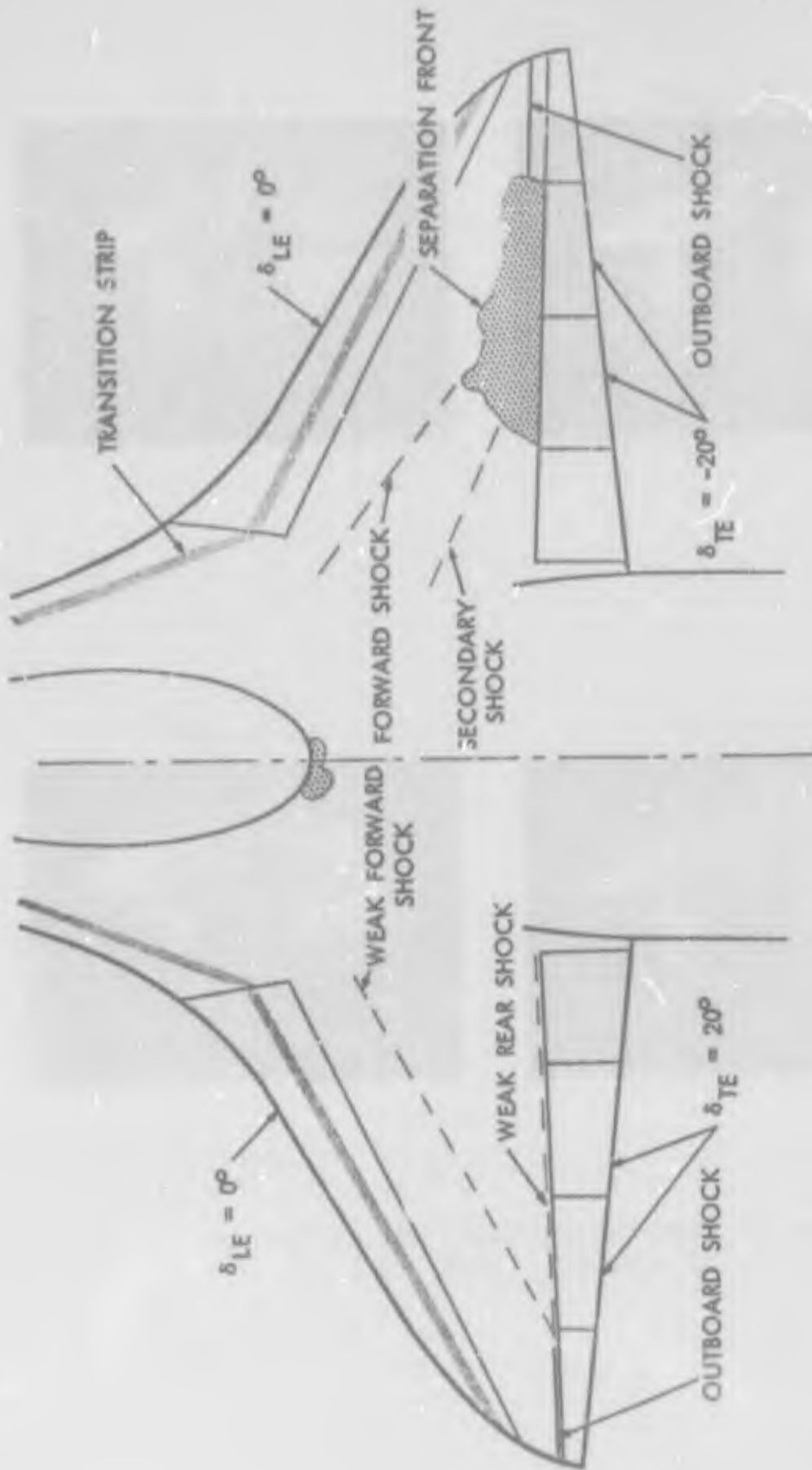


Figure 69a SKETCH OF FLOW PATTERNS FOR DEFLECTED MID-AILERONS  
 $\alpha = 4.44^\circ$ , MACH = 0.90

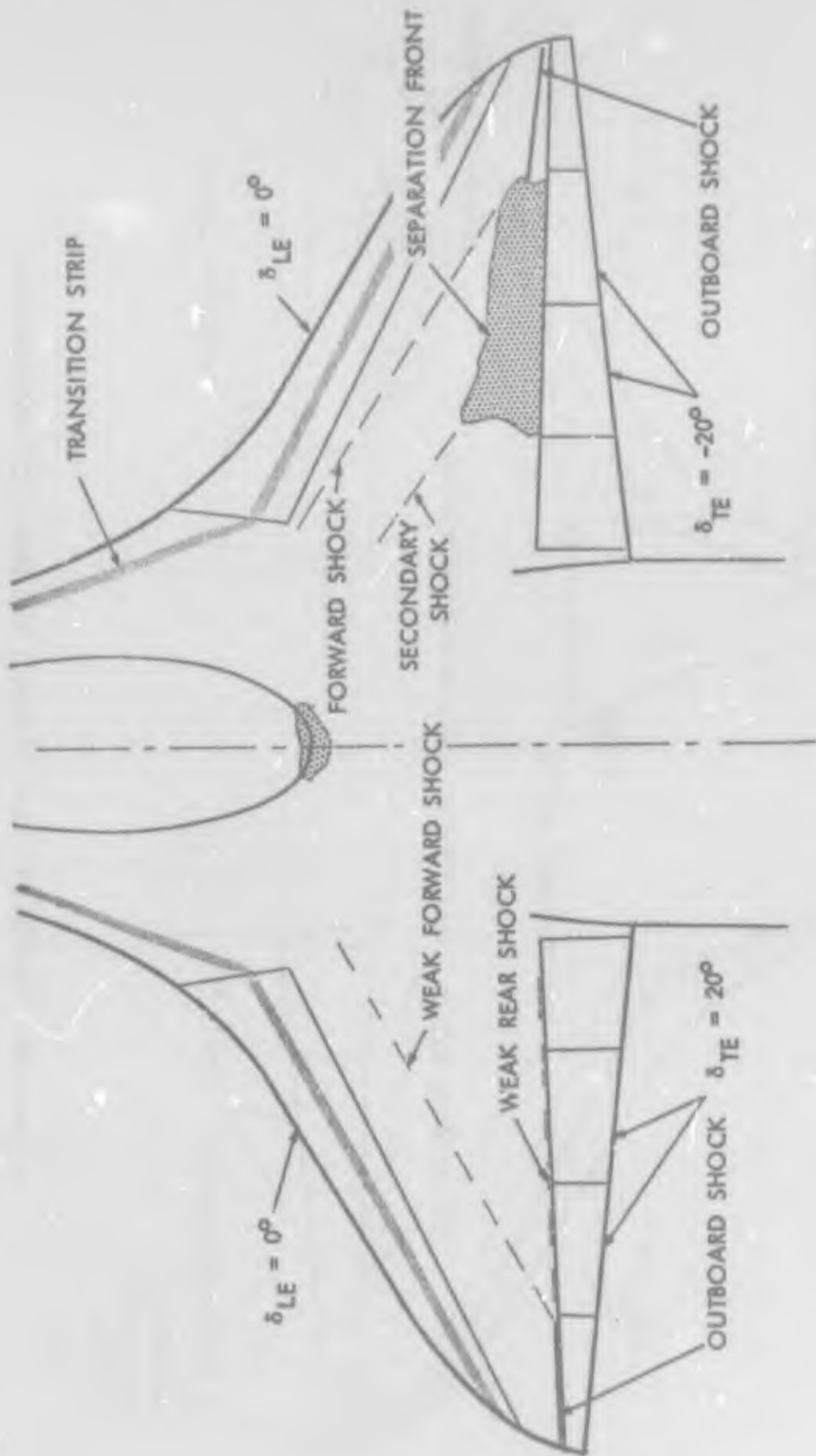


Figure 69b SKETCH OF FLOW PATTERNS FOR DEFLECTED MID-AILERONS

$\alpha = 6.46^\circ$ , MACH = 0.90

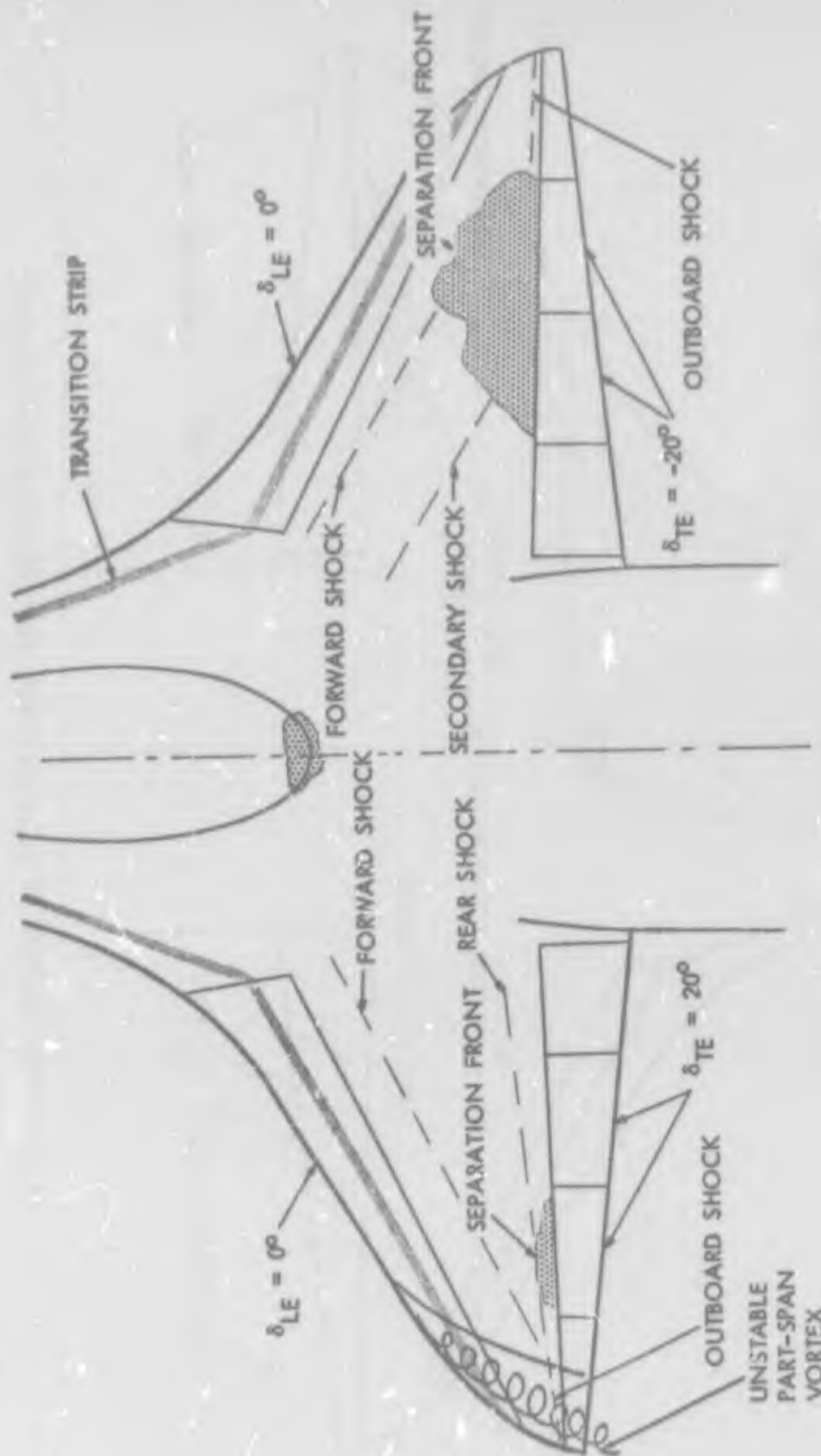


Figure 69c SKETCH OF FLOW PATTERNS FOR DEFLECTED MID-AILERONS  
 $\alpha = 8.75^\circ$ , MACH = 0.90

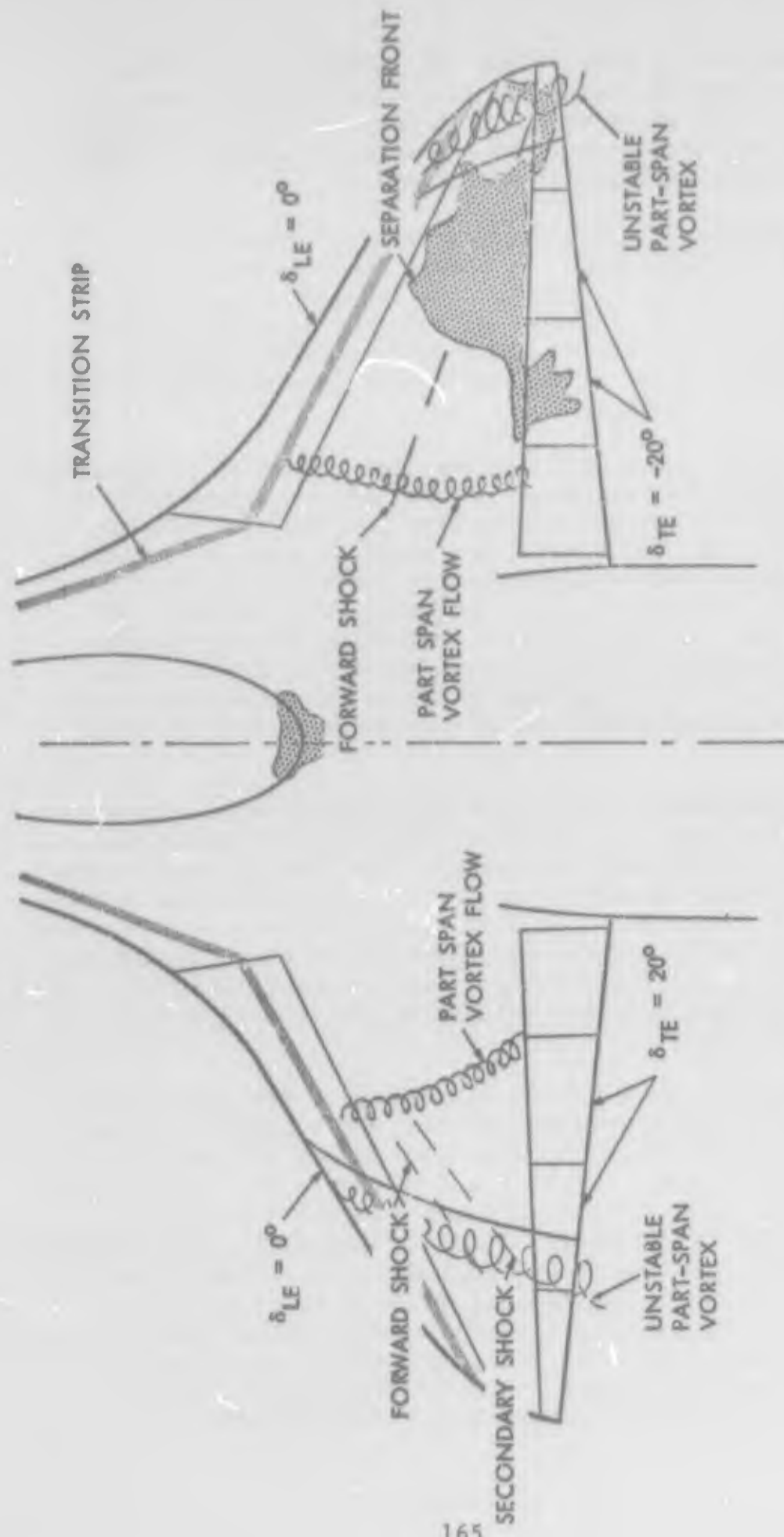


Figure 69d SKETCH OF FLOW PATTERNS FOR DEFLECTED MID-AILERONS

$\alpha = 11.82^\circ$ , MACH = 0.90



inboard instead of a rear shock. An outboard shock exists beyond the separated region and is located slightly more forward than for the clean wing. Note that the large separated region does not extend aft onto the control surface but terminates approximately along the hinge line.

Flow patterns for 6.5 degrees angle of attack are illustrated in Figure 69b. No change from the pattern at the lower angle of attack is evident for the left wing. For the right wing (with trailing-edge-up aileron) both the forward and secondary shocks are noticeably more forward. However, the separated region ahead of the control is only slightly altered in shape by this change.

Flow conditions at 8.8 degrees angle of attack, Figure 69c, illustrate that the rear shock on the left has moved forward and separation is now evident between the shock and the down-deflected control. Because of the angle of view, no specific statement can be made concerning flow conditions on this control surface. An unstable part span-vortex is evident just inboard of the left wing tip, corresponding to leading edge separation in this region. Little change is evident in the shock pattern on the right wing although the separated region ahead of the up-deflected control has grown toward the leading edge.

Major portions of both wings have leading edge separation at 11.8 degrees angle of attack as evidenced by motion pictures of the shed vortices and wing wake. This leading-edge separation predominates outboard near the unstable part span vortices indicated in Figure 69d. Because of this separation, the shock patterns are rather indefinite. However the major separation ahead of the up-deflected control remains quite distinct. Note also that separation is now evident on the inboard portion of the control surface.

In summary, several basic relationships are evident from the oil flow patterns reviewed above. For surfaces with down-deflected trailing edges, leading edge camber and deflection exhibit a major effect on the shock pattern. The leading-edge deflection to minimize shock-induced separation at low-to-moderate angles of attack is noticeably less than that to delay leading-edge separation at the high angles of attack. Note also that a favorable positioning of the forward and aft shocks exists for the moderate aspect ratio curved-leading-edge planform such that a strong outboard shock exists only in the wing tip region. This is particularly helpful in improving control effectiveness for mid-span and

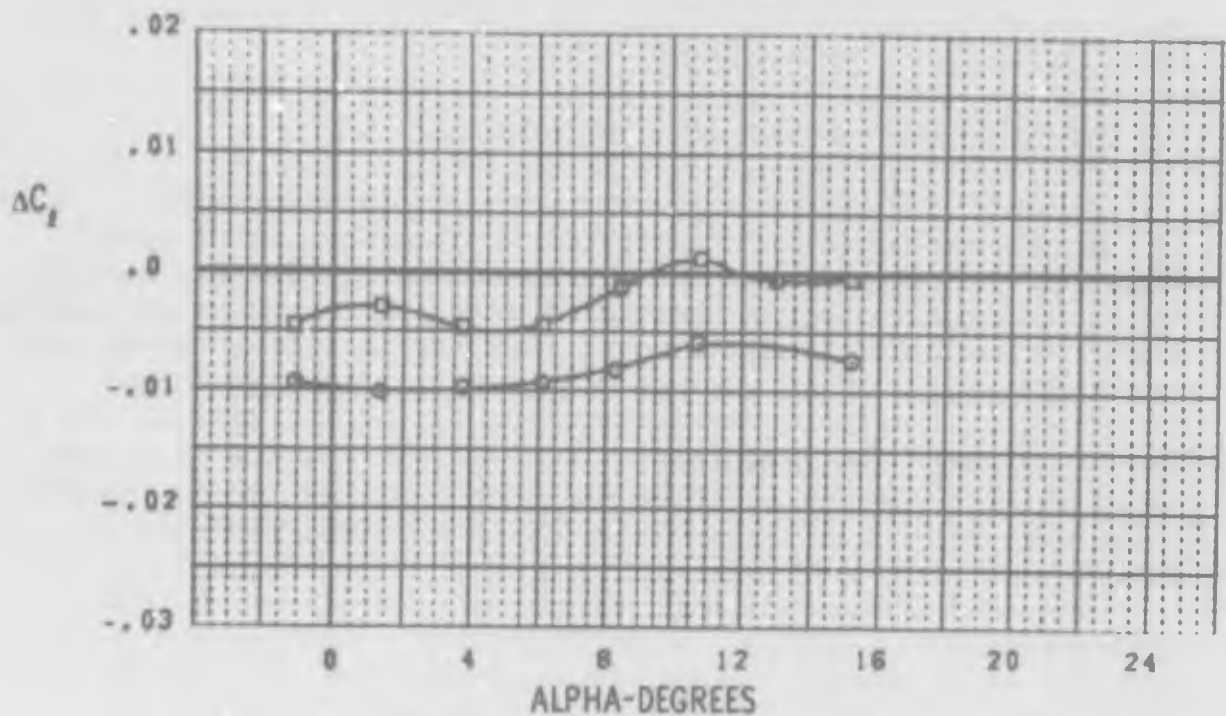
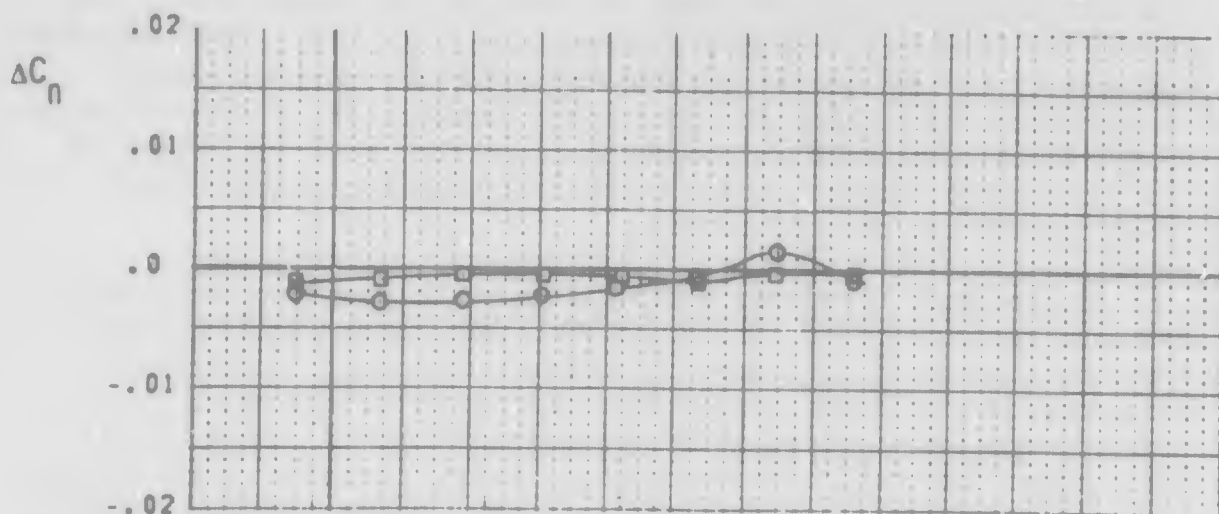
inboard ailerons. For up-deflected trailing edge controls, the control deflection has a major effect on both the shock pattern and the separated region ahead of the control hinge line. In this case, the relationship between shock patterns and separated regions is not as direct as for conventional shock-induced separation. The angle of attack and surface deflection effects on pressure distributions contribute to the size and shape of the separated regions to an extent comparable to that due to shock positions and strengths.

The effect of spanwise location of the aileron on interference loss is given in Figure 70. The data, given in the form of tail on minus tail off force and moment increments illustrates the large losses for the inboard location. These differences are quite startling, particularly in view of the fact that lift, drag, and pitching moment increments are essentially identical for the two locations. Corresponding moment increments are given in Figure 71 to show how the interference increases with surface deflection. Note the marked change with angle of attack associated with the variation in proximity of the wing wake to the horizontal tail.

#### b. Symmetrical Leading Edge Deflection

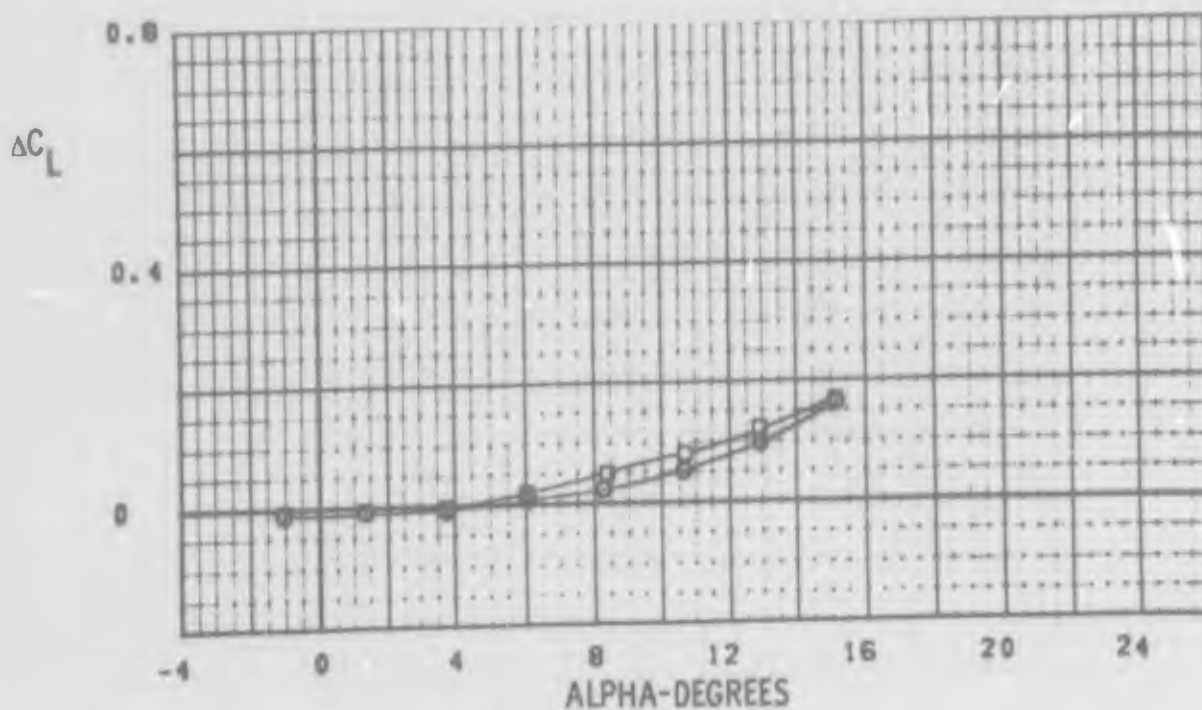
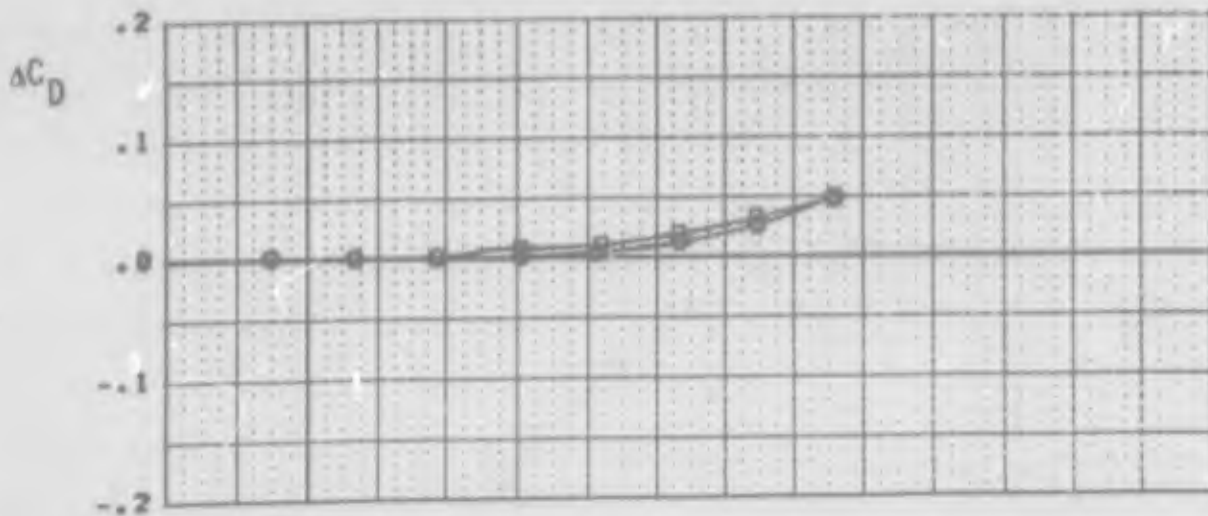
The use of leading edge deflection to increase wing camber was not generally beneficial to aileron control power. Figure 72 illustrates the loss in control effectiveness experienced at low and moderate angles of attack with deflected leading edges. Note however that a small increase in effectiveness does occur for angles of attack near wing stall. No significant differences in aileron characteristics were noted between the K1 and K2 leading edge geometries. Overall, it appears that the basic airfoil section selected for LEDE provides nearly optimum camber, at least for aileron effectiveness considerations.

The test philosophy used to arrive at the leading edge configuration for initial tests of aileron effectiveness is reviewed at this point to provide some guidance for future wind tunnel research programs in this respect. The plan of attack was to first evaluate longitudinal characteristics of various symmetrical leading edge arrangements, horizontal tail off, with no roll control devices (clean trailing edge). Based on this data, a leading edge configuration was chosen that would minimize and delay separation in order to obtain the best control effectiveness at high angles of attack. This rationale



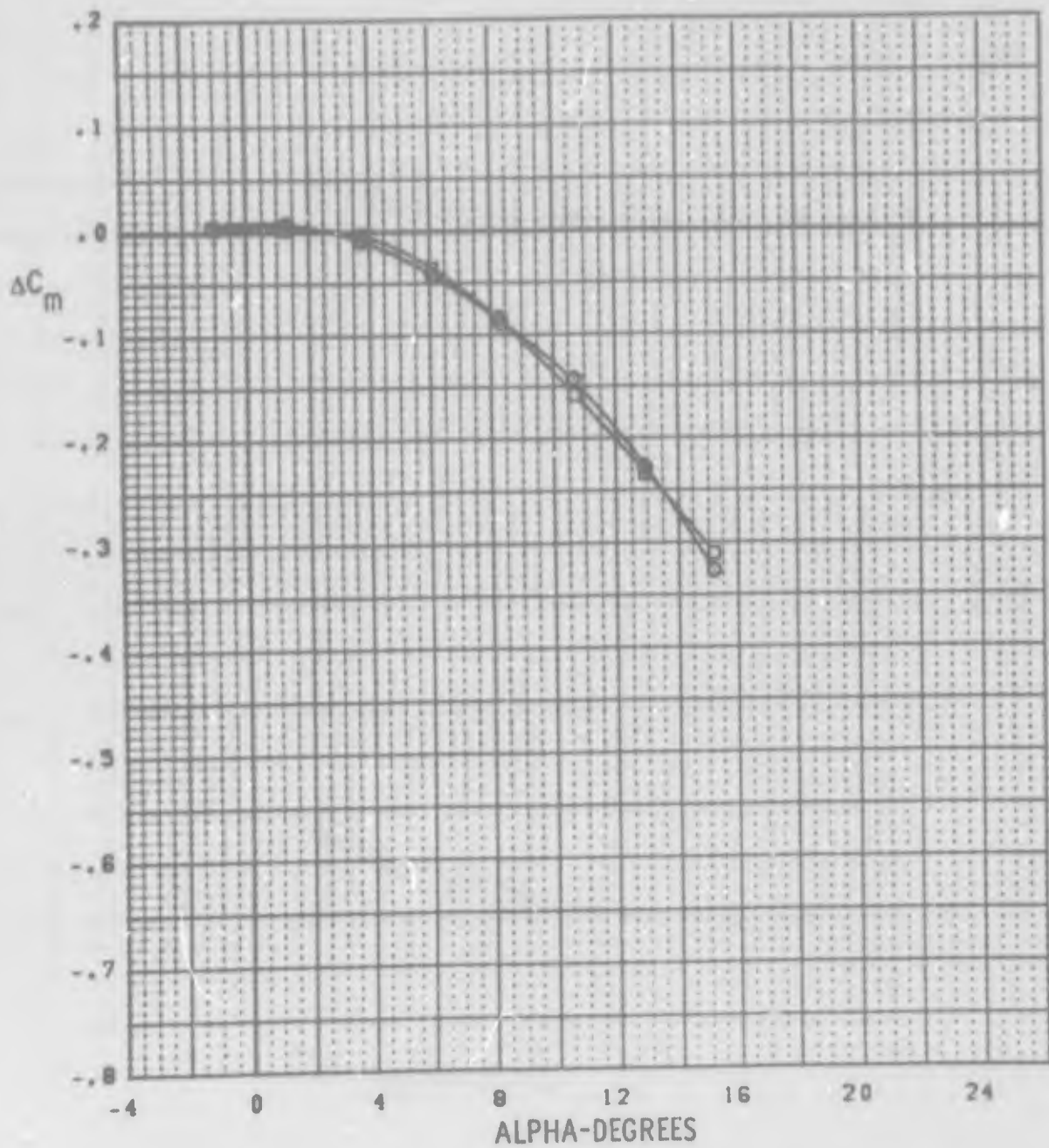
| SYM | TEST                 | INCREMENT | L.E. (L/R) | AILERON (L/R) |
|-----|----------------------|-----------|------------|---------------|
| ○   | PWT 4T TC-043 PN 119 | -PN 112   | K1 10/10   | INBD 10/-10   |
| ◻   | PWT 4T TC-043 PN 133 | -PN 108   | K1 10/10   | MID 10/-10    |

FIGURE 70 HORIZONTAL TAIL INTERFERENCE. RN = 5.2 MILLION  
SMALL AILERON DEFLECTION M = 0.9



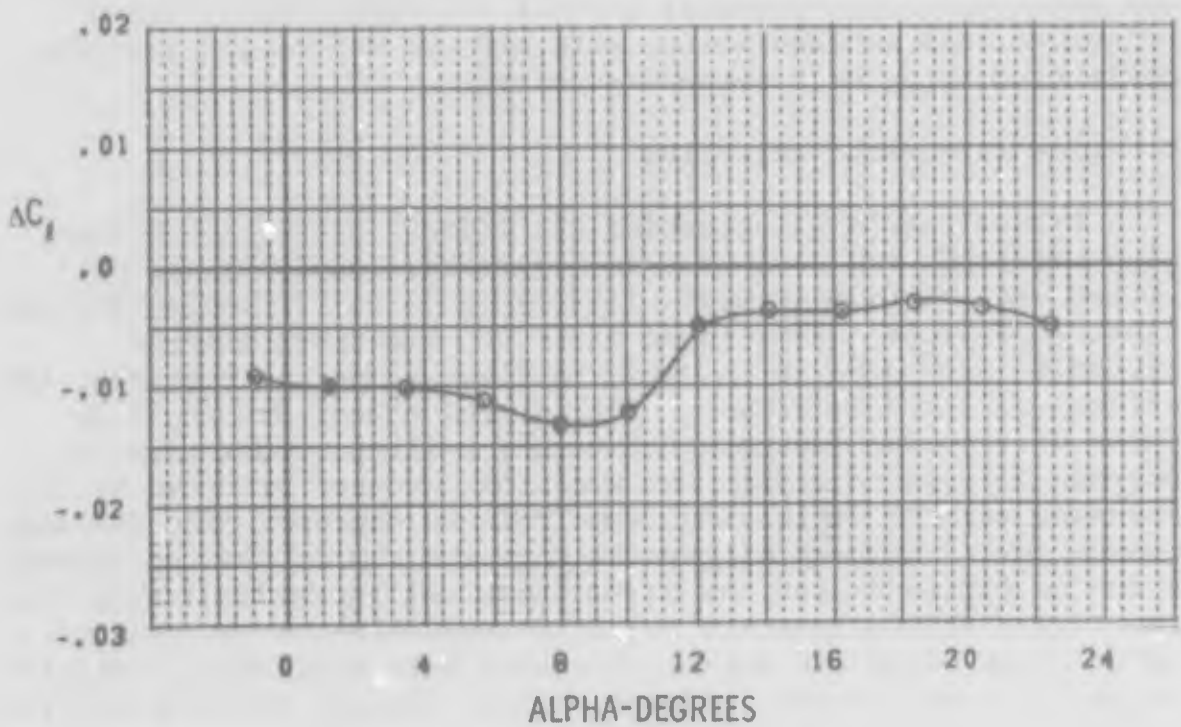
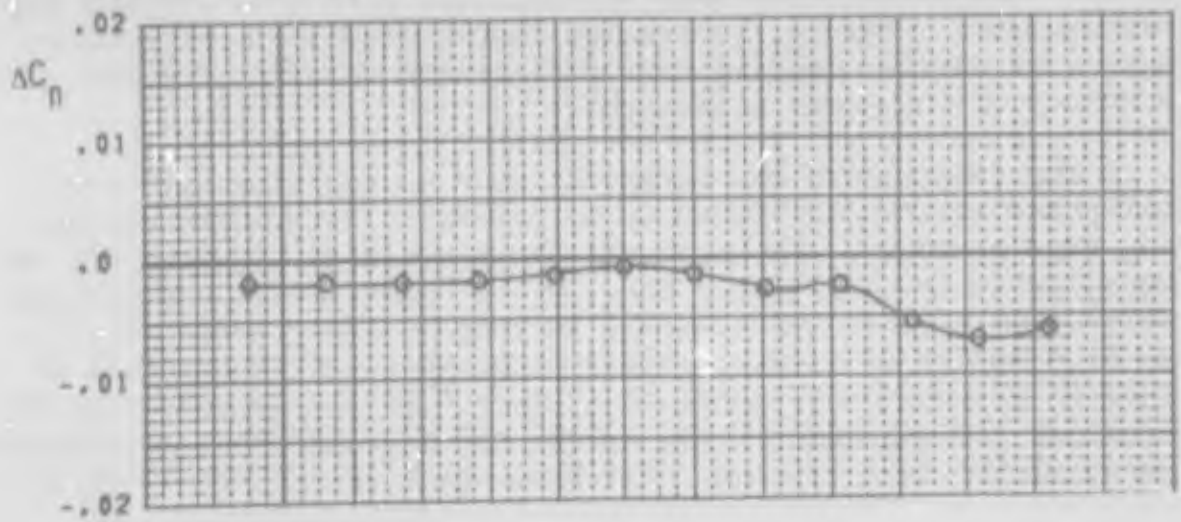
| SYM | TEST          | INCREMENT      | L.E. (L/R) | AILERON (L/R) |
|-----|---------------|----------------|------------|---------------|
| ⊙   | PWT 4T TC-043 | PN 119 -PN 112 | K1 10/10   | INBD 10/-10   |
| □   | PWT 4T TC-043 | PN 133 -PN 108 | K1 10/10   | MID 10/-10    |

FIGURE 70 HORIZONTAL TAIL INTERFERENCE, RN = 5.2 MILLION  
SMALL AILERON DEFLECTION, M = 0.9



| SYM | TEST          | INCREMENT      | L.E. (L/R) | AILERON (L/R) |
|-----|---------------|----------------|------------|---------------|
| ⊙   | PWT 4T TC-043 | PN 119 -PN 112 | K1 10/10   | INBD 10/-10   |
| □   | PWT 4T TC-043 | PN 133 -PN 108 | K1 10/10   | MIO 10/-10    |

FIGURE 70 HORIZONTAL TAIL INTERFERENCE.  $RN = 5.2$  MILLION  
 SMALL AILERON DEFLECTION  $M = 0.9$



| SYM | TEST          | INCREMENT     | L.E. (L/R) | AILERON (L/R) |
|-----|---------------|---------------|------------|---------------|
| ○   | PWT 4T TC-043 | PN 283 -PN501 | K1 0/0     | MID 20/-20    |

FIGURE 71 HORIZONTAL TAIL INTERFERENCE,  $RN = 3.0$  MILLION  
LARGE AILERON DEFLECTION  $M = 0.9$

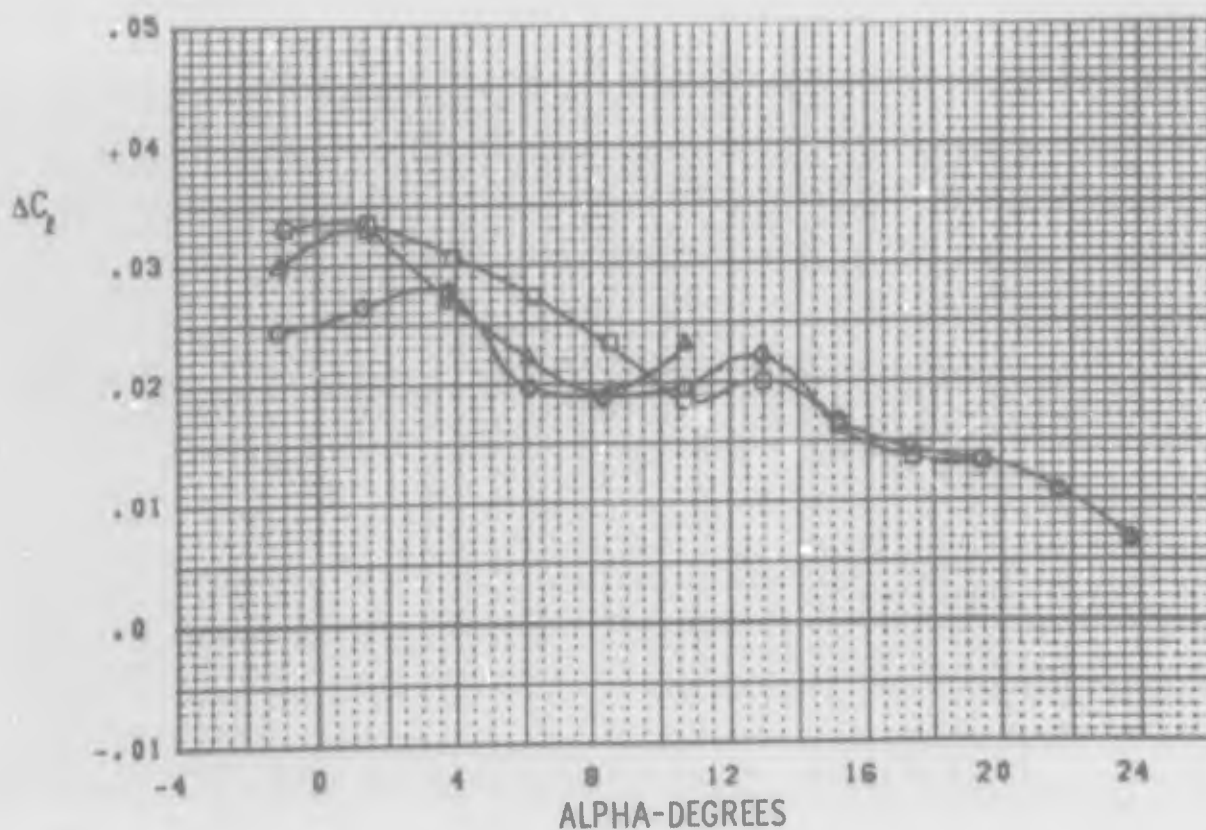
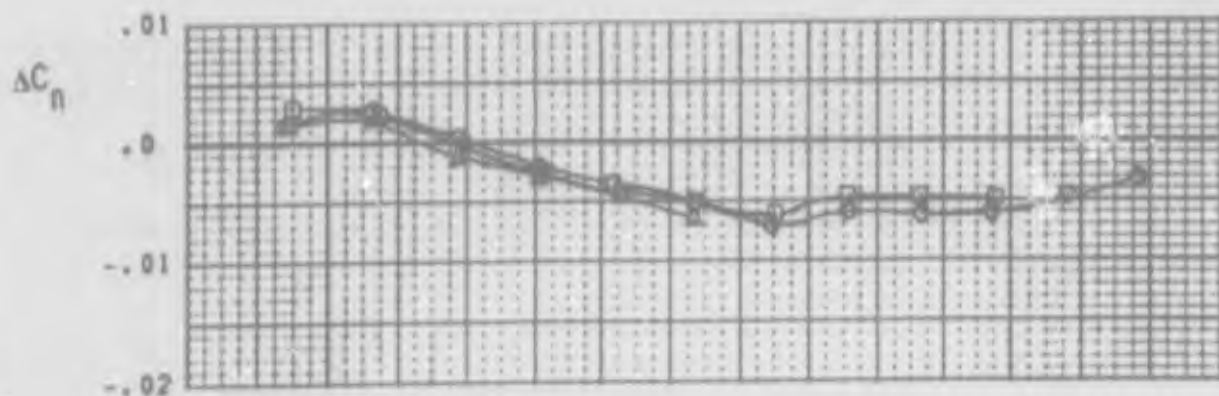
led to the selection of the basic leading edge geometry with ten degrees symmetrical deflection (K1 10/10). The initial test of the various ailerons were accomplished with this leading edge arrangement. However, subsequent checks of aileron effectiveness with smaller leading edge deflections revealed the inadequacy of this test philosophy.

The location of the outboard shock on the wing with down deflected aileron was found to be primarily determined by leading edge geometry. The most aft shock position occurred for the undeflected leading edge. Thus, while symmetrical leading edge deflection yielded improvements in longitudinal characteristics at high angles of attack, little or no gain was experienced in control effectiveness since it is more strongly dependant on the location and strength of the shocks and any attendant separation ahead of the down aileron. For wings with up deflected trailing edge surfaces, the general effects are quite different. In this case the strong adverse pressure gradient due to the trailing edge deflection produces a shock and separation pattern unique to this configuration, with effects due to leading edge deflection being of a secondary nature.

### c. Linearity with Deflection

Typical plots illustrating the effects of aileron deflection magnitude are presented in Figure 73. Analysis was performed with basic increments like these to better define the deflection effects. Additional plots to illustrate aileron linearity were made in an unconventional manner to emphasize the effects of angle of attack. The rolling moment due to 10 degrees aileron was subtracted from the rolling moment with 20 degrees aileron to obtain the additional moment produced by increasing aileron deflection from 10 to 20 degrees. The rolling moment for 20 degrees aileron is thus the sum of the two curves shown in Figure 74 for the mid-aileron configuration. Note that the larger deflections are nearly as effective as the smaller deflections except at angles of attack near wing stall, indicating aileron deflections greater than 20 degrees could be utilized. For Mach numbers of 0.9 and 1.2 the larger deflections are actually more effective at low angles of attack.

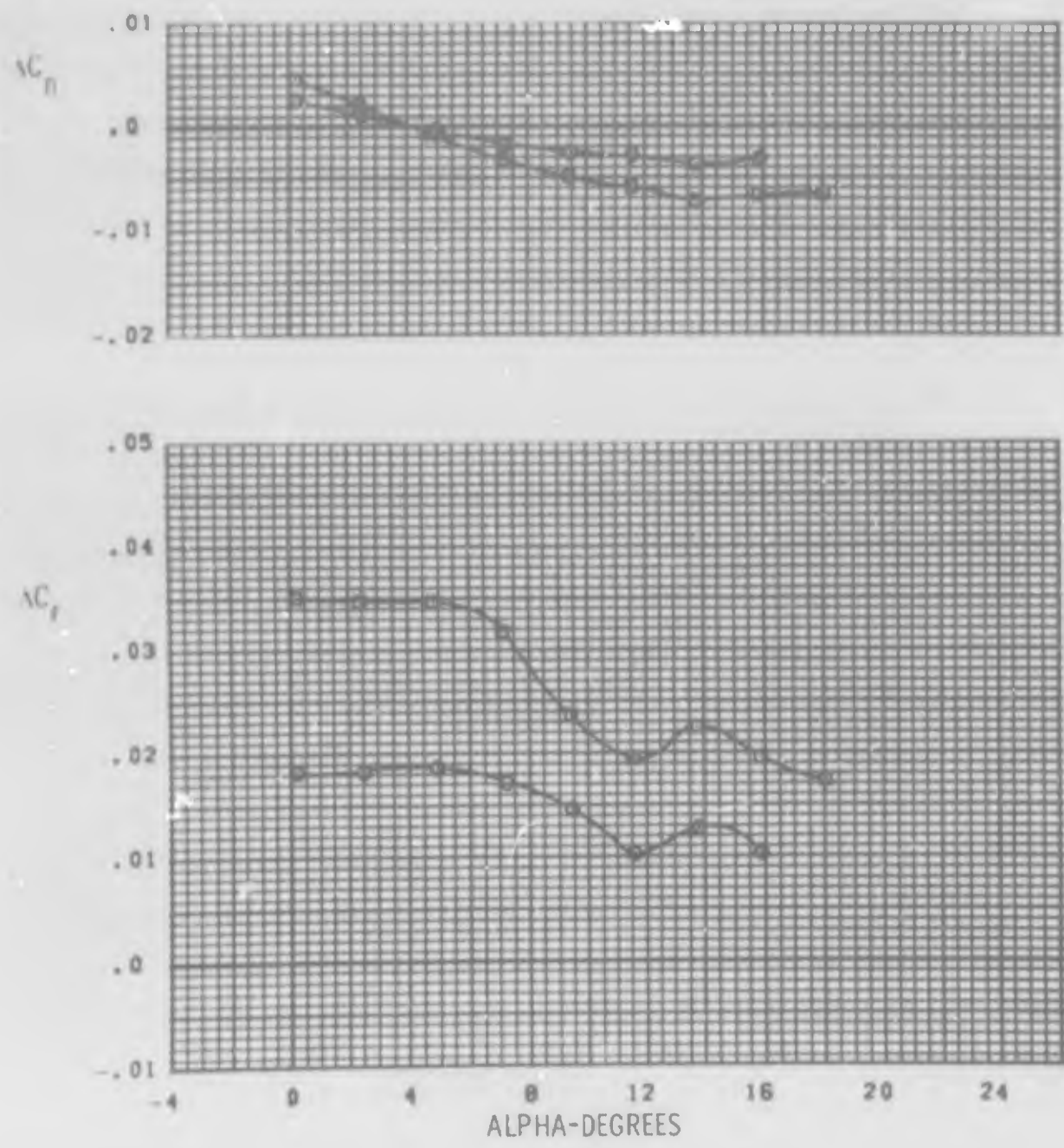
Additional comparisons were made at 0.9 M to understand the reason for the severe loss in effectiveness with angle of attack at the higher control deflection. The available mid-aileron effectiveness data, horizontal tail off, was put in the form used above for the configurations with horizontal tail, see Figure 75. However since the 10 degree aileron data was for 5



| SYM | TEST          | INCREMENT       | L.E. (L/R) | AILERON (L/R) |
|-----|---------------|-----------------|------------|---------------|
| □   | PWT 4T TC-043 | PN 213 - PN 264 | K1 0/0     | MID 20/-20    |
| △   | PWT 4T TC-043 | PN 291 - PN 445 | K1 5/5     | MID 20/-20    |
| ○   | PWT 4T TC-043 | PN 140 - PN 126 | K1 10/10   | MID 20/-20    |

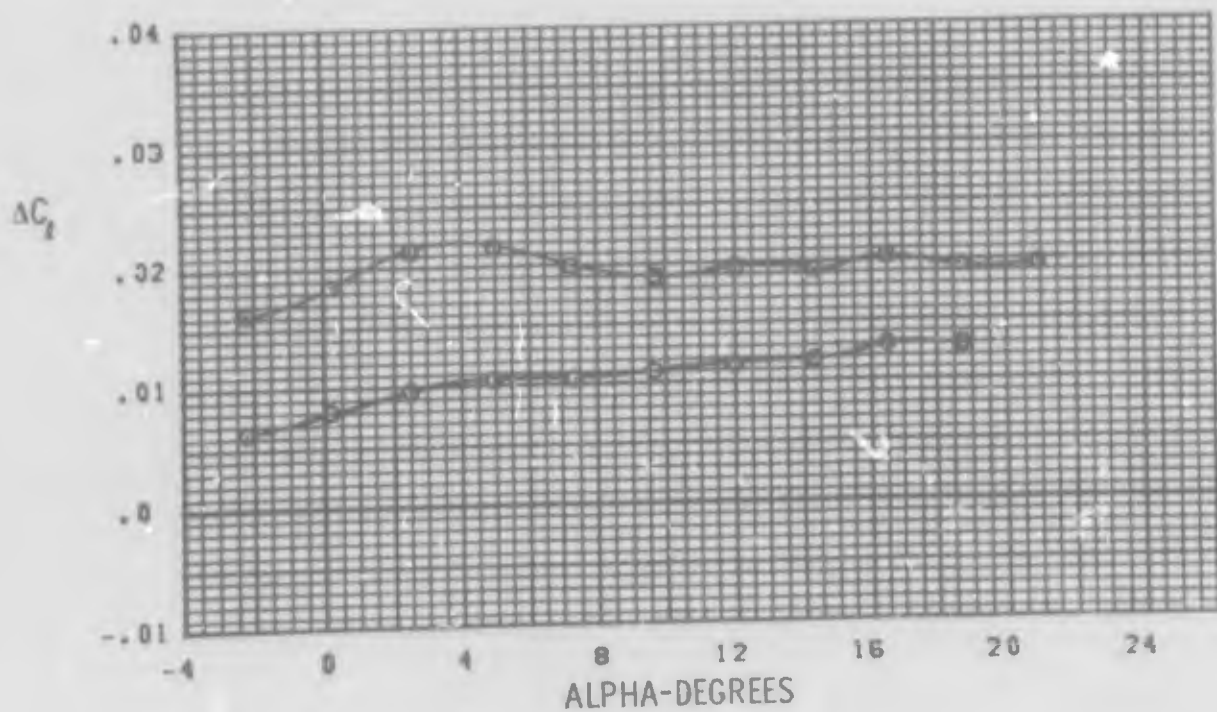
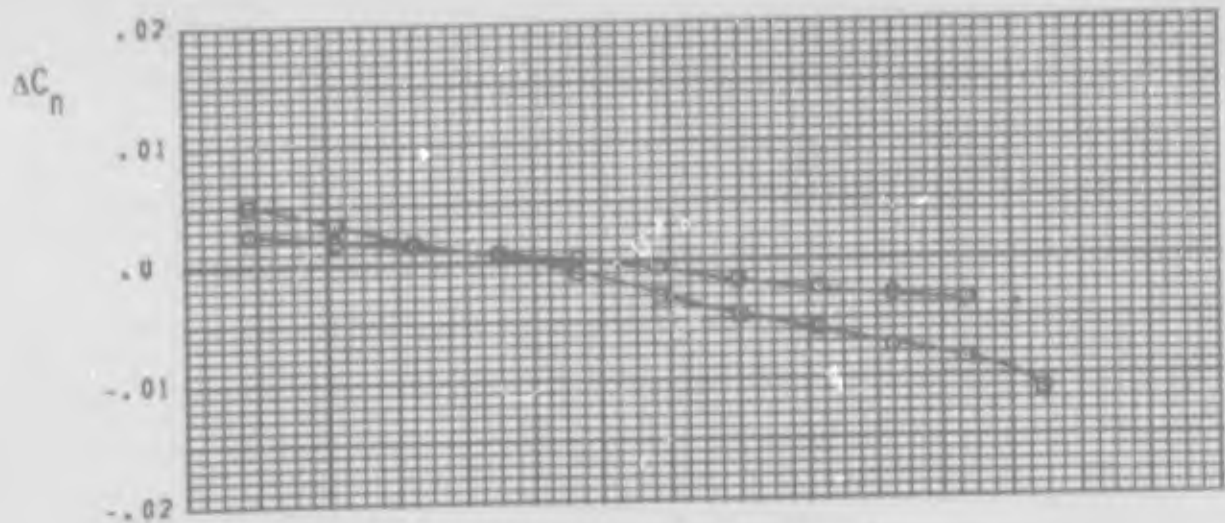
FIGURE 72 SYMMETRICAL L.E. EFFECTS ON MID AILERONS  
M = 0.9





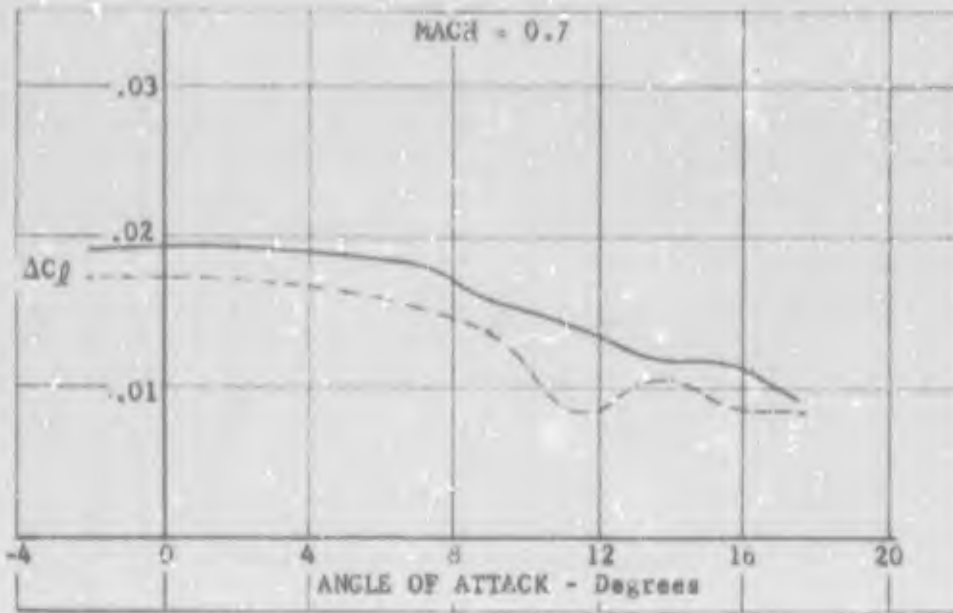
| SYM | TEST          | INCREMENT      | L.E. (L/R) | AILERON (L/R) |
|-----|---------------|----------------|------------|---------------|
| O   | PWT 4T TC-043 | PN 476 -PN 440 | K1 0/0     | MID 10/-10    |
| □   | PWT 4T TC-043 | PN 411 -PN 440 | K1 0/0     | MID 20/-20    |

FIGURE 734 LINEARITY OF AILERON WITH DEFLECTION  
M = 0.8



| SYM | TEST          | INCREMENT      | L.E. (L/R) | AILERON (L/R) |
|-----|---------------|----------------|------------|---------------|
| ⊙   | PWT 4T TC-043 | PN 477 -PN 269 | K1 0/0     | MID 10/-10    |
| ⊗   | PWT 4T TC-043 | PN 414 -PN 269 | K1 0/0     | MID 20/-20    |

FIGURE 73b LINEARITY OF AILERON WITH DEFLECTION  
M = 1.2



K1 Leading Edge 0°/0°  
 10° Aileron  
 Increment for Additional 10° Aileron

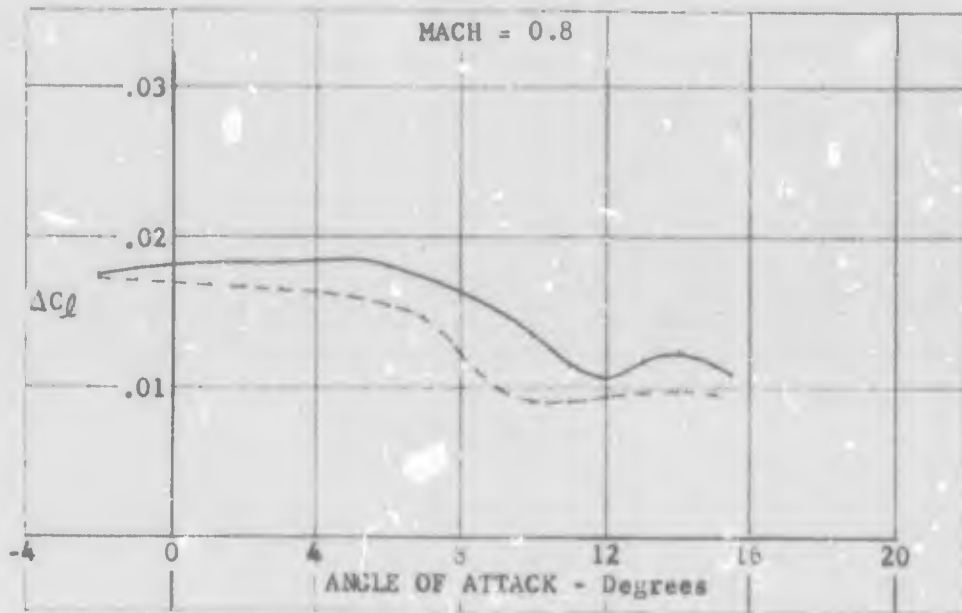
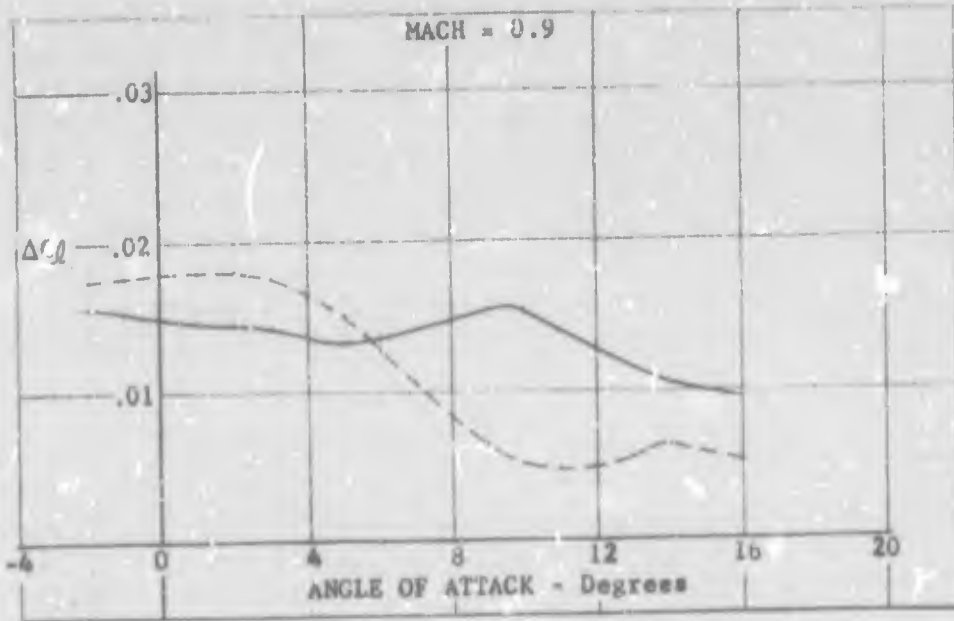


Figure 74 LINEARITY WITH DEFLECTION  
MID SPAN AILERON - HORIZONTAL TAIL ON



K1 Leading Edge 0°/0°

— 10° Aileron

- - - Increment for Additional 10° Aileron

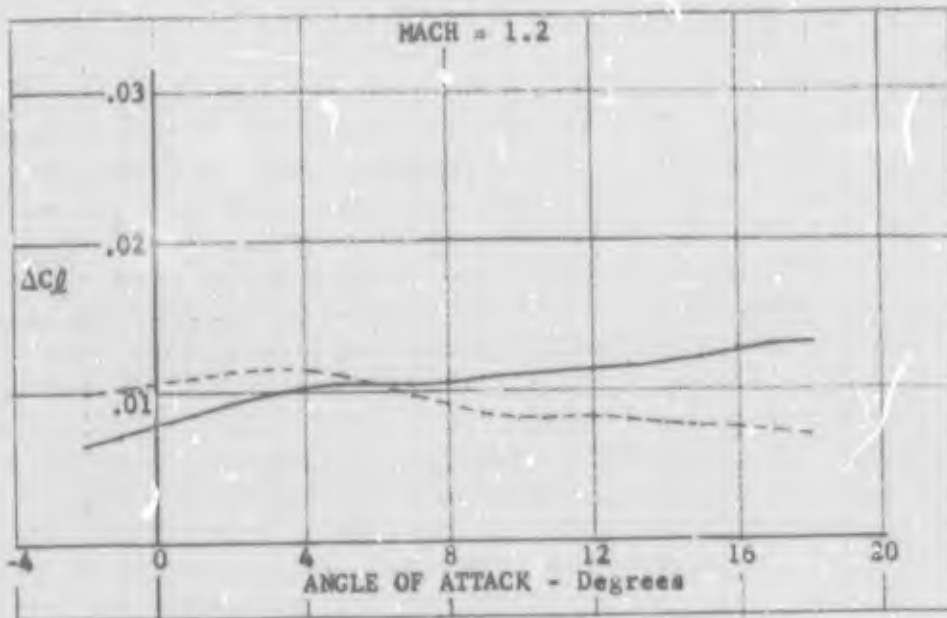
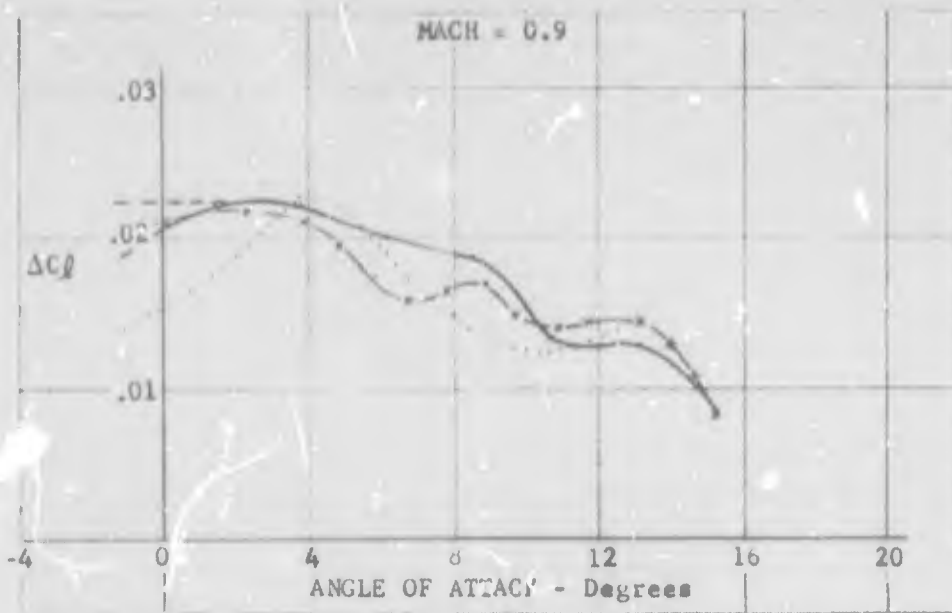


Figure 74 LINEARITY WITH DEFLECTION  
MID SPAN AILERON - HORIZONTAL TAIL ON

and 10 degree symmetrical leading edge deflections while the 20 degree aileron data was obtained only with the undeflected leading edge, some adjustment was necessary. Based upon symmetrical leading edge deflection effects on aileron control, horizontal tail on, the 5 degree leading edge data was adjusted to a constant rolling moment for angles of attack less than  $2^{\circ}$  (indicated in Figure 75 by a short dashed line). The net result is that, horizontal tail off, the control effectiveness at 0.9 M is about equal at large and small aileron deflections. Hence, the loss in control effectiveness tail on at 0.9 M (Figure 74) must be primarily associated with horizontal tail interference effects.

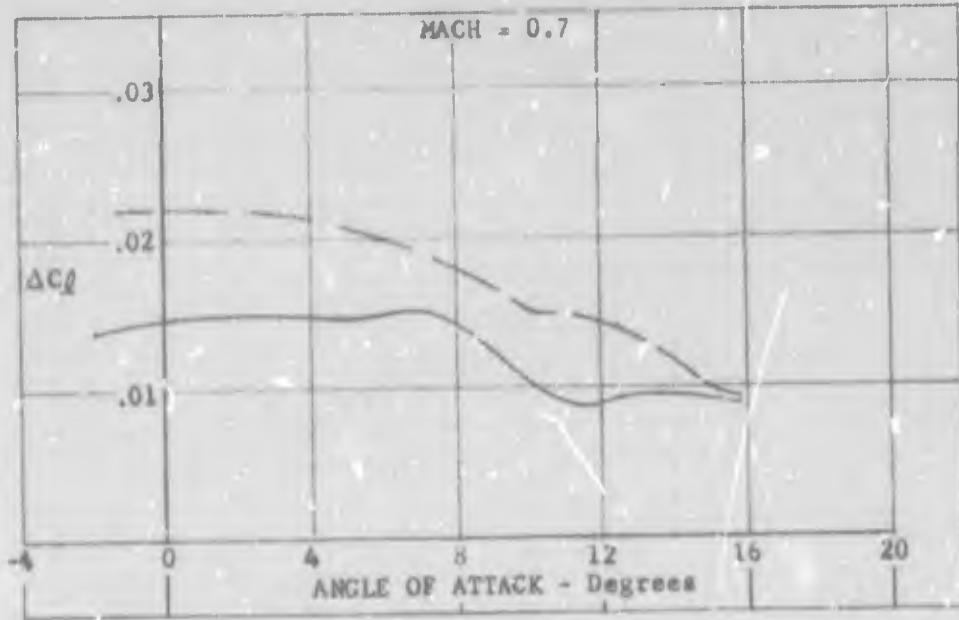
Another interesting aspect of aileron linearity is the relative effectiveness of up versus down deflection. Effectiveness for such one wing panel surfaces are presented in Figure 76. Actual wind tunnel measurements were available for the left aileron 20 degrees down and are shown in this Figure. This data and measurements for 20 degrees differential aileron were used to estimate the rolling moment produced with only the right aileron 20 degrees up. Note that for the transonic Mach numbers, trailing edge up deflection is significantly more effective. The data for 0.8 M and 0.9 M suggest that the estimates for the trailing edge up deflection includes losses or interference effects attributable to the combined asymmetric loading of both ailerons. Note that as the down aileron becomes ineffective the up aileron seems to become more effective.

A comparison of the data for various Mach numbers in Figure 76, reveals that the change in general level of control effectiveness with Mach number in the transonic region is primarily due to effects on the up-deflected surface. The up aileron surface also produces about the same rolling moment at low angles of attack as the equivalent spoiler. (See Figure 77). However, the up aileron deflection does not have the abrupt large loss in effectiveness with angle of attack associated with spoilers. Note that for transonic conditions, the spoiler has somewhat better trends with angle of attack up to about six degrees. However, at about this attitude, an abrupt loss in spoiler effectiveness occurs primarily associated with the start of flow separation on the clean wing. Photographs of oil flow patterns show that the separated region ahead of the up-deflected control is about identical for spoilers and ailerons. (Compare the separated region on the right wing ahead of the spoiler, Figure 78, with that given previously in Figure 68 for mid-aileron. The spoiler appears in Figure 78 as a thin black spanwise line along the 75 percent chord.)



|      |                   |
|------|-------------------|
| Code | L.E. Aileron      |
|      | 5/5 } 10°         |
|      | 10/10 }           |
|      | 0/0 Increment For |
|      | Additional 10°    |

Figure 75 LINEARITY WITH DEFLECTION  
MID SPAN AILERON- HORIZONTAL TAIL OFF



Kl Leading Edge 0°/0°  
 — Left 20° Down  
 - Right 20° Up

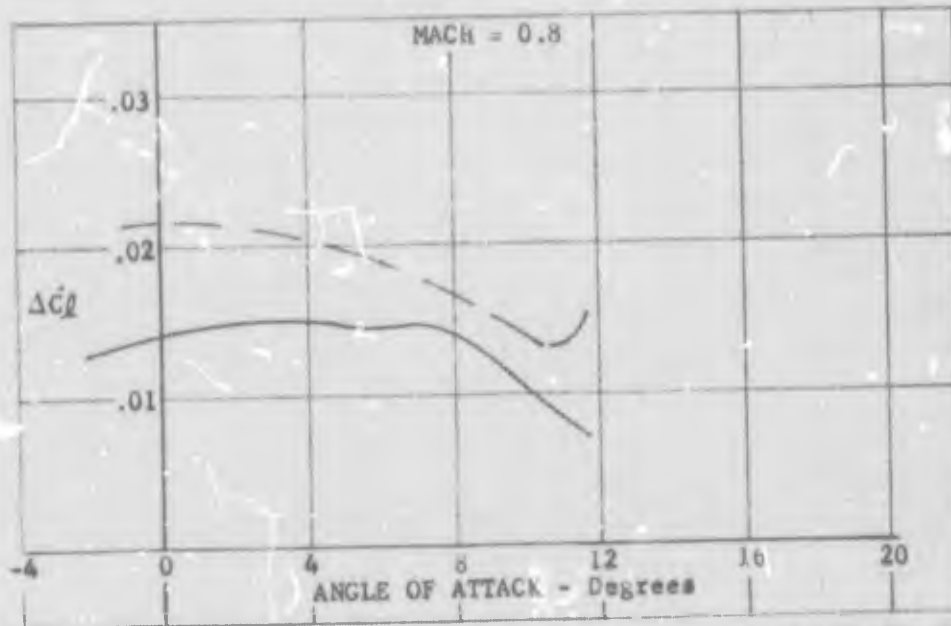
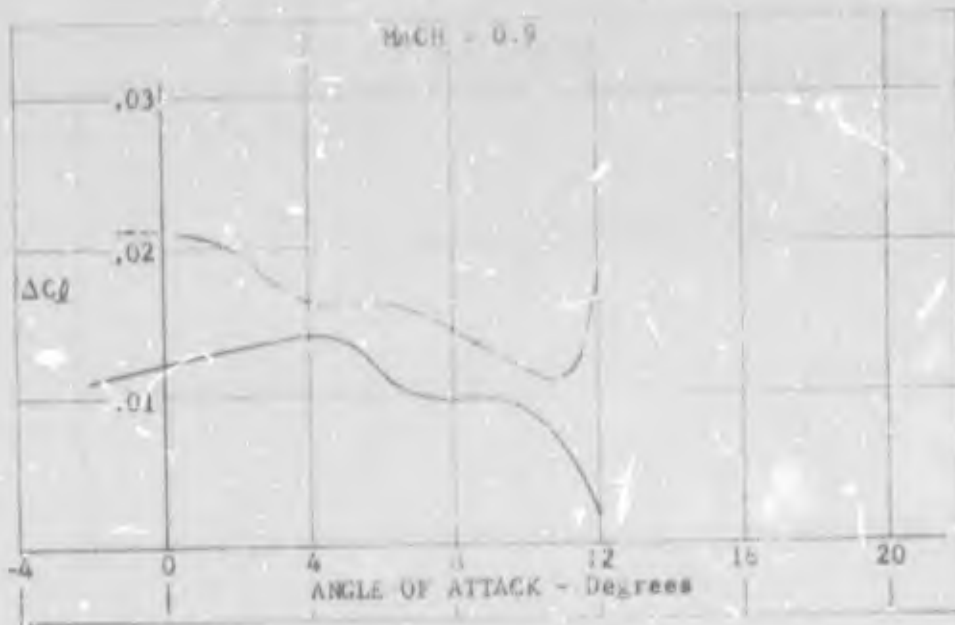


Figure 76 COMPARISON OF UP DEFLECTED AND DOWN DEFLECTED SURFACES  
MID SPAN AILERON



RI Leading edge 0°/70°  
 Left 20° Down  
 Right 20° Up

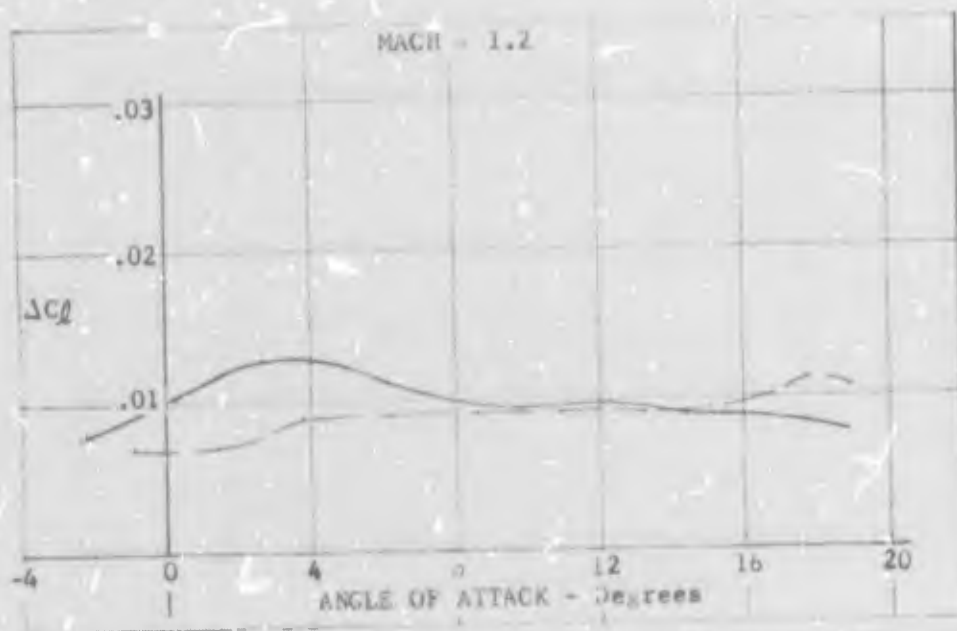


Figure 76 COMPARISON OF UP DEFLECTED AND DOWN DEFLECTED SURFACES  
 MID SPAN AILERON



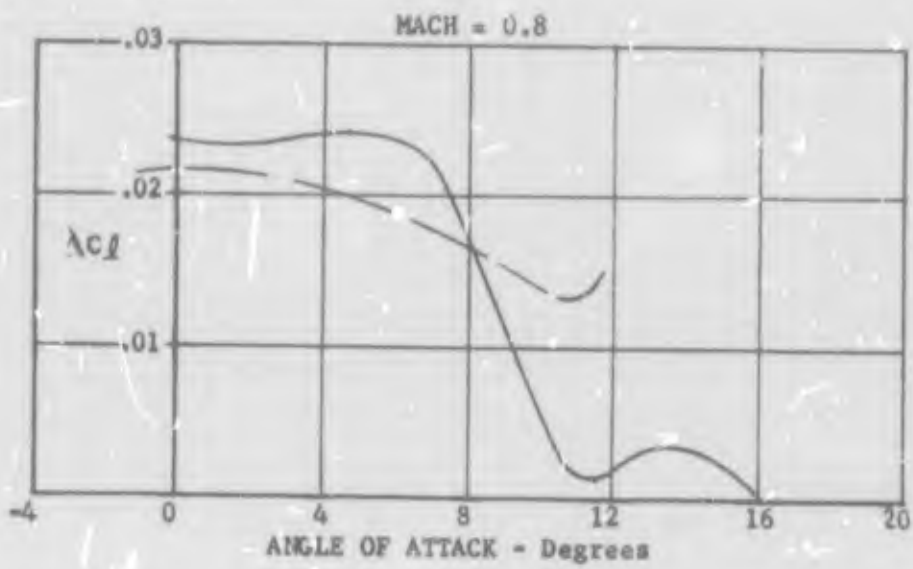
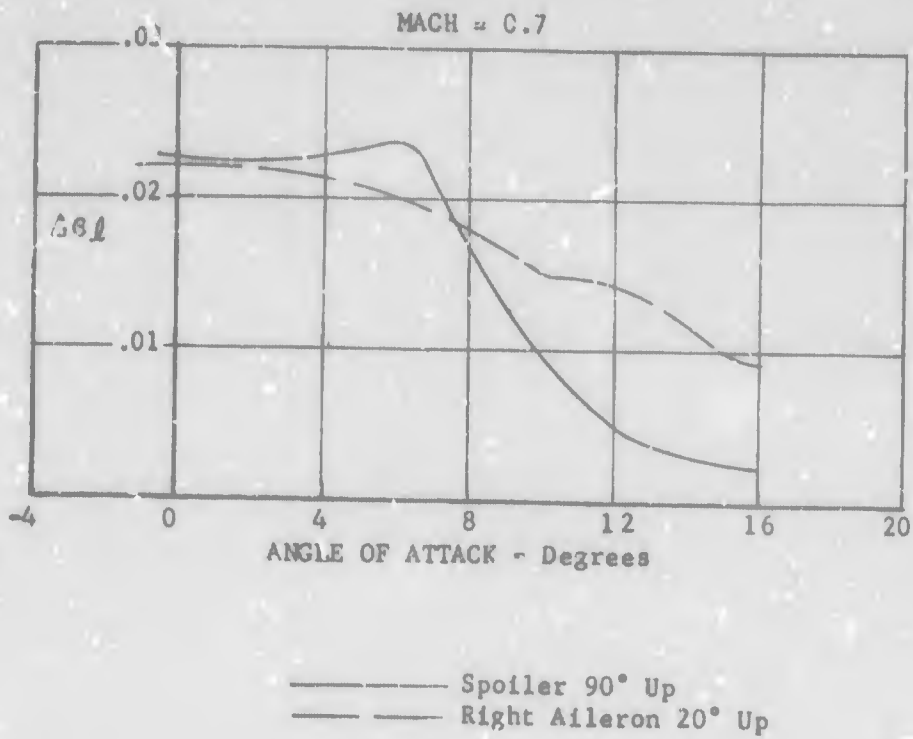


Figure 77 COMPARISON OF UP DEFLECTED MID-AILERON AND SPOILER CLEAN LEADING EDGE

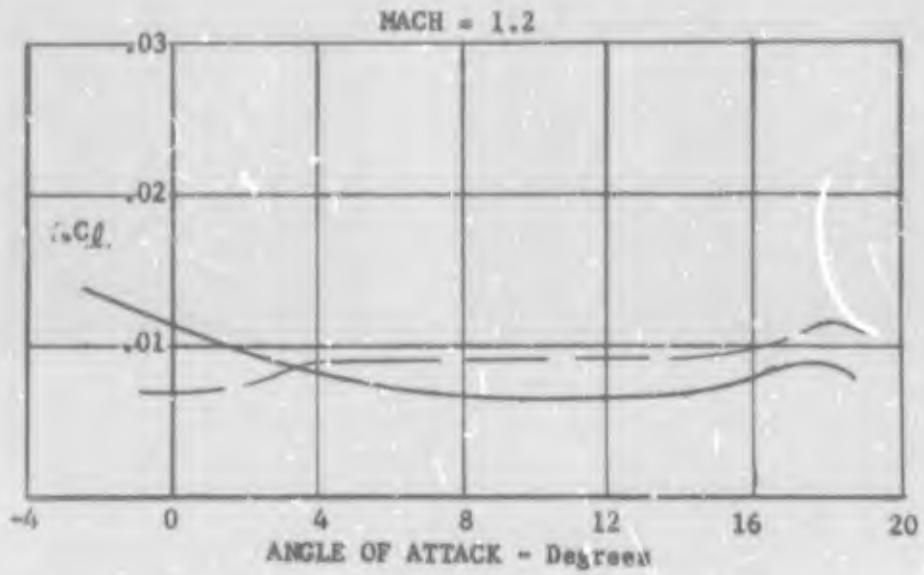
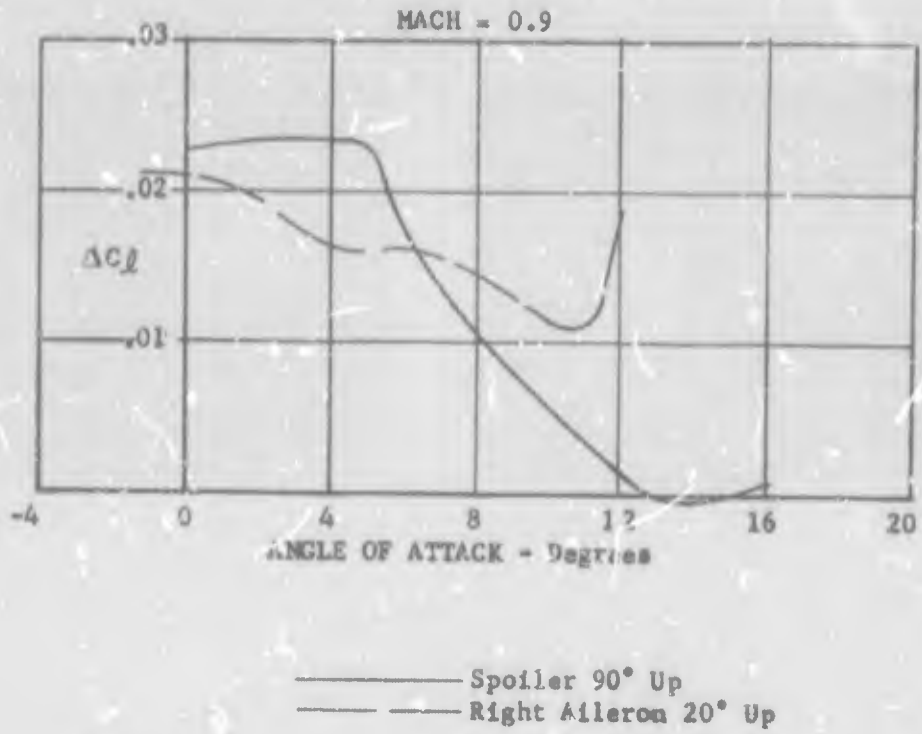


Figure 77 COMPARISON OF UP DEFLECTED MID-AILERON AND SPOILER CLEAN LEADING EDGE

$\alpha = 4.17^\circ$



$\alpha = 6.26^\circ$



$\alpha = 8.66^\circ$



$\alpha = 11.88^\circ$



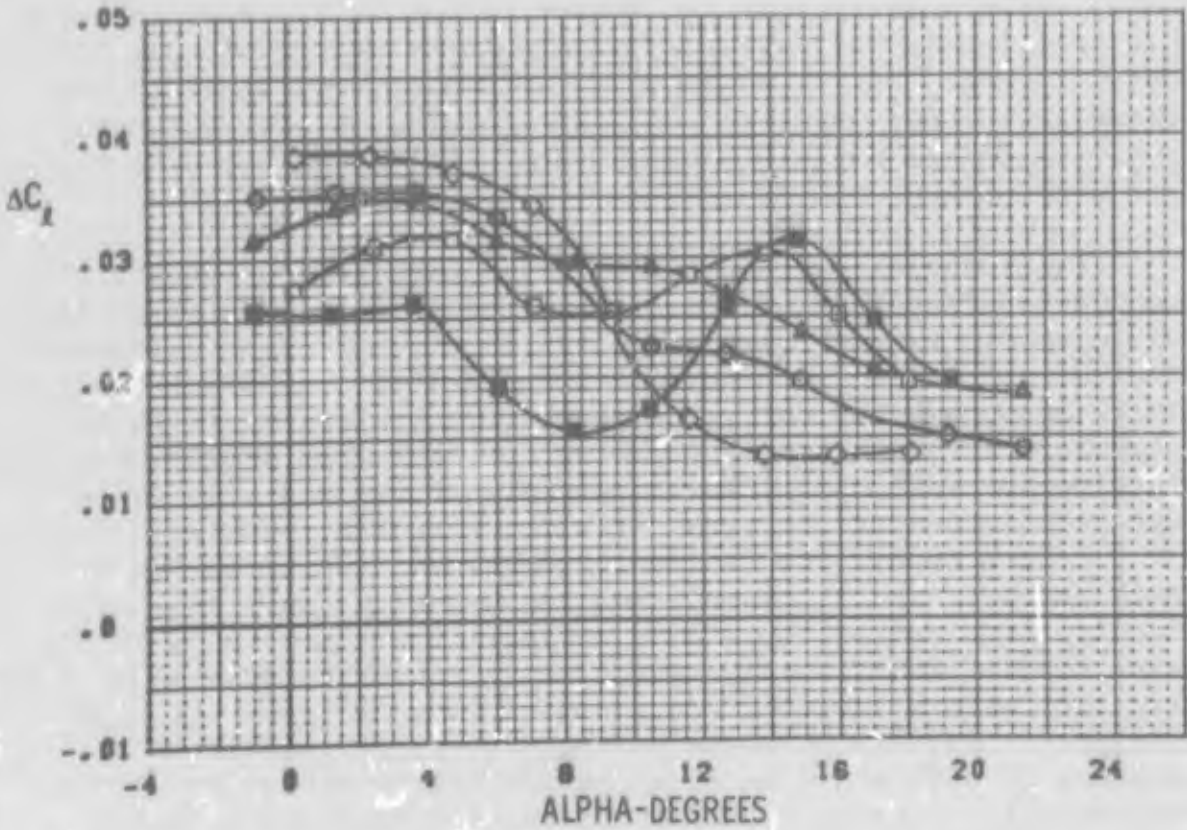
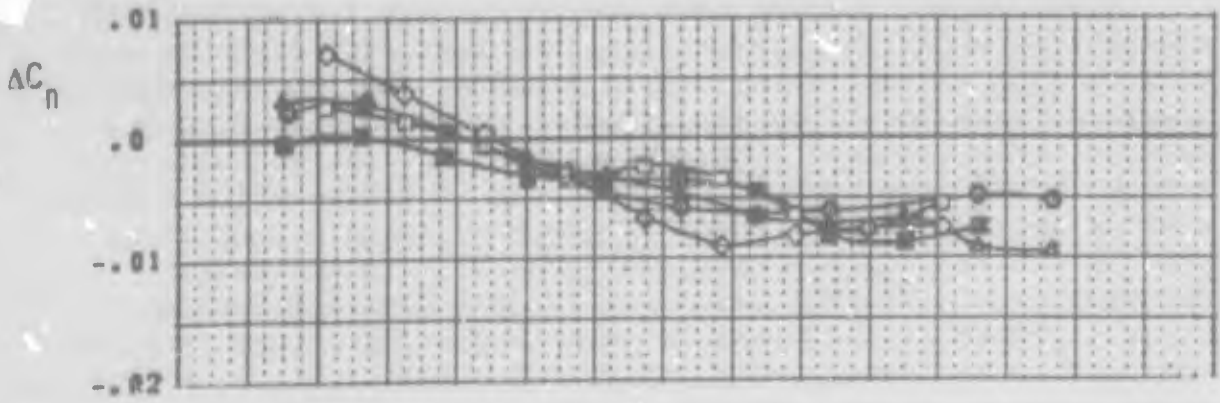
Figure 78 FLOW VISUALIZATION OF SPOILER  
K1 L.E. 0/0 MACH = 0.9

### 3. COMBINED LEADING AND TRAILING EDGE DEVICES

Differential leading edge deflection was investigated in combination with two aileron configurations deflected for positive rolling moment, the mid-span ailerons and the extended span ailerons (made up of the mid-aileron plus the most outboard trailing edge segment). Characteristics for the mid-aileron are noticeably improved by the addition of differential leading edge deflection at high angle of attack transonic conditions, see the 0.8 Mach number data of Figure 79. In particular, the five and ten degree down left leading edge deflections yield improved effectiveness to high angles of attack, suffering only small losses at low attitudes. Differential deflections in the opposite sense, 0/10, (down leading edge with up trailing edge) offer some increase in effectiveness at low attitudes but are undesirable for angles of attack above ten degrees at transonic speeds. For the supersonic condition, differential deflection in this opposite sense shows improved effectiveness over the entire angle of attack range evaluated, see data for 1.2 Mach number.

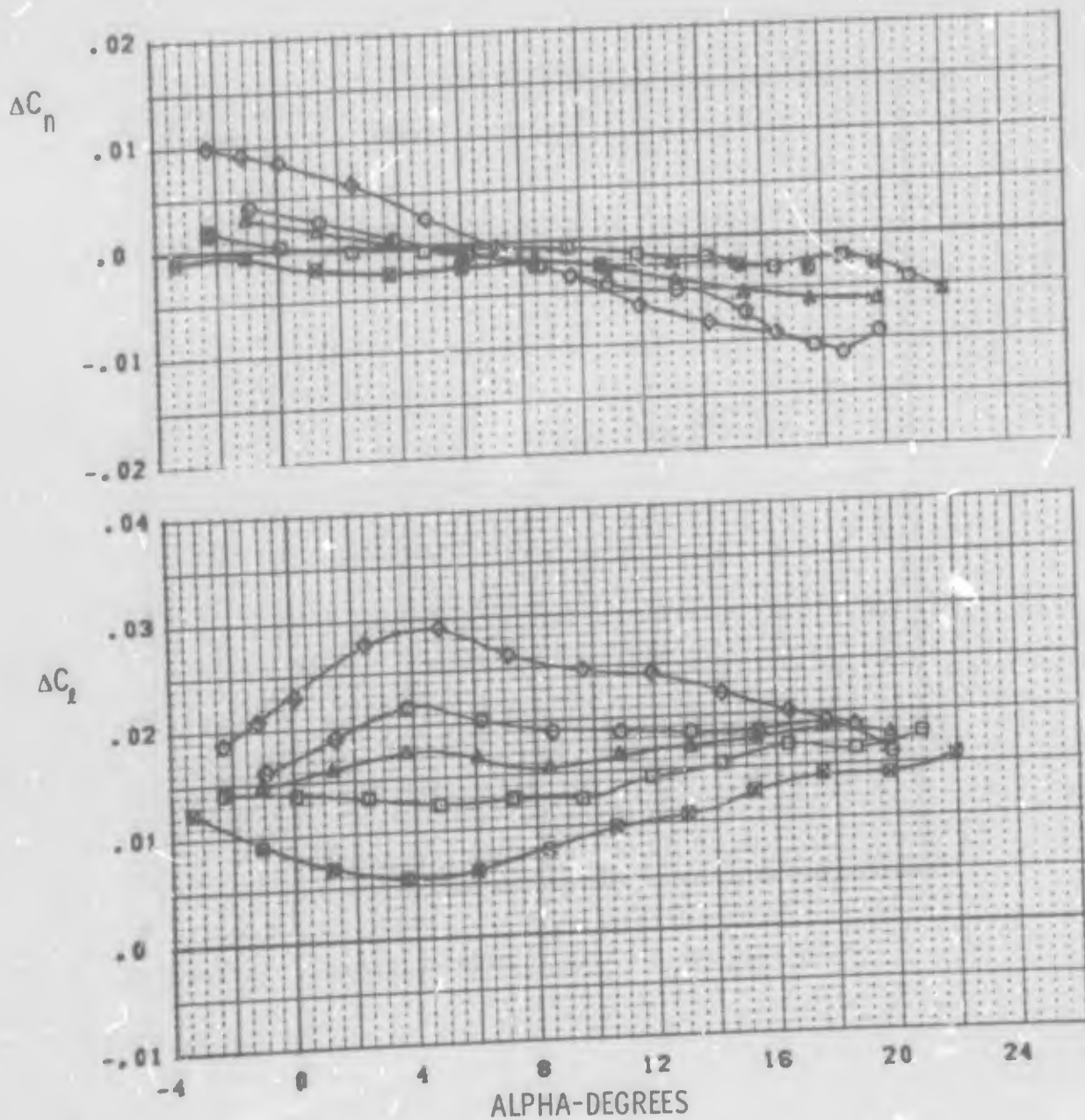
The transonic data for the roll control effectiveness of combined differential deflection of the leading edge flaps and mid-span ailerons is also presented as a function of lift coefficient. The data in Figure 80 more clearly indicate the extent that these combined devices improve roll control at transonic high lift conditions. At 0.7 Mach number marked improvement is attained at lift coefficients between 0.8 and 1.4 with only moderate losses at the lower lift coefficients. Characteristics at 0.8 Mach number are noticeably degraded from those for 0.7 Mach number. The attainable rolling moment is more sensitive to leading edge deflection. Note in particular that the 10/0 degree leading edge is only useful at lift coefficients greater than 1.0 and suffers large effectiveness losses at lower lift coefficients. Further progressive degradation is evident at Mach numbers of 0.85 and 0.9; at these conditions scheduling of the differential leading edge deflection with angle of attack or lift coefficient would be required to obtain the modest benefits at high angles of attack without incurring severe penalties at the lower conditions.

Data obtained for differential leading edge deflection used in combination with the extended span ailerons, Figure 81, have similar trends to those obtained with the mid-aileron. However, in this case, the gains due to inclusion of differential leading edge are smaller than those obtained for the mid-aileron configurations.



| SYM | TEST          | INCREMENT       | L.E. (L/R) | AILERON (L/R) |
|-----|---------------|-----------------|------------|---------------|
| ○   | PWT 4T TC-043 | PN 214 - PN 267 | K1 0/0     | MID 20/-20    |
| ■   | PWT 4T TC-043 | PN 179 - PN 267 | K1 15/0    | MID 20/-20    |
| ▲   | PWT 4T TC-043 | PN 311 - PN 267 | K1 5/0     | MID 20/-20    |
| ◇   | PWT 4T TC-043 | PN 420 - PN 440 | K1 0/10    | MID 20/-20    |
| □   | PWT 4T TC-043 | PN 427 - PN 440 | K1 10/0    | MID 20/-20    |

FIGURE 79a DIFFERENTIAL L.E. FLAP WITH MID SPAN AILERONS  
M = 0.8  
186



| SYM | TEST          | INCREMENT       | L.E. (L/R) |      | AILERON (L/R) |        |
|-----|---------------|-----------------|------------|------|---------------|--------|
| ○   | PWT 4T TC-043 | PN 216 - PN 269 | K1         | 0/0  | MID           | 20/-20 |
| □   | PWT 4T TC-043 | PN 423 - PN 269 | K1         | 10/0 | MID           | 20/-20 |
| △   | PWT 4T TC-043 | PN 313 - PN 269 | K1         | 5/0  | MID           | 20/-20 |
| ■   | PWT 4T TC-043 | PN 181 - PN 269 | K1         | 15/0 | MID           | 20/-20 |
| ◇   | PWT 4T TC-043 | PN 421 - PN 269 | K1         | 0/10 | MID           | 20/-20 |

FIGURE 79b DIFFERENTIAL L.E. FLAP WITH MID SPAN AILERONS  
M = 1.2

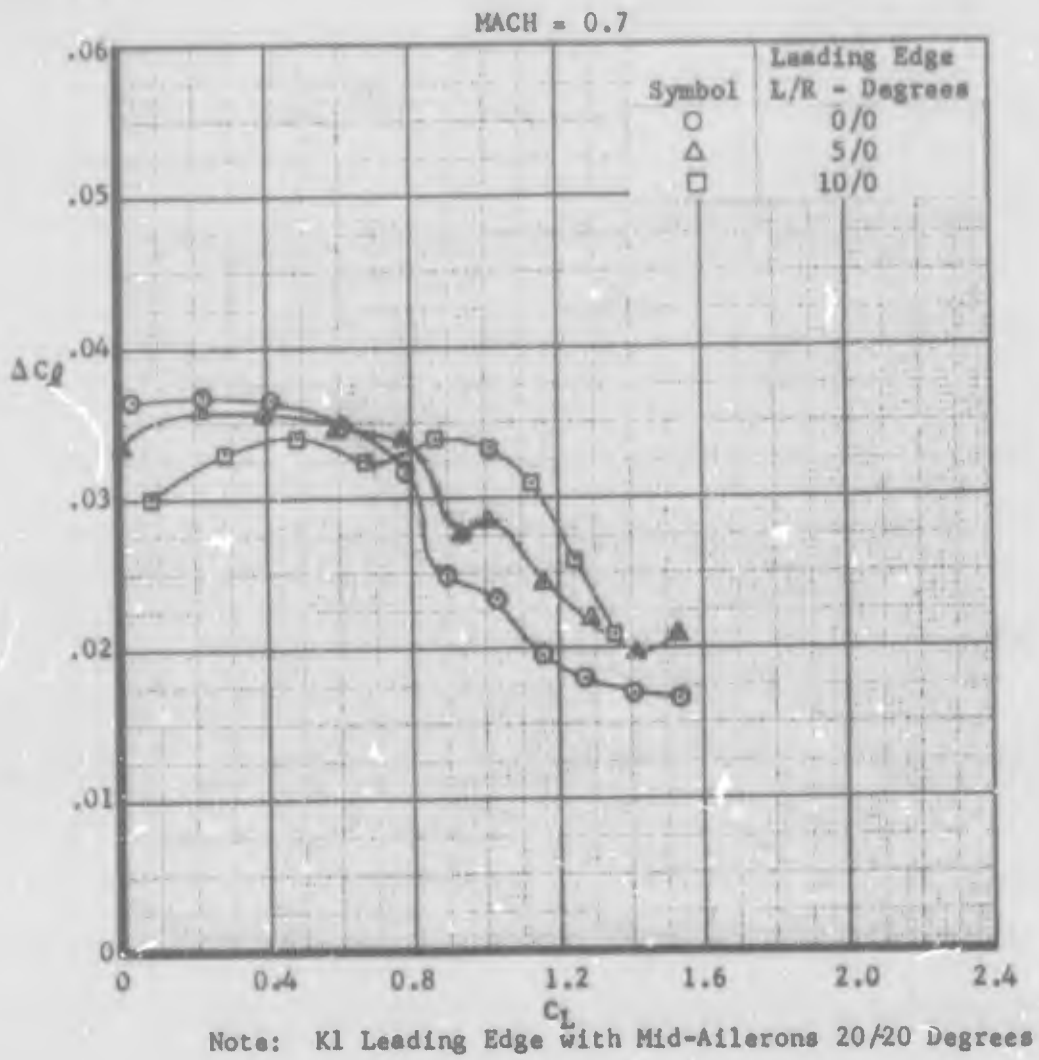


Figure 80a COMBINED LEADING AND TRAILING EDGE ROLL CONTROL  
MACH = 0.7

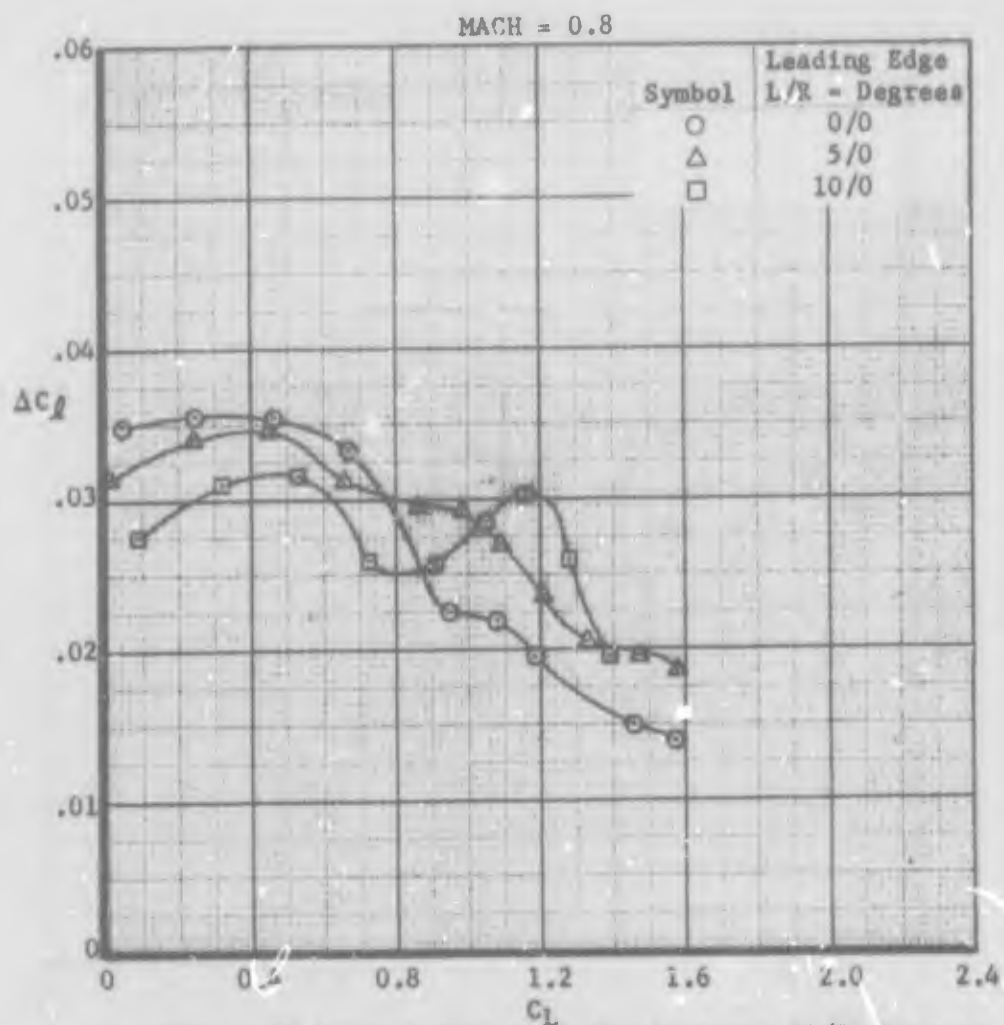
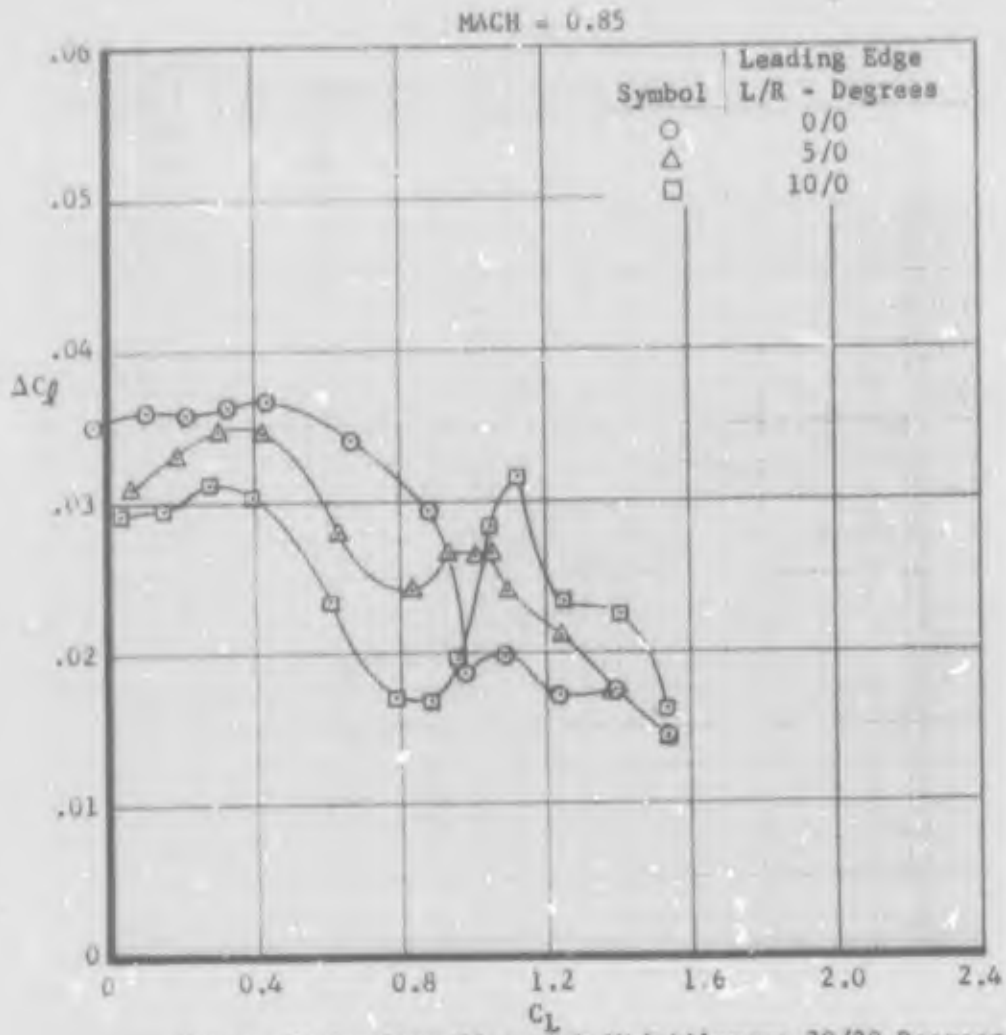


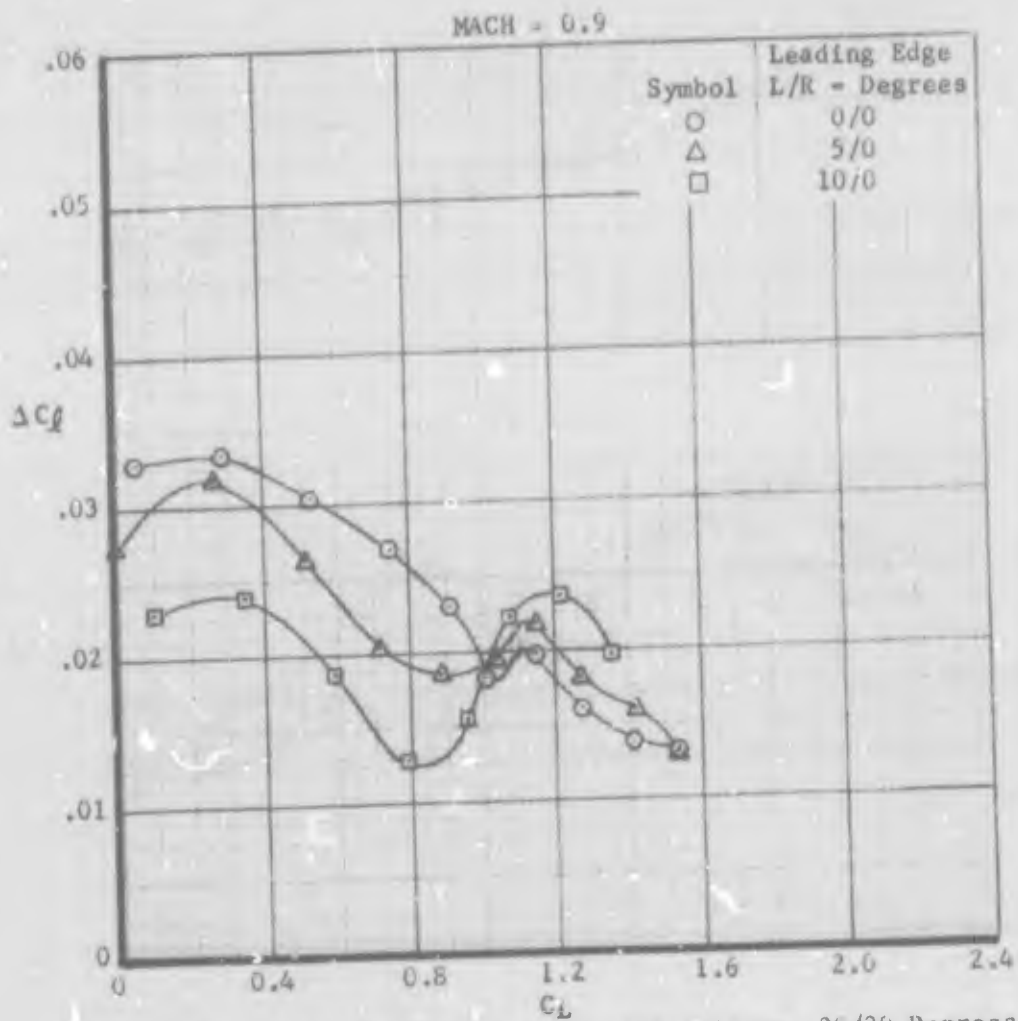
Figure 80b COMBINED LEADING AND TRAILING EDGE ROLL CONTROL  
MACH=0.8





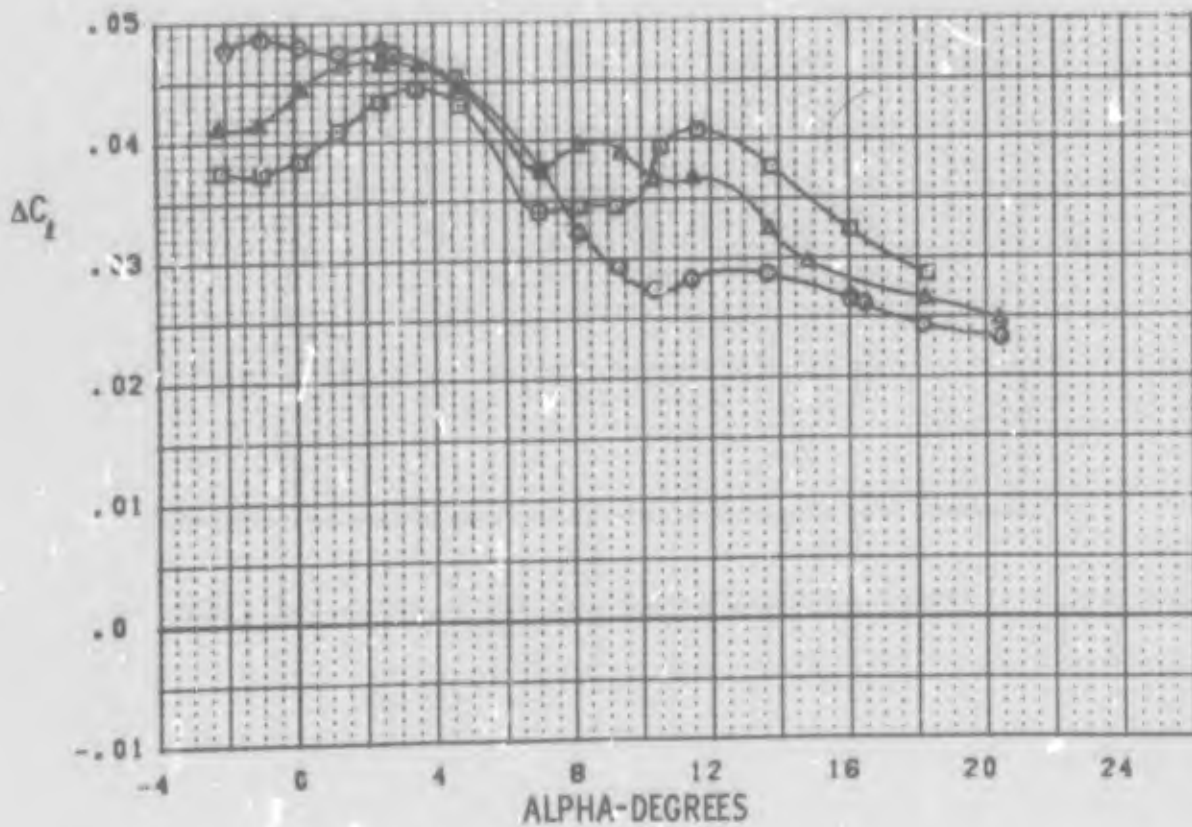
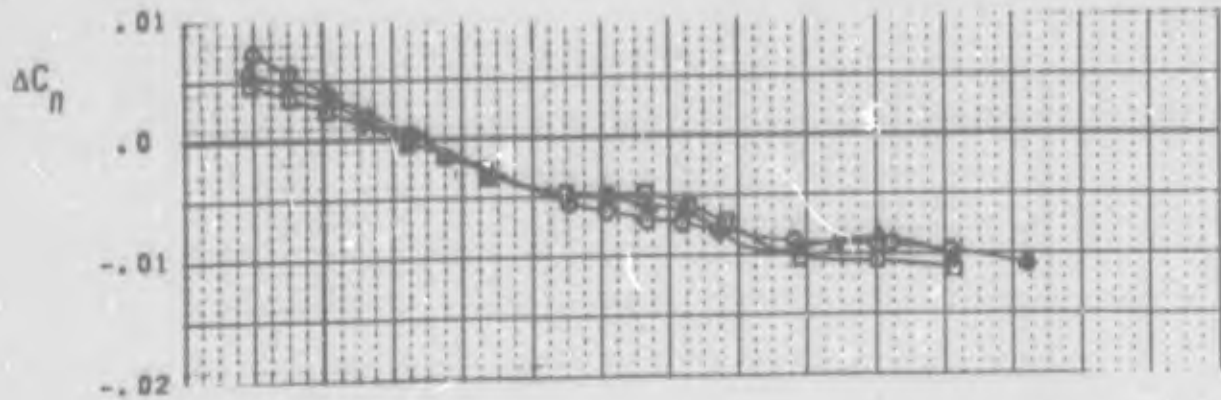
Note: KI Leading Edge with Mid-Ailerons 20/20 Degrees

Figure 80c COMBINED LEADING AND TRAILING EDGE ROLL CONTROL  
MACH = 0.85



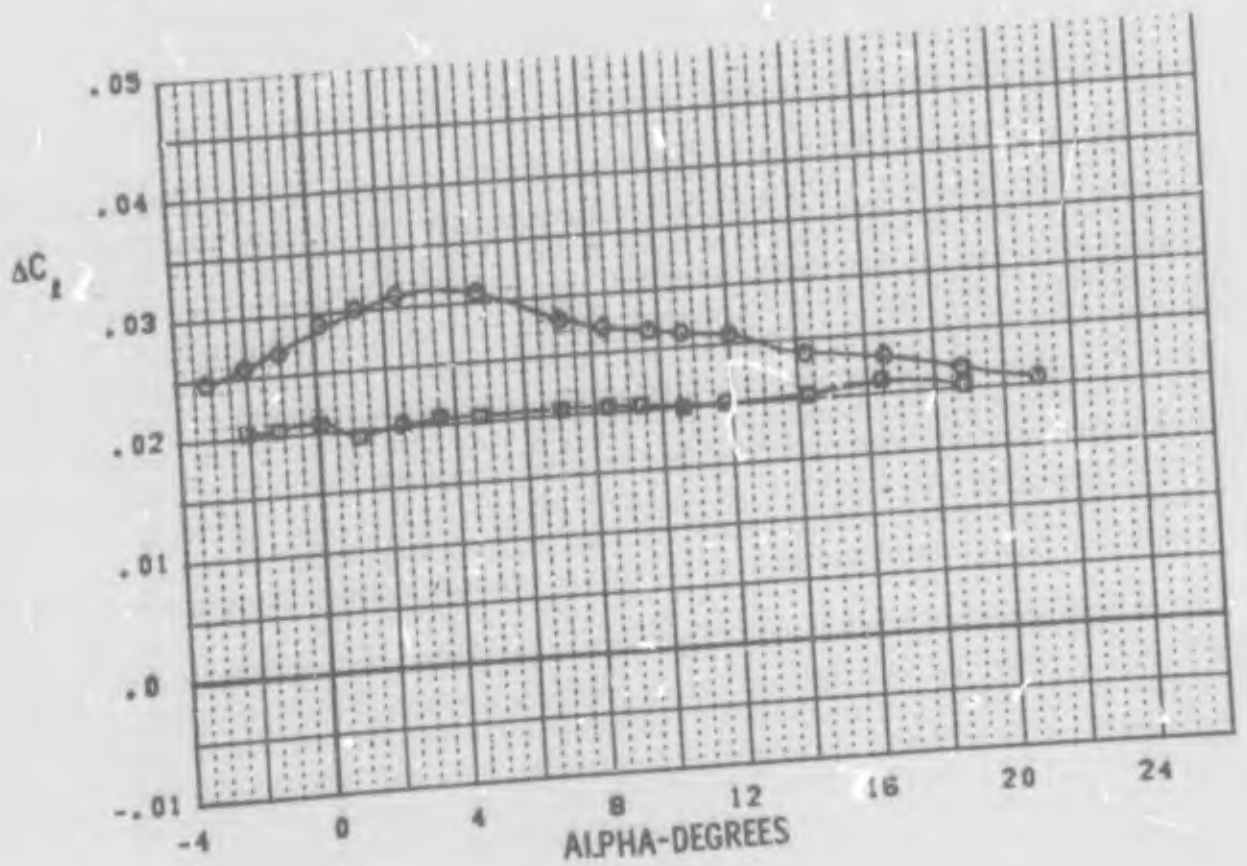
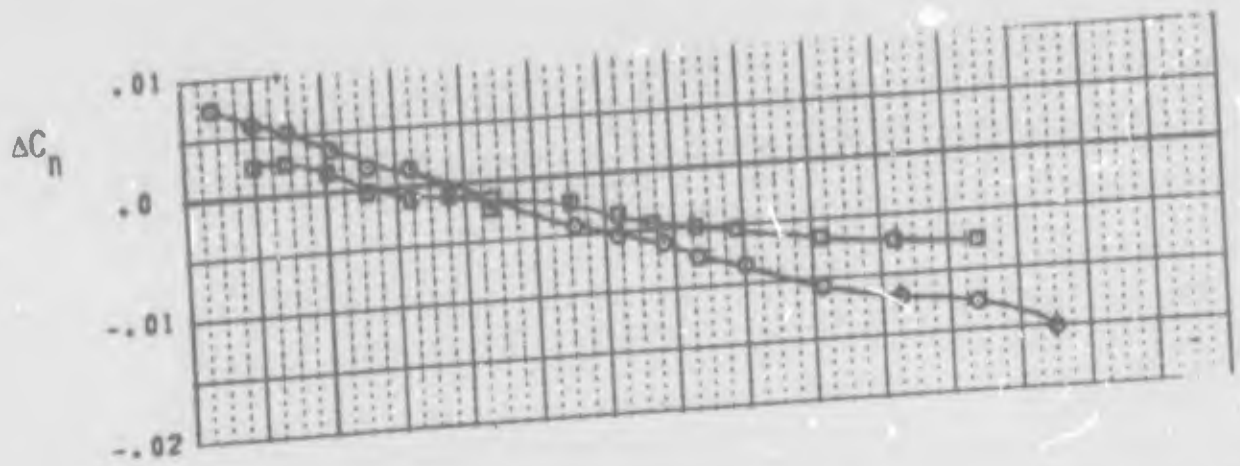
Note: Kl Leading Edge with Mid-Ailerons 20/20 Degrees

Figure 80d COMBINED LEADING AND TRAILING EDGE ROLL CONTROL  
MACH = 0.9



| SYM | TEST           | INCREMENT     | L.E. (L/R) | AILERON (L/R)  |
|-----|----------------|---------------|------------|----------------|
| ○   | PWT 16T TF-216 | PN 62 - PN 50 | K1 0/0     | 3 SEGM. 20/-20 |
| □   | PWT 16T TF-216 | PN 71 - PN 50 | K1 10/0    | 3 SEGM. 20/-20 |
| △   | PWT 16T TF-216 | PN 77 - PN 50 | K1 5/0     | 3 SEGM. 20/-20 |

FIGURE 81a DIFFERENTIAL L.E. FLAP WITH EXTENDED SPAN AILERONS  
M = 0.8



| SYM | TEST           | INCREMENT     | L.E. (L/R) | AILERON (L/R)  |
|-----|----------------|---------------|------------|----------------|
| ○   | PWT 16T TF-216 | PN 61 - PN 54 | K1 0/0     | 3 SEGM. 20/-20 |
| □   | PWT 16T TF-216 | PN 70 - PN 54 | K1 10/0    | 3 SEGM. 20/-20 |

FIGURE 81b DIFFERENTIAL L.E. FLAP WITH EXTENDED SPAN AILERONS  
M = 1.2

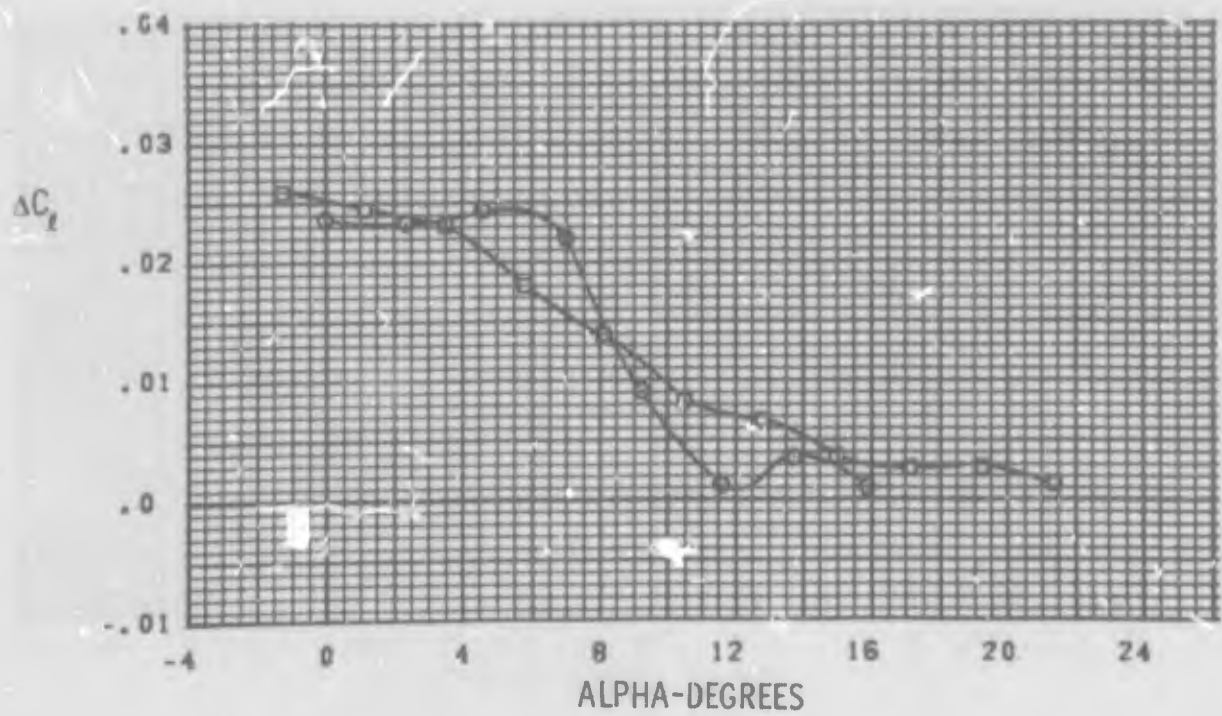
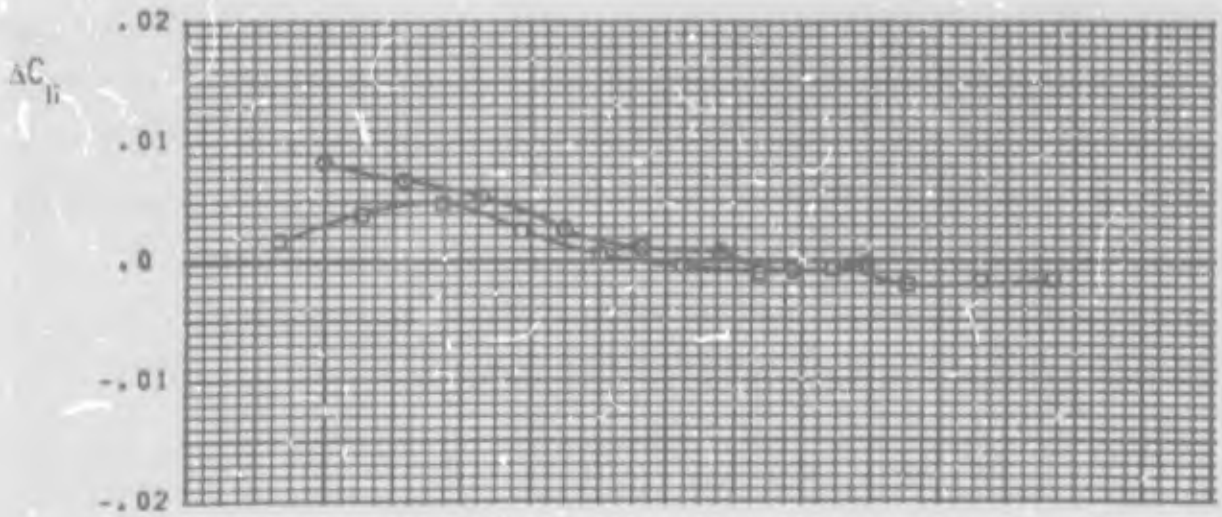
#### 4. VENTED SPOILER

A single geometric arrangement of vented spoiler was tested deflected normal to the upper surface for two symmetrical leading edge deflections. At transonic speeds, as illustrated in the data of Figure 82 for 0.8 Mach number, spoiler effectiveness drops rapidly at angles of attack near stall for the basic wing. The effect of symmetrical leading edge deflection was to yield more gradual losses with angle of attack starting at lower angles. The slightly improved effectiveness at high attitudes for the deflected leading edge was not evident at 0.9 Mach number. For the supersonic case, 1.2 Mach number, effectiveness is less effected by angle of attack, but the general level of effectiveness is much less than predicted by methods of the USAF DATCOM, Reference 12 (see Figure 83).

#### 5. DIFFERENTIAL HORIZONTAL TAIL

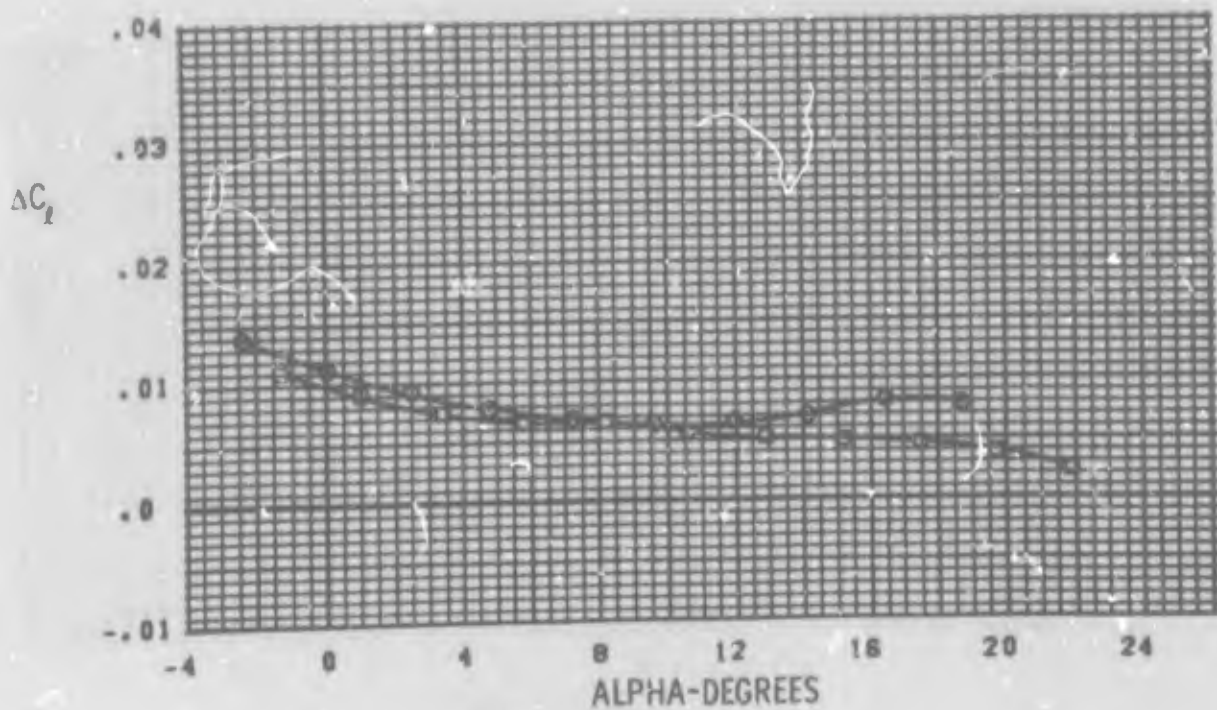
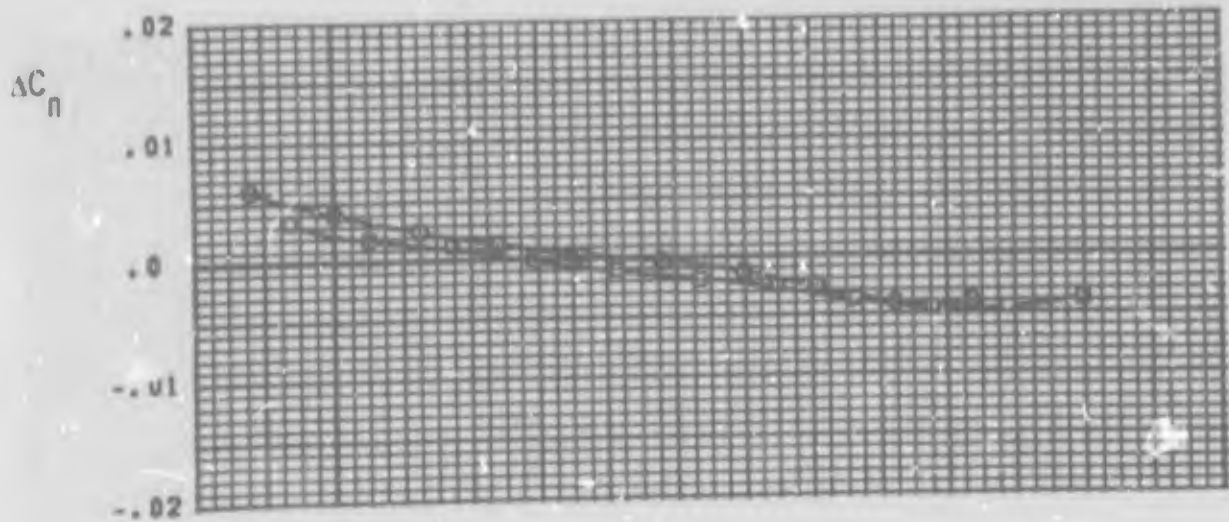
In view of the significant losses in aileron effectiveness due to horizontal tail interference, consideration was given to the use of the horizontal tail as a roll control device. Representative data for this configuration is presented in Figure 84. Note that angle of attack effects on differential horizontal tail roll effectiveness are quite small but the level of effectiveness is so low that the deflections required to produce the desired rolling moments by tail deflection alone could jeopardize the simultaneous use of this surface for longitudinal maneuvering and yield high drag penalties. Also at 1.2 Mach number high adverse yaw occurs at the high angles of attack, particularly in consideration to the rolling moment produced.

Although the horizontal tail is not well suited for primary roll control on a fixed wing configuration such as LEDE, moderate differential deflection shows promise as an auxiliary roll control. In particular, a relatively small differential deflection will cancel the negative rolling moment due to the tail interference of ailerons, by minimizing the asymmetric angle of attack distribution across the horizontal tail. Such an approximately uniform tail angle of attack distribution will allow maximum use of the horizontal tail for maneuvering. The differential tail deflection for the data of Figure 84 was selected on this basis. These measurements confirm that moderate differential deflection cancels aileron-horizontal tail interference to yield significantly improved roll control at the



| SYM | TEST                         | INCREMENT | L.E. (L/R) | SPOILER |
|-----|------------------------------|-----------|------------|---------|
| ○   | PWT 4T TC-043 PN 462 -PN 440 | K1        | 0/0        | RH -90  |
| □   | PWT 4T TC-043 PN 173 -PN 127 | K1        | 10/10      | RH -90  |

FIGURE 82a VENTED SPOILER EFFECTS  
M = 0.8



| SYM | TEST                         | INCREMENT | L.E. (L/R) | SPOILER |
|-----|------------------------------|-----------|------------|---------|
| ○   | PWT 4T TC-043 PN 463 -PN 269 | K1        | 0/0        | RH -90  |
| □   | PWT 4T TC-043 PN 174 -PN 129 | K1        | 10/10      | RH -90  |

FIGURE 82b VENTED SPOILER EFFECTS  
M = 1.2

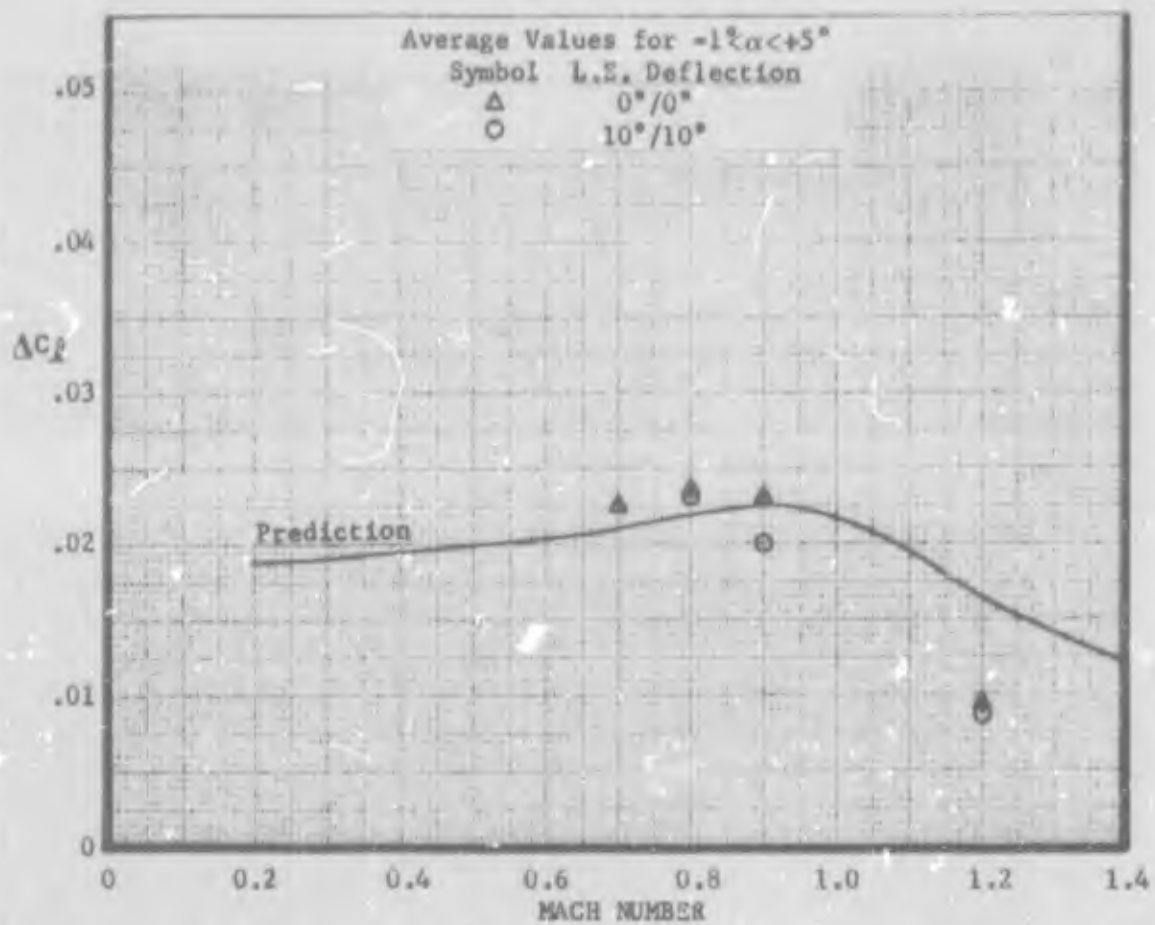
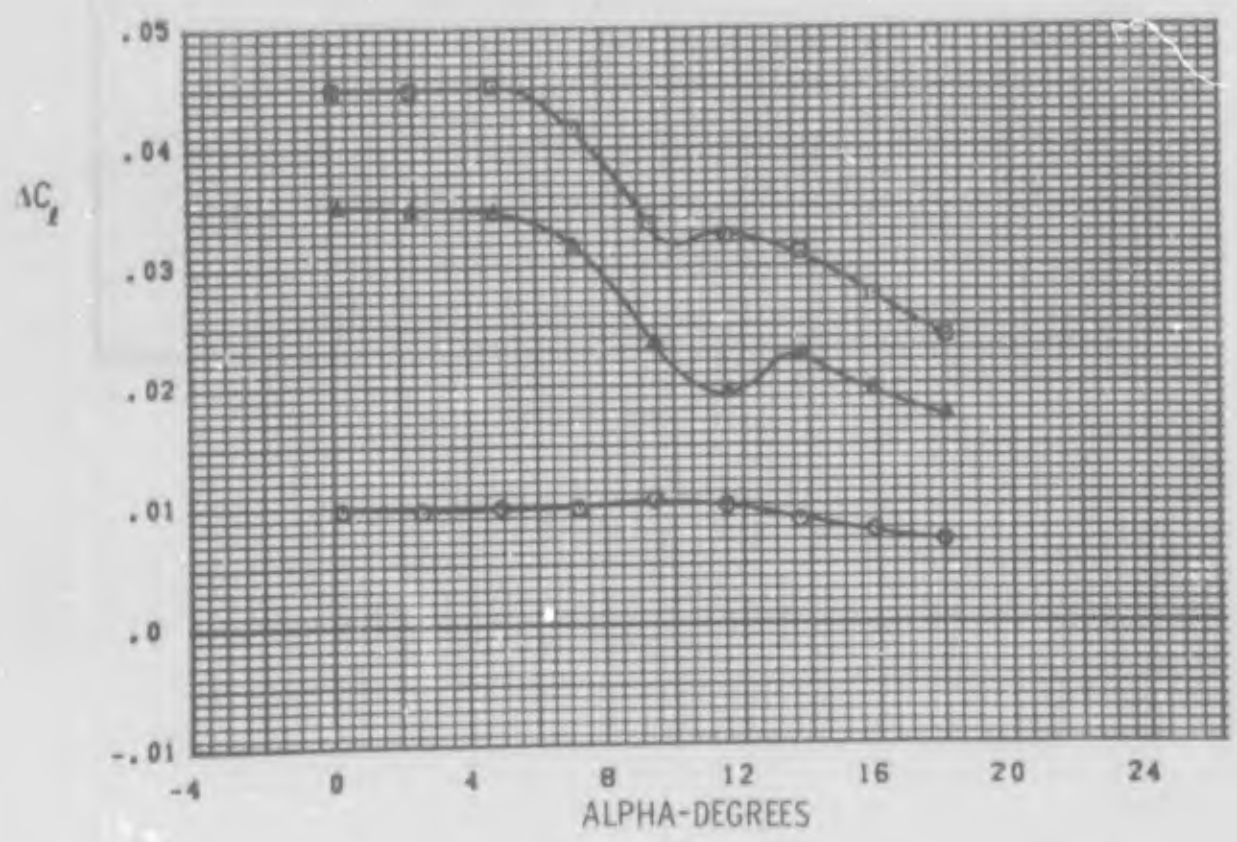
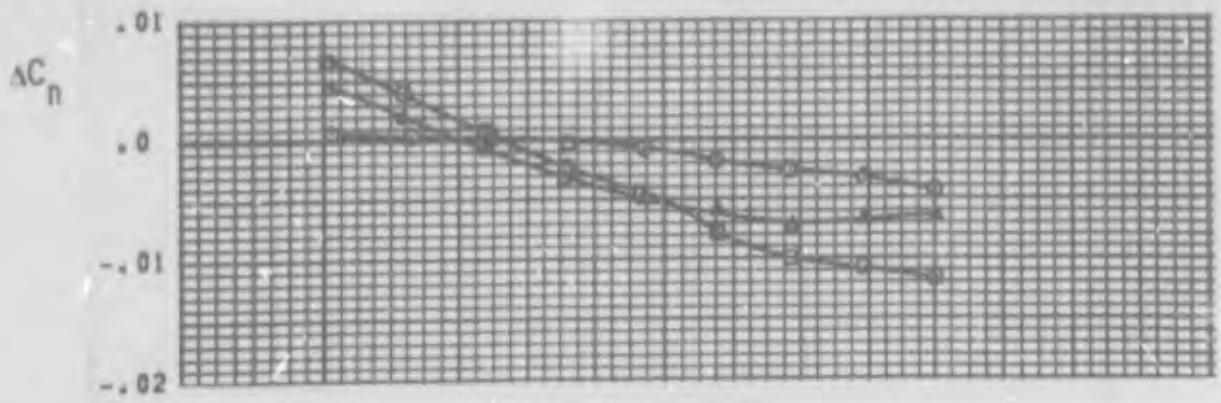


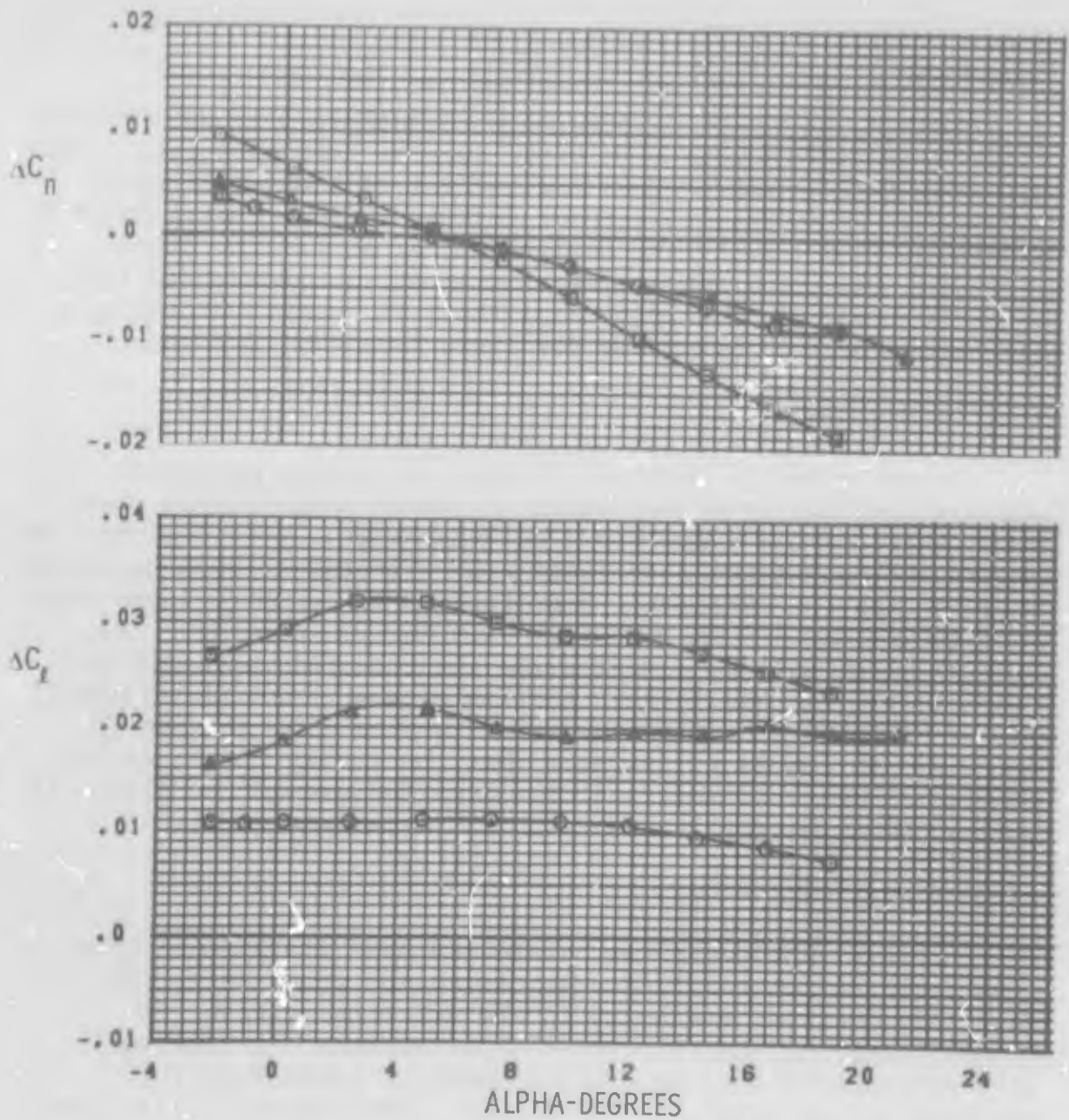
Figure 83 SPOILER ROLLING MOMENT





| SYM | TEST                         | INCREMENT | HORIZ. TAIL (L/R) | AILERON (L/R) |
|-----|------------------------------|-----------|-------------------|---------------|
| ○   | PWT 4T TC-043 PN 487 -PN 440 |           | 4/-4              | NONE          |
| □   | PWT 4T TC-043 PN 493 -PN 440 |           | 4/-4              | MID 20/-20    |
| △   | PWT 4T TC-043 PN 411 -PN 440 |           | 0/0               | MID 20/-20    |

FIGURE 84a DIFFERENTIAL HORIZONTAL TAIL EFFECTS ( CLEAN L.E. )  
M = 0.8



| SYM | TEST          | INCREMENT      | HORIZ. TAIL (L/R) | AILERON (L/R) |
|-----|---------------|----------------|-------------------|---------------|
| ○   | PWT 4T TC-043 | PN 489 -PN 269 | 4/-4              | NONE          |
| ◻   | PWT 4T TC-043 | PN 495 -PN 269 | 4/-4              | HID 20/-20    |
| ▲   | PWT 4T TC-043 | PN 414 -PN 269 | 0/0               | HID 20/-20    |

FIGURE 84b DIFFERENTIAL HORIZONTAL TAIL EFFECTS ( CLEAN L.E.)  
M = 1.2

expense of moderate increases in adverse yaw. Note that the incremental moments produced by asymmetric tail deflection, were not altered by presence of aileron deflection on the wing.

## 6. AUXILIARY DEVICES

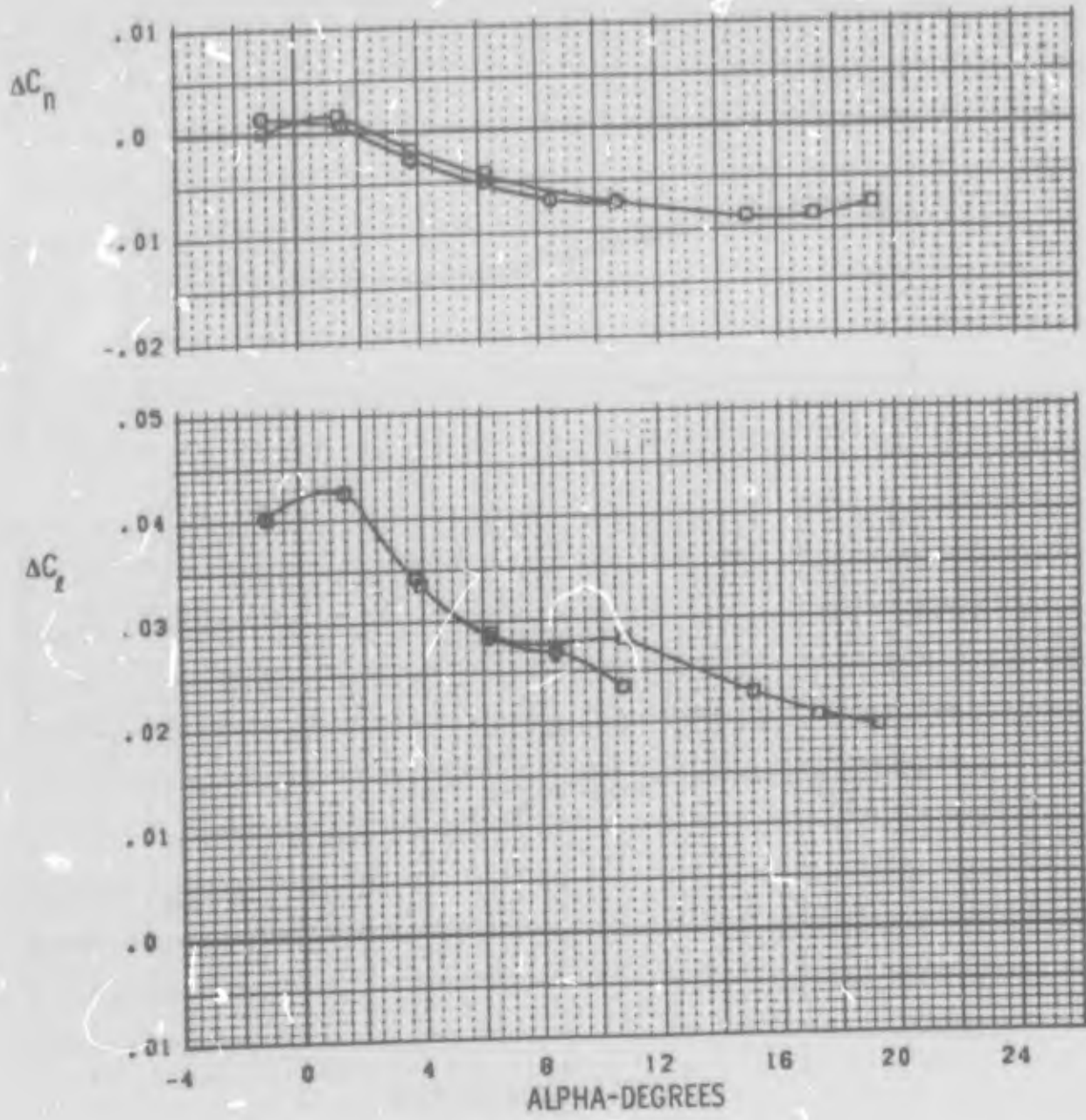
Several different devices were investigated in an auxiliary capacity in combination with basic aileron configurations. For the most part, these devices are typical of items that would be used in an attempt to correct deficient flow conditions of the basic wing. Since the design goal of minimizing shock strengths and delaying flow separation at transonic high lift conditions was apparently accomplished, it is not surprising that little effect was noted for these auxiliary devices.

### a. Vortex Generators

It was noted in Section VI that the vortex generator pattern provided some improvement in basic longitudinal characteristics of the symmetrical configuration. However, the flow separation phenomenon associated with ailerons at high attitudes is such that the attainable improvements in boundary layer characteristics result in little benefit to roll control. The largest gain would be expected for the extended span ailerons since they cover the largest portion of the wing and are significantly influenced by flow conditions at the tip. Figure 85 for 0.9 Mach number illustrates that the change due to vortex generators was a slight rolling moment improvement at angles of attack near wing stall.

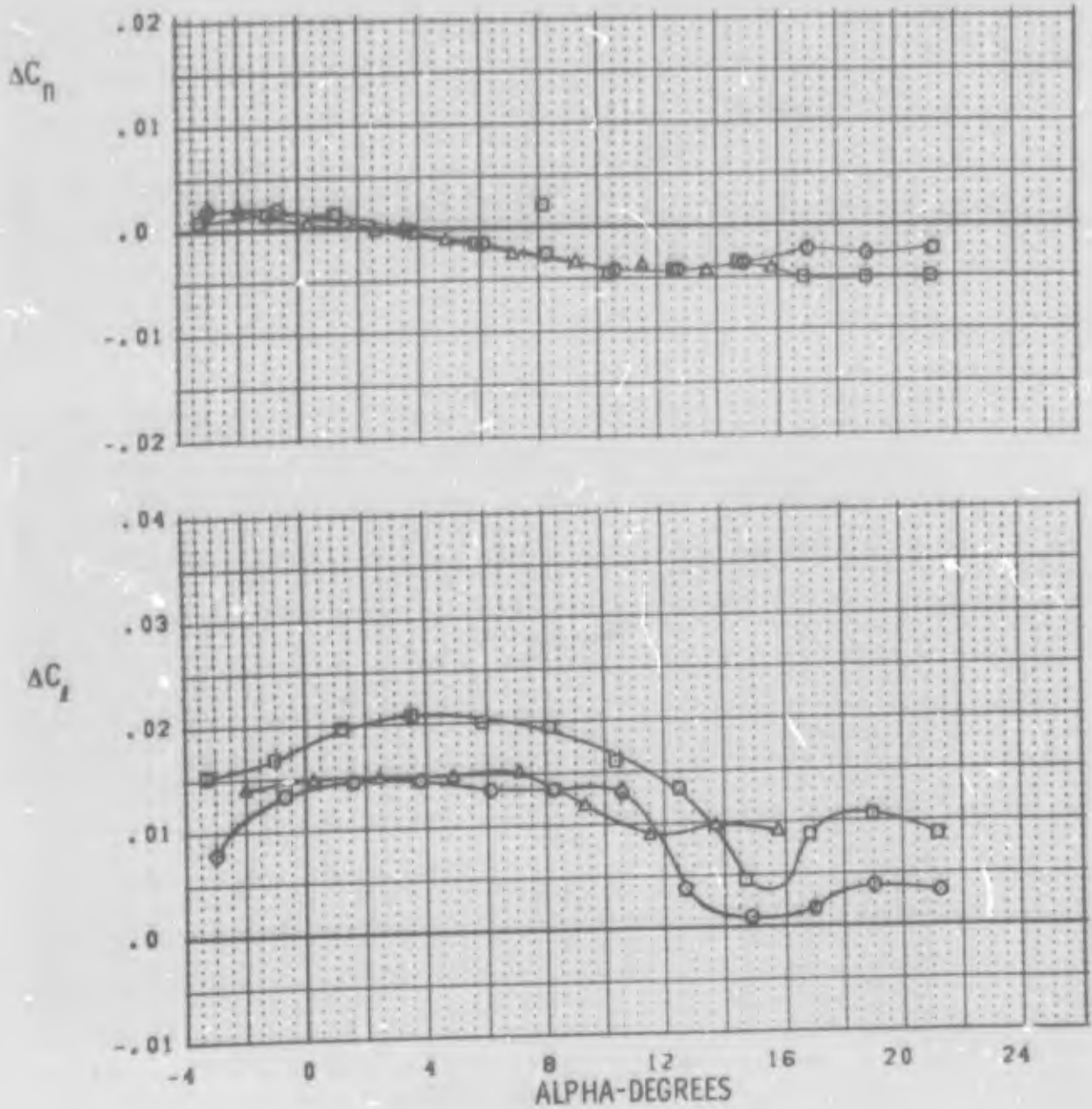
### b. Trailing Edge Droop

Trailing edge droop was considered upon the premise that elimination of up trailing edge deflection would result in favorable pressure gradients on the aft wing portion. A second reason for considering this arrangement is that small flap deflections are one obvious means of increasing lift coefficients at transonic conditions. The symmetric base-line configuration had ten degrees trailing edge deflection for all segments. For roll control, the two mid-aileron segments were differentially deflected ten degrees from the symmetrical droop position. The data in Figure 86 for 0.7 Mach number (typical of all transonic speeds investigated) indicate that the major



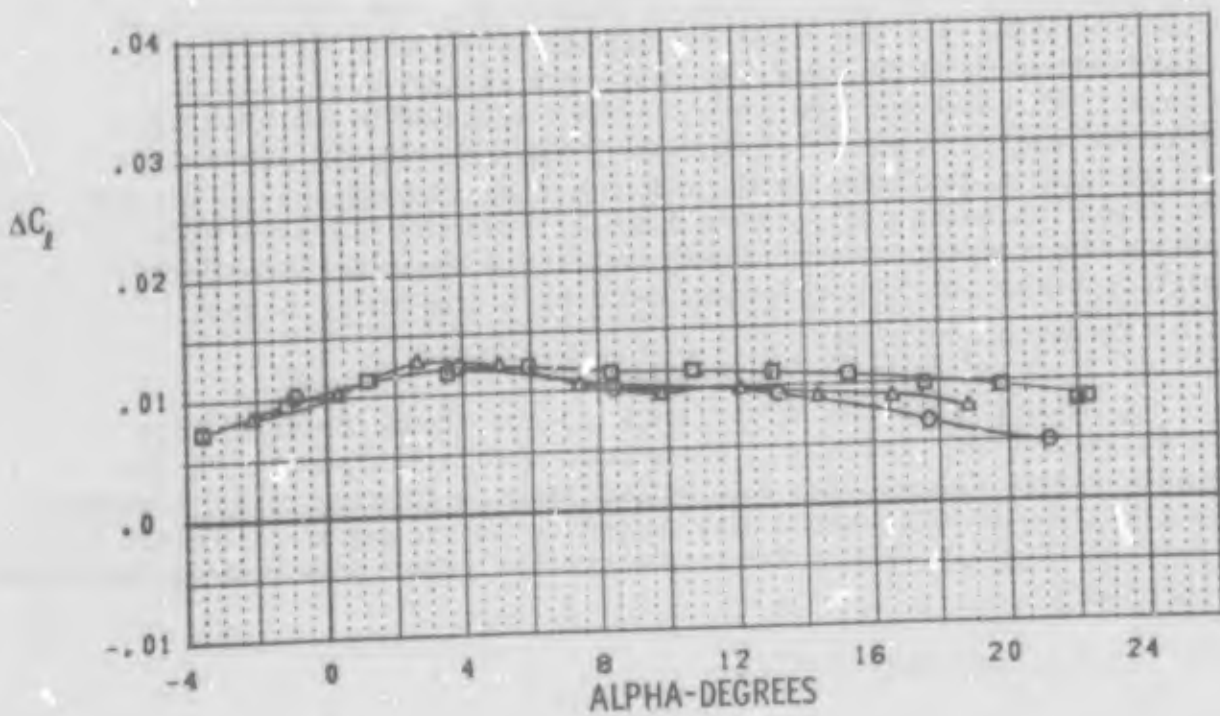
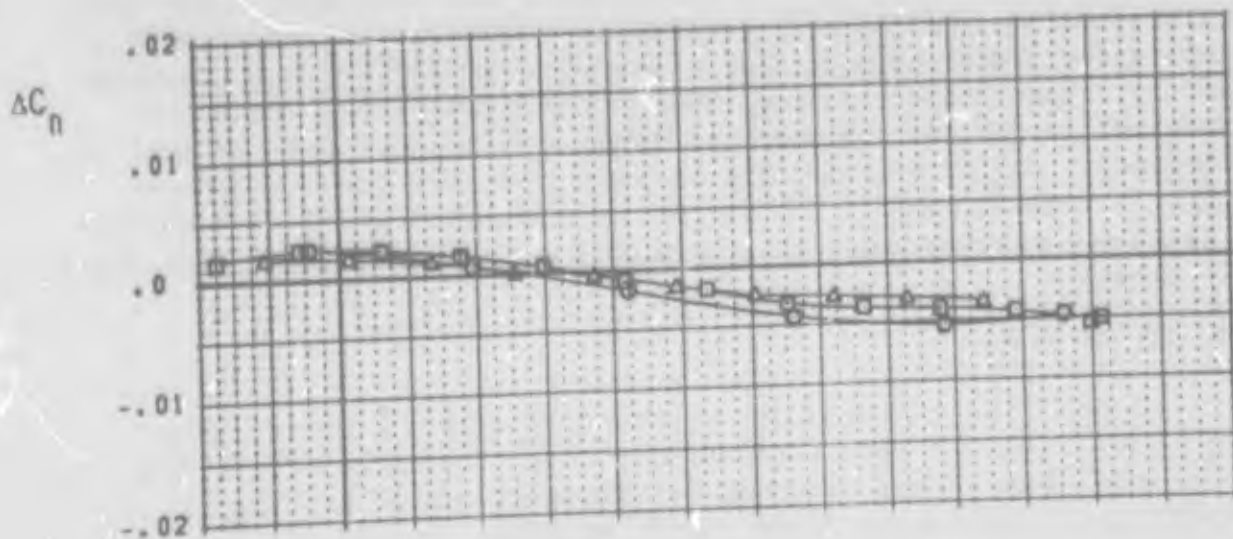
| SYM | TEST          | INCREMENT      | L.E. (L/R) | AILERON (L/R)  |
|-----|---------------|----------------|------------|----------------|
| ⊙   | PWT 4T TC-043 | PN 303 -PN 445 | K1 5/5     | 3 SEGM. 20/-20 |
| ⊠   | PWT 4T TC-043 | PN 227 -PN 241 | K1+VG 5/5  | 3 SEGM. 20/-20 |

FIGURE 85 VORTEX GENERATOR EFFECTS ON EXTENDED SPAN AILERONS  
M = 0.9



| SYM | TEST          | INCREMENT      | L.E. (L/R) | AILERON (L/R)      |
|-----|---------------|----------------|------------|--------------------|
| ○   | PWT 4T TC-043 | PN 202 -PN 128 | K1 10/10   | MID 20/0 +10 DROOP |
| □   | PWT 4T TC-043 | PN 135 -PN 128 | K1 10/10   | MID 10/-10         |
| △   | PWT 4T TC-043 | PN 468 -PN 438 | K1 0/0     | MID 20/0           |

FIGURE 86a TRAILING EDGE DROOP EFFECTS ON MID AILERONS  
M = 0.7



| SYM | TEST          | INCREMENT      | L.E. (L/R) | AILERON (L/R)      |
|-----|---------------|----------------|------------|--------------------|
| ⊙   | PWT 4T TC-043 | PN 201 -PN 129 | K1 10/10   | MID 20/0 +10 DROOP |
| ⊠   | PWT 4T TC-043 | PN 136 -PN 129 | K1 10/10   | MID 10/-10         |
| △   | PWT 4T TC-043 | PN 470 -PN 269 | K1 0/0     | MID 20/0           |

FIGURE 86b TRAILING EDGE DROOP EFFECTS ON MID AILERONS  
M = 1.2

effect is that down aileron deflections are less effective than equivalent up deflections (additional comments on this subject were given previously on the discussion of ailerons, subsection VII 2). Only minor rolling moment differences are directly attributable to the symmetrical droop of the most inboard and tip segments. It is interesting to note that for the supersonic case, 1.2 Mach number, all three arrangements yield essentially identical rolling and yawing moments up to moderately high angles of attack.

#### c. Split Flap

Split flaps were added to the underside of the aileron controls in an attempt to move the shock patterns aft on the wing and thus reduce the region of separated flow. The addition of this type blunt trailing edge for the controls did produce such a result. Note in Figure 87, the reductions in size and more aft position of separated regions for the configurations with the smaller (F2) and larger (F3) split flaps. The changes are particularly noticeable at about 8.4 degrees angle of attack. However, the net result was a loss in control effectiveness at low and moderate angles of attack as shown in Figure 88. This loss is presumed to have been caused by increased horizontal tail interference associated with a lower and thicker wing wake with the split flaps.

#### d. Kruger Glove Flap

A Kruger flap was positioned on the glove leading edge to determine what effect a change on the leading edge of the highly swept inboard portion might have on aileron effectiveness. No significant difference was noted up to an angle of attack of fourteen degrees where balance dynamics precluded testing to higher attitudes.

#### e. Canopy Fairing Effects

The basic LEDE configuration has a fairing on the glove upper surface aft of the canopy to obtain a smooth normal cross sectional area distribution and at the same time accentuate the expansion field on the inboard upper wing surface. A test was accomplished with this fairing removed and showed no change in effectiveness of the mid-span ailerons. Apparently a much larger modification in local geometry is required to produce a noticeable change in control effectiveness. A slight drag

MID-SPAN AILERONS  $10^{\circ}/-10^{\circ}$

$\alpha = 8.34^{\circ}$



$\alpha = 9.08^{\circ}$



AILERONS PLUS F2 SPLIT FLAP

$\alpha = 8.43^{\circ}$



$\alpha = 12.99^{\circ}$



AILERONS PLUS F3 SPLIT FLAP

$\alpha = 8.50^{\circ}$

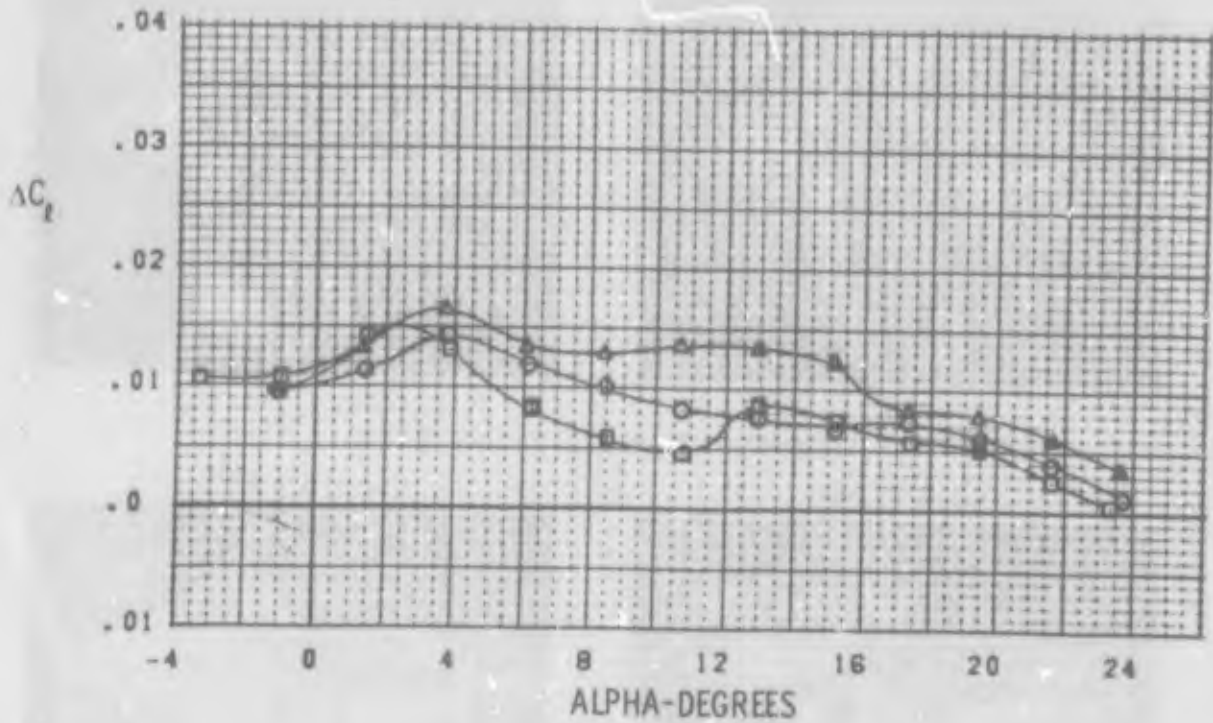
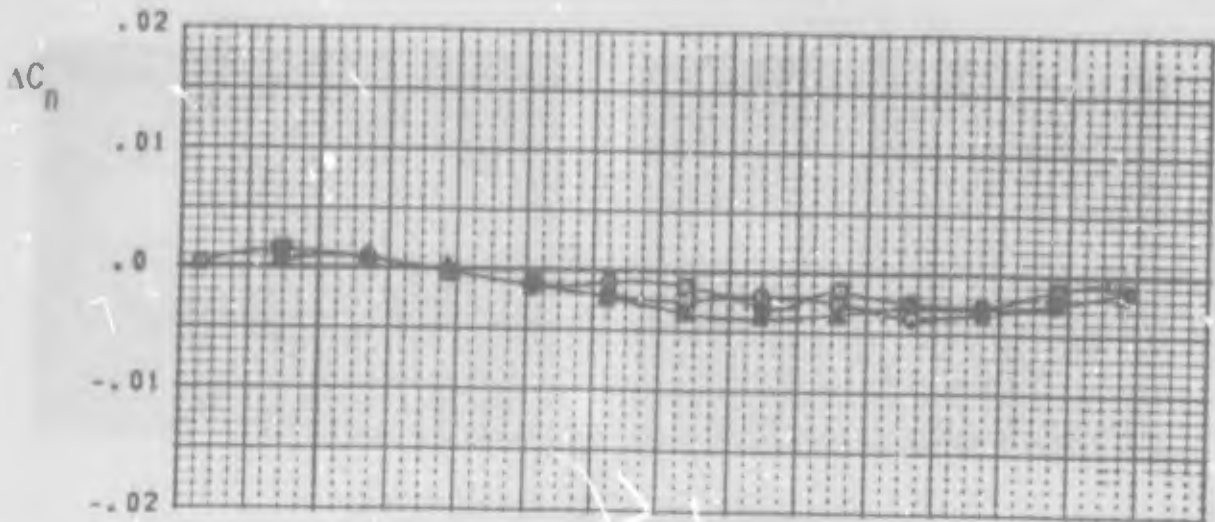


$\alpha = 13.03^{\circ}$



Figure 87 FLOW VISUALIZATION OF SPLIT FLAP EFFECTS  
K1 L.E. 10/10, MACH = 0.9





| SYM | TEST          | INCREMENT      | L.E. (L/R) | AILERON (L/R)  |
|-----|---------------|----------------|------------|----------------|
| ○   | PWT 4T TC-043 | PN 154 -PN 126 | K1 10/10   | MID +F2 10/-10 |
| □   | PWT 4T TC-043 | PN 161 -PN 126 | K1 10/10   | MID +F3 10/-10 |
| △   | PWT 4T TC-043 | PN 133 -PN 126 | K1 10/10   | MID 10/-10     |

FIGURE 88 SPLIT TRAILING EDGE FLAP EFFECTS ON MID AILERON  
M = 0.9

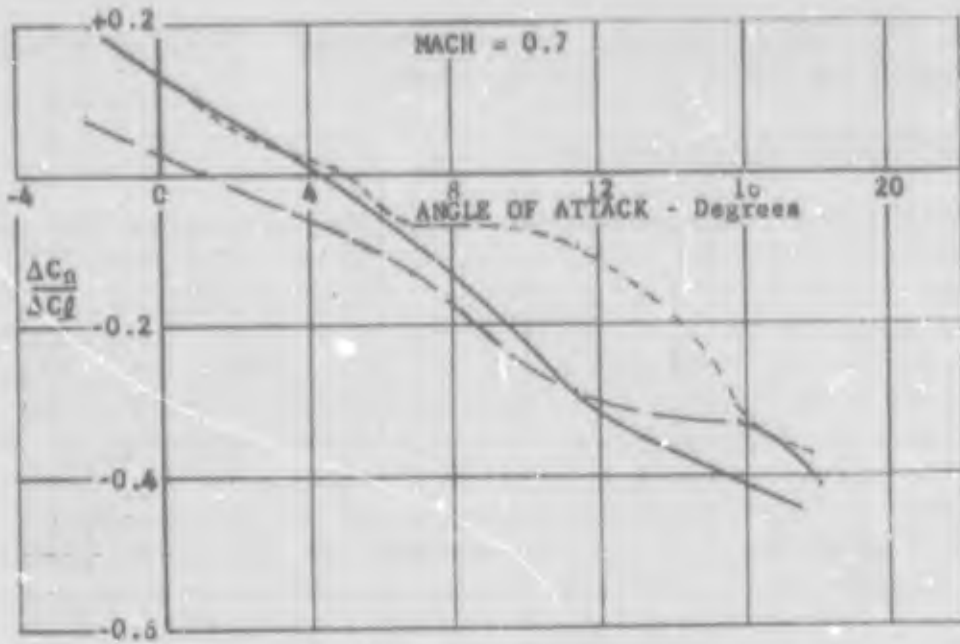
reduction was noted with the fairing removed. This is attributed to a decrease in local aft facing slopes.

## 7. ROLL CONTROL COORDINATION

Coordination characteristics have been evaluated for the lateral control devices found to be suitable. The metric chosen for comparison is the ratio of yawing moment to rolling moment produced by control deflection. This data is presented in Figure 89 for the outboard aileron alone and the mid-aileron alone and in combination with the best differential leading edge deflection, 10/0 degrees. Generally the mid-aileron location yields better coordination than the outboard aileron location considering all Mach numbers and angles of attack tested. (The mid-aileron position is also better than the outboard location from the standpoint of rolling moment at medium to high angles of attack). Use of differential leading edge deflection in combination with mid-ailerons materially reduces adverse yaw in the high range of angle of attack for Mach numbers of 0.7, 0.8, and 0.9 while increasing rolling moment at these conditions. The corresponding coordination obtainable at 1.2 Mach number is not of practical value since use of differential leading edge (in the sense desired for transonic conditions) results in prohibitively large losses in roll control power.

Coordination characteristics for the extended span aileron are given in Figure 90. Trends with angle of attack are identical to those for the outboard and mid-span ailerons. However the improvement for combined aileron and differential leading edge deflection is not as great as when the mid-aileron is used.

The final arrangement considered is mid-ailerons with differential horizontal tail (used to minimize rolling moment losses produced by the horizontal tail). This data is given in Figure 91 along with that for the mid-aileron alone.



L. E. Aileron  
 ——— 0/0 Mid Span  
 - - - -10/0 Mid Span  
 - · - 0/0 Outboard

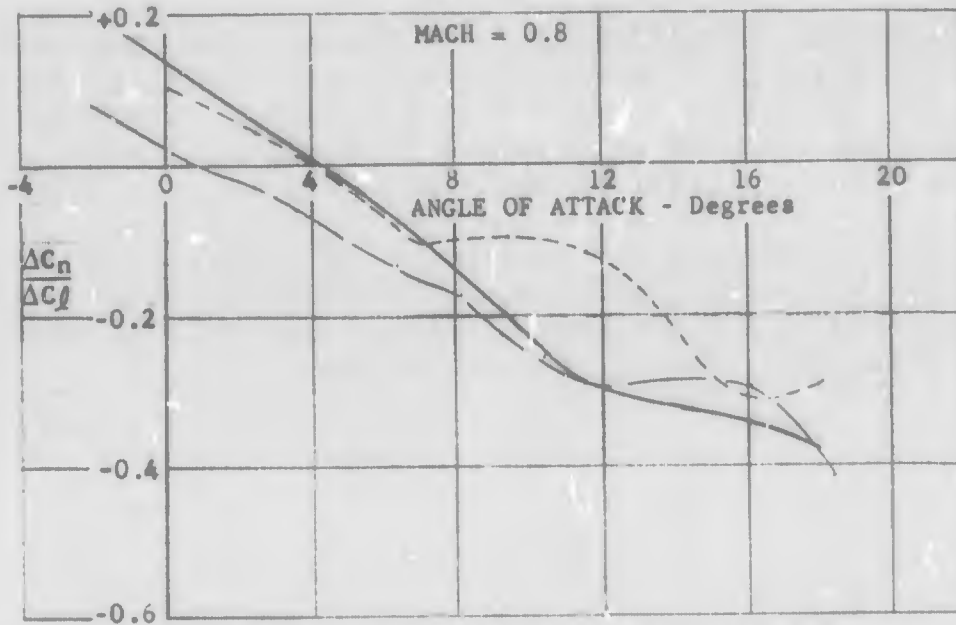
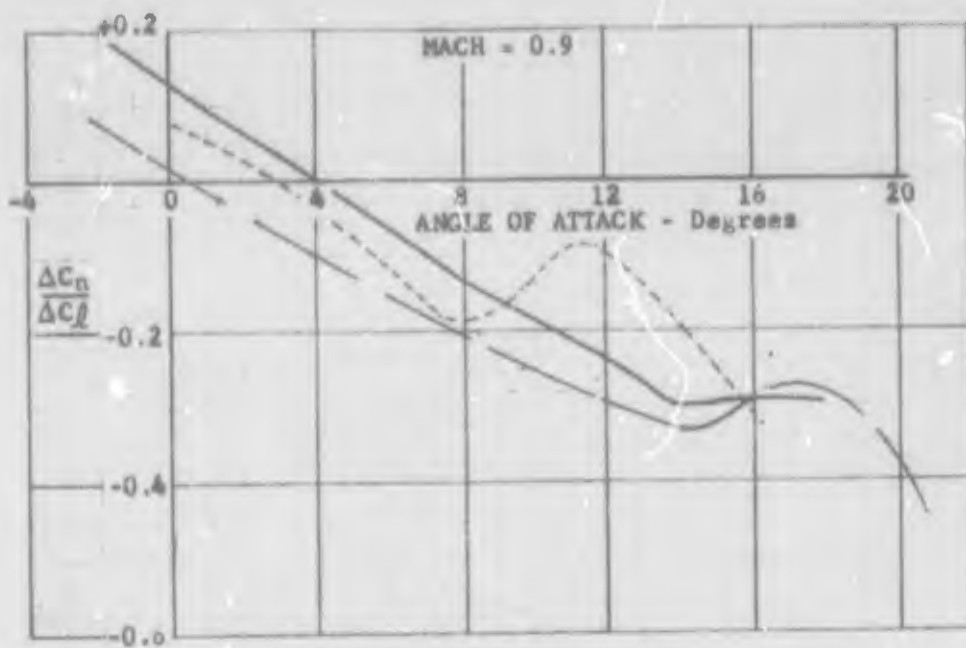


Figure 89 COORDINATION CHARACTERISTICS  
 MID SPAN AND OUTBOARD AILERONS



| L. E. | Aileron       |
|-------|---------------|
| —     | 0/0 Mid Span  |
| - - - | 10/0 Mid Span |
| - · - | 0/0 Outboard  |

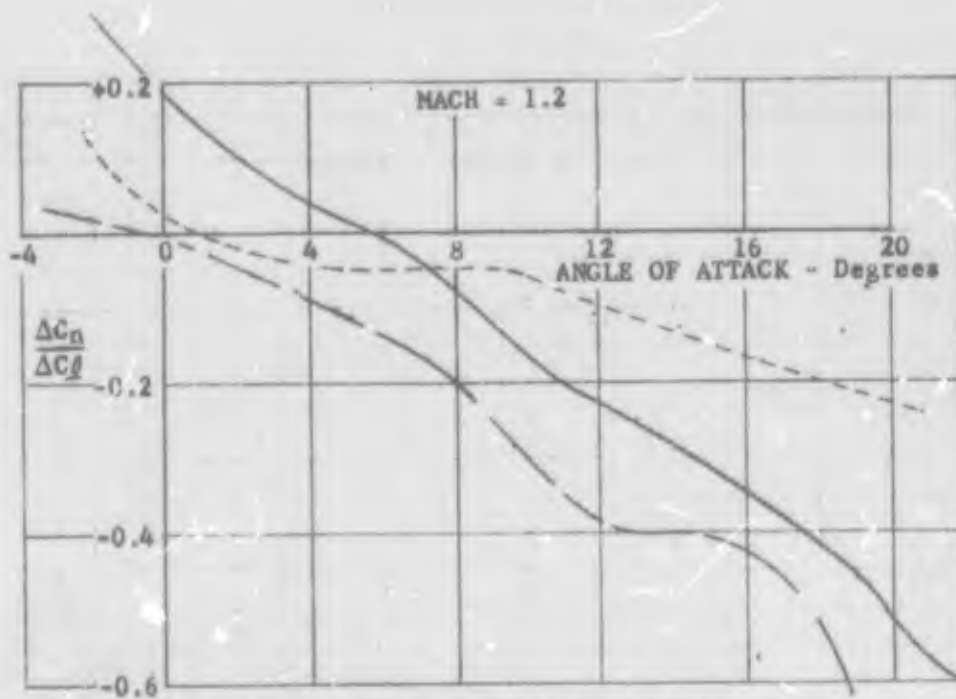
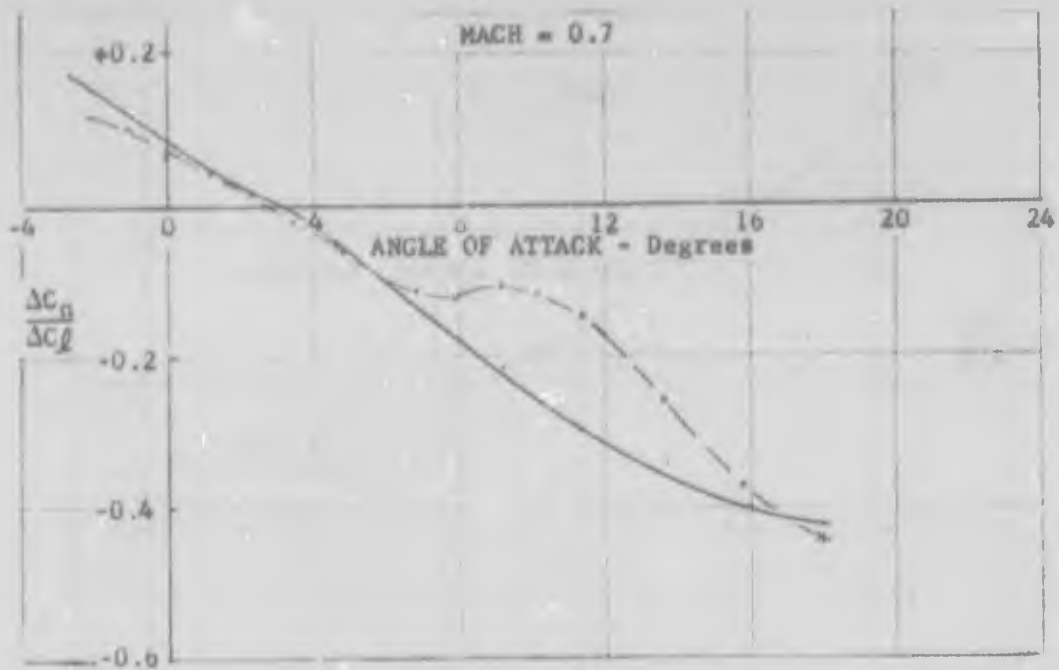


Figure 89 COORDINATION CHARACTERISTICS  
MID SPAN AND OUTBOARD AILERONS



L. E. Deflection  
 0/0  
 x 10/0

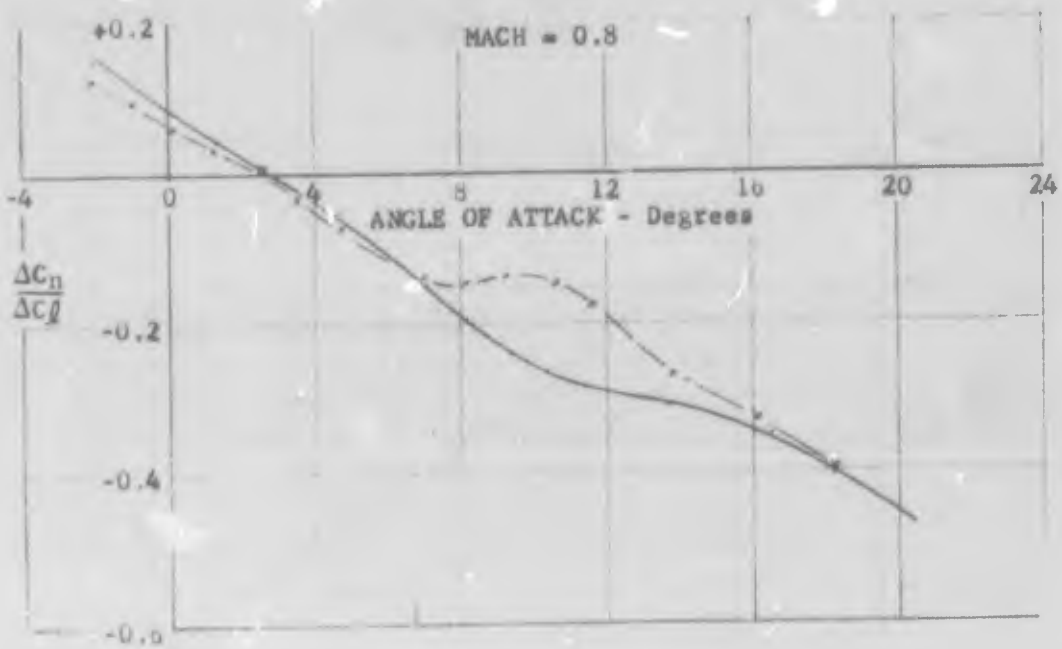
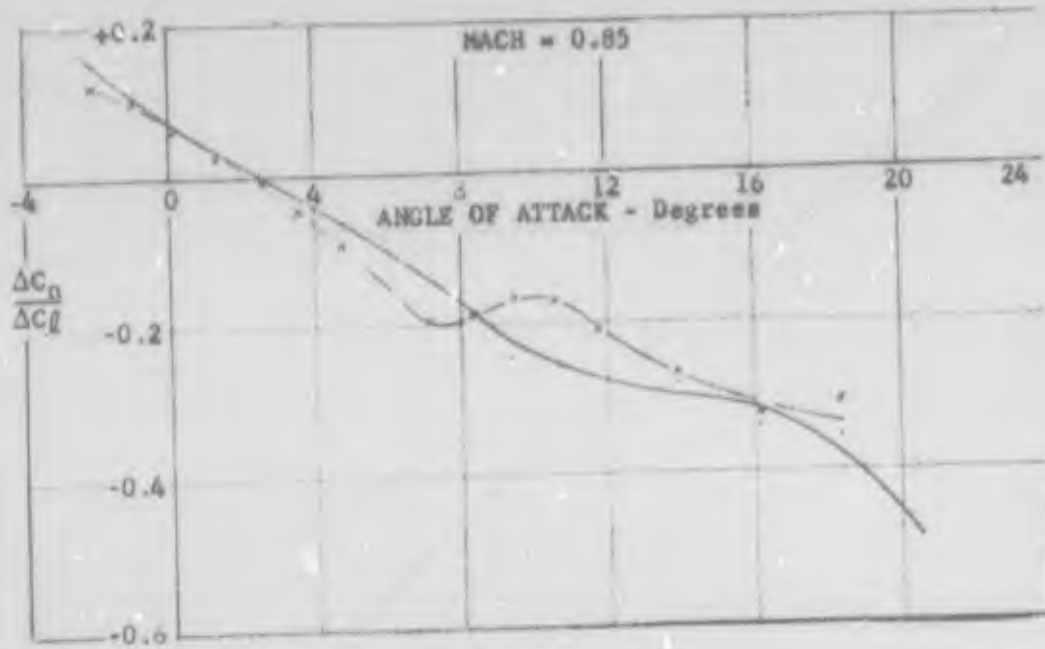


Figure 90 COORDINATION CHARACTERISTICS  
 EXTENDED SPAN AILERONS



L. E. Deflection

o/o

x 10/0

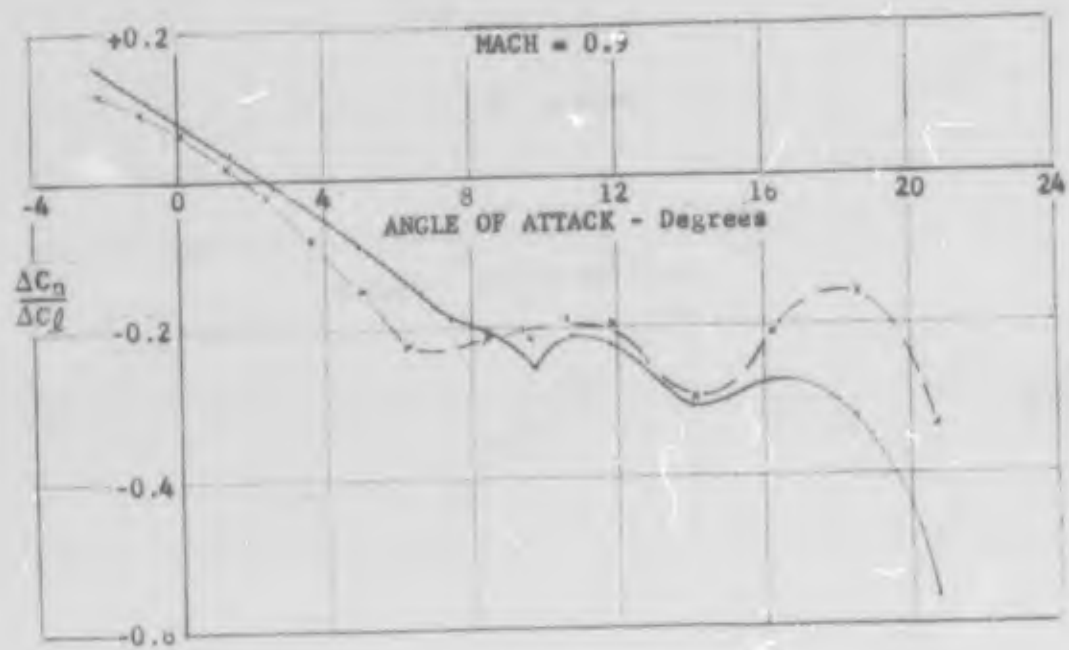


Figure 90 COORDINATION CHARACTERISTICS  
EXTENDED SPAN AILERONS

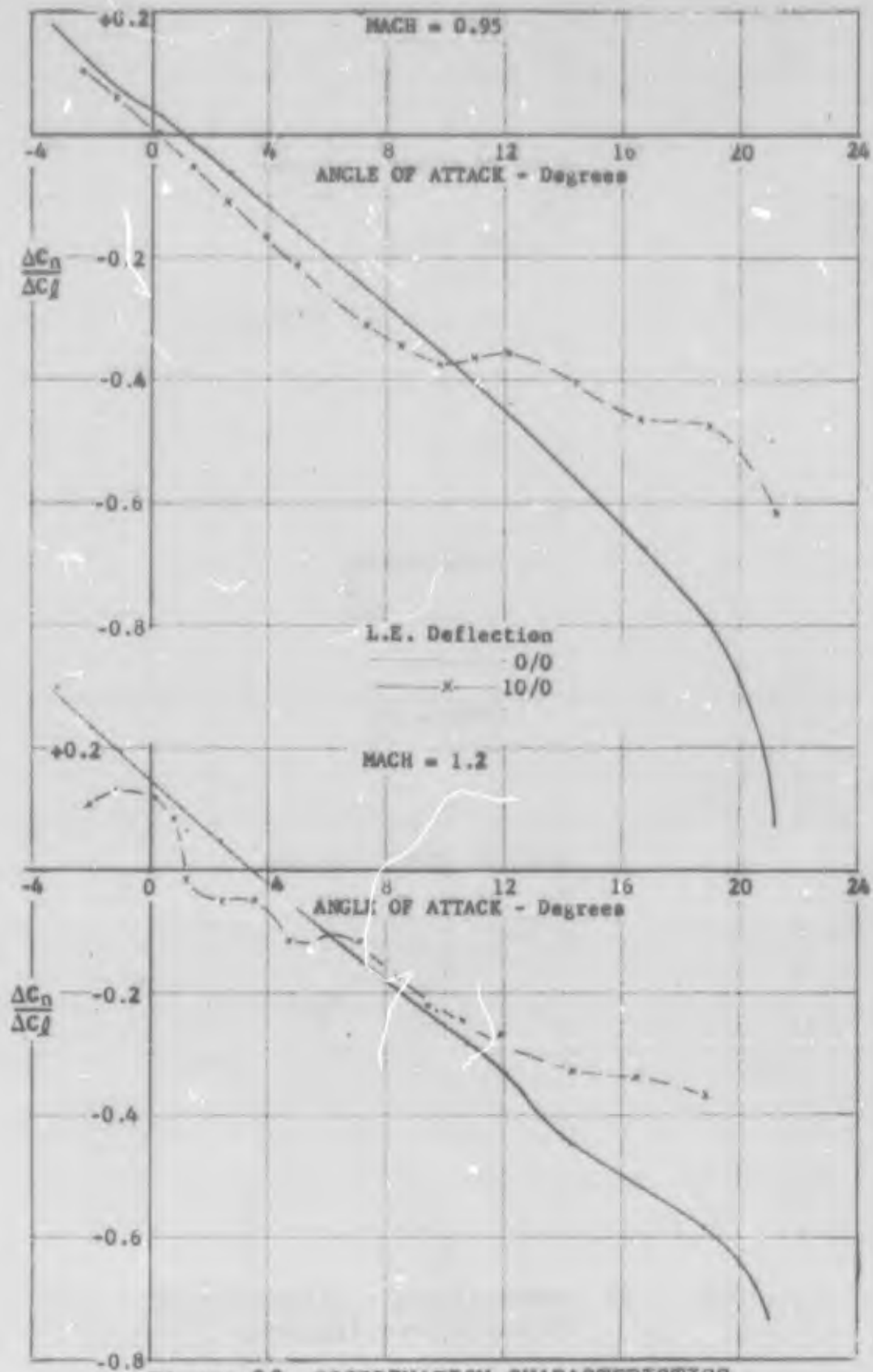
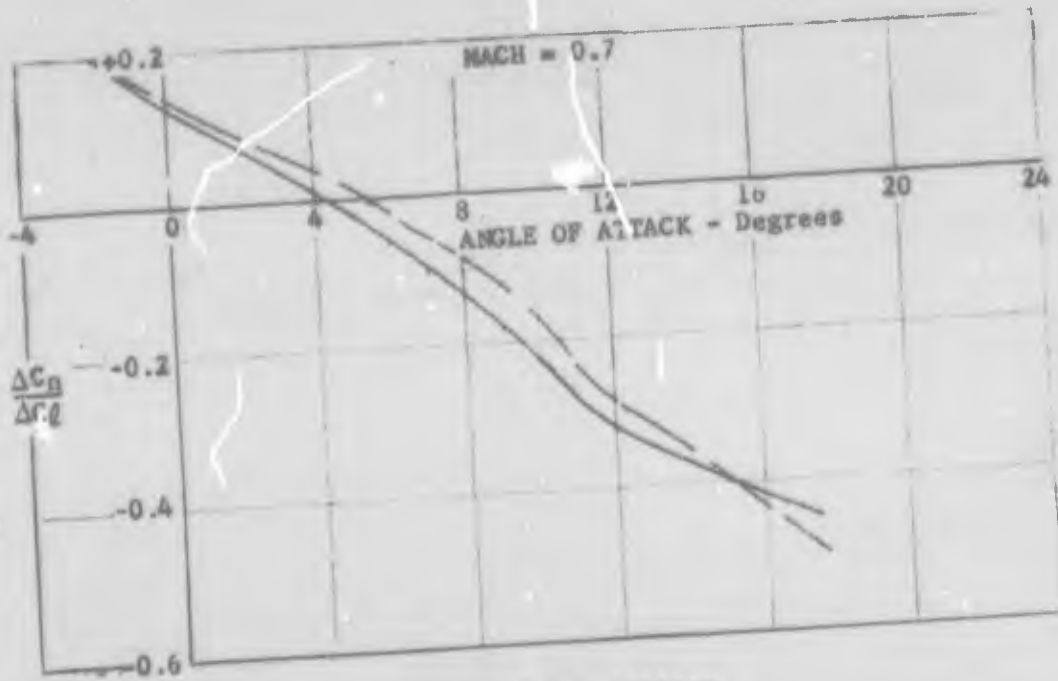


Figure 90 COORDINATION CHARACTERISTICS  
 EXTENDED SPAN AILERONS



| H.T.   | AILERON |
|--------|---------|
| — 0    | ±20     |
| - - 14 | ±20     |

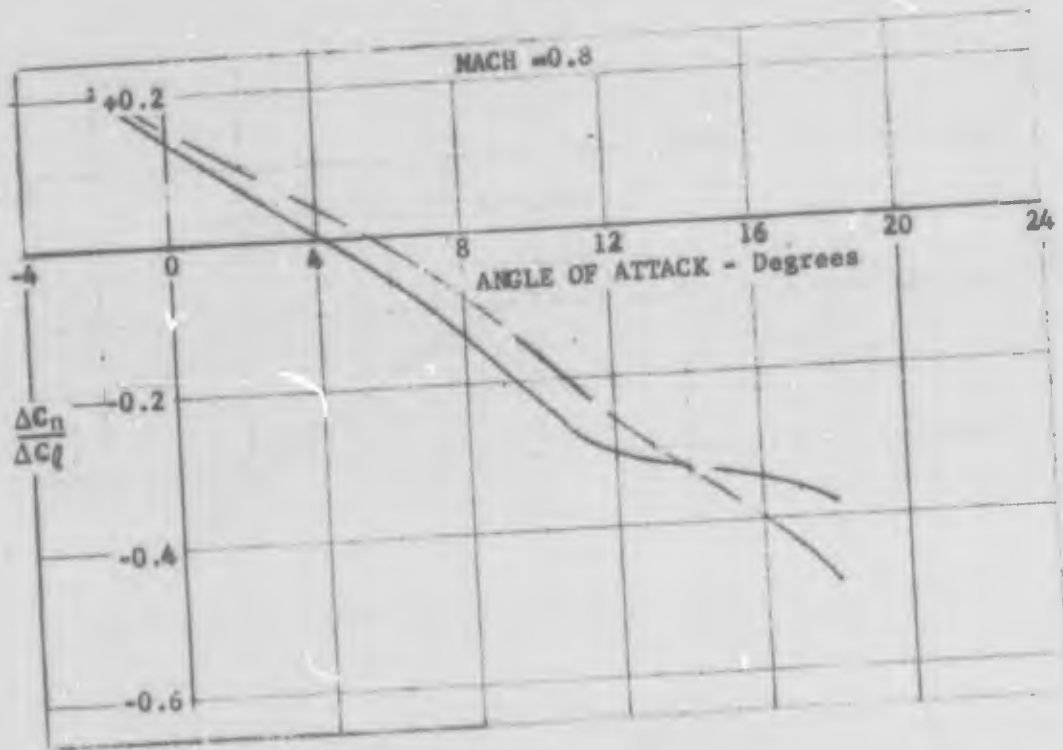


Figure 91 COORDINATION CHARACTERISTICS  
MID AILERON AND DIFFERENTIAL HORIZONTAL TAIL



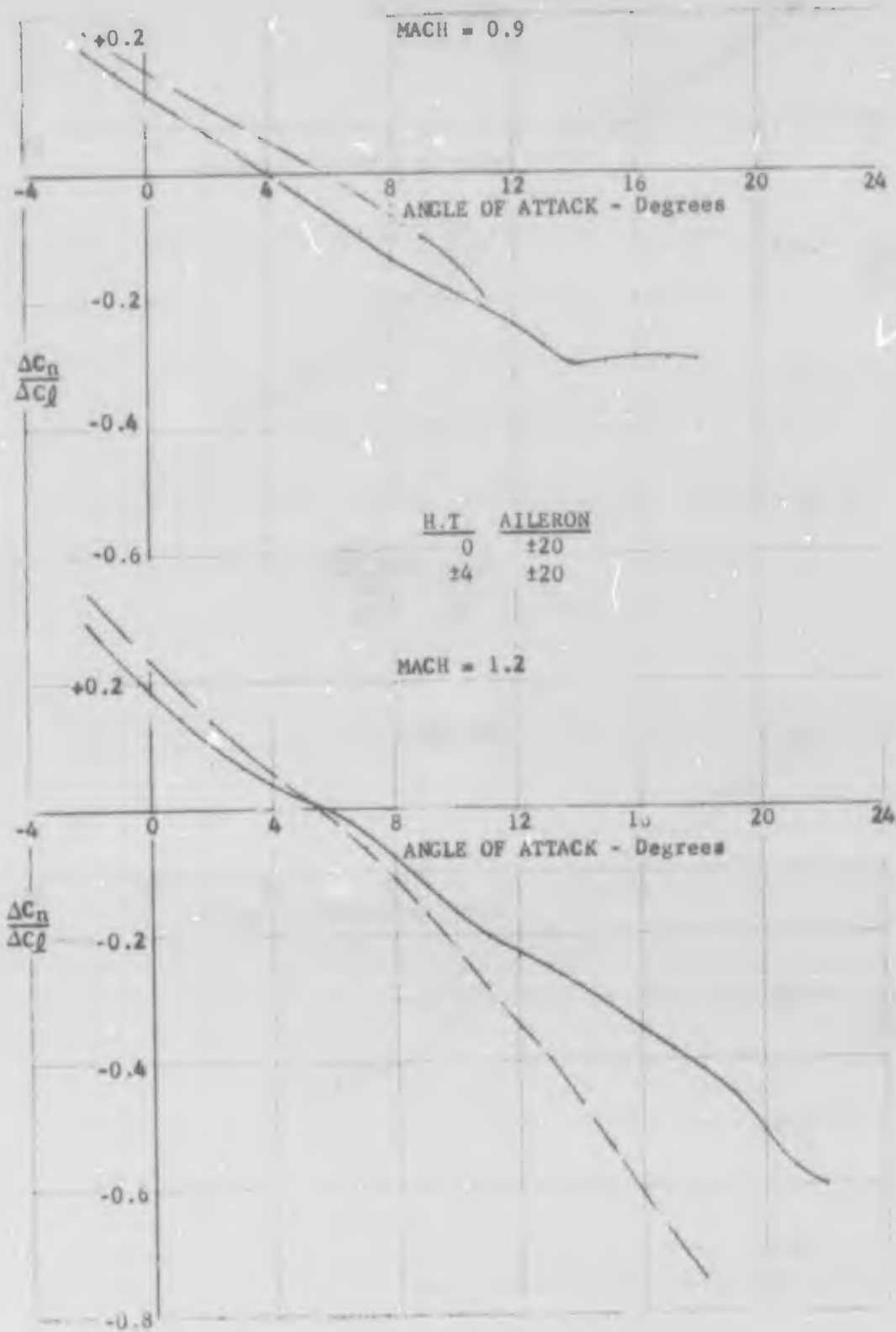


Figure 91 COORDINATION CHARACTERISTICS  
MID AILERON AND DIFFERENTIAL HORIZONTAL TAIL

The best use of differential horizontal tail is as an auxiliary device to improve roll power without seriously degrading coordination.

The results of a generalized lateral coordination study are given in Appendix II in order to relate the individual effects of inertia, stability, and control moments. This information is most clearly related to the control moments in the form of a yawing moment-rolling moment ratio versus angle of attack with  $\omega_r/\omega_l$  as a parameter, Figure 92. In this form, selected bounds on  $\omega_r/\omega_l$  limit the allowable combinations of  $\Delta C_n/\Delta C_l$  and angle of attack or conversely indicate conditions where specific compensation via the flight control system is required.

Coordination data for the mid aileron control has been repeated in Figure 93 using as a boundary  $\omega_r/\omega_l$  not less than 0.8. Consider the 0.7 Mach case, for nominal directional stability the limit is reached at nine degrees angle of attack with aileron alone while inclusion of differential leading edge increase this angle of attack to 10.4 degrees. For the desirable directional stability case, the values are 10.9 and 13.0 degrees. Similar trends are evident at 0.8 Mach number. Beyond these limit angles of attack some form of automatic coordination would be required to maintain  $\omega_r/\omega_l$  above 0.8. The vertical distance between the curve and the corresponding limit is a measure of the magnitude of coordination required. Thus, the use of differential leading edge deflection in combination with mid-aileron allows angle of attack to be increased about two degrees without excessive degradation in lateral coordination and significantly reduces the amount of artificial coordination required in the angle of attack range of ten to sixteen degrees.

It is important to keep the amount of artificial coordination to a relatively small level since scheduling as a function of angle of attack is not easily accomplished. Thus, reduction of adverse yaw at high angles of attack can result in excessive proverse or so called "favorable yaw" at low angles of attack and lead to undesirable pilot coupling tendencies.

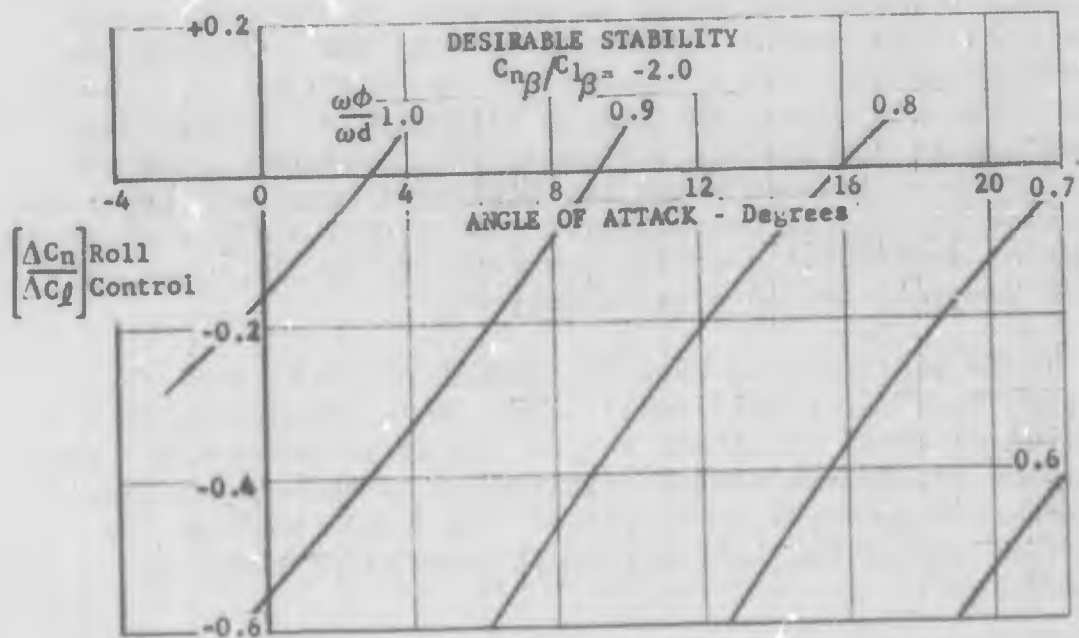
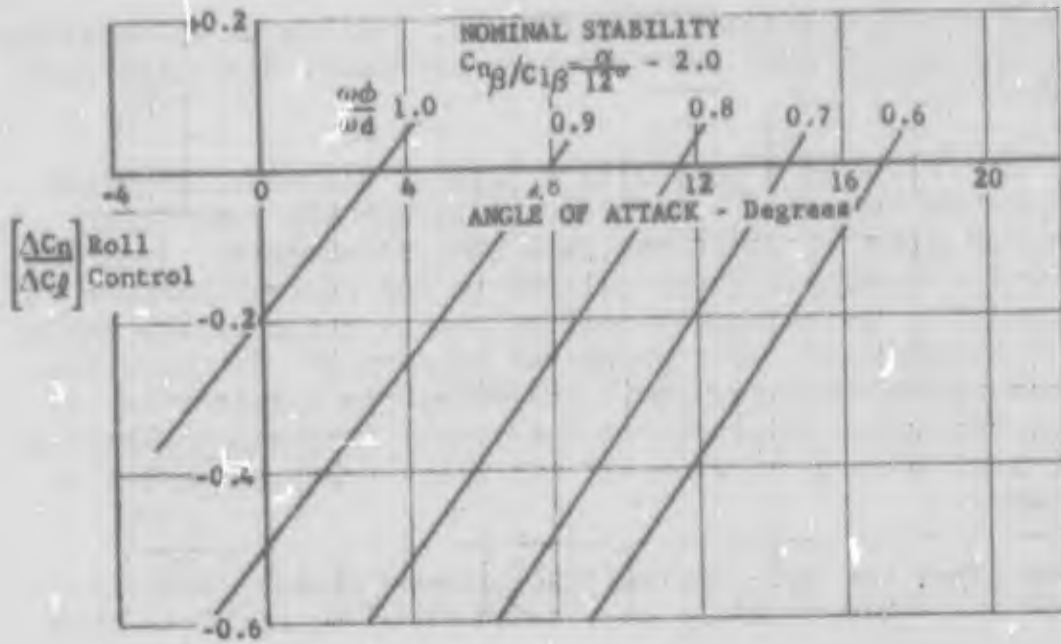


Figure 92 EFFECTS OF CONTROL MOMENT RATIO ON COORDINATION

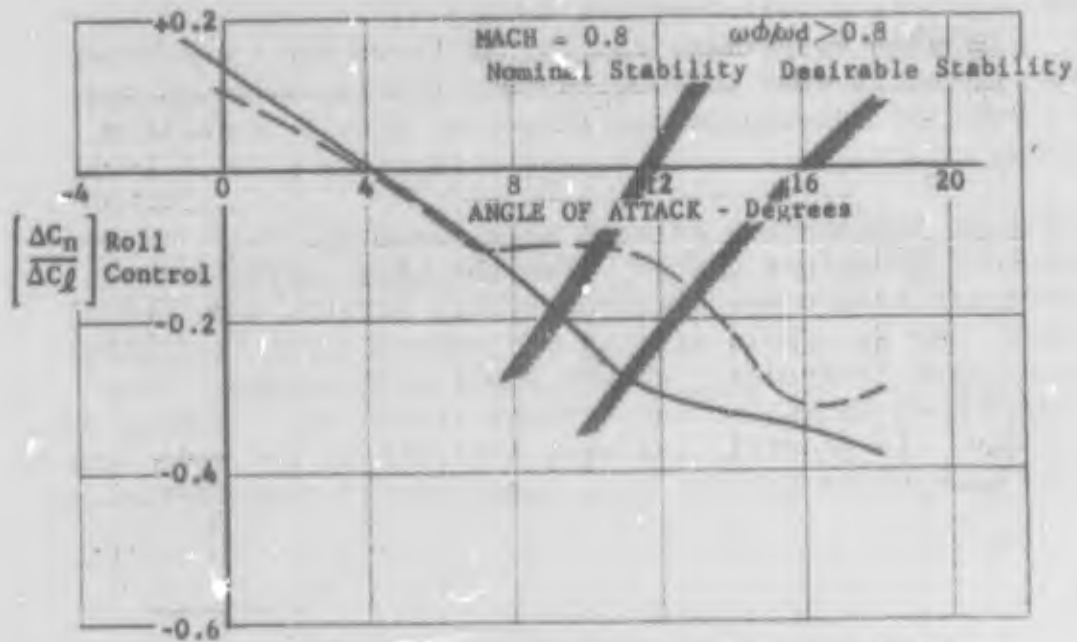
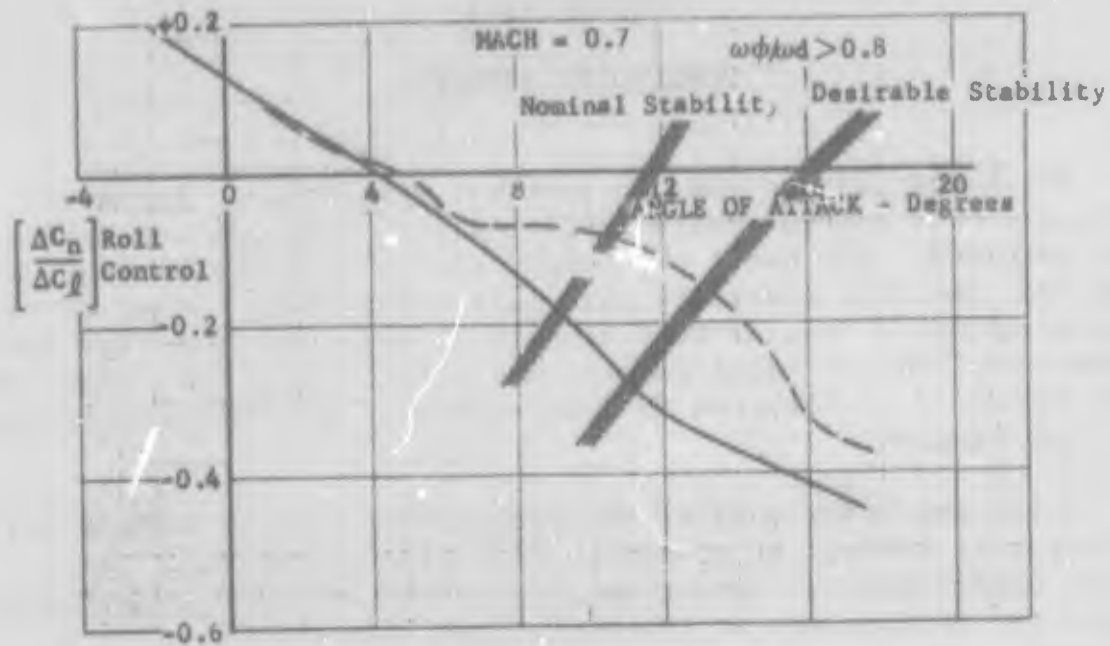


Figure 93 TYPICAL COORDINATION BOUNDARIES  
 MID AILERON

## SECTION VIII

### CONCLUDING REMARKS

The investigation was, in general, successful. Improved transonic roll control characteristics with wing-mounted devices were achieved. The basic philosophy was to generate an improved wing flow field at transonic high lift conditions. Since advanced fighter aircraft designs must achieve an improved wing flow field to meet performance requirements, the results from this study will have immediate application to development of roll control devices for such aircraft.

While the major goal of the program was to investigate and improve roll control at transonic high lift conditions, additional useful results having application to advanced aerodynamic design for performance at transonic high lift conditions were obtained. The experimental program also brought to light serious discrepancies in lift and drag data between results obtained in a small and a large transonic wind tunnel.

#### 1. ROLL CONTROL CONFIGURATIONS

Differential deflection of leading edge flaps does not provide sufficient roll power on moderately swept wing planforms to be used as primary control at transonic conditions. However, there is some indication that this arrangement may be suitable for supersonic conditions on highly swept wing planforms.

Several interesting effects were noted for the various aileron configurations tested. For the LEDE configuration, the strongest effect was horizontal tail interference which overpowers the favorable effects of reduced shock strengths at the inboard locations. Rather small differences in control power were noted for the various symmetrical leading edge deflections. In general, the best deflections for roll control are less than those for the best longitudinal characteristics.

For ailerons, the primary factor is the total camber for the wing section (leading edge deflection, basic section camber, and trailing edge deflection). Leading edge down deflection moved the shock forward and aggravated separation ahead of the down deflected aileron.

Linearity of aileron effectiveness with deflection was generally good up to the largest deflection tested, twenty degrees. It appears that larger maximum deflections, possibly thirty degrees, would be beneficial. Assessment of the relative effectiveness of trailing edge up versus down deflections revealed that the up deflections are more effective at transonic speeds and further that the variations in effectiveness with Mach number are mainly associated with the up deflections. Hence, it appears that further study and exploitation of flow phenomena associated with up deflected ailerons may lead to improved control effectiveness for transonic high lift conditions.

Use of moderate differential leading edge deflection in combination with ailerons affords significant improvement in transonic roll control at high angles of attack and in addition improves coordination characteristics at these conditions. However, the use of such an auxiliary leading edge device results in moderate losses at low angle of attack transonic conditions. This loss is so pronounced at supersonic speeds that if any differential leading edge deflection is employed, the phasing with aileron deflection should be reversed from that for transonic high angle of attack conditions.

Differential deflection of the horizontal tail on the LEDE fixed wing configuration was found to be suited for application as an auxiliary device. Use of such differential tail deflection in moderate amounts with the mid-span ailerons afforded improvement in control power, particularly at high angles of attack, without serious degradation in coordination.

Of the other auxiliary devices evaluated, only the vortex generators were helpful. However, for conditions similar to

those tested, improvements in roll control appear to be limited to a narrow angle of attack range corresponding to onset of flow separation on the mid-span and outboard portions of the wing.

Testing at the highest attainable Reynolds number, within the capability of current transonic wind tunnels, does not appear to be a crucial consideration for obtaining roll control data. For cases such as the LEDE study, where the maximum test angle of attack is limited by static or dynamic balance loads (more critical at the higher static pressures associated with higher Reynolds numbers), it now appears plausible to conduct most evaluations at a moderate Reynolds number that does not compromise maximum angle of attack. These data may then be used with a high confidence level to select the best configurations to be checked at the highest attainable Reynolds number.

## 2. SYMMETRICAL CONFIGURATIONS

Certain aspects of the investigation are particularly pleasing to an aerodynamicist. First and foremost is the fact that the empirically derived wing design worked so well. A significant body of data and some theoretical treatments existed for curved planforms, however, none of this background information fully covered a complete treatment of a planform of relatively high aspect ratio. While the overall integration of planform, airfoil section, twist and camber obviously are important and especially so at transonic speeds, the similarity of results for the basic airfoil and modified leading edge airfoil indicate that the curved leading edge is a powerful factor in the success of the design. A systematic investigation of curved-leading-edge planforms would appear to be a fruitful area of research to advance the state-of-the-art of transonic aerodynamic design.

With respect to the aerodynamic performance of high-lift devices at transonic speeds, the investigation adds to the growing body of data which indicates that the total added camber which can be used at transonic speeds will be more and more

limited as Mach number increases from about 0.7 towards 1.0. At low lift coefficients, trailing-edge flaps appear to be efficient additional-lift producers whereas at high lift coefficients leading-edge flaps appear to be most beneficial. Simultaneous use of leading-edge and trailing-edge flaps at low lift coefficients should probably be limited to relatively small deflections near 0.9 Mach number. The split flap may be a good transonic high-lift device because it does not induce as severe changes in upper surface flow characteristics as a plain flap.

The novel array of vortex generators used in the investigation gave some benefit in reducing the extent of shock-induced flow separation and should be investigated more extensively on conventional wing designs to fully assess its capability in that regard.

### 3. TEST TECHNIQUES

Transonic wind tunnel testing has always presented a major problem with respect to producing results that can be applied at aircraft flight conditions with confidence. The conflicting requirements for high Reynolds number and small model blockage produced a major dilemma. Many years ago guidelines were established for allowable model size with respect to blockage in terms of model cross-section area relative to wind tunnel test section area. In a similar fashion a scaling technique was established which was shown to be valid for aircraft with thin wings at low to moderate lift coefficients. Recent attention to transonic characteristics at high lift conditions has produced results which indicate that the old scaling method may not be valid. As a consequence, there has been a tendency to use larger models to increase the test Reynolds numbers. Often the models are much larger than allowable by the old blockage rules.

Results from the present tests show that very serious effects can occur if models that are too large are used. In particular,



the performance characteristics, i.e., lift and drag, can be seriously altered in an adverse sense. While these effects are not too serious for the present investigation which had the major goal of defining the characteristics of roll control devices, the impact of the degraded performance characteristics on an aircraft conceptual development program could be very serious. Due consideration must be given to this problem for future tests.

Measurements for identical configurations in PWT 4T and 16T had major discrepancies in the drag polars and notable differences in lift characteristics. Effects on the various moments were also noted, mainly at conditions having some flow separation. The measurements suggest that separation effects start at lower angles and progress more gradually in the smaller facility. However, the major interference effects were on lift and drag to the extent that transonic tests of the 22.5 inch span LEDE model in a four foot by four foot test section did not yield accurate baseline longitudinal characteristics at transonic conditions.

Flow visualization, by use of a titanium oxide and oil mixture, proved to be a valuable aid in selecting and analyzing the various roll control configurations. A mixture was found which provided good visualization for about fifteen minutes testing at temperatures up to 140-145 degrees Fahrenheit. Although good detail was evident in the 16 mm films, the attainable black and white prints of single frames were considerably degraded. Overall, the results with black and white film were only slightly better than those with color film. In future tests, a larger camera should be used to obtain better resolution and still retain the advantages which accrue from motion pictures, i.e., observation of dynamic phenomena.

## REFERENCES

1. Kaftan, G., Model and Test Information Report Research Force Model with Wing-Mounted Roll Control Devices (L.E.D.E.) for Transonic High Lift Conditions, General Dynamics, Fort Worth Division, FZT-152, May 1969, Addendum I, August 1969.
2. Rogers, E. W. E., and I. M. Hall, "An Introduction to the Flow About Plane Swept-Back Wings at Transonic Speeds", Journal of the Royal Aeronautical Society, Vol. 64, No. 596, August 1960, pp. 449-464.
3. Pearcey, H. H., "Shock-Induced Separation and its Prevention by Design and Boundary Layer Control", in Boundary Layer and Flow Control (Edited by G. V. Lachmann), Vol. 2, Pergamon Press, New York, 1961, pp. 1251-1254.
4. Benepe, D. B., Compilation of Aircraft Buffet Characteristics, General Dynamics, Fort Worth Division, Aeroanalysis Internal Memorandum No. 251, 7 November 1969.
5. Benepe, D. B. et al., Aerodynamic Characteristics of Non-Straight-Taper Wings, Air Force Flight Dynamics Laboratory Report AFFDL-TR-66-73, October 1966.
6. Bagley, J. A. and J. A. Beasley, The Shapes and Lift-Dependent Drags of Some Sweptback Wings Designed for  $M_0=1.2$ , Royal Aircraft Establishment (Farnborough) Report No. Aero 2620, June 1959.
7. Lock, R. C., "The Aerodynamic Design of Swept-Winged Aircraft at Transonic and Supersonic Speeds", Journal of the Royal Aeronautical Society, Volume 67 No. (June 1963) pp. 325-
8. Lock, R. C. and Bridgewater, "Theory of Aerodynamic Design for Swept Winged Aircraft at Transonic and Supersonic Speeds", Progress in Aeronautical Sciences, Volume 8 (Edited by D. Kücheman), Pergamon Press, New York, 1967, pp. 139-228.
9. Graham, W. J., The Pressure Drag Due to Blunt Leading Edges on Two-Dimensional Airfoils at Transonic and Low Supersonic Speeds, Aeronautical Research Council (Gt. Britain) Report R & M 3465, 1965.

10. Wilby, P. G., The Pressure Drag of an Airfoil with Six Different Round Leading Edges, at Transonic and Supersonic Speeds, Aeronautical Research Council (Gt. Britain) Current Paper No. 921, 1967.
11. Thompson, N. and P. G. Wilby, Leading-Edge Supersonic Velocity Distribution on an Airfoil in a Sonic Stream, Paper Presented to the AGARD Specialists' Meeting on Transonic Aerodynamics, Paris, 18-20 September, 1968.
12. Hoak, D. E., USAF Stability and Control Datcom, Flight Control Division AFFDL, Revised 1968.
13. Thompson, Robert F., and Robert T. Taylor, Effects of a Wing Leading-Edge Flap and Chord-Extension on the High Subsonic Control Characteristics of an Aileron Located at Two Spanwise Positions, NACA RM L55B18a, 1955.
14. Sadoff, Melvin, Fredrick H. Matteson, and Rudolph D. Van Dyke, Jr., The Effects of Blunt-Trailing-Edge Modifications on the High-Speed Stability and Control Characteristics of a Swept-Wing Fighter Airplane, NACA RM A54C31, 1954.
15. Turner, Thomas R., Vernard E. Lockwood, and Raymond D. Vogler, Aerodynamic Characteristics at Subsonic and Transonic Speeds of a 42.7° Swept Back Wing Model Having an Aileron with Finite Trailing-Edge Thickness, NACA RM L8K02, 1949.
16. Pearcey, H. H., IBID pp. 1277-1314.
17. Powers, W. E., Application of Vortex Generators for Boundary Layer Control Through a Shock, United Aircraft Corporation Research Department Report R-95477-6, 1952.
18. Arabian, D. D., Investigation at Transonic Speeds of Loading Over a 30° Swept Back Wing of Aspect Ratio 3, Taper Ratio 0.2 and NACA 65A004 Airfoil Section Mounted on a Body, NACA RM L57G07a, 1957.
19. Haines, A. B., Recent Research Into Some Aerodynamic Design Problems of Subsonic Transport Aircraft, Paper 68-10, B-801 Presented at the Sixth International Congress of the Aeronautical Sciences, Munich 9-13 September, 1968.

20. Luoma, A. A., R. J. Re, and D. L. Loving, Subsonic Longitudinal Aerodynamic Measurements on a Transport Model in Two Slotted Tunnels Differing in Size, NASA TMX-1660, October 1968.
21. Jacocks, J. L., Unpublished AEDC Report
22. Benepe, D. B., Sr., Analysis of Flight-Test and Wind-Tunnel Buffet Intensity Data, General Dynamics, Fort Worth Division, Engineering Research Report, ERR-FW-886, 13 August 1969.
23. Lindsey, Walter F., and Emma Jean Landrum, Compilation of Information on the Transonic Attachment of Flows at the Leading Edges of Airfoils, NACA TN-4204, 1958.
24. Frost, R. C., Editor, GD/FW Aerospace Handbook, General Dynamics, Fort Worth Division Report FZA-381, November 1962.
25. Wenham, R. J., Computer Program ATAC - Air Combat Model, General Dynamics, Fort Worth Division Report FZM-5259, 1969, Confidential.
26. Woodcock, R. J. and D. E. Drake, Estimation of Flying Qualities of Piloted Airplanes, AFFDL TR 65-218, 1966.
27. Creer, Brent Y., et al., A Pilot Study of Lateral Control Requirements for Fighter-Type Aircraft, NASA Memo 1-29-59A, 1959.
28. Williams, Walter C., and William H. Phillips, Some Recent Research on the Handling Qualities of Airplanes, NACA RM H55L29a, 1956.
29. Chawla, J. P., Empirical Formulae for Radii of Gyration of Aircraft, Paper presented at the Eleventh National Conference of the Society of Aeronautical Weight Engineers, Buffalo, New York, 5-8 May 1952.

Unclassified

Security Classification

| DOCUMENT CONTROL DATA - R & D  |  |  |
|--|--|--|
| <i>(Security classification of title, body of abstract and indexing annotation must be entered when the overall report is classified)</i>  |  |  |
| 1. ORIGINATING ACTIVITY (Corporate author)<br>General Dynamics/Fort Worth Division<br>Fort Worth, Texas  |  | 20. REPORT SECURITY CLASSIFICATION<br>Unclassified |
|  |  | 20. GROUP<br>N/A                                   |
| 3. REPORT TITLE<br>Wing Roll Control Devices for Transonic High Lift Conditions - Fixed Wing Configuration   |  |  |
| 4. DESCRIPTIVE NOTES (Type of report and inclusive dates)<br>Final Report (Work accomplished from 1 Jan 1969 to 1 Dec 1969)  |  |  |
| 5. AUTHOR(S) (First name, middle initial, last name)<br>Jack D. McAllister                      Perry D. Whitten<br>David B. Benepe                         Garry Kaftan   |  |  |
| 6. REPORT DATE<br>July 1970  | 7a. TOTAL NO. OF PAGES<br>256  | 7b. NO. OF REFS<br>29                              |
| 8a. CONTRACT OR GRANT NO.<br>F33615-69-C-1225  | 8b. ORIGINATOR'S REPORT NUMBER(S)<br>AFFDL TR-69-124 Part I                        |  |
| b. PROJECT NO<br>8219  |  |  |
| c.<br>821902   | 9b. OTHER REPORT NO(S) (Any other numbers that may be assigned this report)<br>N/A |  |
| 10. DISTRIBUTION STATEMENT<br>This document is subject to special export controls and each transmittal to foreign governments or foreign nationals may be made only with prior approval of the Air Force Flight Dynamics Laboratory (FDCC), Wright-Patterson AFB, Ohio 45433.  |  |  |
| 11. SUPPLEMENTARY NOTES<br>None  | 12. SPONSORING MILITARY ACTIVITY<br>AFFDL<br>Wright-Patterson AFB, Ohio 45433      |  |
| 13. ABSTRACT<br>The Wind Mounted Roll Control Study (Contract F33615-69-C-1225) was an investigation of various methods for improving control effectiveness at high-lift transonic conditions. Emphasis was placed upon the use of leading edge devices as primary controls and also as auxiliary devices with conventional controls. Selected configurations were tested in AEDC 4T facility and limited validation was obtained in the AEDC 16T facility. Control configurations investigated included leading edge flaps and aileron both singly and in combination, as well as spoilers, differential horizontal tail and several auxiliary devices. Use of differential leading edge deflection significantly improved aileron effectiveness at high angle of attack transonic conditions. Because of the important effects that the wing-body configuration has upon wing mounted control devices, considerable data and analysis is presented for the longitudinal characteristics. Testing of the same model in two different size facilities provided significant information on wall interference effects at transonic conditions. |  |  |

DD FORM 1 NOV 68 1473

Unclassified

Security Classification

Unclassified

Security Classification

| 14. KEY WORDS   | LINK A |    | LINK B |    | LINK C |    |
|---|--------|----|--------|----|--------|----|
|   | ROLE   | WT | ROLE   | WT | ROLE   | WT |
| Aerodynamic Controls<br>High Lift<br>Transonic<br>Leading Edge Devices<br>Roll Control<br>Maneuvering |        |    |        |    |        |    |

Unclassified

Security Classification